THESE

présentée à

L'UNIVERSITE DE BRETAGNE OCCIDENTALE

pour obtenir le grade de

Docteur ès-Sciences Physiques

par

Joël PICAUT

SUR LES MECANISMES DES VARIATIONS THERMIQUES

DANS LE GOLFE DE GUINEE

(du semi-diurne à l'interannuel)

Soutenue le 16 mai 1983 devant la commission d'examen

Monsieur	LACOMBE H.	Professeur, Muséum National d'Histoire Naturelle Membre de l'Institut	Président
Messieurs	LE FLOCH J.	Professeur, Université de Bretagne Occidentale	Examinateurs
	MC CREARY J.P.	Directeur Oceanographic Center, Nova University	
	MOORE D.W.	Directeur Joint Institute for Marine and Atmospheric Research, University of Hawaii	
	O'BRIEN J.J.	Professeur, Florida State University	
	SALOMON J.C.	Professeur, Université de Bretagne Occidentale	
	VOITURIEZ B.	Chef du Service Océanographie Physique Centre National d'Exploitation des Océans	

THESE

présentée à

L'UNIVERSITE DE BRETAGNE OCCIDENTALE

pour obtenir le grade de

Docteur ès-Sciences Physiques

par

Joël PICAUT

SUR LES MECANISMES DES VARIATIONS THERMIQUES

DANS LE GOLFE DE GUINEE

(du semi-diurne à l'interannuel)

Soutenue le 16 mai 1983 devant la commission d'examen

Monsieur	LACOMBE H.	Professeur, Muséum National d'Histoire Naturelle Membre de l'Institut	Président
Messieurs	LE FLOCH J.	Professeur, Université de Bretagne Occidentale	Examinateurs
	MC CREARY J.P.	Directeur Oceanographic Center, Nova University	
	MOORE D.W.	Directeur Joint Institute for Marine and Atmospheric Research, University of Hawaii	
	O'BRIEN J.J.	Professeur, Florida State University	
	SALOMON J.C.	Professeur, Université de Bretagne Occidentale	
	VOITURIEZ B.	Chef du Service Océanographie Physique Centre National d'Exploitation des Océans	

A mon Père regretté
qui dès mon plus jeune
âge m'a poussé dans mon
choix pour l'océanographie.

A ma Mère.

A mes Ami(e)s.

"Let me affirm that the freedom to work full time in science, on one's own, with congenial colleagues, unfettered by supervision, with a scientific problem in one's mind when he goes to bed and when he awakes next morning, and to be able to give undivided attention to unraveling some puzzle of nature is a privilege beyond compare."

Henry STOMMEL

SOMMAIRE

REMERCIEMENTS

oooo

Je remercie Monsieur Henri LACOMBE, Membre de l'Institut, pour avoir bien voulu s'intéresser à ce mémoire et assurer la présidence de ce jury. Monsieur Jean LE FLOCH m'a accueilli dès l'origine du Laboratoire d'Océanographie Physique à Rennes, puis à Brest : je n'oublierai jamais nos premières années où il a su me faire communiquer sa passion dévorante pour l'océanographie. Messieurs Jay Mc CREARY, Dennis MOORE et Jim O'BRIEN ont été parmi les premiers Outre-Atlantique à s'intéresser à mes travaux ; leurs encouragements, conseils et assistances ont été vitaux pour la réalisation d'une bonne partie de ces travaux. J'ai été particulièrement touché par le fait qu'ils n'aient pas hésité à venir spécialement des Etats-Unis pour participer à ce jury de thèse. Jean-Claude SALOMON m'a fait l'amitié de siéger dans ce jury, je lui en suis très reconnaissant. Je remercie particulièrement Bruno VOITURIEZ qui, de plus, m'a été d'un très grand support par ses nombreux encouragements et conseils avisés.

Cet ensemble de travaux n'aurait pas été possible sans deux séjours au Centre de Recherches Océanographiques (ORSTOM) de Côte d'Ivoire de septembre 1972 à septembre 1974 et d'octobre 1978 à août 1980, et un séjour au Joint Institute of Marine and Atmospheric Research de l'Université d'Hawaii de mai à octobre 1981. Je tiens donc à remercier chaleureusement l'ensemble de la direction et du personnel de ces deux instituts de recherches, pour avoir organisé ces séjours et les avoir rendus scientifiquement et humainement passionnants. Mes remerciements vont plus spécialement à Rigobert BANHORO pour son assistance technique, Karena YEE pour son accueil, Sharon YOKOGAWA et Linda SMITH pour leur assistance informatique et Roger LUKAS pour ses nombreuses discussions scientifiques. Je suis très reconnaissant envers l'ensemble des membres du Laboratoire d'Océanographie Physique de l'Université de Bretagne Occidentale où j'ai profité d'une bonne ambiance de travail et d'un support technique, en particulier de la part de Chantal MAZE qui a préparé entre autre le ma-

nuscrit de synthèse avec sa très sympathique efficacité.

Plusieurs chercheurs ont participé directement à ces travaux et il en est aussi résulté quelques amitiés profondes. Malgré un climat de scepticisme, Jean-Marc VERSTRAETE a tenu bon pour que, dès 1974, nous démontrions que le Golfe de Guinée est le siège de nombreuses ondes moyennes fréquences. Jacques SERVAIN m'a toujours impressionné par son calme et sa tenacité à trouver la bonne corrélation d'une montagne de données. Jay Mc CREARY et Dennis MOORE ont su me faire un peu comprendre l'art de mettre l'océan équatorial en subtiles équations et Tony BUSALACCHI m'a épuisé à vouloir les résoudre numériquement ! Tous m'ont aussi montré qu'ils savaient se relaxer lors de mémorables soirées.

Je remercie également, George PHILANDER pour avoir cru à la première partie de ce travail, Philippe HISARD, Alain MORLIERE et Jacques MERLE pour leur collaboration et tout particulièrement ce dernier pour ses constants encouragements. Finalement, je suis très reconnaissant à tous les anonymes des stations côtières du Golfe de Guinée, sans qui ce mémoire n'aurait jamais vu le jour.

oooo

AVANT PROPOS

Les principaux travaux que j'ai réalisés depuis une dizaine d'années ont une certaine continuité dans l'étude générale du mécanisme des variations thermiques du Golfe de Guinée. Je les ai regroupés dans le présent mémoire. Il est intéressant de noter que cette continuité est autant le fait du hasard de la recherche et de circonstances externes que d'une évolution spatio-temporelle logique de mon champ d'étude (du semi-diurne dans le Trou sans Fond à l'interannuel dans tout l'Atlantique Tropical!). Un texte résumant et liant les différentes publications ainsi rassemblées s'imposait. Il s'est tout naturellement étendu en un essai de synthèse de ce que j'ai pu apprendre sur le sujet. A ma connaissance, il n'existe pas de document en francais présentant les différences fondamentales entre les océans des basses latitudes et hautes latitudes et résumant les intérêts scientifiques et économiques des océans tropicaux. C'est le but principal de la longue introduction du texte de synthèse. Dans la suite de ce texte, le lecteur pourra être amusé par le mélange de "je" et de "nous". Il n'est pas d'usage fréquent d'utiliser le "je" dans l'écriture scientifique et tout particulièrement en océanographie où le travail du chercheur ne peut être que le résultat de l'effort de toute une équipe. Cependant, dans le cadre du présent mémoire, il est demandé de faire la distinction entre les travaux que j'ai pu faire en collaboration avec d'autres chercheurs et les quelques travaux que j'ai mené "tout seul" (... c'est-à-dire avec d'efficaces marins, techniciens, secrétaires et l'appui intellectuel et psychologique de mes collègues!). Enfin, pour faciliter tant soit peu la tâche du lecteur, j'ai noté d'un astérisque les références des publications suivant ce texte de synthèse.

SUR LES MECANISMES DES VARIATIONS THERMIQUES DANS LE GOLFE DE GUINEE

(du semi-diurne à l'interannuel)

Texte de synthèse

(J. Picaut)

RESUME

Cette revue des mécanismes dynamiques associés aux variations thermiques dans le Golfe de Guinée est basée principalement sur nos travaux depuis une dizaine d'années. Dans l'introduction générale on résume les traits principaux qui différencient fondamentalement les océans des basses latitudes de ceux des plus hautes latitudes. Les conséquences climatiques et économiques des variations thermiques dans les océans tropicaux sont aussi résumées. Le domaine de fréquence de notre étude est divisé en deux bandes. La premiere, définie comme de la moyenne fréquence, concerne essentiellement les ondes de plateau (Picaut et Verstraete, 1976, 1979) forcées par la marée (semi-diurne et semi-mensuelle) et l'atmosphère (40-50 jours de période). Dans la même bande de fréquence les travaux d'autres chercheurs sur les méandres du Sous Courant Equatorial et les ondes océaniques sont aussi résumés. Dans la seconde bande de fréquence, saisonniere et interannuelle, notre revue porte essentiellement sur le mécanisme d'action éloigné du vent de Moore et al. (1978). Les principaux élements de cette théorie sont vérifiés par des analyses de données récentes et historiques, à savoir, corrélation entre la température de surface dans le Golfe de Guinée et tension zonale du vent dans la partie ouest de l'Atlantique Equatoriale (Servain, Picaut et Merle, 1982), et propagations horizontale et verticale du signal côtier d'upwelling dans le Golfe de Guinée (Picaut, 1983). Ce mécanisme d'action éloigné du vent est finallement détaillé grâce à deux modèles. Busalacchi et Picaut (1983) ont forcé un modèle à un mode barocline avec une côte et un vent saisonnier réalistes. McCreary,

Picaut et Moore (1984) ont forcé un modèle linéaire à trois dimensions avec des côtes et un vent annuel simplifiés. Ces études résultantes d'une étroite collaboration entre théoriciens et observateurs ont permis une meilleure compréhension des processus dynamiques de la variabilité dans le Golfe de Guinée.

ON THE MECHANISMS OF THERMAL VARIATIONS IN THE GULF OF GUINEA

(with time scales from semi-diurnal to interannual)

ABSTRACT

This review of dynamic mechanisms associated with thermal variations in the Gulf of Guinea is principally based on our work during the last ten years. In the general introduction we summarize the main features that fundamentally differentiate the low-latitude oceans from the higher ones. The climatic and economic consequences of thermal variations in the tropical oceans are also summarized. The frequency domain of our study is divided into two bands. The first one, defined as medium frequency, focuses mainly on shelf waves (Picaut and Verstraete, 1976, 1979) forced by tides (semi-diurnal and fortnightly) and the atmosphere (period of 40-50 days). In the same frequency range the works of others on Equatorial Undercurrent meanders and oceanic waves are also summarized. For the second frequency band, at seasonal and interannual time scales, our review is mostly concentrated on the remote forcing mechanism of Moore et al. (1978). The main elements of this simple theory are corroborated by analyses of direct and historical observations, i.e. correlation between sea surface temperature in the Gulf of Guinea and zonal wind stress in the western equatorial Atlantic (Servain, Picaut and Merle, 1982), and poleward and vertical propagation of the coastal upwelling in the Gulf of Guinea (Picaut, 1983). This remote forcing mechanism is finally detailed by the use of two numerical models. Busalacchi and Picaut (1983) forced a single baroclinic mode model with realistic coastline and seasonal winds. McCreary, Picaut and Moore (1984) forced a three-dimensional linear model with simplified coastline and annual winds. These studies, resulting from a close collaboration between theoreticians and observationalists, have enabled a better understanding of the dynamical processes of the variability in the Gulf of Guinea.

I. INTRODUCTION

1. Historique et évolution de l'étude de cette variabilité

L'historique de l'océanographie dans le Golfe de Guinée a été très bien décrit par Hisard (1983). Notons avec cet auteur, que dès 1886, il avait été observé une variation saisonnière de la structure hydrologique à l'équateur. Et dès 1906, par la mise en place de la première station côtière à Lomé (Janke, 1923), il a été observé que la température de surface pouvait varier de façon importante sur plusieurs jours. Mais pendant très longtemps, il n'a pas été question d'étudier cette variabilité, il fallait décrire les océans et pour cela on les a traités comme s'ils étaient pratiquement stationnaires. Tout au plus on considérait qu'ils étaient imprégnés d'un bruit, perturbant les mesures océanographiques. Et avec la découverte, dès le début du siècle, des ondes internes haute fréquence, on a limité l'origine de ce bruit aux seules ondes internes de gravité, de quelques minutes à quelques heures de période, et aux ondes internes de marée semi-diurne. Cet état de fait se retrouve au niveau des premiers modèles à moyenne et grande échelle qui eux aussi étaient stationnaires. Citons, pour exemple le modèle de Stommel (1960), extension de la théorie classique d'Ekman aux zones équatoriales.

Curieusement, ce sont les théoriciens qui ont été à l'origine de la découverte de l'énorme variabilité intermédiaire qui nous intéresse. En effet, avec le plan β, Rossby (1939) a introduit le concept mathématique des ondes planétaires dites ondes de Rossby. Dans la bande équatoriale, il a fallu que des météorologues mettent en évidence les singularités des équations de marée de Laplace pour lancer l'idée d'ondes piégées à l'équateur (Matsuno, 1966). L'existence de frontières méridiennes limitait l'extrapolation des théories équatoriales de l'atmosphère à l'océan ; Moore (1968) dans un travail de thèse, qui sert encore de base aux théoriciens équatoriaux, a détaillé les solutions correspondantes. Un grand pas dans l'étude de la réponse d'un océan équatorial à un vent variable a été fait par Lighthill (1969) qui projette la force du vent sur les modes verticaux. Cette idée de traiter mathématiquement le problème comme la somme des ondes forcées et libres pouvant être générées, a laissé sceptiques bien des océa-

nographes de terrain, d'autant plus que tout cet énorme travail théorique avait été fait jusqu'alors sans aucune évidence d'onde *in situ*.

La principale raison de cette avance de la théorie est d'ordre technique. Jusqu'il y a une vingtaine d'années, les mesures océanographiques se faisaient à partir d'un bateau isolé et avec des moyens qui n'avaient pas évolué depuis le début du siècle, comme la bouteille à renversement et le courantomètre Ekman. EQUALANT en 1963-1965 est le premier exemple d'une campagne multinationale dans l'Atlantique Tropical. Mais faute de connaissances préalables, cette opération internationale a surtout servi à décrire les grands traits de la circulation générale. Avec le développement des instruments électroniques et du nombre de navires de recherches, le passage à la connaissance des phénomènes dépendant du temps s'est rapidement effectué. Ce fut le but principal de la partie océanographique de l'expérience GATE en 1974. Auparavant, il y eut quelques tentatives isolées pour saisir cette variabilité en Atlantique Tropical. En particulier, notre laboratoire en 1968 et 1972, avait décrit en moins d'un mois, trois fois deux zones restreintes du Golfe de Guinée, mettant en évidence une surprenante variabilité spatio-temporelle (Le Floch, 1970, 1972). Mais les premières évidences d'ondes équatoriales dans l'Atlantique ont été obtenues par Duing *et al.* (1975) dans les couches de surface et Weisberg *et al.* (1979) dans les couches plus profondes. Citons pour mémoire, les analyses de niveau moyen de Wunsch et Gill (1976) dans le Pacifique Equatorial et la découverte de jets profonds équatoriaux basse fréquence par Luyten et Swallow (1976) dans l'Océan Indien. Ces découvertes en zones équatoriales sont à mettre en parallèle avec celles des tourbillons d'échelle moyenne dans les océans tempérés. Ainsi, il existerait dans l'océan énormément d'énergie dans les échelles de temps allant de quelques jours à quelques années. Le problème, maintenant admis en météorologie, que certaines de ces fluctuations puissent être à l'origine du mouvement moyen est donc posé en océanographie.

L'étude de cette variabilité tropicale pourrait se faire, comme dans les moyennes latitudes, via une statistique d'un ensemble important de mesures systématiques qui aboutirait à un modèle semi-empirique. Mais nous verrons qu'aux basses latitudes, l'identification des mécanismes de cette variabilité est beaucoup plus facile que dans les océans tempérés. Les pro-

grès fantastiques des ordinateurs pourraient laisser penser que cette approche dynamique devrait se limiter à l'élaboration d'un modèle numérique sophistiqué reproduisant cette variabilité. Mais pour espérer vraiment simuler l'océan, un tel modèle nécessiterait l'adjonction de plus en plus d'une physique encore mal connue, et à la limite on aboutirait à un modèle dont les solutions seraient aussi compliquées que l'océan réel, et surtout fortement dépendantes de coefficients d'échanges, réceptacles de notre ignorance. La tendance actuelle est donc à la recherche de modèles simples qui permettent de comprendre le mécanisme de cette variabilité. Ils doivent aussi servir de guide pour les programmes de mesures. Mais ce ne sera que par une collaboration de plus en plus étroite entre les observateurs et les modélisateurs que l'on pourra espérer comprendre, puis simuler, cette énorme variabilité.

2. Particularité des océans équatoriaux

Si l'on s'affranchit des forces astronomiques, les fluctuations océaniques sont régies par des apports de quantité de chaleur par absorption du rayonnement solaire, et de quantité de mouvement par le vent. L'importance relative de ces apports dans les couches proches de la surface est fondamentalement différente suivant la latitude.

Aux moyennes et hautes latitudes, la thermodynamique locale est dominante ce qui explique le succès des modèles unidimensionnels pour simuler les variations thermiques des couches superficielles (Lacombe, 1973). De plus, ces mêmes régions semblent être dominées par la présence de tourbillons à échelle moyenne. Ces mouvements transitoires, à vitesse de phase très faible, contiennent des quantités d'énergie cinétique très importantes dépassant très souvent celles de la circulation moyenne. Leur très grand nombre et l'impossibilité actuelle de relier ces tourbillons à une cause directe les a fait considérer comme de la turbulence à grande échelle. Les techniques spectrales semblent ainsi plus adaptées à leur modélisation.

Aux basses latitudes, il semblerait que les modèles thermodynamiques unidimensionnels ne soient pas applicables. En particulier Merle (1980 a) trouve qu'à l'échelle saisonnière, les variations du contenu thermique de l'Océan Atlantique Equatorial sont dix fois plus importantes que les varia-

tions des flux locaux de chaleur entre l'atmosphère et l'océan. Ainsi, une très importante redistribution de chaleur par une dynamique purement équatoriale semble se produire. A grande échelle, cette dynamique paraît être directement reliée au vent. L'exemple le plus spectaculaire est la renverse du courant de Somalie avec la renverse des vents de mousson. Les modèles océaniques dynamiques, directement forcés par le vent, sembleraient donc être beaucoup mieux adaptés aux problèmes des basses latitudes que des modèles thermodynamiques. L'aptitude des océans correspondants à répondre de manière cohérente et claire aux sollicitations basse fréquence du vent rend beaucoup plus aisée l'étude de sa variabilité. Notons à ce propos que, mis à part quelques cyclones occasionnels, le régime des alizés couvrant les zones tropicales, est beaucoup plus stable et régulier que celui des vents aux plus hautes latitudes.

Nous verrons que cette dynamique équatoriale très particulière est à relier à l'annulation puis au changement de signe de la force de Coriolis au passage de l'équateur. Cette singularité est aussi à l'origine d'un upwelling océanique et d'un contre-courant le long de l'équateur. Ce dernier paraît faire partie d'un ensemble de contre-courants zonaux à trois branches (Khanaichenko, 1974), transportant des quantités d'énergie considérables de l'ouest vers l'est. A l'opposé des océans tempérés, tous ces contre-courants ainsi que les courants de surface océaniques et côtiers sont très rapides et étroits. L'océan équatorial est donc fortement barocline comme le suggère aussi la présence d'une thermocline quasi-permanente marquée. Ce caractère barocline se retrouve à grande profondeur avec la découverte récente de jets zonaux multiples confinés à l'équateur. Luyten et Swallow (1976), dans l'Océan Indien, ont été les premiers à les observer grâce à un nouveau profileur à flotteurs. Les mesures de Hayes et Milburn (1980) et Eriksen (1981) dans le Pacifique et de Weisberg et Horigan (1981) dans le Golfe de Guinée, suggèrent leur existence dans les autres océans équatoriaux. Ces jets auraient une période de quelques mois à l'année et une échelle verticale de quelques centaines de mètres et rendraient compte d'une bonne partie de l'énergie en profondeur des océans équatoriaux.

La théorie et les observations montrent que les ondes internes de quelques minutes à quelques heures de période ne diffèrent pas vraiment

avec la latitude. Par contre, dans le domaine moyenne et basse fréquence, l'effet dynamique de l'annulation à l'équateur de la force de Coriolis et du gradient symétrique du tourbillon planétaire fait de l'équateur un guide d'ondes particulièrement efficace. Ceci est montré par la théorie équatoriale (Moore, 1968 ; Moore et Philander, 1978) : les équations sont linéarisées (méthode des perturbations) ce qui permet de découpler la structure verticale de la structure horizontale. L'océan équatorial est ainsi décomposé en modes barocline et barotrope stationnaires sur la verticale et en modes horizontaux. Ces modes horizontaux sont représentés par des fonctions oscillantes d'Hermite doublées d'une décroissance exponentielle correspondant au piégeage équatorial. Ce piégeage n'affecte pas le mode barotrope, ce qui fait que celui-ci est à traiter au niveau de l'océan global et non au niveau de la zone équatoriale. Les solutions ainsi obtenues sont composées de différents types d'ondes équatoriales :

. Les ondes d'inertie-gravité dont la phase et l'énergie se propagent vers l'est ou vers l'ouest et dont la période va de la journée à la semaine.

. Les ondes mixtes de Rossby-gravité, appelées encore ondes de Yanaï, avec une vitesse de groupe dirigée vers l'est et une vitesse de phase dirigée vers l'est ou vers l'ouest.

. Les ondes de Rossby, avec une vitesse de phase dirigée vers l'ouest, de période supérieure à un mois qui se partagent en ondes dispersives à courte longueur d'onde (quelques centaines de kilomètres) dont l'énergie se propage vers l'est et en ondes presque non-dispersives à grande longueur d'onde (quelques milliers de kilomètres) dont l'énergie se propage vers l'ouest.

. Les ondes non-dispersives de Kelvin dont l'énergie et la phase se propagent vers l'est.

Ces ondes équatoriales couvrent une bande continue de périodes allant de la journée à l'année. Au contraire, dans les latitudes tempérées, il existe un trou spectral entre les deux seuls groupes d'ondes libres possibles : les ondes d'inertie-gravité (période égale ou inférieure à celle d'inertie) et les ondes planétaires de Rossby (période de quelques mois à quelques années). Dans cette bande de fréquence intermédiaire ne peuvent exister que des ondes forcées (Philander, 1979 a). Ainsi, on note qu'il n'existe pas d'ondes libres longues allant vers l'est aux moyennes latitudes,

ce qui expliquerait en partie l'accumulation d'énergie sur les bords ouest des océans. Par contre, le guide d'onde équatorial permet un transfert d'énergie sur le bord est des océans.

Une autre particularité importante des zones équatoriales, conséquence de ce guide d'onde, est leur aptitude à répondre rapidement à un changement dans le régime des vents. Les ondes de Rossby ont un rôle essentiel dans un tel ajustement. Ce sont elles qui établissent le gradient horizontal de densité contre-balançant la tension du vent. De par la célérité importante des modes baroclines équatoriaux, cet ajustement est effectué en quelques mois (Cane, 1979 a-b). Par contre, aux moyennes et hautes latitudes, cela peut prendre jusqu'à une décennie et la variation correspondante du gradient de pression à l'échelle du bassin océanique se fera sur la même échelle de temps. Ainsi donc, la redistribution horizontale de chaleur correspondante est extrêmement lente. En zones équatoriales, ce temps de réponse est beaucoup plus proche des échelles de temps caractéristiques du vent qu'aux latitudes moyennes (Leetma *et al.*, 1981). Cette approche explique en partie pourquoi les modèles forcés par le vent sont plus adaptés aux basses latitudes que les modèles thermodynamiques unidimensionnels de couche homogène qui eux marchent mieux aux latitudes supérieures.

Un autre intérêt de la présence d'ondes équatoriales se propageant rapidement vers l'est ou vers l'ouest, est que des informations peuvent rayonner hors de la zone d'action du vent et réagir très vite et fortement sur des régions éloignées. C'est le phénomène dit de l'action éloignée du vent sur lequel porte une bonne partie de nos travaux. De plus, ce mécanisme pourrait être à l'origine des jets équatoriaux profonds. En effet, d'après Mc Creary (1984) les ondes équatoriales peuvent rayonner aussi vers les profondeurs créant, après d'éventuelles réflexions sur les frontières méridiennes, de multiples jets équatoriaux en profondeur. Cette étude théorique semble être appuyée par les observations récentes de Luyten et Roemmich (1982) dans l'Océan Indien.

Des variations de l'intensité du vent dans la bande équatoriale, ou de son rotationnel dans les zones extra-équatoriales, sont à l'origine de la plupart de ces ondes équatoriales. Mais des instabilités entre les courants ou des fluctuations rapides de la pression atmosphérique peuvent induire les ondes plus courtes d'inertie-gravité (Philander, 1978 a). Notons

que jusqu'à maintenant, ce sont ces dernières qui ont été observées de façon très nette. Le brouillage haute fréquence des couches de surface, la présence de phénomènes locaux non ondulatoires (d'origine thermodynamique ou thermohaline par exemple), le peu de mesures de longue durée et leur caractère non sinusoïdal rendent difficile la détection directe des ondes longues équatoriales. Mis à part les plausibles observations directes de Knox et Halpern (1982) et Eriksen *et al.* (1983), des méthodes indirectes, comme celles que nous allons présenter, permettent de confirmer l'existence des ondes longues équatoriales.

3. Intérêts climatiques et économiques des océans équatoriaux

Les zones tropicales sont caractérisées par une accumulation de chaleur d'origine solaire dans les couches superficielles tout au long de l'année (Hastenrath et Lamb, 1978). Ce sont les seules parties des océans où le bilan thermique océan-atmosphère est largement positif, au contraire des océans aux moyennes et hautes latitudes. Il y a donc des transferts importants d'énergie des tropiques vers les pôles via des processus interactifs océan-atmosphère et de l'advection marine. Il existe aussi un transfert moyen entre les deux hémisphères à travers la zone tropicale puisque le bilan énergétique de chacun des hémisphères n'est pas équilibré (Oort et Vonder Haar, 1976). Des fluctuations à grande échelle et basse fréquence de ces transferts sont à l'origine des variations climatiques de notre planète. Des modèles numériques récents (Shukla, 1975 ; Reiter, 1978) montrent l'importance des courants et des températures de surface des zones équatoriales dans le mécanisme de ces variations climatiques, non seulement dans les tropiques mais aussi aux latitudes plus élevées.

Bjerknes (1966, 1969) a été le premier à présenter une telle interaction océan-atmosphère à grande échelle dans le Pacifique Tropical. Il suggère que la cellule de circulation convective de Walker dans le plan équatorial répond directement aux variations du gradient de température de surface le long de l'équateur. Ce gradient résulte de la présence d'une thermocline qui est profonde dans la partie ouest du bassin équatorial et qui affleure dans la partie est. Ce schéma est complété, au niveau des échanges nord-sud, par la cellule méridienne de Hadley, maintenue par les contrastes thermiques entre les tropiques et les latitudes moyennes. Wyrtki (1975) reprend cette idée en insistant sur la réaction dynamique de l'océan équatorial aux vents. En effet, les variations saisonnières et interannuel-

les de la profondeur de la thermocline dans le plan équatorial semblent directement reliées à l'intensité des vents zonaux, partie basse de la cellule de Walker. Cet exemple de couplage océan-atmosphère dans les tropiques a été modélisé par Mc Creary (1983 a) et semblerait même avoir de l'influence sur le climat du nord du Pacifique et de l'Amérique du Nord (Bjerknes, 1966).

Les tropiques sont aussi les régions qui réagissent très souvent de façon catastrophique aux variations de température de surface. Le schéma précédent a été proposé par Bjerknes comme une explication possible du phénomène bien connu d'El Niño d'accumulation anormale d'eaux chaudes le long des côtes de l'Equateur et du Pérou. Cet événement provoque, entre autres, des pluies dévastatrices sur ces régions côtières. En Atlantique Tropical, il semble exister un phénomène similaire (Hisard, 1980 ; Merle, 1980 b) qui peut amener des pluies torrentielles le long des côtes nord du Golfe de Guinée (Hookey, 1970) et de l'Angola (Hisard et Piton, 1981). En effet, les températures de surface influencent le régime des pluies par contrôle de l'humidité et de la stabilité des basses couches de l'atmosphère. Dans la partie nord de l'Atlantique Tropical, la présence de températures de surface anormales peut avoir un effet important sur la formation des cyclones (Namias, 1969). Et à plus grande échelle, il semblerait qu'il y ait une téléconnexion entre les températures de surface et les sécheresses du Sahel et du Nord du Brésil (Lamb, 1968 ; Hastenrath, 1976 ; Markman et Mc Lain, 1977).

Nous avons vu que le phénomène d'El Niño a d'importantes conséquences sur le climat des côtes de l'Equateur et du Pérou. Mais de par la cessation de l'upwelling côtier correspondant, il peut entraîner une chute considérable du premier stock mondial d'anchois suivie d'une diminution importante du nombre d'oiseaux de mer et donc de la quantité de guano récupérée. En effet, les upwellings participent à un enrichissement actif de la zone euphotique par apport vertical de sels nutritifs qui débouche sur une augmentation de la productivité à travers la chaîne alimentaire. De plus, ces upwellings induisent des changements importants de paramètres physiques comme la température de surface et la profondeur de la thermocline qui conditionnent la concentration des poissons favorisant ainsi leur capture (Evans *et al.*, 1980). Les tropiques sont les régions où les upwellings sont les plus intenses. Ces résurgences d'eaux froides existent de façon quasi-permanente le long des bords nord-est et sud-est des bassins tropicaux et

existent de façon saisonnière dans la partie est de la bande équatoriale, le long des côtes et de l'équateur.

Dans l'Atlantique, l'importance de l'upwelling équatorial comme facteur d'enrichissement a été décrite par Voituriez *et al.* (1982). Les upwellings saisonniers du Golfe de Guinée sont à l'origine de fronts thermiques favorables à la concentration des thons (Stretta, 1977). Ces mêmes upwellings côtiers, couplés avec les apports nutritifs d'origine fluviale influencent les pêcheries de sardinelles (Binet, 1982). Plus au sud, un phénomène pouvant ressembler à El Niño peut perturber les pêcheries d'anchois et de sardinelles des côtes de l'Angola (Hisard et Piton, 1981).

Ainsi, les océans tropicaux, de façons directes ou indirectes, seraient à l'origine des variations climatiques, lesquelles peuvent avoir des répercussions économiques importantes. La prévision d'une bonne partie de ces fluctuations climatiques, ne pourra se faire que grâce à des modèles couplés océan-atmosphère. Mais le caractère hautement non linéaire de ce couplage ne permet pas de garantir actuellement les résultats de tels modèles. En attendant, les océanographes cherchent à mieux connaître la physique de la réponse des océans aux différents forcings.

4. L'intérêt particulier de l'Atlantique Tropical et plus spécifiquement du Golfe de Guinée

a) L'Atlantique Tropical

Nous venons de voir qu'au niveau des catastrophes climatiques, économiques et humaines, l'océan Pacifique Tropical agit avec un maximum d'effets sur ses côtes sud-est, l'océan Atlantique Tropical, par contre, influence plus l'intérieur des continents avec la terrible sécheresse du Sahel. Mais il existe bien d'autres différences entre ces deux océans tropicaux, ne serait-ce que par leur dimension. L'Atlantique est en effet trois fois moins large que le Pacifique. Le temps de réponse des océans tropicaux aux sollicitations basse fréquence du vent étant fonction du temps de parcours des ondes longues baroclines à travers le bassin, il devrait donc être plus grand dans le Pacifique que dans l'Atlantique (Cane, 1979 a-b ; Philander,

1979). Cela va se traduire par une prépondérance du signal saisonnier dans l'Atlantique Tropical (Merle *et al.*, 1980) et du signal interannuel dans le Pacifique (Wyrtki, 1975 ; Hickey, 1975 ; Busalacchi, 1982). Mais les résultats récents d'un modèle linéaire forcé par des vents périodiques (Cane et Sarachik, 1981) suggèrent que cette différence dans la réponse serait plutôt à relier aux écarts dans le régime des vents. En effet, le cycle annuel des vents dans l'Atlantique Tropical est plus évident que dans le Pacifique Tropical (Roden, 1962 ; Wyrtki, 1975 ; Philander et Pacanoswski, 1981 a). Par contre, le cycle semi-annuel dans les vents comme dans leurs réponses, existe dans l'Atlantique Tropical (Merle et Le Floch, 1978 ; Busalacchi et Picaut, 1983) tout comme dans le Pacifique Tropical (Meyers, 1979 ; Busalacchi et O'Brien, 1980), mais il est beaucoup moins important que dans l'Océan Indien (Duīng, 1978 ; Luyten et Roemmich, 1982) qui est principalement soumis aux renverses de la mousson.

b) Le Golfe de Guinée

Contrairement au reste de l'Atlantique Equatorial, soumis à de forts vents zonaux issus des alizés de nord-est et sud-est, le Golfe de Guinée est principalement sous l'influence d'un vent de mousson de secteur sud, d'intensité moyenne. Cette région, qui occupe plus du tiers du bassin équatorial, a été tout particulièrement étudiée en océanographie comme en météorologie de par la présence française depuis de nombreuses années. Ainsi, il existe sur son littoral toute une série de stations côtières de prélèvements journaliers de température de surface dont les plus longues séries excèdent la vingtaine d'années (Figure 1). Cette partie est de l'Atlantique équatorial est caractérisée par une thermocline qui affleure, alors qu'elle est profonde, dans la partie ouest. Il en résulte que les déplacements saisonniers de cette thermocline vont induire des variations importantes de la température de surface (5 à 7° contre 1 à 2° dans l'ouest) qui, nous l'avons vu, ont des répercussions climatiques, économiques et sociales importantes. Cette thermocline très proche de la surface est une des raisons de la vulnérabilité des thons aux techniques de pêches modernes, ce qui explique qu'une bonne partie des thons pêchés dans l'Atlantique Tropical provient du Golfe de Guinée (Evans *et al.*, 1980 ; Fonteneau et Cayré, 1983).

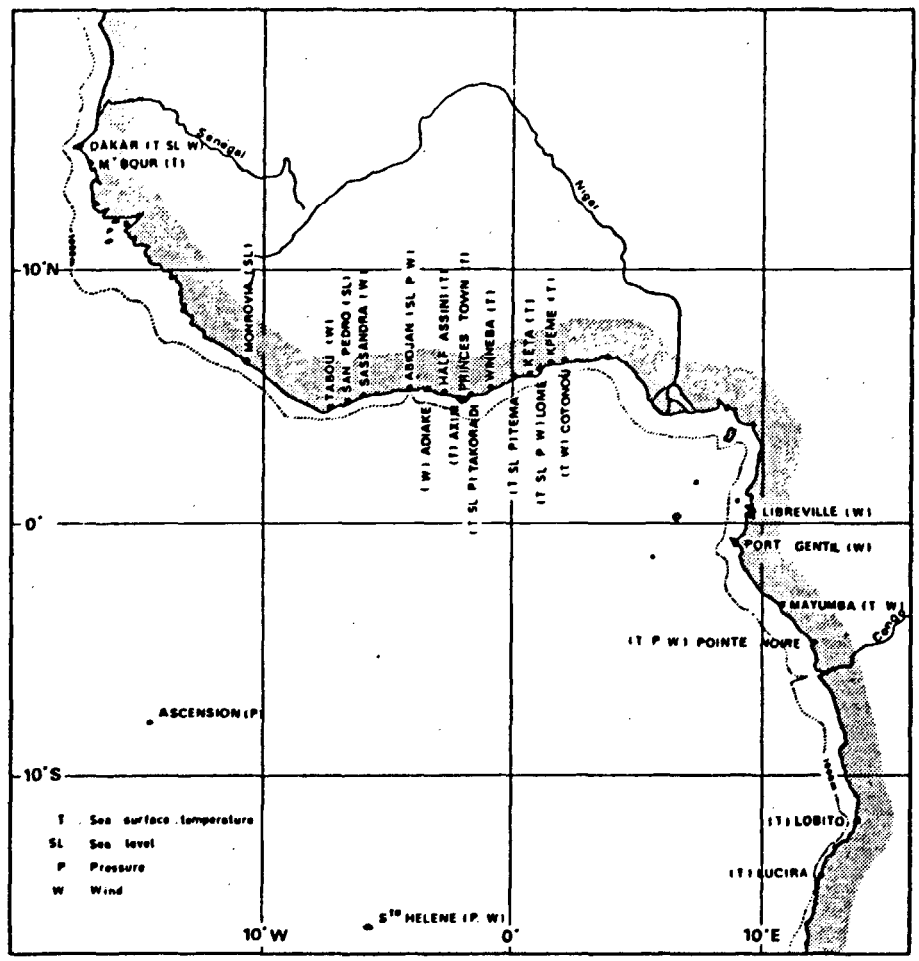

Figure 1 : Le Golfe de Guinée et les stations côtières (d'après Verstraete, Picaut et Morlière, 1980).

Les déplacements saisonniers de cette thermocline sont associés à un phénomène d'upwelling équatorial et côtier qui semble mal expliqué par des concepts classiques comme l'advection ou la théorie d'Ekman (Berrit, 1976 ; Houghton, 1976 ; Bakun, 1978 ; Voituriez, 1980). Un des principaux résultats de notre étude a été de montrer qu'une partie significative de ce phénomène est due à un effet des vents à l'extérieur du Golfe de Guinée, transmis par des ondes équatoriales. Ces variations saisonnières sont contaminées par des fluctuations importantes à plus hautes fréquences qui peuvent être dues à des ondes équatoriales ou à des ondes côtières (Figure 2). En effet, une discontinuité de profondeur (talus continental) ou une pente régulière du fond (plateau continental) offrent également la possibilité de

piéger l'énergie sous forme d'ondes côtières. La côte du Golfe de Guinée, partout proche de l'équateur est une région favorable pour la propagation d'ondes topographiques équatoriales barotropes et baroclines. La présence d'une côte orientée est-ouest, unique dans les zones équatoriales, peut être à l'origine d'un mode supplémentaire des ondes piégées par l'équateur sous la forme d'une onde de Kelvin se propageant vers l'ouest piégée à la côte (Hickie, 1977 ; Philander, 1977). Enfin, dans le même point de vue, plutôt théorique, l'existence d'un fond plat dans le Golfe de Guinée laisse penser que des modes verticaux stationnaires peuvent beaucoup plus facilement s'établir que dans la partie ouest de l'Atlantique Equatorial où le fond est particulièrement irrégulier (Garzoli et Katz, 1981).

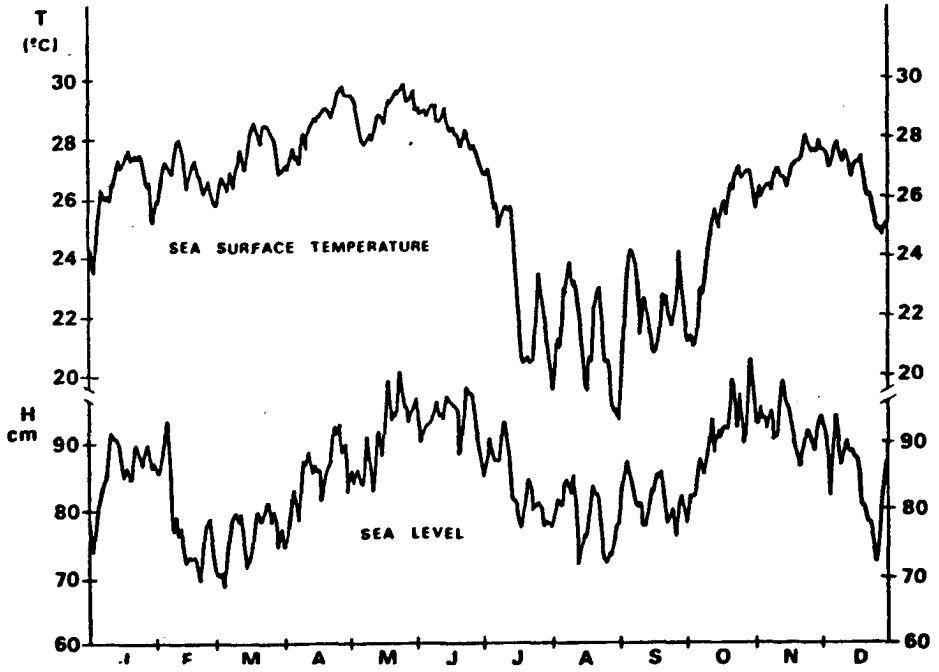

Figure 2 : Variations journalières de température de surface et de niveau moyen en 1974 à Téma (d'après Picaut et Verstraete, 1979).

L'existence d'un Centre de Recherches Océanographiques (ORSTOM) à Abidjan, c'est-à-dire sur cette côte orientée est-ouest et à quelques degrés de l'équateur, est un avantage important pour étudier ces phénomènes équatoriaux.

5. Présentation de la présente étude

Cette étude porte sur les oscillations dont les périodes sont égales ou supérieures à celle de la marée semi-diurne. Nous ne nous intéressons pas aux ondes internes haute fréquence, c'est-à-dire de quelques minutes à quelques heures de périodes. Bien que nous les ayons observées systématiquement dans le Golfe de Guinée depuis 1968 (Trébern-Etienne, 1971), elles ne diffèrent pas vraiment de leurs homologues aux plus hautes latitudes. Dans les modèles à grande échelle que nous avons utilisés, elles seront donc considérées et paramétrisées comme de la turbulence.

Notre domaine d'étude se partage en deux bandes de fréquence. La première, que nous définissons comme de la moyenne fréquence, va du semi-diurne à quatre mois de période et englobe toutes les oscillations que nous avons pu observer, soit à l'aide de points fixes à partir de navire de recherches, soit à l'aide de stations côtières. Nous avons complété cette revue de nos propres travaux par un survol des résultats similaires de quelques autres chercheurs aussi bien à la côte qu'au large. La deuxième bande de fréquence, que nous définissons comme de la basse fréquence, traite du cycle saisonnier et de l'interannuel. La limite entre ces deux domaines est assez floue. Nous avons montré (Picaut, 1983*) que le cycle saisonnier était parfaitement reconstitué à l'aide des cinq premières harmoniques de l'annuel. En fait d'énergétique, il n'existe que les trois premières. Or s'il est facile d'imaginer des événements océaniques annuels et semi-annuels, l'existence d'une onde tiers-annuelle est problématique (Picaut *et al.*, 1978).

Notre étude des moyennes fréquences porte surtout sur les ondes de plateaux forcées par la marée (semi-diurne et semi-mensuelle lunisolaire) et l'atmosphère (45 jours de période). Par contre, le deuxième chapitre concerne surtout le mécanisme des upwellings côtiers et équatoriaux à l'échelle saisonnière et interannuelle.

Dans ces deux bandes de fréquence nous nous intéressons principalement à la dynamique des variations thermiques. Mais une bonne partie de nos observations consiste en température de surface dans le Golfe de Guinée, où la thermocline est toujours proche de la surface. Il ne faut donc pas oublier qu'en plus des mouvements dynamiques de cette thermocline, des processus thermodynamiques sont nécessaires pour mélanger la couche homogène et induire les variations de la température de surface.

II. VARIATION A MOYENNE FREQUENCE

1. Marée interne semi-diurne

La marée est le parfait exemple de réponse océanique à un forcing oscillant. Le cas barotrope a été mathématiquement étudié par Laplace dès 1776 mais il faudra attendre 1940 pour adjoindre de la stratification dans ces équations (Hendershott, 1981). Si le phénomène de marée barotrope est connu depuis l'aurore des temps, il faudra attendre le début du siècle pour les premières observations de marée interne par Nansen. Quelques mesures au point fixe durant la campagne du Météor puis par Varlet (1958) suggèrent leur existence dans le Golfe de Guinée.

En 1973, j'ai effectué une douzaine de sorties avec le NO Reine Pokou du Centre de Recherches Océanographiques de Côte d'Ivoire, en vue d'étudier la variabilité interne induite par le grand canyon sous-marin, au large d'Abidjan, appelé Trou sans Fond. Des mesures en huit points fixes, sur le plateau continental ou la rupture de pente, ont montré la permanence des ondes de marée interne et leur forte amplitude. Ainsi, sur un fond de 200 m, cela se traduit par un déplacement, principalement semi-diurne, des isothermes de plus de 50 m et sur les fonds de 50 m d'environ 30 m. L'utilisation en continu, lors des deux dernières sorties d'un profileur de courant, prêté par l'Université de Miami, a conduit à la mise en forme de 450 profils de courant et de température. Sur la figure 3 sont représentés les résultats du dernier point fixe. On note une très forte cohérence entre le déplacement vertical des isothermes, la composante parallèle à la côte des courants et le niveau moyen mesuré à quelques milles. Les températures au fond peuvent ainsi varier de près de 6° en quelques heures. Les oscillations de courants, pratiquement en opposition de phase entre les couches de surface et celle au fond, suggèrent la dominance du premier mode barocline.

Cet ensemble de mesures et travaux a été repris et développé par Park (1979). Ses principaux résultats peuvent se résumer ainsi : en présence d'une faible pente, ces oscillations sont assez bien expliquées par la théorie linéaire des ondes internes. Si le fond est bien incliné, le déplacement des masses d'eaux, suivant la pente et sous l'action du courant de

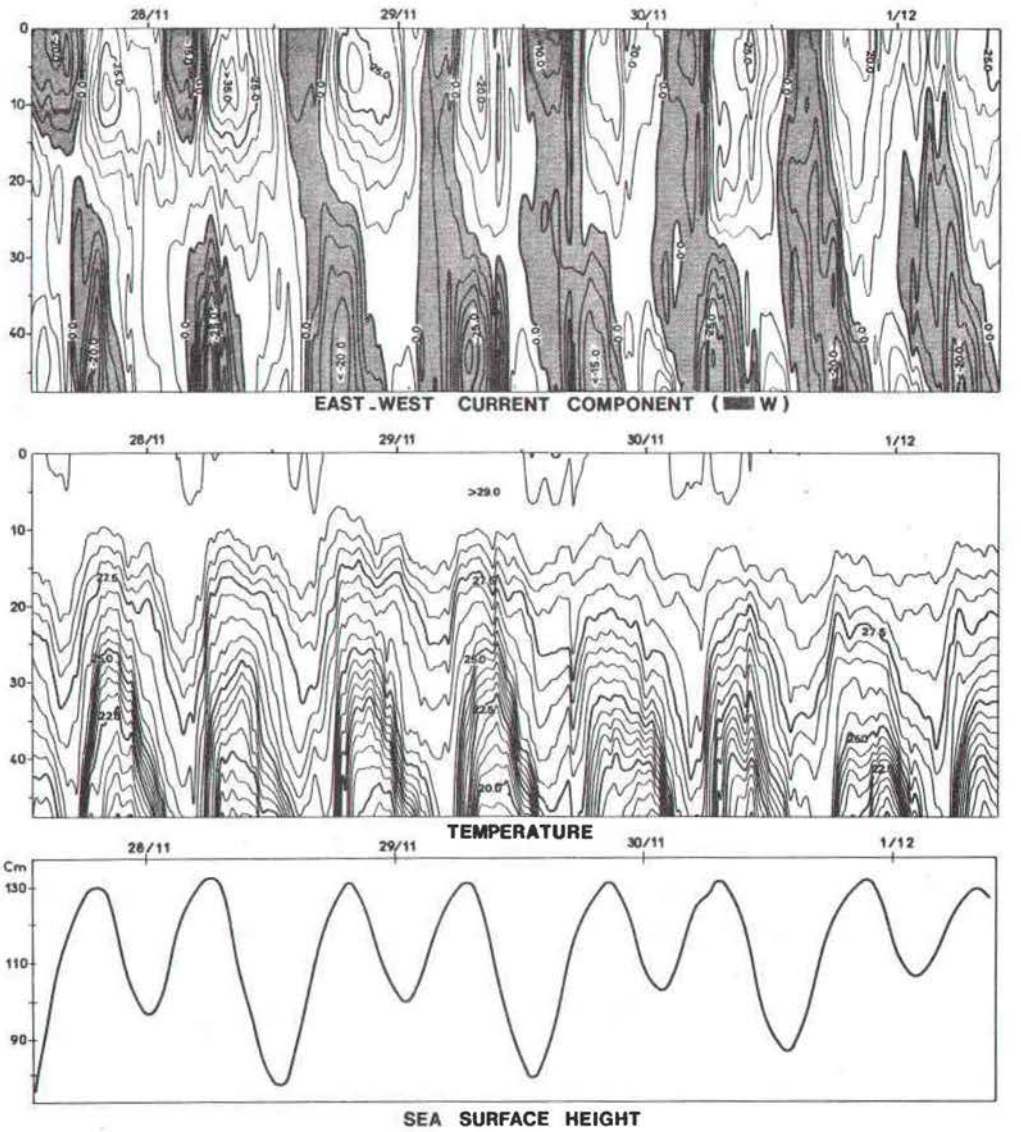

Figure 3 :, Marée interne observée sur un fond de 52 m au large d'Abidjan à partir de 298 profils de courant et de température et niveau moyen correspondant mesuré à la côte (d'après Picaut et Verstraete, 1979).

marée barotrope, peut être prépondérant. Enfin, il ne faut pas totalement négliger les déplacements baroclines résultant de l'effet du courant de marée barotrope à travers le gradient horizontal de densité qui équilibre le courant de Guinée. Les changements de la stratification moyenne au passage des saisons marines (Morlière et Rébert, 1970) semblent affecter les caractéristiques internes de ces oscillations. En particulier, durant la saison chaude, une analyse portant sur les courants montre que le premier mode barocline est fortement dominant et égal en amplitude au mode barotrope. L'adaptation du modèle de Prinseberg (1971) au plateau continental ivoirien et du modèle de Cavanié (1969) au canyon sous-marin Trou sans Fond montre que ces ondes internes peuvent être générées par l'action du courant de marée sur le talus continental et sur les rebords du Trou sans Fond.

Concernant la répartition spectrale de ces ondes internes, Park (1979) note l'existence de faibles oscillations diurnes. A partir de mesures avec une chaîne à thermistances sur près de six mois, nous avons réussi à séparer les ondes internes semi-diurnes M_2 et S_2, la première étant évidemment prépondérante (Picaut et Verstraete, 1979 *).

Ces marées internes que l'on retrouve aussi au large des côtes du Golfe de Guinée peuvent être à l'origine d'erreurs dans l'interprétation des mesures hydrologiques (Defant, 1950), c'est pourquoi, elles seront, si possible, filtrées dans le reste de notre étude. Par contre, elles semblent être une source importante de l'agitation interne des océans et des mélanges. Wunsch (1975) trouve qu'au moins 10 % de l'énergie des marées barotropes est transféré dans les marées internes, ce qui par comparaison est similaire à l'apport d'énergie dans la circulation générale.

Ces oscillations internes sont aussi importantes au niveau de la chaîne alimentaire par les interactions qu'elles pourraient avoir sur le phytoplancton (Kamykowski, 1974). Elles semblent aussi avoir une influence directe sur la répartition des poissons. En effet, une expérience de 24 traits de chalut toutes les deux heures sur le plateau ivoirien, encadrée par quatre jours de mesures physiques en continu, semble montrer que des mouvements de certains poissons correspondent aux variations de température dues aux marées internes (Caverivière et Picaut, communication personnelle).

2. Ondes côtières

Dès le début de mon premier séjour au Centre de Recherches Océanographiques de Côte d'Ivoire (septembre 1972 - septembre 1974), j'ai été frappé par l'amplitude des variations à moyenne fréquence des températures mesurées à la station côtière bi-hebdomadaire au large d'Abidjan et à la sation côtière journalière du warf de Lomé au Togo. Les températures de surface peuvent en effet varier jusqu'à 5° en moins d'une semaine (voir Fig. 2 pour exemple). Une première analyse spectrale, sur ces séries de température et sur une série marégraphique d'un peu plus d'un an effectuée à Abidjan, met en évidence des maxima d'énergie dans la bande des 3 à 60 jours de période. Cette première étude a été reprise, sur une plus grande échelle, à partir de mai 1974 en collaboration étroite avec J.M. Verstraete. Nous avons ainsi mis sur support informatique les données d'un maximum de stations côtières au Togo-Bénin-Ghana et Côte d'Ivoire et incité les autres centres ORSTOM de Dakar et Pointe Noire à en faire autant. Les séries chronologiques de 27 stations (Figure 1), comportant des mesures généralement journalières, de températures, niveau moyen, pression atmosphérique et vent ont été ainsi systématiquement analysées. Parallèlement, nous avons maintenu une chaîne à thermistance sur un fond de 65 m au large d'Abidjan, pendant près de six mois. Sur la figure 4 correspondante, obtenue après filtrage des fluctuations dues aux marées internes semi-diurnes, il apparaît que ces oscillations moyenne fréquence intéressent toute la couche d'eau. Sur cette même figure, on notera que l'upwelling de l'été boréal semble se déclencher en profondeur dès la mi-mai créant un minimum thermique (21°) en surface, fin juillet.

Ces séries chronologiques ont été soumises à un ensemble de traitements statistiques comme l'analyse spectrale, la corrélation croisée, la décomposition en série de Fourier, l'analyse harmonique de marée, le filtrage passe-bande et la démodulation complexe. Ces analyses nous ont permis de mettre en évidence des oscillations océaniques côtières plus énergétiques dans les bandes de périodes allant de 3 à 9 jours, 13-15 jours et 40-50 jours (Picaut *et al.*, 1978 ; Verstraete *et al.*, 1980*).

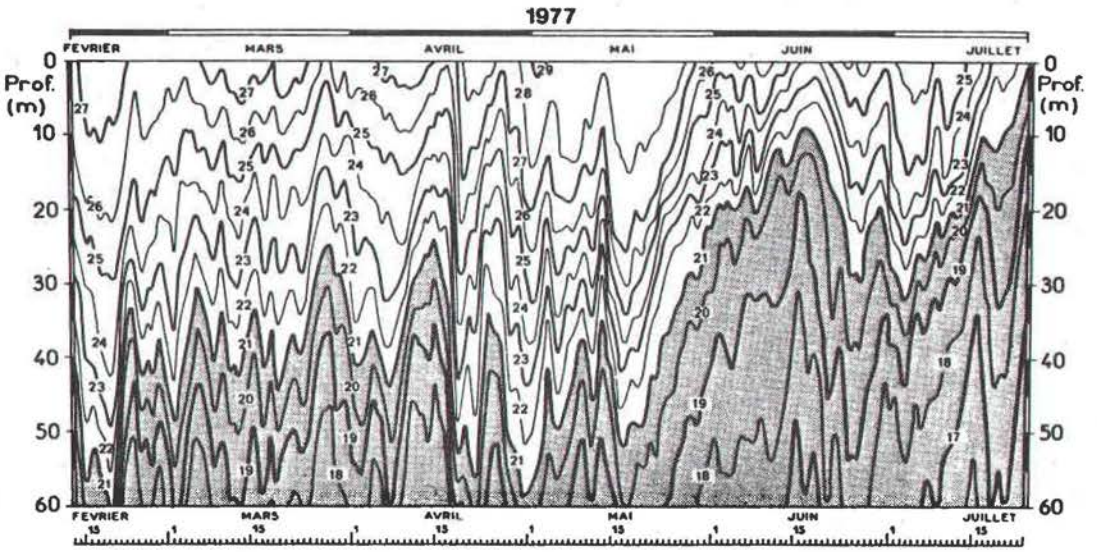

Figure 4 : Variation de la structure thermique sur un fond de 65 m au large d'Abidjan du 11 février au 25 juillet 1977, à partir de données de surface et d'une chaîne de thermistance après élimination des oscillations dues aux marées internes (d'après Verstraete et Picaut, 1983).

a) 3 à 9 jours de période

. Une oscillation vers 3 jours de période semble être forcée par l'atmosphère.

. Une oscillation dans les alizés dans les périodes allant de 3 à 6 jours (Krishamurti et Krishamurti, 1980), probablement reliée aux ondes atmosphériques africaines se propageant vers l'ouest (Arnold, 1966), pourrait forcer une onde océanique que nous avons trouvée dans cette même gamme de période. Houghton (1979) et Mc Grail (1979) notent cette même oscillation à partir de mesures de courants sur le plateau continental du Ghana, du Libéria et de Sierra Léone. Il faut noter que le long de la côte nord du Golfe de Guinée, la période d'inertie correspond à ces mêmes valeurs.

. L'atmosphère forcerait aussi une onde océanique vers 9 jours de période. A partir des mesures de courant, Houghton (1979) retrouve cette oscillation qui semble s'atténuer à l'approche du fond. Dans une étude d'ondes de plateau barotropes dans le plan β, Beer (1978 a) indique que cette

onde pourrait correspondre au deuxième mode.

b) Période semi-mensuelle

1974 est l'année particulière où apparaît de façon très nette une oscillation semi-mensuelle dans les températures de surface de la saison d'upwelling, époque durant laquelle la thermocline est la plus proche de la surface (Figure 2). Houghton et Beer (1976), avec les mesures des stations côtières de Cotonou et du Ghana de cette même période, montrent que cette oscillation se propage vers l'ouest à une vitesse moyenne de 64 cm/s. Simultanément, Picaut et Verstraete (1975), par une analyse spectrale de toutes les séries chronologiques de température de surface, ont trouvé un maximum d'énergie autour de quinze jours de période se propageant le long de la côte nord du Golfe de Guinée avec une vitesse approximative de 75 cm/s. Nous avons poursuivi cette étude par la collecte d'un maximum de données marégraphiques dans cette même région et avons alors montré que cette oscillation existe toute l'année dans le niveau moyen (Figure 2), mais surtout qu'elle se compose de deux ondes (Figure 5). La première correspond à l'onde semi-mensuelle lunaire Mf (13,66 jours de période) et a une phase constante tout au long de ces côtes. La deuxième a une période de 14,76 jours, ce qui correspond à celle de l'onde semi-mensuelle luni-solaire Msf. Cette onde se propage vers l'ouest sur au moins 1500 km de la côte nord du Golfe de Guinée avec une vitesse moyenne de phase de 53 cm/s (Figure 6) et de 675 km de longueur d'onde (Picaut et Verstraete, 1979*). Ces ondes particulièrement énergétiques (Figure 5) ont un effet important sur la structure thermique et induisent des oscillations verticales des isothermes de sub-surface tout au long de l'année.

De par la petitesse de la force astronomique luni-solaire semi-mensuelle, nous en avons déduit que l'onde Msf est très probablement le résultat d'une interaction non-linéaire entre les deux ondes de marée semi-diurne M_2 et S_2. On vient de voir que des ondes internes M_2 et S_2 existent vraisemblablement tout le long des côtes du Golfe de Guinée. Elles pourraient forcer une onde de 14,76 jours de période via un processus non-linéaire. Mais il semble difficile d'imaginer que des ondes de 15 à 20 km de longueur d'onde puissent forcer localement une onde de 675 km de longueur d'onde . Il

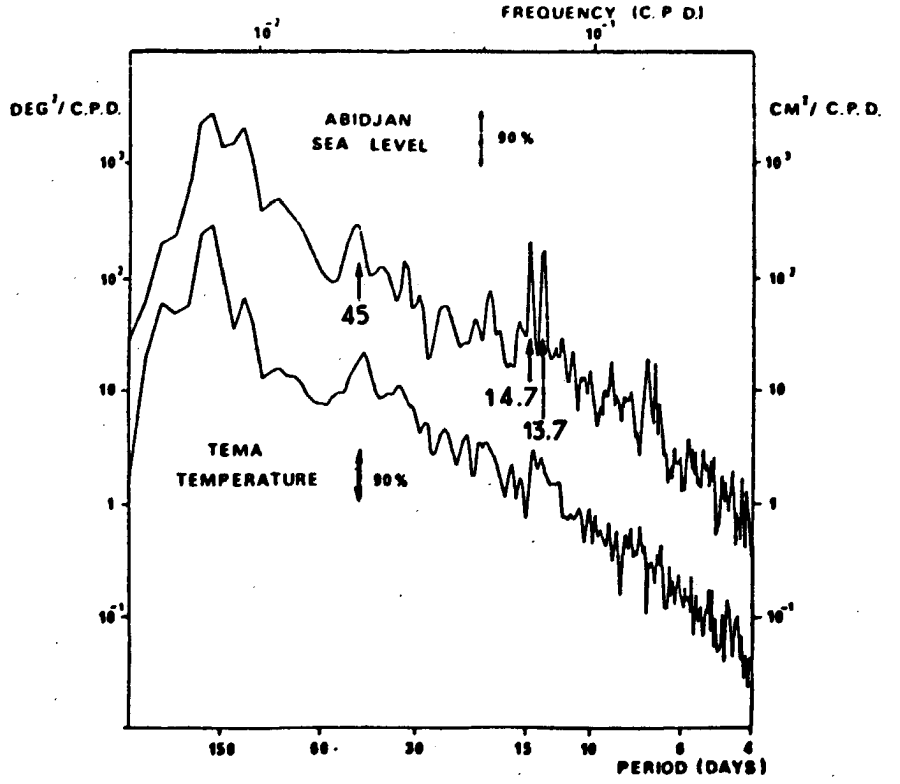

Figure 5 : Spectre de 10 années de niveau moyen à Abidjan et de 13 années de température de surface à Téma (d'après Picaut de Verstraete, 1979).

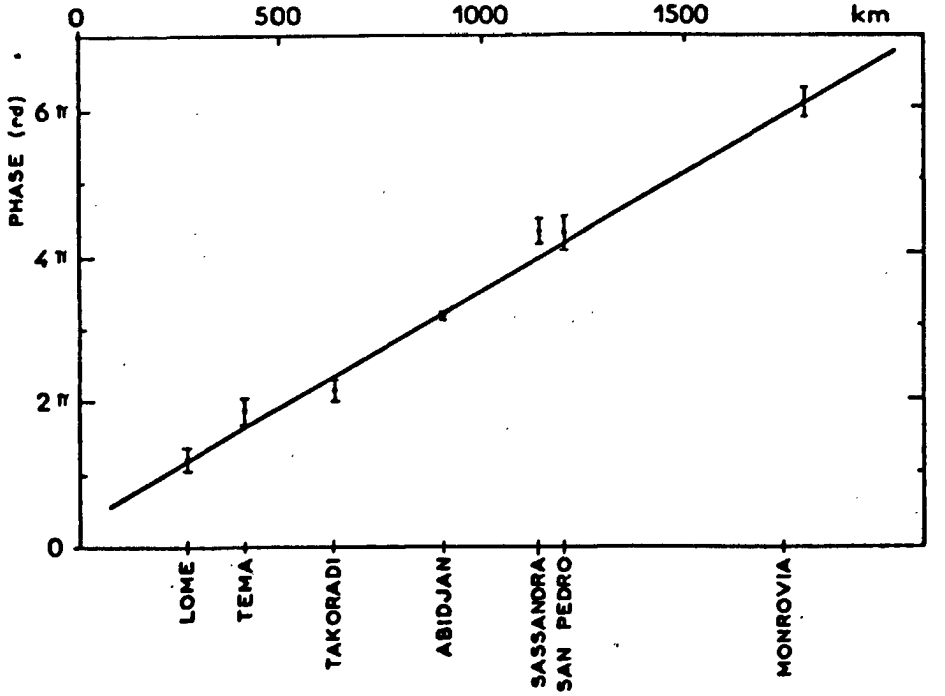

Figure 6 : Variation de la phase de l'onde de 14,7 jours de période le long de la côte nord du Golfe de Guinée (d'après Picaut et Verstraete, 1979).

nous a été plus facile d'imaginer une interaction non-linéaire entre les ondes de marée barotropes M_2 et S_2 dans la région du Golfe de Guinée où le plateau continental est le moins profond et le plus large, à savoir son coin nord-est. Une onde serait alors générée se propageant en laissant les petits fonds à droite, donnant ainsi un très bel exemple de forcing éloigné. Il a été suggéré que cette onde pouvait être une onde de plateau topographique (Philander, 1979), une onde interne de Kelvin (Houghton et Beer, 1979) ou une onde équatoriale topographique (Mysak, 1978 a-b ; Picaut et Verstraete, 1979*). Par des analyses récentes de mesures de courant, Houghton (1979) trouve que l'énergie associée à cette onde est piégée sous la thermocline et pense que le modèle de Wang et Mooers (1976) d'une onde hybride de plateau topographique modifiée par la stratification serait plus approprié. Il existe des contradictions entre tous ces modèles. L'onde ne peut être barotrope puisqu'elle se manifeste par des fluctuations importantes d'isothermes. Par contre, nous avons montré (Picaut et Verstraete, 1979*) que quand la stratification change sur le plateau continental, avec l'arrivée de la saison d'upwelling, la célérité de cette onde ne change pas. Clarke et Battisti (1983), en utilisant un modèle à topographie réaliste et à stratification continue dans un plan β, trouvent que l'onde observée coïnciderait avec le deuxième mode calculé, mais surtout que la célérité correspondante dépendrait essentiellement de la stratification en dessous de 150 m. Comme cette dernière ne change pratiquement pas avec les saisons marines, ce dernier modèle expliquerait ainsi la constante observée de la célérité.

c) 40 à 50 jours de période

Avant de passer dans cette bande de fréquence, notons que nous avons trouvé une onde assez peu énergétique à 31,8 jours de période correspondant à la marée mensuelle Msm (Verstraete *et al.*, 1980*).

Nos premières études sur les séries chronologiques des stations côtières du Golfe de Guinée nous ont permis de mettre en évidence une onde de 40-50 jours de période (Picaut et Verstraete, 1976*). Des analyses spectrales faites sur le niveau moyen corrigé de l'effet barométrique et sur la température de surface en diverses stations du Golfe de Guinée montrent un maximum d'énergie, dans cette bande de période, significatif à 90 %. Des

calculs de déphasage par spectres croisés et par corrélations croisées après filtrage passe bande, semblent indiquer que, le long des côtes nord du Golfe de Guinée, cette onde serait stationnaire. L'existence de pics d'énergie autour de la même bande de fréquence dans la pression atmosphérique et le vent mesuré au sol, suggère que cette onde côtière puisse être forcée par l'atmosphère. Ce mode de génération semble confirmé par les tracés des spectres de courant de Houghton (1979) où l'on peut noter, sur le plateau continental, une décroissance du maximum d'énergie correspondant à l'approche du fond.

Les travaux de Madden et Julian (1971, 1972) prouvent qu'il existe une onde atmosphérique de même période sur au moins le Pacifique et l'Océan Indien. Cette oscillation serait le résultat d'une circulation cellulaire à grande échelle se propageant vers l'est dans le plan équatorial. Elle pourrait exciter une onde équatoriale de Kelvin dans l'océan (Philander, 1977) mais nous verrons dans la section suivante qu'il ne semble pas exister d'onde équatoriale dans cette gamme de période. Des études complémentaires seraient nécessaires pour comprendre la liaison entre l'onde atmosphérique et l'onde côtière que nous avons mise en évidence.

Pour clore cette discussion sur les ondes côtières, il nous faut citer les travaux de Portolano (1981) sur toutes les stations côtières du Sénégal, bien que cela concerne une zone un peu en dehors de notre centre d'intérêt. Il trouve que les températures de surface de cette région sont sollicitées par les déplacements basse fréquence à grande échelle de la zone intertropicale de convergence (ITCZ) et par les variations moyenne fréquence de l'intensité et de la direction du vent local.

3. Ondes océaniques

Mes études moyenne fréquence portant essentiellement sur les mesures effectuées aux stations côtières, je n'ai pas été amené à m'intéresser directement aux ondes océaniques de l'Atlantique Equatorial. Cependant, il m'est apparu nécessaire de résumer les principales découvertes dans ce domaine. Dans la plupart des cas, elles n'ont été possibles que grâce à la mise en place de mouillages de longue durée et GATE a été le premier exemple d'une expérience où des mouillages dans l'Atlantique Equatorial ont pu être

maintenus pendant trois mois. Ces travaux et ceux qui ont suivi, ont montré la présence de mouvements énergétiques dans les bandes de périodes allant de 3 à 5 jours, 9-10 jours, 14-18 jours et de l'ordre du mois.

a) 3 à 5 jours de période

Nous avons vu qu'il existait des oscillations de l'ITCZ de 3 à 6 jours de période. Elles pourraient générer une réponse barotrope par le forcing de pression ou une réponse barocline par le forcing du vent (Beer, 1978 b). Les mesures de GATE ont permis de trouver une telle oscillation qui serait cohérente d'un point de vue dynamique avec une onde équatoriale d'inertie-gravité. Cette onde semblerait tirer son énergie du courant moyen (Weisberg *et al.*, 1980). Si des ondes similaires paraissent correspondre à un mode résonnant dans le Pacifique (Wunsch et Gill, 1976) il ne semble pas que cela soit le cas dans l'Atlantique (Philander et Duing, 1980). Des études de déplacement de la thermocline, à partir de trois écho-sondeurs inversés, ancrés près de l'équateur dans la partie ouest du bassin, donnent un maximum d'énergie commun autour de 3,75 jours de période. Une comparaison avec le diagramme de dispersion autorise à rejeter le cas d'une onde libre. Par contre, une analyse de cohérence avec le vent, déduit de ces écho-sondeurs inversés, montre que cette oscillation pourrait être une onde d'inertie-gravité forcée par l'atmosphère dans cette partie ouest de l'océan (Garzoli et Katz, 1981). Des mesures similaires à 4°W suggèrent que cette onde piégée par l'équateur pourrait être libre dans la partie est (Miller, 1981).

b) 9 à 10 jours de période

Par des mesures courantométriques effectuées à 26 et 28°W à proximité de l'équateur, Weisberg *et al.* (1980) ont trouvé une oscillation à 9-10 jours de période. Elle se propagerait vers l'ouest et vers le haut, ce qui implique une énergie descendante. Du point de vue dynamique, elle peut correspondre au deuxième mode méridien d'une onde d'inertie-gravité, mais Philander (1978 a) estime qu'il s'agit plutôt d'une onde mixte de Rossby-gravité. Cette onde pourrait être forcée par l'atmosphère et Bubnov *et al.* (1980) la retrouvent en sub-surface dans la plupart des niveaux de mesures

de deux mouillages à 10°W. Dans la couche de surface elle est masquée par les méandres du Sous Courant Equatorial.

c) 14 à 18 jours de période

Neumann et William (1965), à l'aide de drogues-parachutes, ont été les premiers à noter la présence de méandres à l'équateur. Rinkel (1969) par des mesures répétées à l'équateur vers 8°W trouve des oscillations du Sous Courant Equatorial avec une période d'environ 14 jours. Plus récemment avec Le Floch (1972), nous avons observé que dans le Golfe de Guinée, le maximum de salinité associé à ce sous courant se déplace de façon régulière de 40 milles de part et d'autre du parallèle 0°15'S, avec une période approximative de 16 jours.

Les mesures faites à partir de bateaux, mouillages et satellites ont apporté un maximum d'informations sur ces méandres entre 0° et 30°W (Duing *et al.*, 1975). Ils oscillent à la période moyenne de 16 jours, à ± 1 degré de l'équateur et intéressent surtout les deux cents premiers mètres en se propageant vers le haut avec une célérité approximative de 50 m par jour. Ils se propagent aussi horizontalement vers l'ouest avec une vitesse de phase moyenne de 1,35 m/s, ce qui donne une longueur d'onde d'environ 1850 km et se traduit au niveau des courants par une assymétrie de la composante zonale (Duing et Hallock, 1980).

Monin (1972, cité par Bubnov *et al.*, 1980) a proposé un modèle inertiel des méandres du Sous Courant Equatorial qui coïnciderait en période avec celle observée. Des mesures directes de vents et par dérive des nuages observés par satellite mettent en évidence une fluctuation des alizés autour de 15 jours de période qui se propagerait vers l'ouest avec une longueur d'onde d'environ 4000 km (Krishnamurti et Krishnamurti, 1980). L'atmosphère pourrait ainsi forcer ces méandres océaniques sous forme d'une onde mixte de Rossby-gravité. Mais un problème demeure, dû à la différence de longueur d'onde entre ces ondes océaniques et atmosphériques. Hallock (1980) à partir d'un modèle barocline trouve que la réponse dominante à un vent fluctuant méridien est une onde de Rossby-gravité dont les caractéristiques ressemblent à celle de l'onde de 14-18 jours de période observée. Finalement,

Philander et Duing (1980 a) suggèrent que ces méandres, bien qu'assez peu instables, puissent croître rapidement sous l'action d'un forcing important dont les échelles sont comparables.

d) 30-32 jours de période

A l'aide des mouillages de surface du Passat à 10°W et du Trident à 26° et 28°W, Weisberg (1980) note que les méandres à 16 jours de période, dominants dans les couches de surface, se mélangent avec une fluctuation à 32 jours de période. Cette dernière apparaît nettement au-dessous du Sous Courant Equatorial. Durant la même opération GATE, Brown (1980) trouve une oscillation similaire dans les températures de surface mesurées par satellite vers 3°N, là où le gradient thermique horizontal, lié aux courants zonaux, est maximum. Des mesures de sub-surface de plus longue durée dans le Golfe de Guinée, retrouvent cette oscillation dans la composante méridienne des courants et permettent de bien définir ses caractéristiques (Weisberg *et al.*, 1980). Sa période moyenne est de 31 jours et elle se propage vers l'ouest et vers le haut avec des longueurs d'onde de 1200 km et 100 m. Le flux d'énergie associé se propage vers l'est et vers le bas avec une vitesse de groupe de 16 cm/s et de 0,014 cm/s respectivement. Cette onde mixte de Rossby-gravité, modulée par les variations saisonnières, est piégée à l'équateur selon une décroissance exponentielle de 210 km.

Cette onde semble formée en surface par une instabilité entre le courant Sud Equatorial et le Contre Courant Equatorial Nord (Philander, 1978 b) pour rayonner vers l'est et en profondeur, ce qui justifierait son importance dans les couches profondes du Golfe de Guinée où elle explique les deux tiers de la variance de la composante méridienne (Weisberg *et al.*, 1979).

Toutes ces études prouvent l'existence et l'importance d'ondes piégées à l'équateur et à la côte dans l'Atlantique Equatorial. Ces ondes sont très souvent énergétiques et semblent avoir de l'importance au niveau des courants moyens. Un calcul d'énergie cinétique du mouvement moyen, par Crawford et Osbron (1980) montre que l'énergie apportée par le vent est en partie perdue par la turbulence et en partie sert à créer le gradient zonal

de pression. Le taux d'énergie apportée aux oscillations et méandres est significatif mais ne peut être estimé avec précision. Les changements importants du gradient zonal de pression, ainsi généré par le vent, sont les éléments dominants des variations saisonnières de l'Atlantique Equatorial (Katz *et al.*, 1977 ; Merle, 1980), variations que nous allons maintenant étudier.

III. VARIATIONS BASSE FREQUENCE : LA REPONSE DE L'ACTION ELOIGNEE DU VENT DANS LE GOLFE DE GUINEE

1. Présentation de l'upwelling du Golfe de Guinée

De par la présence des Centres de Recherches Océanographiques (ORSTOM) de la République du Congo, de la Côte d'Ivoire et du Sénégal et du Fishery Research Unit du Ghana, nous avons maintenant une assez bonne connaissance des variations saisonnières du Golfe de Guinée. Quatre saisons marines ont été ainsi mises en évidence dans les couches superficielles (Berrit, 1958 ; Morlière, 1970) : une grande saison chaude de février à mai, une grande saison froide de juin à début octobre, une petite saison chaude de novembre à mi-décembre et finalement une petite saison froide de mi-décembre à janvier. La décomposition en série de Fourier de ce cycle saisonnier (Merle et Le Floch, 1978) et l'analyse spectrale de plus longues séries chronologiques (Picaut *et al.*, 1978) montrent que l'alternance de ces saisons marines peut s'interpréter, pour une bonne part, comme la superposition de deux ondes annuelle et semi-annuelle. Les travaux de White (1977), Meyers (1979 a-b) et Lukas (1981) dans l'océan Pacifique et de Luyten et Roemmich (1982) dans l'Océan Indien, penchent pour une réalité physique des ondes annuelles et semi-annuelles dans les océans tropicaux. Tout simplement ces deux ondes pourraient être dues à l'influence climatique des deux hémisphères. Mais il ne faut pas écarter le fait que ces deux ondes puissent être le résultat d'un artefact de la décomposition mathématique de Fourier d'un signal saisonnier irrégulier.

La grande saison froide, qui domine ce cycle saisonnier, est caractérisée par l'arrivée d'un upwelling le long de l'équateur et des côtes nord et sud du Golfe de Guinée. Cet upwelling est relié aux déplacements de

la thermocline (Morlière et Rébert, 1972 ; Houghton, 1976 ; Merle, 1980 b), mais n'a pu être expliqué valablement par l'effet local du vent (Berrit, 1976 ; Houghton, 1976 ; Bakun, 1978), le rayonnement solaire (Merle, 1980 a), l'advection par les courants (Citeau *et al.*, 1980 ; Houghton, 1981) et l'accroissement du mélange vertical à l'équateur (Voituriez et Herbland, 1979 ; Voituriez *et al.*, 1982). Le long de la côte nord du Golfe de Guinée, une partie de cet upwelling pourrait être induite par l'accroissement du Courant de Guinée, directement par ajustement géostrophique relevant la thermocline (Ingham, 1970 ; Philander, 1979 b) ou indirectement par un effet dynamique sur le Cap des Trois Pointes et le Cap des Palmes au Ghana et Côte d'Ivoire (Marchal et Picaut, 1977). Pour une revue de ces divers mécanismes, voir Picaut (1983*).

Le Golfe de Guinée est caractérisé par une thermocline toujours très proche de la surface, au contraire de la partie ouest de l'Atlantique Equatorial. Cette pente zonale de la thermocline dans toute la bande équatoriale de l'Atlantique est soumise à des variations saisonnières qui se traduisent par le basculement de cette pente autour d'une zone de pivotement située vers les 25°-30°W (Merle, 1980 a). Katz *et al.* (1977) et Lass *et al.* (1983) ont relié les variations de la pente dynamique correspondante, à l'ouest du Golfe de Guinée, avec les variations saisonnières de la tension zonale des vents dans la même région. Il est donc possible que le cycle saisonnier du Golfe de Guinée puisse être en bonne partie le résultat d'un ajustement à l'échelle du bassin équatorial.

2. La théorie de l'action éloignée du vent

Durant le FINE Workshop (FGGE-INDEX-NORPAX-Equatorial Workshop), qui se tenait à la Scripps Institution of Oceanography en Californie du 27 juin au 12 août 1977, le petit groupe de français dont je faisais partie a présenté aux théoriciens américains le problème de l'upwelling du Golfe de Guinée. Des discussions, basées sur les données que nous avions apportées, les toutes nouvelles théories équatoriales (Moore et Philander, 1978) et une récente explication théorique d'El Niño (Wyrtki, 1975 ; Mc Creary, 1976 ; Hulburt *et al.*, 1976), ont permis de suggérer que cet upwelling pouvait être induit par un accroissement du vent zonal dans la partie ouest de l'Atlanti-

que Equatorial (Moore *et al.*, 1978*).

Le contexte théorique de cette hypothèse a été illustré par deux modèles à gravité réduite dans lesquels les vents d'est limités à la partie ouest du bassin se mettent à souffler soudainement (O'Brien *et al.*, 1978 ; Adamec et O'Brien, 1978). Une accumulation d'eaux se produit le long des côtes du Brésil, créant un gradient zonal de pression qui vient à équilibrer la tension du vent, en accord avec les travaux de Katz *et al.* (1977) et Lass *et al.* (1983). En amont de la zone d'action du vent, un upwelling équatorial se produit et se propage vers l'est, le long du guide d'ondes équatoriales, sous la forme d'une onde équatoriale de Kelvin. A l'arrivée sur les côtes africaines, cette onde se réfléchit sous la forme de paquets d'ondes équatoriales de Rossby, symétriques par rapport à l'équateur et se propageant vers l'ouest et de deux ondes de Kelvin côtières se propageant vers le nord et vers le sud. Tout cet ensemble d'ondes permet ainsi au signal d'upwelling, généré dans la partie centrale de l'Atlantique Equatorial, de rayonner dans tout le Golfe de Guinée. Ce schéma théorique, basé à l'époque sur peu de faits physiques, nous a servi de guide pour la collecte et le traitement de données en vue de confirmer ou d'infirmer cette nouvelle hypothèse.

3. Propagation de l'upwelling saisonnier

Au cours de mon deuxième séjour au Centre de Recherches Océanographiques de Côte d'Ivoire, d'octobre 1978 à août 1980, j'ai assuré la maintenance des nouvelles stations de prélèvements journaliers de température de surface que J.M. Verstraete avait installées en mai 1977. En tout, six nouvelles stations côtières qui venaient s'ajouter aux neuf autres du Bénin, Togo et Ghana. Et fin 1979, nous disposions de près de trois années de mesures systématiques sur plus de 1200 km de la côte nord du Golfe de Guinée. Il a été vu que le cycle saisonnier décrit par ces séries chronologiques est fortement parasité par tout un ensemble d'oscillations à plus haute fréquence dont certaines peuvent se propager. L'utilisation d'un filtre passe-bas a permis d'éliminer toutes les oscillations de périodes égales ou inférieures à 45 jours. Une analyse de corrélation avec décalage (Figure 7) centré sur la grande saison froide m'a permis de mettre en évidence la propagation de l'upwelling de l'été boréal le long des côtes du Ghana et de la Côte d'Ivoire

(Picaut, 1983*). Une analyse similaire mais limitée au phénomène de la petite saison froide montre que l'upwelling de l'hiver boréal se propage de la même manière (Roy, 1981).

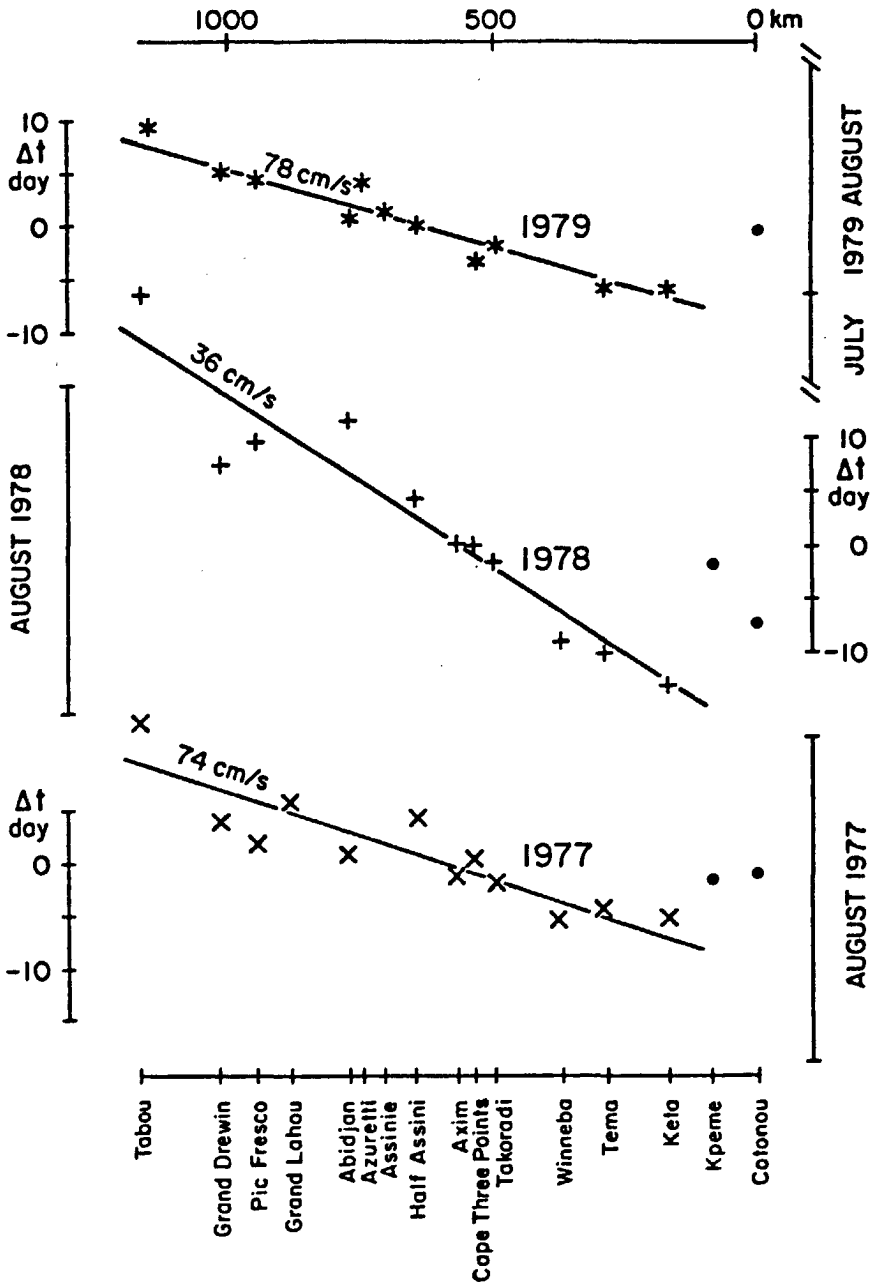

Figure 7 : Propagation de l'upwelling saisonnier, le long des côtes nord du Golfe de Guinée, à partir des données des stations côtières journalières en 1977, 1978 et 1979 (d'après Picaut, 1983).

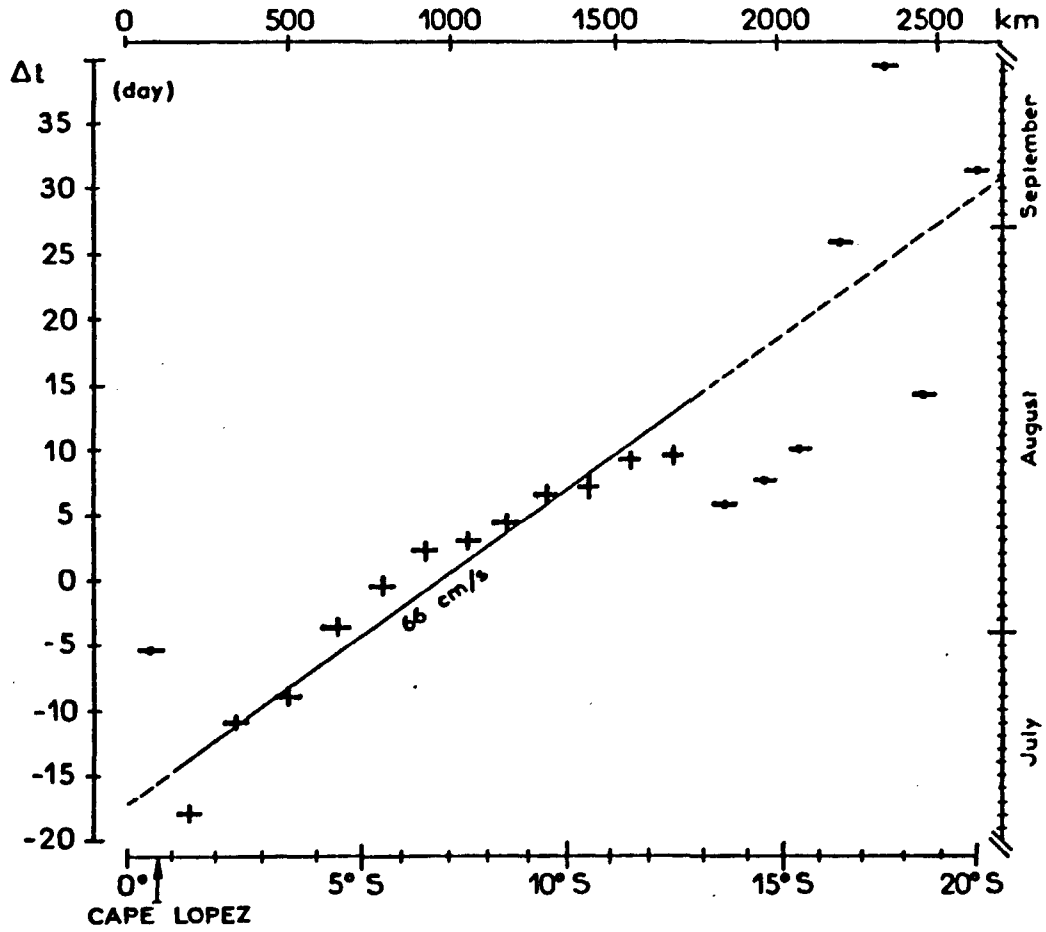

Figure 8 : Propagation de l'upwelling saisonnier le long des côtes sud du Golfe de Guinée à partir des données de température de navires marchands moyennées par mois et par carrés de 1° (d'après Picaut, 1983).

Mis à part Pointe Noire, il n'existe plus de stations côtières le long de la côte sud. Grâce aux fichiers prétraités, de données historiques collectées par les navires marchands, aimablement fournis par S. Hastenrath, W. Wooster et A. Bakun, j'ai pu montrer que des moyennes mensuelles climatologiques de température de surface par carré de 1°, permettaient de retrouver cette propagation le long des côtes du Ghana et de Côte d'Ivoire. L'utilisation de ces données historiques sur une année type devant la côte sud du Golfe de Guinée a permis de découvrir une propagation du signal du grand upwelling de l'équateur jusqu'à au moins 13°S (Figure 8). Par contre, il n'a pas été possible de retrouver une telle propagation côtière de l'équateur jusqu'à la frontière du Ghana. Le signal d'upwelling n'apparaît probablement

pas nettement dans les températures de surface du coin nord-est du Golfe de Guinée qui est caractérisé par une thermocline relativement profonde et une accumulation d'eaux dessalées (Berrit, 1973). Une analyse de corrélation a permis cependant de noter un décalage de 28 jours entre les passages du signal d'upwelling côtier à l'équateur et à la frontière du Ghana. Ce déphasage est le temps nécessaire pour une onde de 0,6 m/s de célérité pour cheminer tout le long du coin nord-est du Golfe de Guinée. Cette vitesse de phase est du même ordre de grandeur que celles observées sur les figures 7 et 8. Il est donc possible d'imaginer que le signal de l'upwelling équatorial se partage entre deux signaux côtiers se propageant le long des côtes nord et sud du Golfe de Guinée. Finalement, il n'a pas été possible de trouver une propagation nette le long de l'équateur (Picaut, 1983*). Cela peut être dû aux difficultés pour les températures de surface de rendre compte du signal d'upwelling et en particulier sur une année type, mais aussi au fait que le long de l'équateur il peut y avoir interférence entre les ondes équatoriales de Kelvin se propageant vers l'est et de Rossby se propageant vers l'ouest (Cane et Sarachick, 1981).

Entre 1957 et 1964, 217 stations hydrologiques ont été régulièrement effectuées par l'ORSTOM sur un site à 38 km au sud d'Abidjan sur le talus continental. Une analyse similaire aux précédentes m'a permis de mettre en évidence la propagation verticale du signal d'upwelling (Picaut, 1983*). Il se produirait à 300 m un mois et demi avant la surface (Figure 9). En aucun cas, la théorie classique d'Ekman ne pourrait expliquer une telle profondeur et encore moins ce déphasage progressif jusqu'à la surface. Nous verrons que la superposition d'ondes forcées au large du Golfe de Guinée peut être à l'origine d'un tel phénomène (Mc Creary, Picaut et Moore, 1984*).

4. Corrélations locale et éloignée entre la tension du vent et la température de surface

Cette mise en évidence de propagation de l'upwelling saisonnier nous ayant incité à croire en la théorie de Moore *et al.* (1978*), J. Servain, J. Merle et moi-même avons décidé d'analyser simultanément les tensions de vent et leur réponse possible au niveau de la température de surface (Servain *et al.*, 1982 a*-b). Ce travail a été facilité par S. Hastenrath qui a mis à

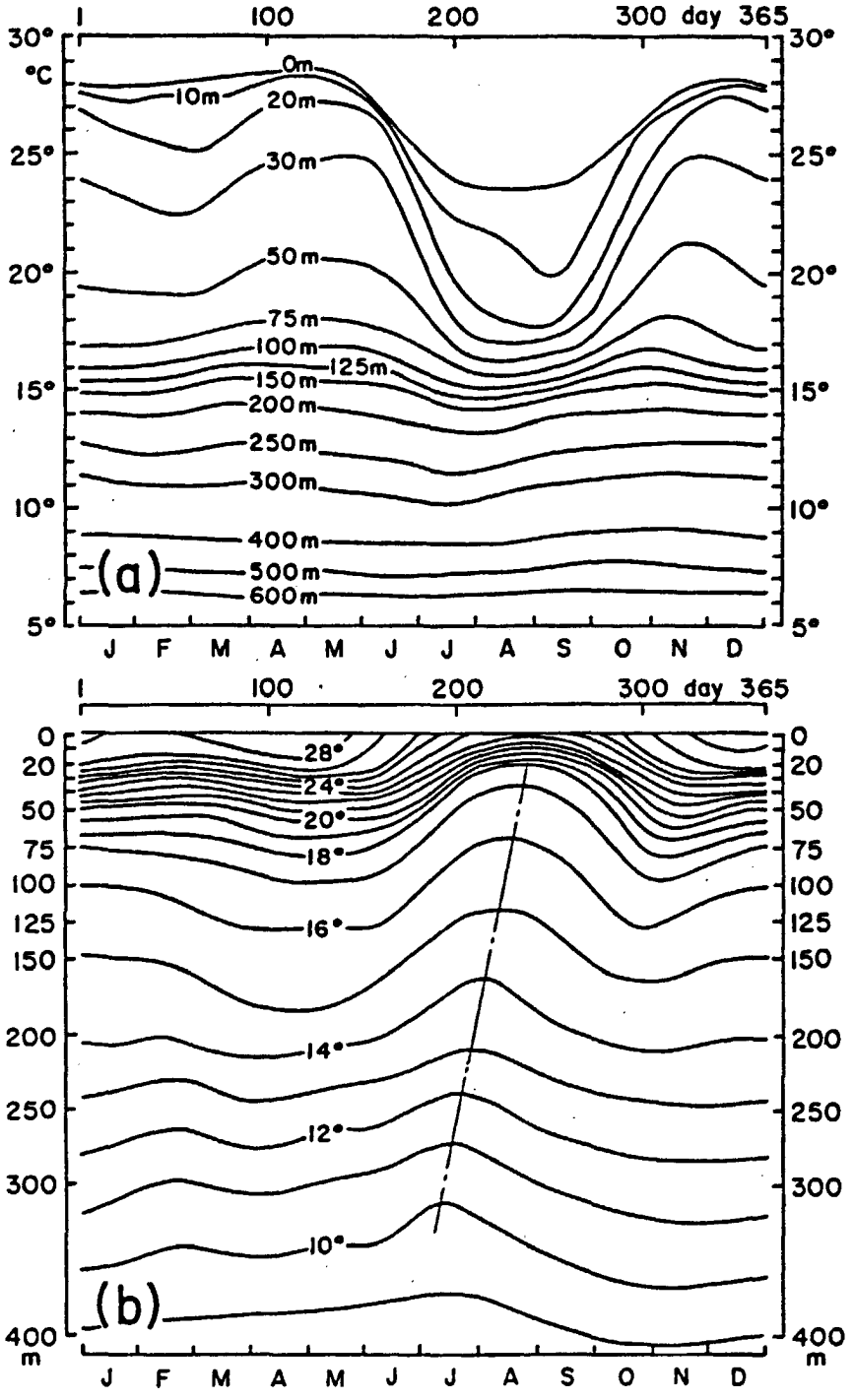

Figure 9 : a) Cycle saisonnier de température reconstitué aux profondeurs standards à partir des données de la station hydrologique au sud d'Abidjan.

b) Cycle saisonnier des profondeurs d'isothermes à partir des données de la Figure 9 a.

(d'après Picaut, 1983).

la disposition de J. Merle un fichier des vents et des températures de surface collectés par les navires marchands, moyenné par mois et par carré de 5° de côté sur toute la période 1911-1972.

Une partie des études précédentes a été effectuée sur une année moyenne, ce qui conduit à lisser considérablement les phénomènes propres à des années particulières. De plus, sur une année type, l'événement dominant, tant dans les vents que les températures de surface, est à période annuelle. Ce fait rend donc caduque toute tentative de corrélation entre des moyennes climatiques de températures de surface et de vents. En retirant le cycle saisonnier moyen des deux jeux de données pluri-annuelles vent-température de surface, une corrélation significative entre les données non-saisonnières résultantes doit être un indicateur beaucoup plus évident de processus dynamiques réels. Nous avons d'abord montré que les anomalies thermiques mensuelles de surface dans le Golfe de Guinée sont spatialement cohérentes et qu'elles diffèrent sensiblement des régions extérieures. Puis nous avons mis en évidence la très bonne corrélation existant entre les anomalies mensuelles de la tension du vent zonal dans la partie ouest de l'Atlantique Equatorial et les anomalies mensuelles de la température de surface dans le Golfe de Guinée, et ce avec une avance d'environ un mois (Figure 10). Ce décalage pourrait correspondre à une propagation d'une onde équatoriale de Kelvin de la zone d'action du vent au Golfe de Guinée, à la vitesse approximative de 1 m/s. Par opposition, les corrélations locales entre les anomalies mensuelles de tension du vent zonal et méridien et les anomalies de température de surface dans le Golfe de Guinée, sont très faibles (Figure 10).

Ces derniers résultats sont importants car ils font intervenir directement le moteur (vent) et sa réponse océanique éloignée (température de surface) et apportent ainsi un argument positif supplémentaire à la théorie de Moore *et al.* (1978*). Mais ces analyses de corrélation n'impliquent pas nécessairement une relation directe de cause à effet. Une telle relation rationnelle ne pourra apparaître qu'à travers une étude détaillée de processus physiques par une confrontation judicieuse modèles - observations. Les modèles numériques simplifiés de O'Brien *et al.* (1978) et Adamec et O'Brien (1978) ont été surtout construits pour illustrer l'idée théorique de Moore *et al.* (1978*) et ne prétendaient pas détailler les mécanismes de

l'océan réel. D'autres modèles simplifiés ont été élaborés pour illustrer d'autres mécanismes possibles ; citons ceux de Philander et Pacanoswski (1981 b) soumis à un vent régulier de secteur sud et de Cane et Sarachick (1981) forcé sur tout le bassin équatorial par des vents zonaux périodiques. Mais dans notre cas, la nécessité d'arriver à un certain degré de simulation nous a conduit à mettre en oeuvre des modèles un peu plus réalistes.

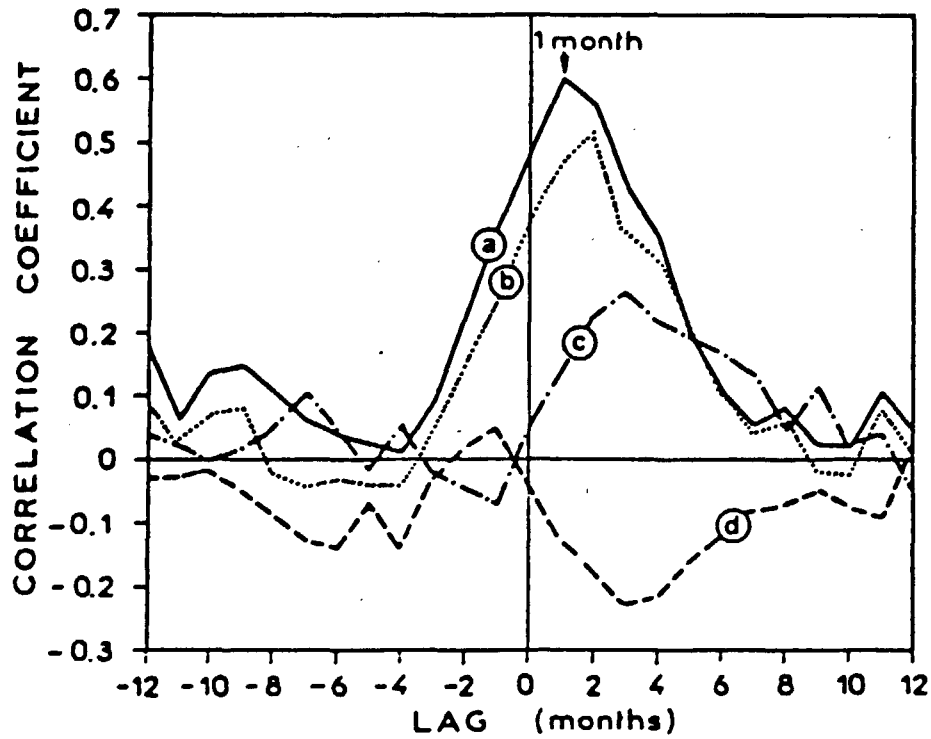

Figure 10 : Corrélation avec décalage. Courbe a : anomalies de tension du vent zonal dans l'ouest de l'Atlantique Equatorial avec les anomalies de température de surface dans la partie ouest du Golfe de Guinée. Courbe b : anomalies de tension du vent zonal dans l'ouest de l'Atlantique Equatorial avec les anomalies de température de surface dans la partie nord du Golfe de Guinée. Courbe c : anomalies de tension du vent zonal dans la partie ouest du Golfe de Guinée avec les anomalies de température de surface dans la même zone. Courbe d : anomalies de tension du vent méridien dans la partie ouest du Golfe de Guinée avec les anomalies de température de surface dans la même zone. (d'après Servain, Picaut et Merle, 1982 a).

Dans l'introduction, il a été soulevé le danger des modèles numériques trop sophistiqués aussi, nous avons préféré procéder en deux étapes. Dans un premier modèle (Busalacchi et Picaut, 1983*), on sacrifie la résolution verticale mais on injecte le vent saisonnier observé sur une année moyenne dans un bassin aux côtes réalistes. Dans un deuxième modèle (Mc Creary, Picaut et Moore, 1984*), on simplifie fortement les vents et les côtes mais on somme les solutions sur les modes verticaux, ce qui permet d'avoir une très grande résolution verticale.

5. Modèle à gravité réduite forcé par les vents saisonniers moyens (Busalacchi et Picaut, 1983*)

Ce modèle linéaire est aussi appelé modèle à mode unique ou modèle à une couche et demi. En effet, il ne comporte que deux couches, la deuxième est au repos et le vent agit en déplaçant horizontalement la première couche et verticalement la pycnocline séparant les deux couches. Ce modèle s'étend sur une bonne partie de l'Atlantique Tropical (Figure 11) et est forcé par les vents issus de l'atlas d'Hastenrath et Lamb (1977), moyenne par carré de 1° et par mois de 60 années d'observations à partir de navires marchands.

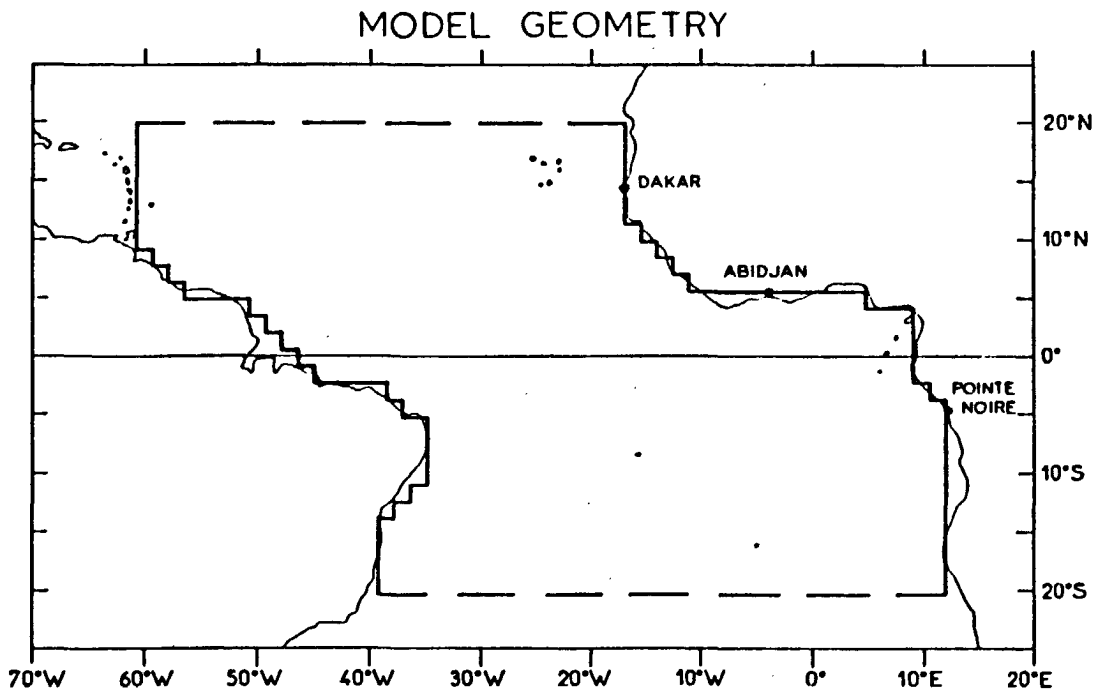

Figure 11 : Comparaison de la géométrie du modèle à mode unique avec le bassin Atlantique Tropical. Les frontières au nord et au sud sont des frontières ouvertes. Ce modèle est forcé par les vents saisonniers moyens déduits de 60 années d'observations par les navires marchands (d'après Busalacchi et Picaut, 1983).

D'après Schopf et Harrison (1983) une perturbation du champ de hauteurs dynamiques répond d'une manière linéaire aux premiers modes baroclines du système, au contraire de la thermocline qui est plus sensible aux modes de rang élevé, mais aussi aux termes non-linéaires. Les résultats d'autres modèles (Philander et Pacanoswski, 1981 b ; Mc Creary, Picaut et Moore, 1983*), nous ayant incités à utiliser la gravité réduite du deuxième mode barocline calculée à partir d'observations dans l'Atlantique Equatorial, il a été préférable de comparer les résultats de ce modèle avec les hauteurs dynamiques sur une année moyenne observées par Merle et Arnault (1983). Dans l'ensemble, cette comparaison est relativement bonne, principalement au niveau du champ moyen et de sa variation annuelle. En particulier, ce modèle reproduit correctement les variations saisonnières du Golfe de Guinée (Figure 12).

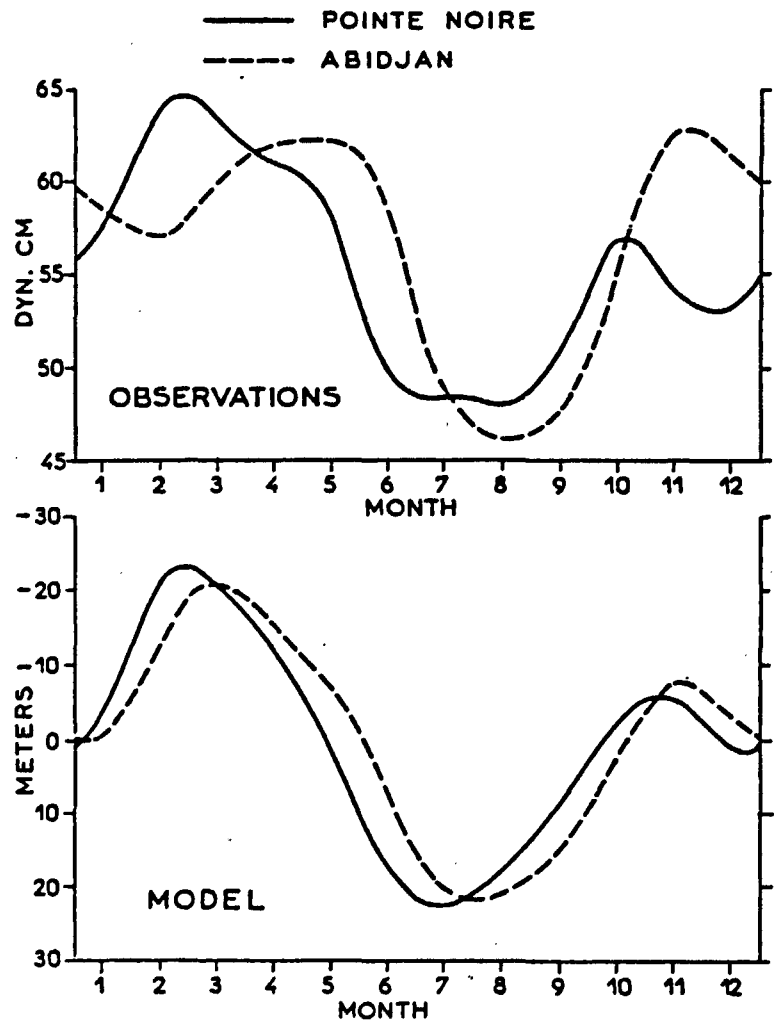

Figure 12 : Comparaison des hauteurs dynamiques 0/300 db et de la profondeur de la pycnocline du modèle au large de Pointe Noire et d'Abidjan. Les valeurs négatives correspondent à une pycnocline plus profonde que la moyenne annuelle (d'après Busalacchi et Picaut, 1983).

Il faut remarquer que ces résultats dépendent fort peu de la vitesse du deuxième mode choisi (dans la limite de ± 30 %) et pratiquement pas de la viscosité horizontale. De plus, ces calculs ont été faits antérieurement à ceux de Merle et Arnault (1983), il ne s'agit donc pas du tout d'un ajustement à des observations.

Cette assez bonne simulation nous a permis de retourner au développement des équations gouvernant le modèle et de relancer celui-ci avec des masques sur des portions géographiques du vent. Ainsi nous est apparu le détail des mécanismes pouvant reproduire les variations saisonnières dominantes de l'Atlantique Tropical. Ces variations sont caractérisées dans la partie nord-ouest du bassin par un basculement méridien autour d'une ligne correspondant à la position moyenne de l'ITCZ (vers 5°-10°N). Le long de l'équateur, il existe un pivotement de la pycnocline autour d'un point situé vers 25°-30°W (Merle, 1980 a). Cette réponse périodique forcée par le vent sur une année type, est une combinaison, dépendant de l'espace géographique, de réponses forcées localement, d'ondes de Kelvin, d'ondes de Rossby et de multiples ondes réfléchies par les côtes. Cette étude de mécanismes montre que dans le modèle le basculement, au nord de la position moyenne de l'ITCZ, est entièrement dû aux effets locaux du vent via le pompage d'Ekman. Au sud de cette ligne, le basculement en sens opposé est une combinaison d'effets locaux et d'effets éloignés apportés principalement par des ondes de Rossby. En accord avec les travaux de Katz *et al.* (1977) et Lass *et al.* (1983), nous trouvons que le gradient zonal de pression dans la partie ouest de la bande équatoriale est, durant toute l'année, en équilibre avec la tension zonale du vent local. Au contraire, dans la partie de bande équatoriale du Golfe de Guinée, il n'y a pas d'équilibre entre le gradient zonal de pression et la tension du vent local. Dans cette bande équatoriale, la réponse du modèle est en bonne partie la superposition d'ondes équatoriales de Kelvin excitées par le vent zonal équatorial à l'ouest du Golfe de Guinée et d'ondes de Rossby issues de leurs réflexions sur les côtes africaines. Cette réflexion induit aussi une réponse symétrique qui se propage le long des côtes nord et sud du Golfe de Guinée (Figure 13). Des études spécifiques, dans lesquelles le modèle était forcé par différentes portions géographiques du vent, ont permis de saisir le détail des variations saisonnières du Golfe de Guinée. Le vent zonal équatorial à l'ouest de 10°W est responsable de presque toute

la réponse annuelle du modèle dans le Golfe de Guinée. Le vent zonal annuel à l'est de 10°W a un effet secondaire le long de la côte nord, orientée est-ouest, qui en plus est annulé par l'action du vent méridien sur la côte orientée nord-sud. Ces résultats suggèrent que la grande saison froide peut être en bonne partie due à une action du vent en dehors du Golfe de Guinée. Dans cette même région, la moitié de l'oscillation semi-annuelle de la pycnocline du modèle est la réponse à des variations de la composante zonale du vent équatorial à l'ouest de 10°W. Le reste de cette oscillation provient des effets combinés des vents zonaux et méridiens dans le Golfe. Ainsi, il semblerait que la petite saison froide puisse être le résultat de la variabilité du vent autant à l'intérieur qu'à l'extérieur du Golfe de Guinée.

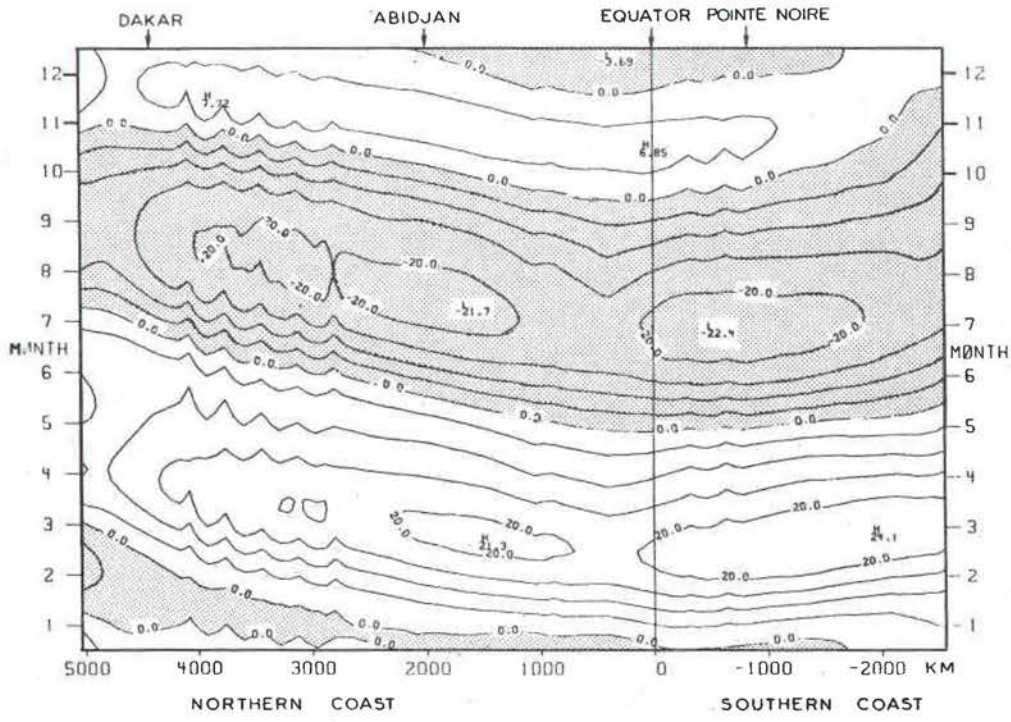

Figure 13 : Déplacement saisonnier de la pycnocline du modèle (en mètres), le long des côtes nord et sud du Golfe de Guinée. Les zones ombrées correspondent à une pycnocline moins profonde que la moyenne annuelle (d'après Busalacchi et Picaut, 1983).

6. Modèle à trois dimensions forcé par un vent annuel simplifié (Mc Creary, Picaut et Moore, 1984*)

Ce modèle est une adaptation au problème de l'action éloignée du vent dans l'Atlantique Equatorial, des modèles linéaires de Mc Creary (1981 a-b ; 1983 b) qui ont permis d'étudier la dynamique des sous-courants équatoriaux et côtiers et des jets profonds. Ils sont une extension du modèle non visqueux de Lightill (1969) par l'adjonction d'une diffusion de chaleur et de quantité de mouvement en profondeur, ce qui permet d'avoir des résultats réalistes. Le modèle considéré est forcé par la portion de vent oscillant à la fréquence annuelle, limitée à la zone équatoriale et à l'ouest de 20°W (Figure 14). Les solutions sont représentées comme le développement des modes baroclines du système, en fait la sommation sur les quinze premiers modes suffit. Le profil vertical moyen de densité utilisé a été déterminé à partir de données hydrologiques historiques de toute la bande équatoriale de l'océan Atlantique. On calcule la solution d'un mode particulier non pas par la méthode classique de résolution numérique par intégration dans le temps, mais en supposant, comme dans beaucoup de modèles de marée, une dépendance du temps de la forme $e^{-i\sigma t}$, σ étant la fréquence annuelle.

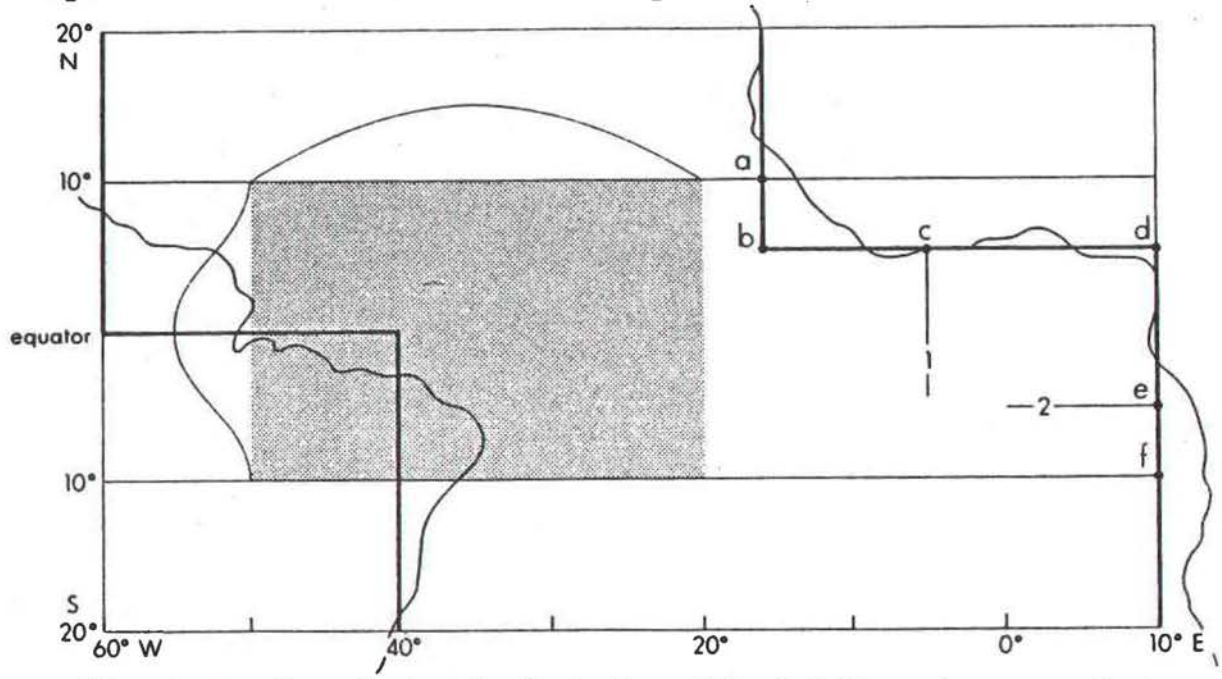

Figure 14 : Comparaison de la géométrie du modèle à 3 dimensions avec le bassin Atlantique Tropical. Les frontières au nord et au sud sont des frontières ouvertes. La région ombrée correspond à la zone d'action du vent et le trait fin autour schématise son profil en x, y. La tension du vent oscille à la fréquence annuelle et arrive à un maximum de 0,5 dyne/cm^2 au centre de cette zone (d'après Mc Creary, Picaut et Moore, 1984).

Du fait de l'absence de vent dans le Golfe de Guinée, la réponse dans cette région est le résultat du rayonnement d'un ensemble d'ondes équatoriales de Kelvin excitées par le vent à l'ouest. Ces ondes se superposent de façon cohérente de manière à former un faisceau étroit d'énergie qui se propage rapidement vers l'est et lentement vers le bas, selon la pente σ/N, N étant la fréquence de Väisälä au niveau considéré. Ce faisceau se réfléchit sur la côte africaine sous la forme d'un ensemble de faisceaux de Rossby qui, se propageant avec une pente plus importante que le faisceau de Kelvin, affecte la structure profonde du Golfe de Guinée. Les faisceaux d'énergie réfléchis les plus évidents correspondent au premier mode horizontal équatorial de Rossby et à un mode piégé le long de la côte nord, orientée est-ouest, très similaire à un faisceau d'ondes côtières de Kelvin. D'autres faisceaux de Rossby se superposent pour générer des jets côtiers le long des côtes méridionales (Figure 15). Cette figure représente la section verticale du champ de courant le long de la côte africaine de 5°S à 10°N. La continuité des courants et sous-courants côtiers sur toute cette section montre que ces courants sont bien causés par la réflexion d'un faisceau équatorial de Kelvin. Cette figure illustre aussi très bien la propagation verticale des courants selon une célérité comparable avec celle que j'ai observée au sud d'Abidjan. De même, il existe pratiquement dans toute cette section, une propagation horizontale des champs de courant et de densité, dirigée vers les pôles et avec des vitesses de phase généralement du même ordre de grandeur que celles observées.

Ce modèle met en évidence une différence importante observée entre les côtes du Golfe de Guinée. Le long de la côte orientée est-ouest, la présence d'un faisceau de Kelvin, côtier, fait que les structures de densité et de courants sont piégées à la côte. De par la présence de faisceaux de Rossby à la côte orientée nord-sud, ces mêmes structures sont étendues beaucoup plus au large. Finalement, on peut noter que ce modèle suggère qu'il puisse exister en sub-surface au large de Dakar, un faisceau d'énergie issue de la réflexion des ondes équatoriales excitées par le vent à l'ouest du Golfe de Guinée (Figure 15).

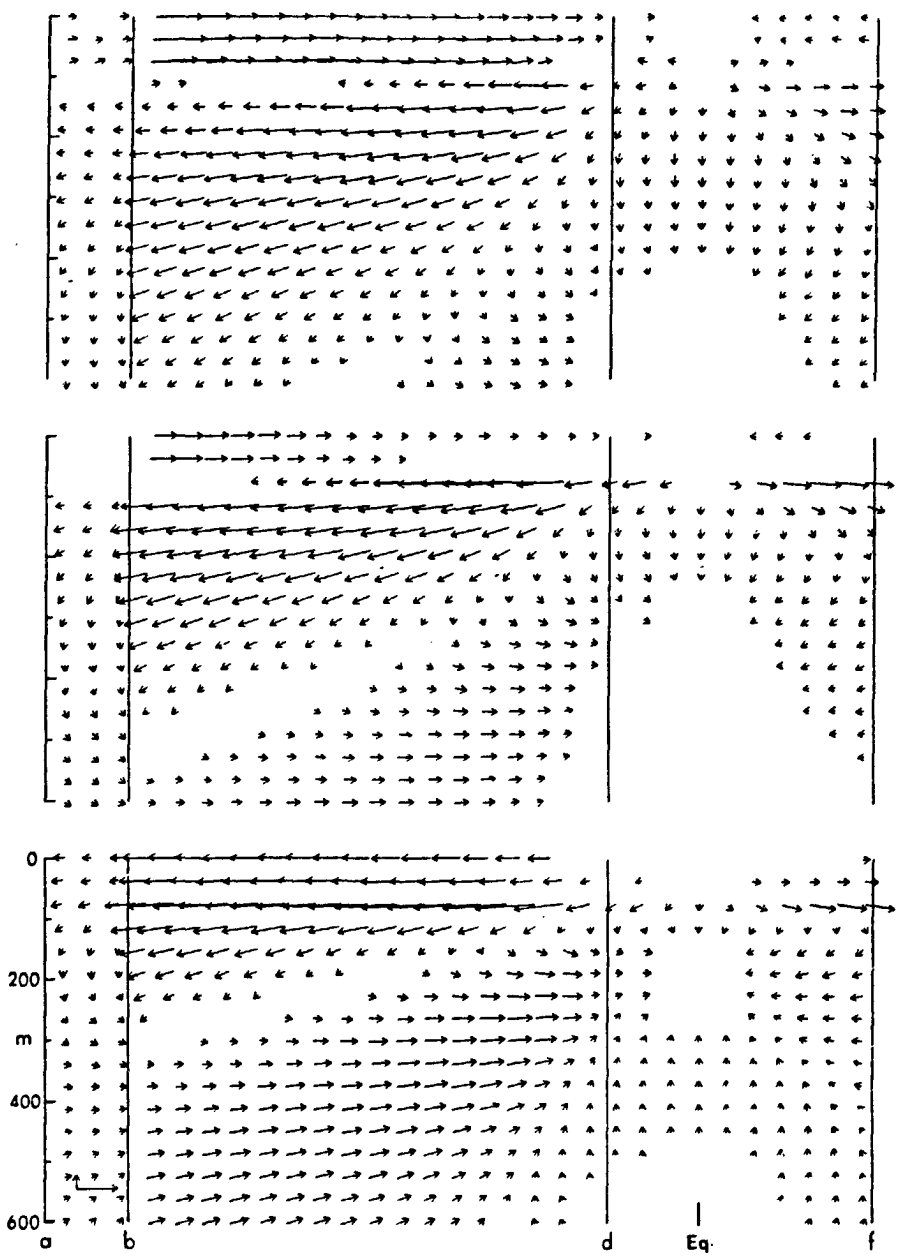

Figure 15 : Section verticale des courants le long des côtes nord et sud du Golfe de Guinée des points a-f de la figure 14 à t = 6,8 et 10 mois. Les échelles des courants situées dans la partie inférieure de la figure correspondent à 0,001 cm/s et 10 cm/s dans les directions verticale et horizontale (d'après Mc Creary, Picaut et Moore, 1984).

7. Discussion et conclusion

Nos observations suggèrent que l'upwelling saisonnier côtier du Golfe de Guinée se propage vers le nord et vers le sud à partir de l'équateur et verticalement tout au moins au sud d'Abidjan. Nous avons aussi trouvé une bonne corrélation entre les variations non saisonnières de la tension de vent zonal dans l'ouest de l'Atlantique Equatorial et les variations non saisonnières de la température de surface du Golfe de Guinée et ce, avec un décalage d'un mois, le temps pour une onde équatoriale de Kelvin de se déplacer à environ 1 m/s de la zone d'action du vent au Golfe de Guinée. Ces deux résultats d'observations sont les éléments dominants de la théorie de l'action éloignée du vent de Moore *et al.* (1978*), illustrée par les modèles de O'Brien *et al.* (1978) et Adamec et O'Brien (1978). Mais ces modèles sont tellement simplifiés qu'il est presque étonnant que nos observations concordent si bien. Aussi, nous allons conclure ce chapitre en discutant des résultats des récents modèles traitant de ce mécanisme.

Dans les modèles de O'Brien *et al.* (1978) et Adamec et O'Brien (1978), le vent zonal, limité à la partie ouest de l'Atlantique Equatorial, est lancé de façon impulsionnelle. Ce vent excite un front d'ondes équatoriales de Kelvin dont la propagation apparaît de façon très nette, de même que celles des ondes réfléchies de Rossby et de Kelvin côtières résultantes. Ainsi, la phase de la réponse dans le Golfe de Guinée est directement liée à l'instant de l'accroissement brutal du vent et à la célérité de toutes ces ondes. A l'opposé, Cane et Sarachik (1981) ont étudié la réponse linéaire d'un simple mode barocline à un vent périodique, indépendant de la coordonnée zonale, dans un bassin limité par deux simples côtes orientées nord-sud. Dans ce modèle, la réponse périodique est une superposition complexe d'ondes de Rossby, d'ondes équatoriales de Kelvin et d'ondes de Rossby issues de la réflexion des ondes de Kelvin à la frontière est. Il n'est donc pas possible de pouvoir suivre une onde équatoriale de Kelvin. De plus, à la fréquence annuelle, les ondes côtières de Kelvin ne peuvent exister qu'au-dessus de la latitude critique qui, à titre indicatif, est d'environ 50° pour le premier mode barocline et de 5° pour le dixième mode. Il n'y a donc plus de relation simple entre le forcing et sa réponse dans le Golfe de Guinée. Le modèle linéaire de Busalacchi et Picaut (1983*), similaire au précédent, mais utili-

sant des côtes et des vents réalistes, a une solution équatoriale beaucoup plus proche du forcing périodique que du forcing impulsionnel. Par contre, il permet de retrouver une propagation côtière vers les pôles dans le Golfe de Guinée (Fig. 13) et suggère que dans cette même région la réponse annuelle est principalement issue de l'action éloignée du vent. Cette propagation le long de la côte orientée nord-sud est probablement due à l'utilisation de viscosité horizontale et aux harmoniques de la fréquence annuelle dans la tension du vent.

Le modèle linéaire à trois dimensions de Mc Creary, Picaut et Moore (1984*), forcé par un vent annuel à l'ouest de 20°W, retrouve la propagation verticale observée au sud d'Abidjan. L'utilisation de nombreux modes baroclines autorise l'énergie à pénétrer lentement en profondeur. Ainsi, le faisceau équatorial de Kelvin et les faisceaux réfléchis de Rossby ne vont plus complètement interférer comme dans les modèles précédents, permettant ainsi de retrouver le piégeage équatorial et côtier et rendant possible la visualisation des ondes de Kelvin. Une autre explication, pour la présence d'ondes côtières et équatoriales de Kelvin dans un modèle à trois dimensions, est la disparition des ondes de Rossby dans les couches de surface par les termes non linéaires (Philander et Pacanoswski, 1981 a). De plus, ces auteurs trouvent que dès que l'on limite un vent de période proche de l'annuelle à la partie centrale du bassin, à l'est de cette zone les ondes de Kelvin deviennent apparentes et la réponse dans cette région, tout comme dans le modèle de Mc Creary, Picaut et Moore (1984*), est directement associée à cette onde se propageant vers l'est. Au contraire des modèles à mode unique, il ne semble donc pas que dans des modèles à trois dimensions il y ait de différences fondamentales entre une action éloignée d'un vent périodique et une action éloignée d'un vent impulsionnel.

Il faut noter de plus que l'utilisation de vents moyens sur une année type lisse considérablement les événements propres à chaque année. Les analyses de données de vent historiques par Servain *et al.* (1982 a*) et les mesures directes du vent sur le rocher Saint Paul près de l'équateur à 29°W par Garzoli *et al.* (1982) semblent montrer que l'accroissement des alizés à l'ouest du Golfe de Guinée est souvent du type impulsionnel. Un calcul interannuel similaire à celui de Busalacchi et O'Brien (1981) est en

cours de préparation pour comprendre les différences entre le cycle saisonnier moyen et le signal saisonnier d'années individuelles (Picaut *et al.*, 1983).

Cet ensemble de travaux a démontré qu'une partie importante des variations saisonnières dans le Golfe de Guinée était due à des effets du vent zonal à l'ouest du Golfe. Le premier modèle a surtout permis d'avoir des indications sur l'importance dans la réponse de la répartition spatiale et en fréquence des vents. Le deuxième modèle a détaillé le mécanisme de liaison entre le forcing éloigné et sa réponse dans le Golfe de Guinée. Ces deux modèles semblent donc complémentaires. On pourrait objecter que dans l'un des modèles l'énergie pénètre en profondeur, ce que ne permet pas l'autre. D'après Mc Creary, Picaut et Moore (1984*), le Golfe de Guinée, en subsurface, est principalement sollicité par le premier mode horizontal de faisceau d'énergie réfléchie de Rossby. Comme ce faisceau ne dépasse guère 300 m dans le Golfe de Guinée, la comparaison dans cette même région de la profondeur de la pycnocline du modèle de Busalacchi et Picaut (1983*) avec les hauteurs dynamiques 0/300 db, n'est pas du tout incompatible. Plus à l'ouest, la réponse semble principalement locale et les faisceaux de Rossby peuvent disparaître en profondeur ou être dissipés par les termes non linéaires.

Mais toute cette étude est bien évidemment trop simple pour prétendre expliquer tous les aspects des variations saisonnières dans le Golfe de Guinée. Par exemple, les changements importants du courant de Guinée entre 2° et 4°N sont mal expliqués dans nos deux modèles, d'après Philander (1979 b) et Anderson (1979), ils pourraient être dus à l'influence des vents méridiens du Golfe de Guinée. Rappelons que nos deux modèles ignorent l'advection, la topographie du fond, les effets thermohalins et thermodynamiques et qu'ils ne permettent pas de reproduire des variations de température de surface. Malheureusement, de par sa grande fréquence de mesures, c'est encore cette seule température de surface qui peut actuellement nous donner des informations précises sur les variations saisonnières et interannuelles des océans.

IV. CONCLUSION GENERALE

Nous venons de présenter les principaux résultats d'un travail qui apporte quelques informations sur les variations thermiques dans le Golfe de Guinée. Faute d'une étude fine, les marées internes au large d'Abidjan n'ont pu être que décrites et les tentatives de modélisation de Park (1979) ne permettent pas de conclure sur leurs modes de génération et de propagation. Par contre, l'oscillation à 14,7 jours de période, sollicitant au moins toute la zone côtière du nord du Golfe de Guinée, a été beaucoup plus étudiée. Si nous avons maintenant quelques idées précises sur sa structure interne et sa propagation, il n'en est pas de même de son mode de génération, on peut imaginer qu'elle puisse être forcée par une interaction non-linéaire entre les deux ondes de marée barotropes M_2 et S_2. Une autre oscillation aussi importante (1 à 2° d'amplitude en surface) a été mise en évidence le long des côtes du Golfe. Elle serait peut-être stationnaire et très probablement forcée par une oscillation atmosphérique à 40-50 jours de période. Plus au large, les méandres du Sous Courant Equatorial et les ondes profondes étudiées par Weisberg *et al.* (1979) montrent l'importance des oscillations moyenne fréquence dans l'ensemble du Golfe de Guinée.

Dans le domaine des variations saisonnières et interannuelles nous nous sommes surtout attaché à un mécanisme original faisant intervenir le vent zonal à l'ouest de notre zone d'intérêt. Au départ quelques vagues observations et des idées très théoriques ont autorisé à imaginer le processus dit de l'action éloignée du vent de Moore *et al.* (1978*). Le retour à des observations sur le terrain ou historiques, a permis de retrouver les éléments importants de cette théorie simplifiée : corrélation température de surface - vent à l'ouest, propagation côtière vers les pôles. Le détail de ce mécanisme d'action du vent à longue distance a pu être suivi grâce à la mise en oeuvre de deux modèles numériques élaborés dont les produits ont été comparés avec les observations. Cette étude, résultat d'une collaboration très étroite entre théoriciens et observateurs, a donc permis de comprendre une partie de la physique de ce processus responsable probablement de la moitié ou plus des variations saisonnières et interannuelles dans le Golfe de Guinée.

L'énergie importante associée aux ondes moyenne fréquence pose le problème de la génération de courants moyens par ces oscillations. A la côte elles peuvent induire de grandes variations dans les upwellings saisonniers (Houghton, 1976). Elles sont probablement à l'origine des déplacements importants des fronts thermiques, zones de très forte concentration en thons (Stretta, 1977). Des études détaillées de ces ondes moyenne fréquence doivent donc permettre de mieux comprendre la dynamique côtière et par la même de préciser les conditions limites de modèles océaniques sophistiqués.

Dans le domaine basse fréquence, nous avons déjà souligné la difficulté de mettre en évidence les ondes équatoriales correspondantes. Si la présence d'un plateau continental réaliste ne semble pas affecter la réflexion de ces ondes sur les frontières océaniques (Suginohara, 1981), le phénomène de réflexion sur le fond ne semble pas résolu. Il en est de même de la dissipation de ces ondes ce qui pose le problème crucial de la mémoire des océans équatoriaux. Un autre point important est de connaître le mécanisme de transfert d'énergie de l'atmosphère vers l'océan et de savoir combien de cette énergie va traverser la thermocline (Philander, 1978 a) pouvant ainsi générer des jets profonds (Mc Creary, 1983). Le reste de cette énergie va participer aux échanges entre les bords du bassin équatorial et le rôle des trois contre-courants équatoriaux dans ce transfert est fort mal connu. Enfin, la réaction de l'océan sur l'atmosphère, élément dominant semble-t-il de la climatologie est relativement peu étudiée et elle nécessite une meilleure collaboration entre météorologues et océanographes.

Des modèles numériques plus sophistiqués faisant intervenir les termes non-linéaires et de la thermodynamique devraient aider à résoudre certains de ces problèmes. Mais c'est par de nombreuses mesures bien spécifiques et surtout une coopération encore plus étroite entre théoriciens et observateurs que l'on pourra espérer avancer dans ces recherches. Dans l'Atlantique Tropical, les expériences SEQUAL (Seasonal Response of the Equatorial Atlantic) et FOCAL (Français Océan et Climat dans l'Atlantique Equatorial) devraient permettre de résoudre certains de ces aspects et si les buts sont centrés sur les variations saisonnières, des études moyenne fréquence pourront se développer grâce aux mouillages équatoriaux et aux écho-sondeurs inversés. Le Pacifique est particulièrement détaillé avec EPOCS (Equatorial

Pacific Ocean Climate Studies), PEQUOD (Pacific Equatorial Ocean Dynamics) et les constants efforts sur El Niño et l'Oscillation du Sud associée. Tous ces grands programmes vont se prolonger par l'expérience sur 5-10 années TOGA (Tropical Ocean Global Atmosphere).

Mais si des techniques hautement élaborées comme les satellites nous permettent d'avoir de bonnes indications sur les températures de surface et avant la fin de la décade sur les tensions de vent, il ne faudra pas avant longtemps négliger les mesures simples facilement dépouillables et interprétables. Et si l'image, le long des côtes africaines d'une bonne vingtaine de personnes munies de leur seau et de leur thermomètre, peut faire sourire, il n'est pas inutile de rappeler que ce modeste travail repose en grande partie sur ces mesures quotidiennes.

REFERENCES

Adamec, D. et J.J. O'Brien (1978) : The seasonal upwelling in the Gulf of Guinea due to remote forcing. J. Phys. Oceanogr., 8 (6), 1050-1060.

Anderson, D. (1979) : Low latitude seasonal adjustment in the Atlantic. (Manuscrit non publié).

Arnold, J.E. (1966) : Easterly wave activity over Africa in the Atlantic with a note on the Intertropical Convergence Zone during early July 1961. SMRP Research Paper. University of Chicago. 65, 24 pp.

Bakun, A. (1978) : Guinea current upwelling. Nature, 271. 147-150.

Beer, T. (1978a) : Non-divergent shelf waves on the Ghana continental shelf. Goephys. Astrophys. Fluid Dyn., 9, 219-227.

Beer, T. (1978b) : Tropical waves. Rev. Geophys. Space Phys., 16(4), 567-582.

Berrit, G.R. (1958) : Les saisons marines à Pointe Noire. Bull. Inf. C.O.E.C., 6, 335-360.

Berrit, G.R. (1973) : Recherches hydroclimatiques dans les régions côtières de l'Atlantique tropical oriental. Etat des connaissances et perspectives. Bull. Mus. Nat. Hist. Nat. Paris, 148, Ecologie Générale 4, 85-99.

Berrit, G.R. (1976) : Les eaux froides côtières du Gabon à l'Angola sont-elles dues à un upwelling d'Ekman ? Cah. ORSTOM, Sér. Océanogr., 14, 273-278.

Binet, D. (1982) : Relation between climate and Fishery in the Gulf of Guinea. Trop. Oc. At. News, 11, 1-2 (manuscrit non publié).

Bjerknes, J. (1966) : A possible response of the atmosphere hadley circulation to equatorial anomalies of ocean temperature. Tellus, 18, 820-829.

Bjerknes, J. (1969) : Atmospheric teleconnections from the equatorial Pacific. Mon. Wea. Rev., 97, 163-172.

Bubnov, V.A., V.M. Vasilenko et L.M. Krivelevich (1980) : The study of low-frequency variability of currents in the Tropical Atlantic. Deep Sea Rech. GATE suppl. II, 26, 199-216.

Busalacchi, A.J. (1982) : Wind driven variability of the tropical Pacific and Atlantic Oceans. Ph. D. Dissertation. The Florida State University, 138 pp.

Busalacchi, A.J. et J.J. O'Brien (1980) : The seasonal variability in a model of the Tropical Pacific. J. Phys. Oceanogr. 10, 1929-1951.

Busalacchi, A.J. et J.J. O'Brien (1981) : Interannual variability of the equatorial Pacific in the 1960's. J. Geophys. Res., 86, 10901-10907.

Busalacchi, A.J. et J. Picaut (1983) : Seasonal variation from a model of the tropical Atlantic. J. Phys. Oceanogr., 13, 1564-1588.

Brown, O.B. (1980) : Observation of long period sea surface temperature variability during GATE. Deep Sea Res., suppl. II, 26, 103-124.

Cane, M.A. (1979a) : The response of an equatorial ocean to simple wind stress patterns : I. Model Formulation and analytic results. J. Mar. Res., 37(2), 233-252.

Cane, M.A. (1979b) : The response of an equatorial ocean to simple wind stress patterns : II. Numerical results. J. Mar. Res., 37(2), 253-299.

Cane, M.A. et E.S. Sarachik (1981) : The response of a linear equatorial ocean to periodic forcing. J.Mar. Res., 39, 651-693.

Cavanié, A. (1969) : Sur la génèse et la propagation d'ondes internes dans un milieu à deux couches. Cah. Océanogr., 21(9).

Citeau, J., G.R. Berrit et L. Verseci (1980) : The upwelling in the Guinea Gulf as observed by Meteosat. Proceeding of a workshop on applications of existing satellite data to the study of the ocean surface energies. University of Wisconsin Press, 233-237.

Clarke, A.J. et D.S. Battisti (1983) : Identification of the fortnightly coastal wave in the Gulf of Guinea. J. Phys. Oceanogr., 13, 2192-2200.

Crawford, W.R. et T.R. Osbron (1980) : Energetics of the Atlantic equatorial undercurrent. Deep Sea Res. GATE suppl. II to vol. 26, 309-324.

Defant, A. (1950) : Reality and illusion in oceanographic surveys. J. Mar. Res., 9, 120-138.

Duĭng, W. (1978) : The Somali current : past and recent observations. FINE Workshop Proceedings, Nova University Press.

Duĭng, W., P. Hisard, E. Katz, J. Meincke, L. Miller, V. Moroshkin, G. Philander, A.A. Ribnikov, K. Voigt et R. Weisberg, (1975) : Meanders and long waves in the equatorial Atlantic. Nature, Vol 257, N° 5525, 280-184.

Duĭng, W. et Z. Hallock (1980) : Equatorial waves in the upper central Atlantic, Deep Sea Res., GATE suppl. II, 26, 161-178.

Ericksen, C.C. (1981) : Deep currents and their interpretation as equatorial waves in the western Pacific Ocean. J. Phys. Oceanogr., 11, 48-70.

Ericksen, C.C., M.B. Blumenthal, S.P. Hayes et P. Ripa (1983) : Wind-generated equatorial Kelvin waves observed across the Pacific ocean. J. Phys. Oceanogr., 13, 1622-1640.

Evans, R.N., D.R. Mc Lain et R.A. Bauet (1979) : Atlantic skipjack tuna : influences of the environment on their vulnarability to surface year. Southwest Fisheries Center, report no. LJ-79-38, 21 pp.

Fonteneau, A. et P. Cayré (1983) : Statistique de la pêcherie thonière FISM durant la période de 1969 à 1981. Rec. Doc. Scient. ICCAT, 18, 1, 72-82.

Garzoli , S. et E.J. Katz (1981) : Observations of inertia-gravity waves in the Atlantic from inverted echo sounders during FGGE, J. Phys. Oceanogr., 11, 1463-1473.

Garzoli , S., E.J. Katz, H.J. Panitz et P. Speth (1982) : In situ wind measurements in the equatorial Atlantic during 1979. Océanol. Acta., 5, 281-288.

Hallock, Z. (1980) : On wind-excited equatorially trapped waves in the presence of mean currents. Deep Sea Res., GATE suppl. II, 26, 261-284.

Hayes, S.P. et H.B. Milburn (1980) : On the vertical structure of velocity in the eastern equatorial Pacific. J. Phys. Oceanogr., 10, 633-635.

Hastenrath, S. (1976) : Variations in low-latitude circulation and extreme climatic events in the tropical Americas. J. Atm. Sci., 33, 202-215.

Hastenrath, S. et P. Lamb (1977) : Climatic atlas of the tropical Atlantic and eastern Pacific oceans. University of Wisconsin Press, 112 pp.

Henderschott, M.C. (1981) : Long waves and ocean tides. Evolution of Physical oceanography, MIT Press, Warren et Wunsch editeurs, 292-341.

Hickey, B. (1975) : The relationship between fluctuations in sea level, wind stress and sea surface temperature in the equatorial Pacific. J. Phys. Oceanogr., 5, 460-475.

Hickie, B.J. (1977) : The effects of coastal geometry on equatorial waves (Free modes of the Gulf of Guinea). (Manuscrit non publié).

Hisard, P. (1980) : Observation de réponses de type "El Niño" dans l'Atlantique tropical oriental Golfe de Guinée. Océan. Acta, 3, 69-78.

Hisard, P. (1983) : Deux précurseurs de l'étude du Golfe de Guinée au 19ème siècle : Charles Philippe de Kerhallet et John Young Buchanam. Océanogr. Tropic. 18, 95-101.

Hisard, P. and B. Piton (1981) : Interannual variability in the eastern tropical Atlantic during the last decades. In Recent Progress in Equatorial Oceanography. Nova University Press, 297-306.

Houghton, R.W. (1976) : Circulation and hydrographic structure over the Ghana continental shelf during the 1976 upwelling. J. Phys. Oceanogr., 6, 909-924.

Houghton, R.W. (1979) : Characteristics of the fortnightly shelf wave along the Ghana coast. J. Geophys. Res., 84, C10, 6355-6361.

Houghton, R.W. (1981) : Temperature variations in the Gulf of Guinea. Trop. Oc. Atm. News., 8, 1-3 (manuscrit non publié).

Houghton, R.W. et T. Beer (1976) : Wave propagation during the Ghana upwelling. J. Geophys. Res., vol 8, N° 24, 4423-4429.

Hookey, P. (1970) : Revenge of the Gods ; Weather, 25, 425-428.

Hulburt, H.E., J.C. Kindle and J.J. O'Brien (1976) : A numerical simulation of the onset fo El Niño. J. Phys. Oceanogr., 6, 621-631.

Ingham, M.C. (1970) : Coastal upwelling in the northwestern of Gulf of Guinea. Bull. Marine Sci., 20, 2-34.

Janke, J. (1920) : Strömungen und Oberflächentemperaturen im Golfe von Guinea. Archiv. der Deutschen Seewarte, 6, 1-68.

Kamykowski, D. (1974) : Possible interactions between phytoplancton and semi diurnal internal tides. J. Marine Res., 32, 67-89.

Katz, E.J. et collaborateurs (1977) : Zonal pressure gradient along the equatorial Atlantic. J. Marine Res., 35, 293-307.

Khanaichenko, N.K. (1974) : Le système des contre-courants équatoriaux dans l'océan. Editeurs : Guidrometeoizdat - Leningrad 1974. Traduction de P. Hisard et H. Rotchi. CRO-ORSTOM. Abidjan. 100 pp.

Knox, R.A. et D. Halpern (1982) : Long range Kelvin wave propagation of transport variations in Pacific Ocean equatorial currents. J. Mar. Res., 40 (Suppl.), 329-339.

Krishnamurti, T.N. et Krishnamurti, R. (1980) : Surface meteorology over the GATE A-scale. Deep Sea Res., GATE, suppl. II, 26, 29-62.

Lacombe, H. (1973) : Modèles simples de prévision de l'état thermique de la mer et de l'immersion de la thermocline. Ann. Hydrogr. SHOM. Paris.

Lamb, P.J. (1978) : Case studies of tropical Atlantic surface circulation pattern during recent sub-Saharan weather anomalies, 1967-1968. Mon. Wea. Rev., 106, 482-491.

Lass, H.U., V. Bubnov, J.M. Huthance, E.J. Katz, J. Meincke, A. de Mesquita, F. Ostapoff, et B. Voituriez (1982) : Seasonal changes of the zonal pressure gradient in the equatorial Atlantic west of 10°W during the FGGE year. Ocean Acta., 6, 3-11.

Le Floch, J.F. (1970) : La circulation des eaux d'origine sub tropicale dans la partie orientale de l'Atlantique Equatoriale étudiée en relation avec les mesures faites à bord du N.O. Jean Charcot en mai 1968. Cah. ORSTOM, Sér. Océanogr., 3, 77-113.

Le Floch, J.F. (1972) : Undercurrent system in the eastern part of the equatorial Atlantic. Papier présenté à l'Institut Für Meereskunde Université de Kiel, novembre 1972.

Leetma, A., J.P. Mc Creary et D.W. Moore (1981) : Equatorial currents : observations and theory. Evolution of Physical Oceanography, MIT Press, Warren et Wunsch editeurs, 184-196.

Lightill, M.J. (1969) : Dynamic response of the Indian Ocean to the onset of the Southwest Monsoon. Phil. Trans. Roy. Soc. Lond. A265, 45-93.

Lukas, R.B. (1981) : The termination of the Equatorial Undercurrent in the eastern Pacific. Ph. D. Dissertation. University of Hawaii. 127 pp.

Luyten, J.R. et J.C. Swallow (1976) : Equatorial undercurrents. Deep Sea Res., 23, 1005-1007.

Luyten, J.R. et D.H. Roemmich (1982) : Equatorial currents at semi-annual period in the Indian Ocean. J. Phys. Oceanogr., 12, 406-413.

Madden, R. et P. Julian (1972a) : Further evidence of global scale 5 day pressure wave. J. Atmosph. Sci., 29, 1464-1469.

Madden, R. et P. Julian (1972b) : Description of global scale circulation in the tropics with a 40-50 day period. J. Atmosph. Sci., 29, 1109-1123.

Marchal, E. et J. Picaut (1977) : Répartition et abondance évaluées par échointégration des poissons du plateau ivoiro-ghanéen en relation avec les upwellings locaux. J. Rech. Oceanogr., Vol II, N° 4, 39-57.

Markman, C.G. et D.R. Mc Lain (1977) : Sea Surface temperature related to rain in Ceara, northeastern Brazil. Nature, 265, 320-323.

Matsuno, T. (1966) : Quasi-geostrophic motions in the equatorial aera J. Meteor. Soc. Jap., 44, 25-42.

Mc Creary, J.P. (1976) : Eastern tropical response to changing wind systems with application to El Niño. J. Phys. Oceanogr., 6, 632-645.

Mc Creary, J.P. (1981a) : A linear stratified model of the equatorial undercurrent. Phil. Trans. Roy. Soc. London, 298, 603-635.

Mc Creary, J.P. (1981b) : A linear stratified ocean model of the coastal undercurrent. Phil. Trans. Roy. Soc. London, 302, 385-413.

Mc Creary, J.P. (1983a) : A model of tropical ocean-atmosphere interaction. Mont. Weat. Rev., 111, 370-387.

Mc Creary, J.P. (1983b) : Equatorial beams. J. Mar. Res., 42, 395-430.

Mc Creary, J.P., J. Picaut et D.W. Moore (1984) : Effect of annual remote forcing in the eastern tropical Atlantic. J. Mar. Res., 42, 45-81.

Mc Grail, D.W. (1979) : Topographically controlled mesoscale flow anomalies on the continental shelf off southern sierra Leone and Liberia. J. Phys. Oceanogr., 9, 327-336.

Merle, J. (1980a) : Seasonal heat budget in the equatorial Atlantic Ocean. J. Phys. Oceanogr., 10, 464-469.

Merle, J. (1980b) : Variabilité thermique annuelle et interannuelle de l'océan Atlantique equatorial Est. L'hypothèse d'un "El Niño" Atlantique. Océan.Acta., 3, 209-220.

Merle, J. et J.F. Le Floch (1978) : Cycle annuel moyen de la température dans les couches supérieures de l'Océan Atlantique intertropical. Océan. Acta., 1, 271-276.

Merle, J., M. Fieux et P. Hisard (1980) : Annual signal and interannual anomalies of sea surface temperature in the eastern equatorial Atlantic. Deep Sea Res., GATE suppl. II, 26, 77-101.

Merle, J., et S. Arnault (1983) : Seasonal variability of dynamic topography in the tropical Atlantic Ocean. (soumis à J. Mar. Res.).

Meyers, G. (1979a) : on the annual Rossby wave in the tropical North Pacific Ocean. J. Phys. Oceanogr., 9, 663-674.

Meyers, G. (1979b) : Annual variation in the slope of the 14°C isotherm along the equator in the Pacific Ocean. J. Phys. Oceanogr., 9, 885-891.

Miller, L. (1981) : Acoustic measurements of dynamic height and wind speed in the eastern Equatorial Atlantic. Recent Progress in Equatorial Oceanography, Nova University Press, Mc Creary-Moore et Witte editeurs, 325-334.

Moore, D.W., (1968): Planetary-gravity waves in an equatorial ocean. Ph. D. thesis, Harvard University, 201 pp.

Moore, D.W. et S.G.H. Philander, (1977): Modeling of the tropical oceanic circulation. The sea, Vol. 6, E. Goldberg, et al., Eds., Wiley-Interscience, 319-361.

Moore, D.W., P. Hisard, J.P. Mc Creary, J. Merle, J.J. O'Brien, J. Picaut, J.M. Verstraete et C. Wunsch, (1978) : Equatorial adjustment in the eastern Atlantic. Geophys. Res. Letters, 5, 637-640.

Morlière, A. (1970) : Les saisons marines devant Abidjan. Doc. Sc. Centre Rech. Océanogr. Abidjan, 1, 1-15.

Morlière, A. et J.P. Rébert (1972) : Etude hydrologique du plateau continental ivoirien. Doc. Sci. Centre Rech. Océanogr. Abidjan, 3, 1-30.

Mysak, L.A. (1978a) : long period equatorial topographic waves. J. of Phys. Oceanogr., 8, 302-314.

Mysak, L.A. (1978b) : Equatorial shelf waves on an exponentiel shelf profile. J. Phys. Oceanogr., 8, 458-467.

Namias, J. (1969) : On the causes of the small number of Atlantic hurricanes in 1968. Mon. Wea Rev., 97, 346-348.

Newmann, G. et R.E. William (1965) : Observations of the equatorial undercurrent in the Atlantic Ocean at 15°W during EQUALANT I. J. Geoph. Res., 70,

O'Brien, J.J., D. Adamec et D.W. Moore (1978) : A simple model of equatorial upwelling in the Gulf of Guinea. Geophys. Res. Letters, 5, 641-644.

Oort, A. et T.H. Vonder Haar (1976) : On the observed annual cycle in the ocean atmosphere heat balance over the northern hemisphere, J. Phys. Oceanogr., 6, 781-800.

Park, Y.H. (1979) : Contribution à l'étude de la génération et de la propagation des marées internes au large de la Côte d'Ivoire. Thèse de 3e cycle, Université de Bretagne Occidentale, 180 pp.

Philander, S.G.H. (1977) : The effect of coastal geometry on equatorial waves. (Forced waves on the Gulf of Guinea), J. Mar. Res., 35, 509-523.

Philander, S.G.H. (1978a) : Forced oceanic waves. Rev. Geophys. Space. Phys., 16, 15-46.

Philander, S.G.H. (1978b) : Instabilities of zonal equatorial currents. part II, J. Geophys. Res., 83, 3679-3682.

Philander, S.G.H. (1979a) : Variability of the tropical oceans. Dyn. Atm. Ocean., 3, 191-208.

Philander, S.G.H. (1979b) : Upwelling in the Gulf of Guinea. J. Mar. Res., 37, 23-33.

Philander, S.G.H. et W. Duïng (1980a) : The oceanic circulation of the Tropical Atlantic and its variability during GATE. Deep. Sea Res., GATE supl. II, 26, 1-28.

Philander, S.G.H. et R.C. Pacanoswski (1980b) : the generation and decay of equatorial currents. J. Geophys. Res., 85, 1123-1136.

Philander, S.G.H. et Pacanoswski (1981a) : Response of equatorial oceans to periodic forcing. J. Geophys. Res., 86, 1903-1916.

Philander, S.G.H. et R.C. Pacanoswski (1981b) : The oceanic response to cross equatorial winds (with application to coastal upwelling in low latitudes). Tellus, 33, 204-210.

Picaut, J. (1983) : Propagation of the seasonal upwelling in the eastern equatorial Atlantic. J. Phys. Oceanogr., 13, 18-37.

Picaut, J. et J.M. Verstraete (1975) : low frequency oscillations of temperature and sea level along the coast of the Guinea Gulf. Papier présenté à l'UGGI, Grenoble 25 août - 6 septembre.

Picaut, J. et J.M. Verstraete, (1976) : Mise en évidence d'une onde de 40-50 jours de période sur les côtes du Golfe de Guinée. Cah. O.R.S.T.O.M., sér. Océanogr., 14, 3-14.

Picaut, J., J.M. Verstraete et A. Morlière (1978) : Ondes forcées par la marée et l'atmosphère le long des côtes du Golfe de Guinée. Rapport CNEXO. Université de Bretagne Occidentale, 78 pp.

Picaut, J. et J.M. Verstraete (1979) : Propagation of a 14.7 day wave along the northern coast of the Guinea Gulf. J. Phys. Oceanogr., 9, 136-149.

Picaut, J., J. Servain, Y. Gouriou, P. Lecomte, N. Merabet, M. Seva, A.J. Busalacchi, J.P. Mc Creary, D. Moore et B. Burtchy (1983) : Modélisation et observations des variations thermiques basse fréquence dans l'Atlantique Tropical. Rapport CNEXO, Université de Bretagne Occidentale, 242 pp.

Portolano, P. (1981) : Contribution à l'étude de l'hydroclimat des côtes Sénégalaises. ORSTOM, Centre Océanogr. Dakar-Thiaroye, 69 pp.

Prinseberg, S.I. (1971) : Internal wave generation from a step like, constant slope continental shelf. Ph. D. dissertation, Université du Michigan.

Reiter, E.R. (1978) : The interannual variability of the ocean-atmosphere system. J. Atm. Sci., 35, 349-370.

Rinkel, M.O. (1969) : Some features of relationships between the Atlantic Equatorial Undercurrent and its associate salinity core. Proc. Symp. Oceanogr. Fish. Resources Tropical Atlantic, UNESCO. Paris; 193-212.

Roden, I.G. (1962) : On sea surface temperature, cloudiness and wind variations in the Tropical Atlantic. J. Atmosph. Sci., 19, 66-80.

Rossby et collaborateurs (1939) : Relation between variations in the intensity of the zonal circulation of the atmosphere and the displacements of the semi-permanent centers of action. J. Marine Res., 2, 38-55.

Roy, C. (1981) : Sur le phénomène de la petite saison froide dans le Golfe de Guinée. Rapport de D.E.A., Université de Bretagne Occidentale, 38 pp.

Schopf, P.S. et D.E. Harrison (1982) : On equatorial Kelvin waves and El Nino : I. Influence on initial stages on waves-induced currents and warming. J. Phys. Oceanogr., 13, 936-948.

Servain, J., J. Picaut et J. Merle (1982a) : Evidence of remote forcing in the equatorial Atlantic Ocean. J. Phys. Oceanogr., 12, 457-463.

Servain, J.,J. Picaut et J. Merle (1982b) : Mise en évidence d'un couplage à longue distance entre le vent et la température de surface dans l'Atlantique Equatorial. C.R. Acad. Sc. Paris., t. 294, 789-792.

Shukla, J. (1973) : Effects of Arabian sea surface temperature on Indian Ocean summer monsoon : a numerical experiment with the GFDL model. J. Atm. Sci., 32, 503-511.

Stommel, H. (1960) : wind drift near the equator. Deep Sea Res., 6, 298-302.

Stretta, J.M. (1977) : Température de surface et pêche thonière dans la zone frontale du Cap Lopez (Atlantique tropical oriental) en juin et juillet 1972, 1974 et 1975. Cah. ORSTOM, Sér. Océanogr. 15, 163-180.

Suginohara, N. (1981) : Propagation of coastal trapped waves at low latitudes in a stratified ocean with continental shelf slope. J. Phys. Oceanogr., 11, 1113-1122.

Trébern-Etienne, A. (1971) : Contribution à l'étude des mouvements internes de l'océan dans le Golfe de Gascogne et dans le Golfe de Guinée (ondes internes, turbulence). Thèse de 3e cycle. Université de Bretagne Occidentale, 122 pp.

Varlet, F. (1958) : le régime de l'Atlantique près d'Abidjan (Côte d'Ivoire). Etudes Eburnéennes, 7, 97-222.

Verstraete, J.M., J. Picaut et A. Morlière (1980) : Atmospheric and tidal observations along the shelf of the Guinea Gulf. Deep Sea Res., 26 (Suppl. II), 343-356.

Verstraete, J.M. et J. Picaut (1983) : Variation du niveau de la mer, de la température de surface et des hauteurs dynamiques le long de la côte nord du Golfe de Guinée. Océanogr. Tropic., 18, 139-162.

Voituriez, B. (1980) : The equatorial upwelling in the eastern Atlantic. problem and paradoxes, Coastal Upwelling , édité par F.A. Richards, A.G.U., Washington, D.C., 95-106.

Voituriez, B. et A. Herbland (1979) : The use of the salinity maximum of the Equatorial Undercurrent for estimating nutrient enrichment and primary production in the Gulf of Guinea. Deep. Sea Res., 26, 77-83.

Voituriez, B., A. Herbland et R. Le Borgne (1982) : L'upwelling équatorial de l'Atlantique Est pendant l'Expérience Météorologique Mondiale (PEMG). Océan. Acta., 5, 301-314.

Wang, D.P. et C.N.K. Mooers (1976) : Coastal trapped waves in a continuous stratified ocean, J. Phys. Oceanogr., 6, 853-867.

Weisberg, R.H. (1980) : Equatorial waves during GATE and their relation to the mean zonal circulation. Deep Sea Res., GATE suppl. II, 26, 179-198.

Weisberg, R.H., A. Horigan et C. Colin (1979) : Equatorially trapped Rossby-gravity wave propagation in the Gulf of Guinea. J. Marine Res., 37, 67-86.

Weisberg, R.H., L. Miller, A. Horigan et J.A. Knauss (1980) : Velocity observations in the equatorial thermocline during GATE. Deep Sea Res., GATE suppl. II, 26, 217-248.

Weisberg, R.H., et A. Horigan (1981) : Low-frequency variability in the equatorial Atlantic. J. Phys. Oceanogr., 11, 913-920.

White, W.B. (1977) : Annual forcing of baroclinic long waves in the tropical North Pacific Ocean. J. Phys. Oceanogr., 7, 50-61.

Wunsch, C. (1975) : Internal tides in the ocean. Rev. Geophysics, 13, 167-182.

Wunsch, C. et A.E. Gill (1976) : Observations of equatorially trapped waves in Pacific Sea level variations. Deep Sea Res., 23, 371-390.

Wyrtki, K. (1975) : El Niño. The dynamic response of the equatorial Pacific ocean to atmospheric forcing. J. Phys. Oceanogr., 5, 572-584.

JANUARY 1979 JOURNAL OF PHYSICAL OCEANOGRAPHY VOLUME 9

Propagation of a 14.7-Day Wave along the Northern Coast of the Guinea Gulf

JOËL PICAUT

Laboratoire d'Océanographie Physique, Université de Bretagne Occidentale, 29200 Brest, France

JEAN MARC VERSTRAETE

Antenne O.R.S.T.O.M. au Centre Océanologique de Bretagne, B.P. 337, 29200, Brest, France

(Manuscript received 8 March 1978, in final form 25 July 1978)

ABSTRACT

Long time series of sea level and sea surface temperatures measured at different coastal stations along the northern coast of the Gulf of Guinea are analyzed statistically. The results indicate that pronounced fortnightly oscillations in sea level are composed of two waves: one is the lunar fortnightly tide Mf (13.661-day period) which has a constant phase all along the coast. The other wave has a period of 14.765 days which is the period of the luni-solar fortnightly tide Msf; this wave propagates westward along the east-west oriented coastline with a mean phase speed of 53 cm s^{-1} and a wavelength of 675 km. These waves have important effects on the thermal structure and give rise to strong vertical oscillations of the subsurface isotherms throughout the year. The sea surface temperature, however, has pronounced oscillations around the Msf frequency during the upwelling season (June–September) only. The 14.765-day wave is of tidal origin and is due to a nonlinear interaction of the M_2 and S_2 (barotropic or baroclinic) tides but the generation mechanism is obscure.

1. Introduction

Extensive oceanographic studies over the past 10 years, mainly by the French Office O.R.S.T.O.M. in the Ivory Coast, and by the Fishery Research Unit of Ghana, have increased our knowledge of the general hydrography, circulation and seasonal variations in the Gulf of Guinea considerably. (Varlet, 1958; Longhurst, 1962; Morlière, 1970; Lemasson and Rébert, 1973; Houghton, 1976). There are several reasons why the interaction between the ocean and atmosphere in the Gulf of Guinea is of particular interest.

First, the atmospheric forcing in the area is very regular and is not subject to sudden and dramatic changes as is the case in higher latitudes. As a result tide gage data from this meteorologically quiet area do not merely mirror noisy meteorological forcing but could provide information about the dynamics of the ocean, about the fundamental modes of oscillations of the tropical Atlantic, and possibly about the effects of coastal geometry on equatorial waves (Philander, 1977).

Second, the coastal upwelling observed each year along the northern coast of the Gulf during the Northern Hemisphere summer exhibits a number of perplexing features. These upwellings were noted for the first time by Schott (1944) and considerable efforts have since been made to understand their mechanism (see Houghton, 1976). A simple model of Ekman upwelling driven by the local winds is irreconcilable with the observations. Although the winds over the Gulf are monsoonal, their intensity does not change drastically at the coast during the summer monsoon, and it is probable that the coastal phenomena could be part of large-scale equatorial processes. During the FINE (FGGE/Index/NORPAX Equatorial) workshop at the Scripps Institution of Oceanography (27 June–12 August 1977) Moore *et al.* (1978) proposed that remote forcing by the increase of the wind stress in the western part of the equatorial Atlantic could explain these coastal upwellings. O'Brien *et al.* (1978) have developed these ideas in a simple baroclinic numerical model of upwelling. Another approach to the problem is given by Philander (1978) who shows that the strong cross-equatorial winds between June and September can cause coastal upwellings along the northern coast of the Gulf.

Third, the northern coast of the Gulf of Guinea is an interesting region to extend the studies of trapped shelf waves which have been observed along north-south oriented coastlines off Oregon (Mooers and Smith, 1968; Cutchin and Smith, 1973), off the North Carolina Coast (Mysak and Hamon, 1969), off Florida (Brooks and Mooers, 1977), and off the Australian eastern and western coasts (Hamon, 1966; Mysak, 1967). These traveling waves are energized by atmospheric forcing. Cartwright (1969) gives the only example of a diurnal tidally induced continental shelf wave.

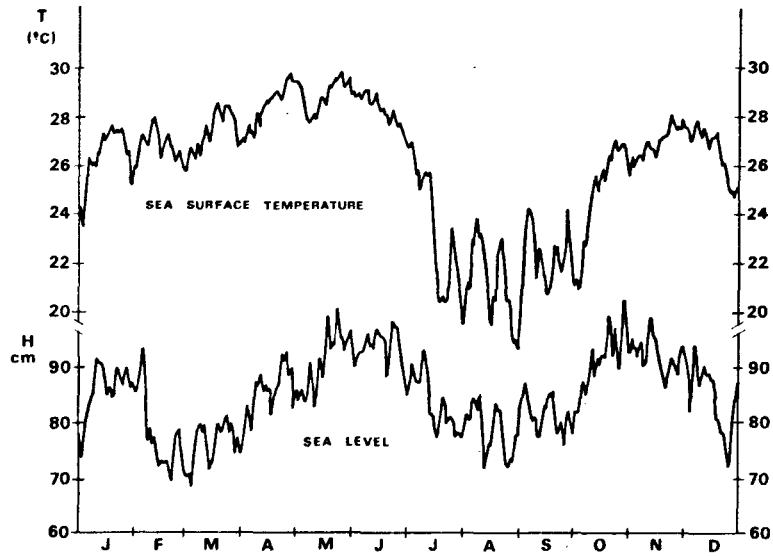

FIG. 1. Daily sea surface temperature and sea level during 1974 at Tema.

The analyses of long time series available at different coastal stations along the northern coast of the Gulf of Guinea show the presence of many low-frequency oscillations. Most of them are induced by tidal and atmospherical forcing (Picaut and Verstraete, 1976; Verstraete *et al.*, 1978).

A wave with a period of about 15 days that exists throughout the year is easily revealed by a visual inspection of the mean sea level (Fig. 1). By looking at the coastal sea surface temperature, this oscillation clearly appears during the upwelling season (July–September) when the thermocline is very close to the surface. Temperature measurements below the surface, with a thermistor chain off Abidjan, show that this wave is present throughout the year (see Fig. 2). Its appearance at the surface in the non-upwelling season is masked by the mixed surface layer.

The purposes of this paper are 1) to document the existence of a westward propagating fortnightly wave along the west-east oriented coastline of the Gulf of Guinea and 2) to evaluate hypotheses concerning the generation of this wave.

2. Data analysis

a. The data

All the data used for this study are listed in Table 1 and the locations are given by Fig. 3. They cover a period between 1951 and 1977 and were

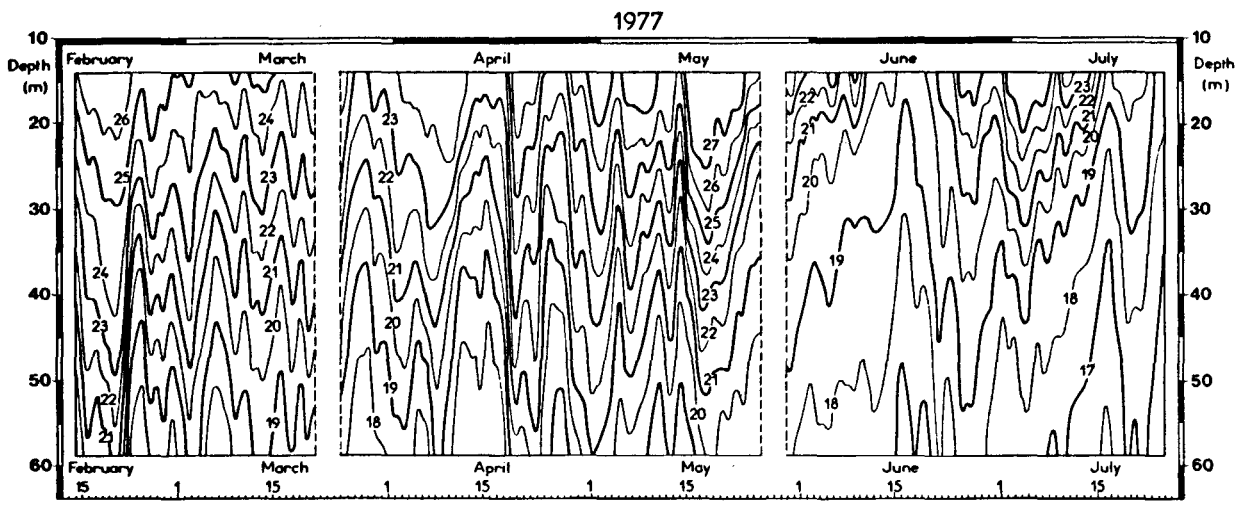

FIG. 2. Low-pass filtered isotherms (Dermerliac filter) at the Aanderaa thermistor chain mooring off Abidjan at a depth of 65 m, from 11 February to 25 July 1977.

TABLE 1. List of the coastal stations and the collected data.

State	Location	Parameter	Data length	Time origin	Remarks
Benin	Cotonou	SST	16 years	1 Apr 1958	Nansen bottle; 0, 5, 8 m depths; T, S; 0800 GMT; wharf
Togo	Kpémé	SST	6 years	1 Jan 1970	Nansen bottle; T, S; 0800, 1200, 1600 GMT; wharf
	Lomé	SST	3 years	1 Jan 1951	Nansen bottle; T, S; 0800, 1200, 1600 GMT; wharf
		SST	2 years	1 Jan 1967	Nansen bottle; T, S; 0800 GMT; wharf
		SL	2 years	9 Jan 1966	High and low tides; 4% of gaps
		SL	6 years	6 Feb 1970	High and low tides; 5% of gaps
Ghana	Keta	SST	9 years	1 May 1968	Bucket sample; T, S; 0800 GMT; beach
	Tema	SST	14 years	1 Jan 1963	Bucket sample; T, S; 0800 GMT; harbor breakwater
		SL	8 years	1 Jan 1969	Mean of 24 h observations
		SL	1 year	1 Jan 1976	Hourly observations
	Winneba	SST	7 years	1 Jan 1970	Bucket sample; T, S; 0800 GMT; beach
	Takoradi	SST	9 years	1 May 1968	Bucket sample; T, S; 0800 GMT; beach
		SL	8 years	1 Jan 1969	Mean of 24 h observations
		SL	2 years	1 Jan 1976	Hourly observations
	Cape Three Points	SST	3 years	1 Jan 1974	Bucket sample; T, S; 0800 GMT; beach
	Princestown	SST	5 years	1 May 1968	Bucket sample; T, S; 0800 GMT; beach; station closed down and replaced by Cape Three Points
	Axim	SST	9 years	1 May 1968	Bucket sample; T, S; 0800 GMT; beach
	Half Assini	SST	8 years	1 Jan 1969	Bucket sample; T, S; 0800 GMT; beach
Ivory coast	Abidjan	T	12 years	29 Mar 1966	Twice a week; Nansen bottle; 0, 5, 10, 15, 20 m depths; T, S; 0930 GMT; in 30 m water depth
		T	165 days	11 Feb 1977	Thermistor chain; 14–59 m depths; Δt = 20 mn; in 66 m water depth
		SL	10 years	9 Jan 1967	High and low tides
		SL	1 year	1 Jan 1971	Hourly measurements
		SL	27 months	1 Jan 1974	Hourly measurements
	Sassandra	SL	304 days	5 Jan 1965	High and low tides
	San Pedro	SL	50 months	1 Apr 1973	High and low tides; 10% of gaps
	Tabou	SST	21 months	1 Apr 1958	Bucket sample; T; 0650, 1200, 1800 GMT; beach
		SST	10 months	18 Aug 1968	Bucket sample; T; 0700 GMT; beach; 20% of gaps
Liberia	Monrovia	SL	338 days	22 Sep 1953	Hourly measurements

collected by the Centre de Recherches Océanographiques (ORSTOM) and Service Hydrographique in Ivory Coast, the Fishery Research Unit and the Survey Department in Ghana, the Service Hydrographique and ORSTOM in Togo and the Service des Pêches in Bénin.

The sea surface temperatures were measured from a bucket sample at the beach or with a Nansen bottle on the wharf, two or three times per day. In these analyses we used the measurements near 0800 GMT.

The hourly measurements of sea level at Mon-

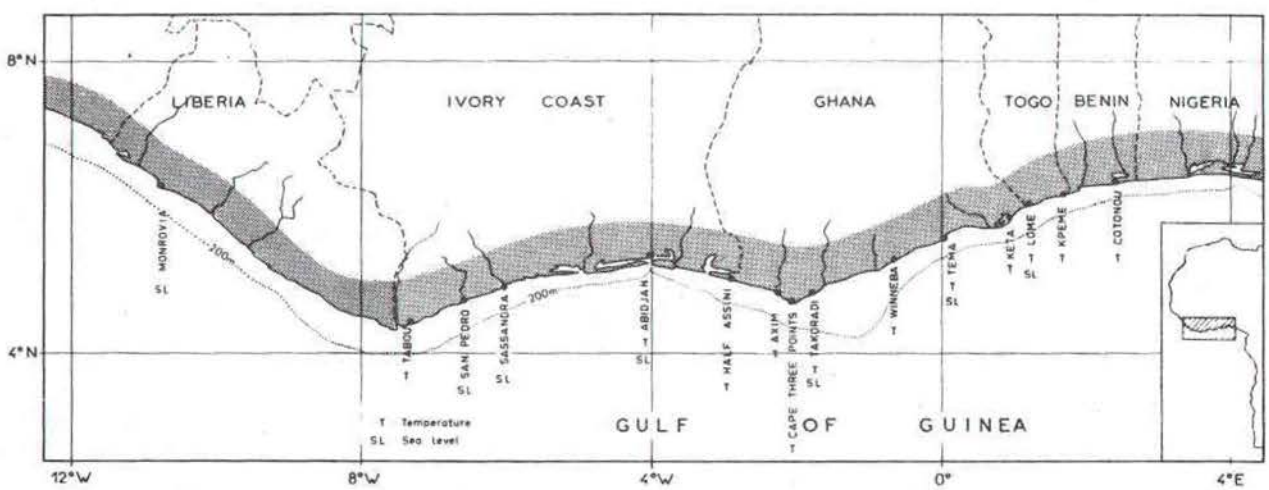

FIG. 3. Location of the coastal stations along the northern coast of the Guinea Gulf.

rovia were generously given by G. Philander. In order to simplify the digitizing of analog records we have extracted the high and low tides from the tidal records at San Pedro, Sassandra, Abidjan and Lomé, and have taken as the daily mean sea level the mid-tide level. For Tema and Takoradi, on the other hand, we collected the mean of 24 consecutive hourly observations of the water levels.

These two types of daily mean sea level could suffer from aliasing of the fundamental tidal constituents (Godin, 1972; Demerliac, 1973). Therefore, we also obtained hourly observations for three years at Abidjan, one year at Tema, and two years at Takoradi, in order to estimate the possible errors introduced by aliasing.

At Lomé, Tema, Takoradi and San Pedro, the tide gages are positioned in or near the harbor entrance where there are no perturbations from any lagoons or rivers. At Abidjan the tide gage is at the entrance of the Vridi Canal and one must be on the lookout for spurious variations from the lagoon during the rainy season. At Sassandra the tide gage had been working on the wharf for less than one year. We have no information about the position of the tide gage in Monrovia Harbor.

b. Determination of the period of the oscillations

Usually the analysis of the sea level first requires corrections for the isostatic variations due to the atmospheric pressure (Hamon, 1966). In a recent paper (Picaut and Verstraete, 1976), we have shown that such a correction is unnecessary in the present area.

The present analysis of the sea level time series that exceed five years gives evidence of several significant peaks, particularly near the periods of 45, 14.7 and 13.7 days. With the longest time series, the one from Abidjan, we are able to separate the two last peaks and find maxima of energy at periods of 14.73 and 13.73 days. These values are very close to those of Msf and Mf[1] (Fig. 4). To obtain the period of the two peaks more accurately, we made numerous spectral analyses of the sea level at Abidjan with a variable length of the autocorrelation interval. If the variations are small and the mean lengths much shorter than those of the time series, the spectral density found in all these analyses are of the same order and may overlap each other. This fact allows us to put the results on the same graph (Fig. 5). The autocorrelation length varied from 298 to 306 days. On this graph the usual bandwidth for a simple spectral analysis is given above the two peaks. With the refined treatment, our resolution is eight times higher. The two maxima are now found to be exactly at 13.66 and 14.77 days. This

[1] Mf is the lunar fortnightly tide (13.661 days) and Msf the luni-solar synodic fortnightly tide (14.765 days).

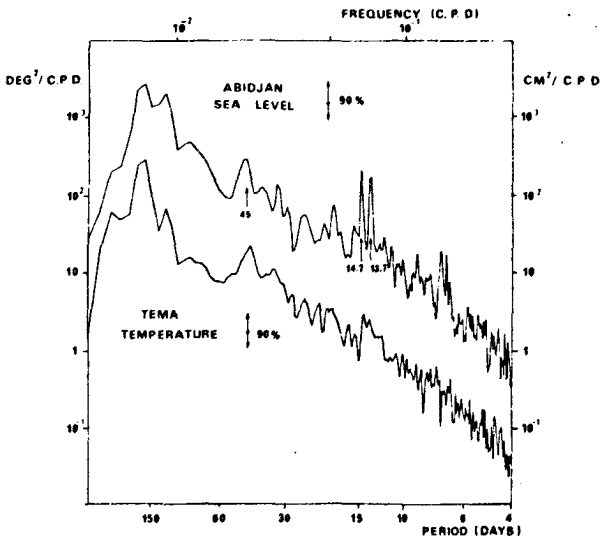

FIG. 4. Autospectra of mid-tide sea level at Abidjan (10 years) and sea surface temperature at Tema (13 years).

establishes that these two peaks correspond exactly to the Mf (13.6608 days) and Msf (14.7653 days) periods.

If these two oscillations are of purely tidal origin, they must be represented by two lines above a continuous noise. The Mf tide is not an integral subharmonic of the Msf tide, so we choose a record length such that the Mf and Msf frequencies are as close as possible to harmonics of the record length. Fig. 6 gives the result of the Fourier analysis with 2922 daily mean sea level data points at Abidjan. The two lines at 14.757 and 13.654 days are far above the continuous noise, with an amplitude of 1.20 and 1.14 cm, respectively. Such a small noise level may be explained by the stability of meteorological conditions in the Gulf of Guinea and probably by the good quality of the measurements at Abidjan.

c. Elimination of possible aliasing

With a sampling frequency of q and in the presence of an oscillation with frequency f, apparent oscillations appear at the frequencies $q-f$, $q+f$, $2q-f$, $2q+f$, ...

Table 2 gives the mean result of a harmonic analysis of hourly measurements of the sea level at Monrovia, Abidjan, Takoradi and Tema, for the most important tidal constituents of periods less than one month.

The analyses of sea surface height are made with two types of "daily mean sea level": the mid-tide level and the 24 hourly average. Table 3 gives the residue coefficients for the main tidal constituents with these two types of "daily mean sea level". The average lets through 3.5% of the M_2 tide and with a sampling frequency of 1 cycle per day (cpd)

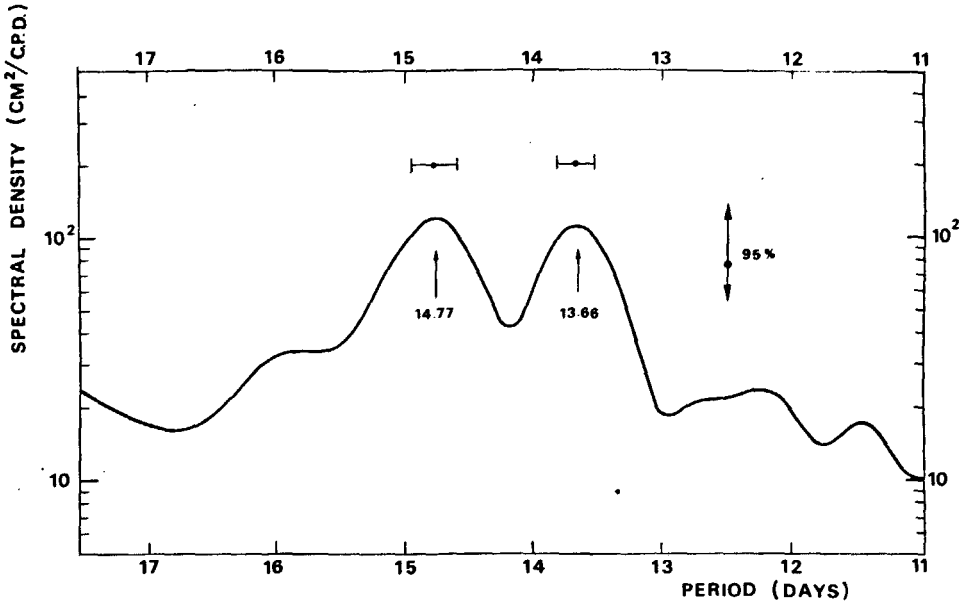

FIG. 5. Detailed spectral analysis of Abidjan sea level.

may give a fictitious Msf oscillation as large as the real phenomenon (Table 2). The mid-tide level has been estimated for each day by the mean of the four nearest low and high tides of the day, so the effective sampling is 0.966 cpd; with 5.9% of the K_2 tide it may give an aliased oscillation at the Mf frequency about eight times smaller than the real one.

In order to control these factors, we have used, on all the hourly measurements of sea level at Abidjan, a special filter that spans 72 h (Demerliac, 1973), and have calculated the corresponding daily mean sea level. Table 4 presents the harmonic analysis of the daily mean sea level, the 24 hourly average, the mid-tide level and the hourly meas-

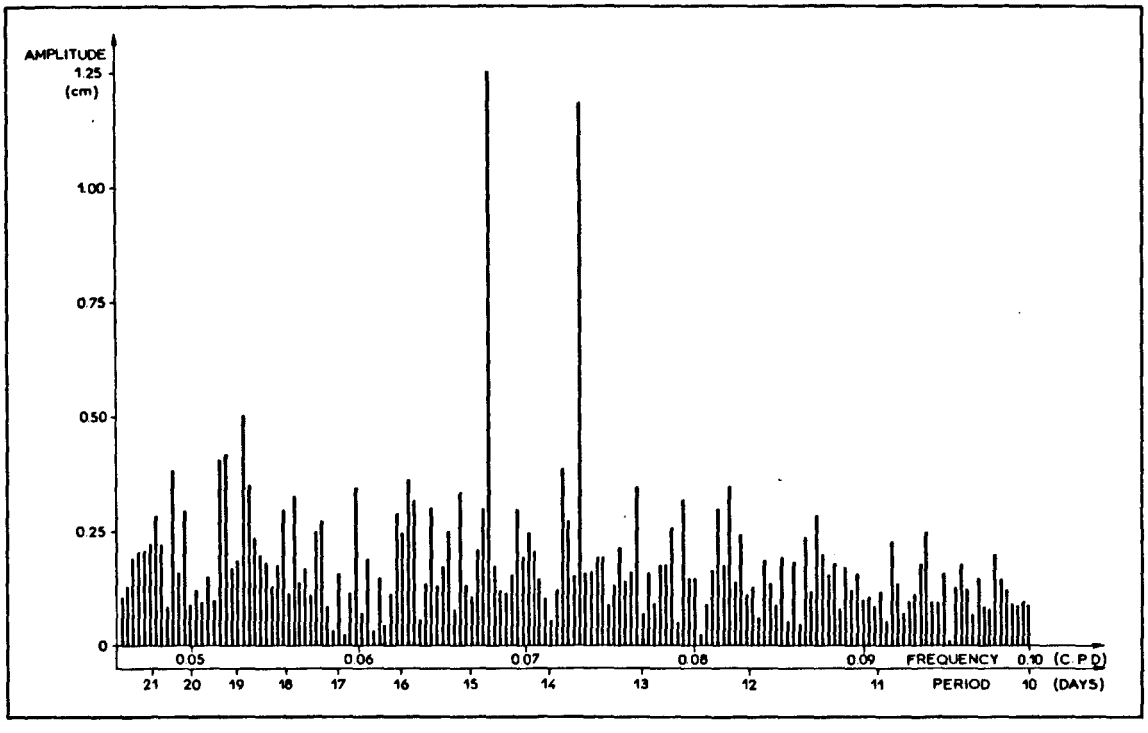

FIG. 6. Fourier analysis of Abidjan mid-tide sea level (8 years).

urements. It is clear that the average perturbs the Msf result considerably, whereas the mid-tide level does not disturb the Mf result significantly.

We have spectrally analysed the 27 consecutive months of hourly sea level at Abidjan, after using the Demerliac filter. The comparison with mid-tide level spectra shows a very good agreement between these two types of data (Fig. 7). Hence the mid-tide level is much better adapted for the study of low-frequency phenomena than the 24 hourly average, which may give significant aliasing.

Puzzling results with this "daily mean sea level" (see Section 4) show clearly the importance of these precautions. We can now be sure that the Mf and Msf oscillations of the sea level are real phenomena.

During the entire year, we find strong semi-diurnal internal waves all along the continental shelf (Fig. 13). During the upwelling season (July–September) it is possible for the thermocline to rise very close to the surface so that daily sea surface temperature measurements could give fictitious Msf results.

In the present study we use two types of sea surface temperature data. One set of data has been taken from the beach, the other at the end of the wharfs or the piers in water 5–8 m deep.

In both cases, the internal waves would have broken some distance away thus eliminating possible aliasing. During the 1974 Ghana upwelling season, Houghton (1976) found a very high correlation between Tema Harbor daily measurements of temperature at 0830 GMT and low-pass filtered data of hourly temperature measurements at a depth of 12 m on the shelf. The filter he used is a cosine one that spans 75 h. This reduces the M_2 considerably.

Special attention has been given to the sea surface temperature from the wharf of Lomé. Comparison of the spectrum for three years measurements at 0800, 1200, 1600 GMT, and for the mean measurements reveals no significant difference in the period range 4–100 days.

We conclude that fortnightly oscillations of the sea surface temperature are real. Visual inspection of the Demerliac filtered temperature as measured with a thermistor chain off Abidjan (Fig. 2) shows clearly such an oscillation, especially in March and April 1977.

TABLE 2. Mean amplitude of the main tidal components at Tema, Takoradi, Abidjan and Monrovia.

Constituent	M_2	S_2	K_1	N_2	K_2	P_1	O_1
Period (h)	12.42	12.00	23.93	12.66	11.97	24.07	25.82
Amplitude (cm)	38.13	13.28	9.94	8.49	3.75	2.83	2.11

Constituent	Mf	Msf	Mm
Period (days)	13.66	14.76	27.55
Amplitude (cm)	1.80	0.88	1.00

3. Origin of the Mf and Msf oscillations

When tidal phenomena propagate on the shelf, they are modified by the bottom and coastal topography so that higher or compounded harmonic waves are created (Le Provost, 1976). These secondary components are the result of the presence of nonlinear advection terms uu_x, uv_x, vu_y, vv_y and the quadratic friction terms. If the tidal forcing is a pure harmonic of frequency ω, $u = u_0 e^{i\omega t}$, the quadratic term uu_x contains a frequency 2ω; also, if the tidal forcing contains two frequencies ω_1 and ω_2, the quadratic term in uu_x will have higher harmonics at $2\omega_1$ and $2\omega_2$ and two compounded harmonics at $\omega_1 - \omega_2$ and $\omega_1 + \omega_2$. Such higher frequency waves created by nonlinearity or by friction are common in the present area. Detailed harmonic analysis of the hourly measurements at Monrovia, Abidjan and Tema shows the presence of 10 waves of this type, with an amplitude higher than 0.5 cm. In the lower range, the Mf oscillation could be due to such an interaction between the K_2 and M_2 tides and the Msf due to an interaction between the M_2 and S_2 tides.

A question remains: are the observed Mf and Msf tides in response to the driving tidal potential or are they due to a nonlinear interaction between the M_2, S_2 and K_2 tides?

While the semidiurnal and diurnal tidal constituents have been studied extensively, this is not so in the case of the semi-monthly tides. Recent studies of the lunar fortnightly tide in the Pacific (Wunsch, 1967) and in the world ocean (Maksimov, 1966;

TABLE 3. Residues of different tidal filters.

Method	Constituent						
	M_2	S_2	K_1	N_2	K_2	P_1	O_1
24 h average	−0.03516	0.00000	−0.00274	−0.05445	0.00276	0.00275	0.07537
Mid-tide	0.00000	0.05461	−0.04079	−0.02945	0.05905	−0.03485	0.04329
Doodson filter	−0.00058	0.00000	0.00015	0.00171	0.00033	−0.00013	0.00299
Demerliac filter	−0.00004	0.00000	0.00000	−0.00014	0.00000	0.00000	0.00041

TABLE 4. Mean results of the harmonic analysis at Abidjan with four different types of sea level data.

Type of data	Constituent			
	Msf		Mf	
	A (cm)	*G* (deg)	*A* (cm)	*G* (deg)
24 hourly average	0.66	130	1.27	11
Mid-tide level	0.91	189	0.98	8
24 h average after using the Dermerliac filter	0.79	195	1.25	11
Hourly measurements	0.81	195	1.31	12

Lisitzin, 1974; Kagan *et al.*, 1976) show that this tide is not exactly an equilibrium tide. Nevertheless, the deviation from the equilibrium tide seems to be a minimum near the equator.

The long-period equilibrium tides can be computed from the following equations:

$$W = V(1 - 3\sin^2\phi)\cos\psi,$$

$$\Delta H = \frac{W}{g}(1 + k - h),$$

where W is the potential of the disturbing force, V the relative coefficient, ϕ the geographical latitude, ψ the argument, ΔH the disturbance in mean sea level, g the acceleration of the earth's gravity and $(1 + k - h)$ a factor representing the resilient and elastic properties of the earth's yielding crust, usually estimated to be 0.67.

This equilibrium equation gives for the Mf and Msf constituents:

$$\Delta H_{Mf} = 1.402(1 - 3\sin^2\phi)\cos 2s,$$

$$\Delta H_{Msf} = 0.123(1 - 3\sin^2\phi)\cos(2s - 2h).$$

With $\phi = 5°$ in the present area, we obtain

$$\Delta H_{Mf} = 1.37 \text{ cm},$$

$$\Delta H_{Msf} = 0.12 \text{ cm}.$$

The mean results of the harmonic analysis of Monrovia, Abidjan, Takoradi and Tema give (Table 2) 1.80 cm for Mf and 0.88 cm for Msf.

The amplification factor of 1.3 for Mf is in good agreement with the observation of Maksimov (1966). Kagan *et al.* (1976) explain the deviation by the dynamic tidal theory. On the other hand, we have seen that Mf could be due to the interaction of the tidal constituents K_2 and M_2, but the amplitude of K_2 is 10 times less than that of M_2 (Table 2). The symmetric compound tide MK_4 $(M_2 + K_2)$ is very weak in the present area and it would probably exist if $(M_2 - K_2)$ were present.

All these facts tend to prove that observed Mf oscillation is of purely astronomical origin.

An amplification factor of 7.4 for the Msf oscillation is inconsistent with the equilibrium theory and even with the dynamic one. M_2 and S_2 are the most important tides in our area (Table 2) and we find a wave MS_4 $(M_2 + S_2)$ of the same order as the observed Msf wave. The observed 14.76-day wave is probably induced by a nonlinear interaction on the shelf between the semidiurnal tides M_2 and S_2.

Offshore, the analysis of tidal observations at Ascension Island in the equatorial Atlantic (Cartwright, 1971, and private communication) gives a significant amplitude (0.9 cm) at the Mf frequency but not at the Msf frequency. In the equatorial Pacific, Wunsch (1967) observes the Mf tide at many islands but the Msf only at Canton Island.

4. Wave propagation

Houghton and Beer (1976) presented evidence of a westward propagating wave with a mean phase speed of 64 cm s^{-1} and a period around 14.5-day (800 km wavelength) in the region east of Cape Three Points during the upwelling season of 1974. In our IUGG paper (Picaut and Verstraete, 1975) we have shown preliminary results of the spectral analysis of some sea surface time series between Tabou and Cotonou. The temperature data indicate that in the neighborhood of the fortnightly frequency, there is an energetic wave with a westward phase speed of roughly 75 cm s^{-1}. On the other hand, the sea level data analyzed by Houghton and Beer show no phase propagation between Tema and Takoradi. This perplexing result is confirmed by our calculations, although we do find westward phase propagation from Ghana to the Ivory Coast in the sea level at a period of 14.7 days.

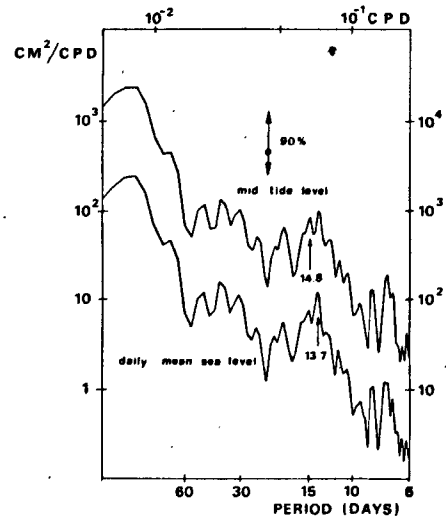

FIG. 7. Autospectra of mid-tide sea level and daily mean sea level. Daily mean sea level obtained by Demerliac filtering of hourly measurements at Abidjan (27 months).

We have tried to make a more detailed cross-spectral analysis by using data from all the coastal stations in Fig. 3. For the sea level at Tema, Takoradi and Abidjan, we find a very strong coherence for the Mf and Msf frequencies; unfortunately, the coherence drops at Lomé and San Pedro. This can be explained by the poor quality of these two sets of data. Furthermore, the time series of Sassandra and Monrovia are too short to give precise information around the fortnightly frequency with spectral analysis. A harmonic analysis seems to be more convenient for this problem. For this purpose, with B. Simon, we adapted a program developed by the French Hydrographic Service (Simon, 1974) for the analysis of daily mean sea level. Table 5 gives the mean results of yearly sea level harmonic analysis.

In Section 2 we have seen that the long-period tide results given by harmonic analysis, on the mid-tide level, are very close to those given by hourly measurement (Table 4). On the other hand, the 24 hourly average gives an entirely fictitious Msf oscillation. So for the Msf result of Tema and Takoradi, we use the hourly measurements for one year at Tema and two years at Takoradi. The mean results with the 24 h/average give an amplitude A of 2.00 cm and a Greenwich phase G of 67° for Tema and $A = 1.66$ cm, $G = 55°$ for Takoradi; with such values, the phase difference between Tema and Takoradi is nearly null (no propagation) instead of 51° (Table 5) for the real values (westward propagation of 121 cm s^{-1}). So for the Msf analysis we use the hourly measurement at Tema and Takoradi.

In Table 5 the mean amplitude and phase for Mf and Msf are given, in addition to error estimates. These error estimates are based on the concept of estimation of a deterministic sinusoidal signal embedded in a random noise background. For further explanations see Wunsch (1967) and Middleton (1947). The high noise level at San Pedro is due to the presence of some gaps in the time series and probably is due to a poor offset of the tide recorder. This could perturb the long-period analysis (Desnoës, 1975). Error estimates are also large for short time series (Sassandra, Monrovia). Nevertheless, Table 5 shows clearly that the Mf oscillation does not propagate. On the other hand, the phase difference for the Msf oscillation increases regularly from Lome to Monrovia. In Fig. 8, we observe a westward propagation of 53 cm s^{-1}, which gives a wavelength of 675 km.

In the case of the sea surface temperature we must distinguish between the whole year and the upwelling season (June to early October) when the thermocline rises to the surface so that the temperature fluctuations can reach the surface (Fig. 1). We did the following analyses on all our sea surface temperatures:

- Autospectral and cross-spectral analyses.
- Fourier analyses on the longest series.
- Harmonic analyses on the whole year and on the upwelling season.
- Cross-correlation centered on the upwelling season.

Cross-spectral analysis reveals generally the presence of a maximum of energy density around the fortnightly frequency but rarely at the exact frequencies of Mf and Msf. The coherence between the stations is generally strong on the eastern side of Cape Three Points but is much lower on the western side. This is probably due to a cape effect which gives a permanent upwelling downstream (east) of Cape Three Points and an accumulation of warm water upstream (Marchal and Picaut, 1977) so that the oscillations may not appear on the upstream side.

A Fourier analysis of the sea surface temperature also fails to separate the Mf and Msf signals. (See Fig. 9). Fig. 10 shows the phase propagation of the fortnightly oscillations. It is approximately 42 cm s^{-1}. Data for the entire year, and for the upwelling season only, give essentially the same result.

The background noise, associated with mixing in a shallow surface layer, presumably blurs the distinction between the Mf and Msf signals in sea surface temperature. Harmonic analysis of the subsurface thermistor chain data (166 days) shows the Msf amplitude to be twice as large as the Mf amplitude.

TABLE 5. Mean results of yearly sea level harmonic analysis.

Station		Lome	Tema	Takoradi	Abidjan	Sassandra	San Pedro	Monrovia
Time duration (years)		5	1	2	10	0.83	4	0.93
Msf	A (cm)	0.83 ∓ 0.32	0.46 ∓ 0.21	0.73 ∓ 0.22	1.24 ∓ 0.13	1.46 ∓ 0.57	0.40 ∓ 0.32	0.90 ∓ 0.49
	G (deg)	214 ∓ 28	336 ∓ 32	27 ∓ 23	206 ∓ 10	61 ∓ 29	59 ∓ 48	20 ∓ 37
Time duration (years)		5	7	8	10	0.83	4	0.93
Mf	A (cm)	1.34 ∓ 0.42	1.69 ∓ 0.22	1.89 ∓ 0.20	0.99 ∓ 0.17	2.10 ∓ 0.59	2.19 ∓ 0.46	1.80 ∓ 0.57
	G (deg)	0 ∓ 24	0 ∓ 11	357 ∓ 10	359 ∓ 14	11 ∓ 22	346 ∓ 17	8 ∓ 24

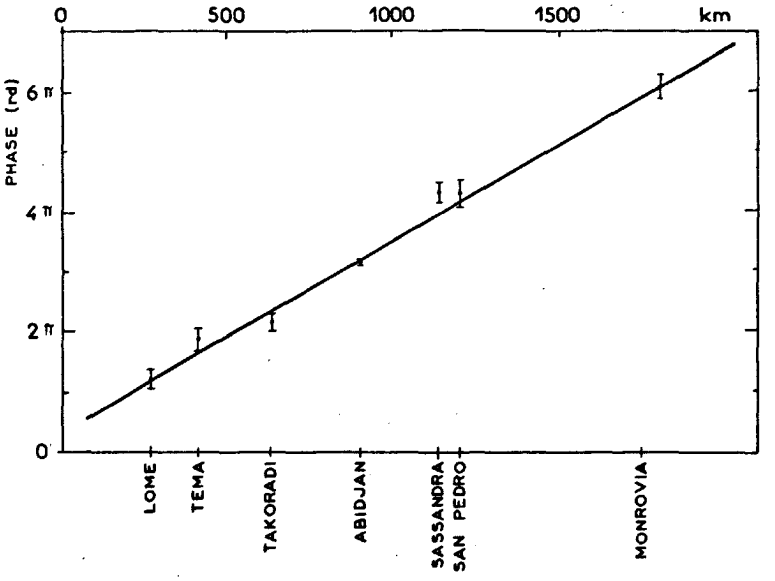

FIG. 8. Sea level phase variation at the Msf frequency along the coast.

To study the phase propagation more closely, we made a cross-correlation analysis of sea surface temperature data taken over 122 days during the upwelling season. In order to discern more clearly the possible fortnightly oscillation from other variations (45-day wave, seasonal variation, . . .) we have submitted all the time series to a bandpass filter centered on 15 days. About half of the 456 cross-correlation analyses reveal the presence of a significant fortnightly oscillation. On each of these analyses, the day lag, corresponding to the maximum of cross-correlation, gives an estimate of the phase speed of the fortnightly wave. Despite a large dispersion of individual results (from 25 to 117 cm s^{-1}), the mean value of 54 cm s^{-1} is highly significant.

Note that the acceleration seems to appear in this westward propagation between Winneba and Takoradi. This result is corroborated by the Msf

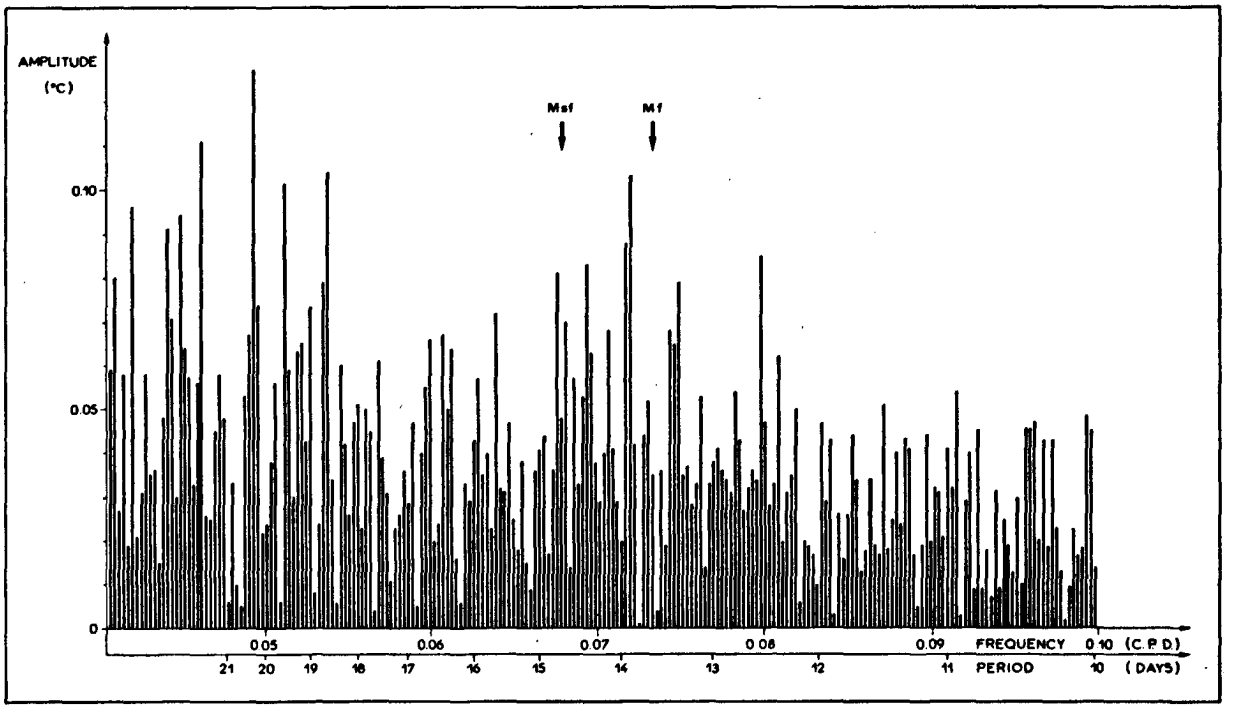

FIG. 9. Fourier analysis of sea surface temperature at Tema (14 years).

phase difference between Tema to Takoradi, for the sea level (121 cm s^{-1}). It might be explained by the increase of the shelf width in this area (Fig. 3).

Morliere and Rébert (1973) have shown that stratification on the shelf changes significantly in the upwelling season (Fig. 2). Table 6 gives the mean results of harmonic analyses for the whole year and for 147 days centered on the upwelling season [according Godin (1970), 147 days are enough to separate the Mf and Msf frequencies]. No variation appears between these two types of analyses, so that the wave propagation seems not to be affected at all by the variation of stratification.

5. Hypotheses concerning the generation of the wave

The fortnightly wave can either be forced nonlocally, in which case it must satisfy the dispersion relation for a freely propagating wave, or it can be forced locally all along the coast, in which case its frequency and wavenumber (and hence phase speed) is determined by that of the forcing function.

a. Nonlocally forced free waves

Since the period of the wave is precisely that of the Msf tide, its origin must be tidal. This eliminates atmospheric forcing as a generation mechanism and also eliminates the 14–18 meanders of the Undercurrent described by Duing *et al.* (1975) from the list of possible causes. A possibility that remains is

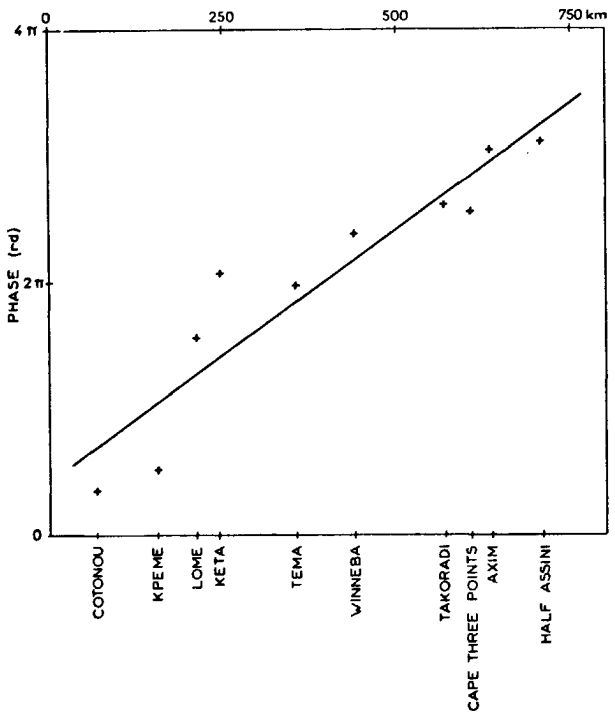

FIG. 10. Sea surface temperature mean phase variation along the coast at the Mf and Msf frequencies.

TABLE 6. Mean results of harmonic analyses for the whole year and around the upwelling season (147 days) with the sea level data

Station		Lome	Abidjan	San Pedro
Number of analyses		5	10	4
Yearly results	A (cm)	0.83	1.24	0.40
	G (deg)	241	206	59
Upwelling season results	A (cm)	0.59	1.43	0.95
	G (deg)	239	204	61

a nonlinear interaction of the barotropic M_2 and S_2 tides in a relatively small region. The "wavemaker" in this small region (which could be the shallow northeast corner of the Gulf of Guinea for example) could then generate waves that propagate freely westward along the coast. If this were indeed the generation mechanism, then the waves would attenuate with increasing distance from the region of forcing. Our data do not show a systematic attenuation of the amplitude. Nonetheless, we consider the free waves that could possibly propagate westward along the coast.

1) Internal Kelvin wave

Philander (1977) has shown that a wave with a period of 14.7 days and a wavelength of 650 km does not satisfy the dispersion relation for a free internal Kelvin wave. Houghton (private communication) has evidence that the amplitude of the observed wave attenuates above the thermocline so that it cannot be an internal Kelvin wave.

2) Topographic shelf wave

Of the various theories related to nondivergent waves associated with sharp changes in depth, we refer to the Robinson (1964) and Mysak (1968) models because their choice of the bottom topography fits conveniently the bathymetry of the Guinea Gulf continental shelf. We have calculated the dispersion relation for numerous sections of the shelf between Monrovia and the Gulf of Biafra. There is only one large area where we find (ω,k) in agreement with a 14.76-day period and a 675 km wavelength, the North shelf area of the Gulf of Biafra. A second possible area is off Takoradi. All the other sections give a theoretical speed at the Msf frequency about 50% slower than the observed speed which is unsatisfactory.

This analysis is for nondivergent waves on an f-plane. In two recent papers, Mysak (1978a,b) investigates the properties of zonally propagating long-period equatorial waves on an equatorial beta plane with topography. He assumes that the motions are barotropic and nondivergent and that the iso-

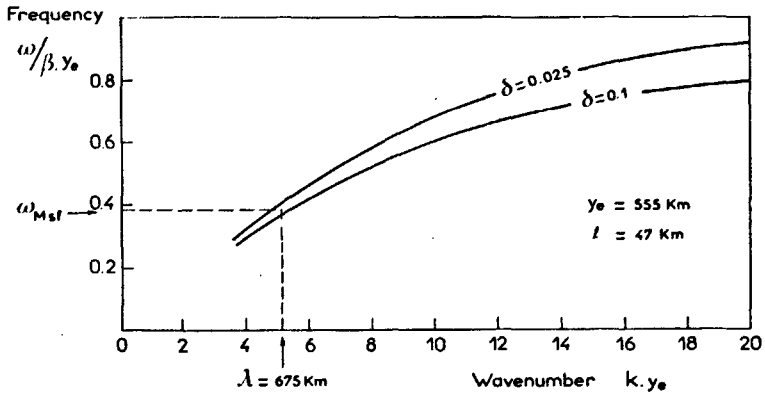

FIG. 11. Dispersion relation for an equatorial topographic wave.

baths are parallel to the equator. He applies his model to the present 14.7-day wave for two types of shelf: a step shelf and an exponential shelf with a mean shelf width of 100 and 92 km, respectively. He obtains a theoretical wavelength of 1300 km for the first profile and 580 km for the second one. However, these topographic values do not fit well the mean shelf of the Ghana and Ivory Coast.

Following Mysak (1978a), we made the calculations for the step shelf profile

$$H(y) = \begin{cases} H_1, & y_e < y < y_e + l \\ H_2, & -\infty < y < y_e \end{cases}$$

where y_e is the distance from the equator of the shelf edge, l the shelf width, H_1 the shelf depth and H_2 the ocean depth.

In terms of the nondimensional frequency $\Omega = \omega/\beta y_e$ and wavenumber $\kappa = ky_e$, the dispersion relation found is

$$\Omega = \frac{-\kappa(1-\delta)\sinh\chi r}{\chi(\delta\sinh\chi r + \cosh\chi r)},$$

where

$$\chi = \left(\kappa^2 + \frac{\kappa}{\Omega}\right)^{1/2}, \quad \delta = H_1/H_2,$$

$$r = l/y_e, \qquad \beta = 2\Omega_E/R,$$

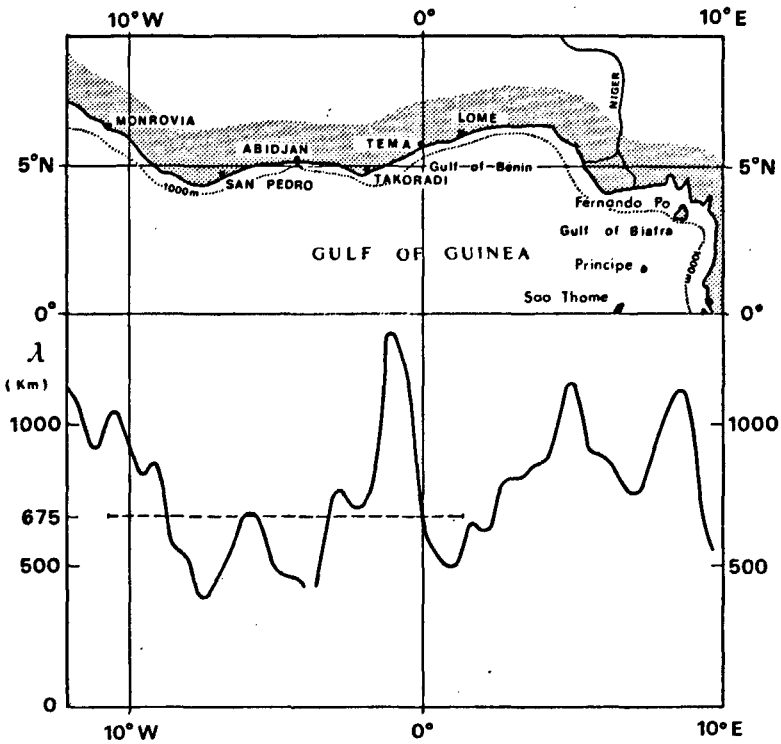

FIG. 12. The theoretical wavelength in the Gulf of Guinea at the Msf period.

and Ω_E and R, respectively, the rate of the earth's rotation and the earth's radius. We have used the 1000 m depth contour to estimate the width of the shelf and $H_2 = 4000$ m for the ocean bottom. Between Monrovia and Lomé we estimate the mean width l to 47 km and the mean y_e to 555 km ($\varphi = 5°N$). Fig. 11 gives the corresponding dispersion relation. We first note that the variations of the shelf depth are unimportant.

At the Msf frequency, with $\delta = H_1/H_2 = 0.025$, we obtain a theoretical wavelength of 722 km, which is very close to the mean observed 675 km wavelength between Monrovia and Lomé.

On Fig. 12 we have plotted the theoretical wave-

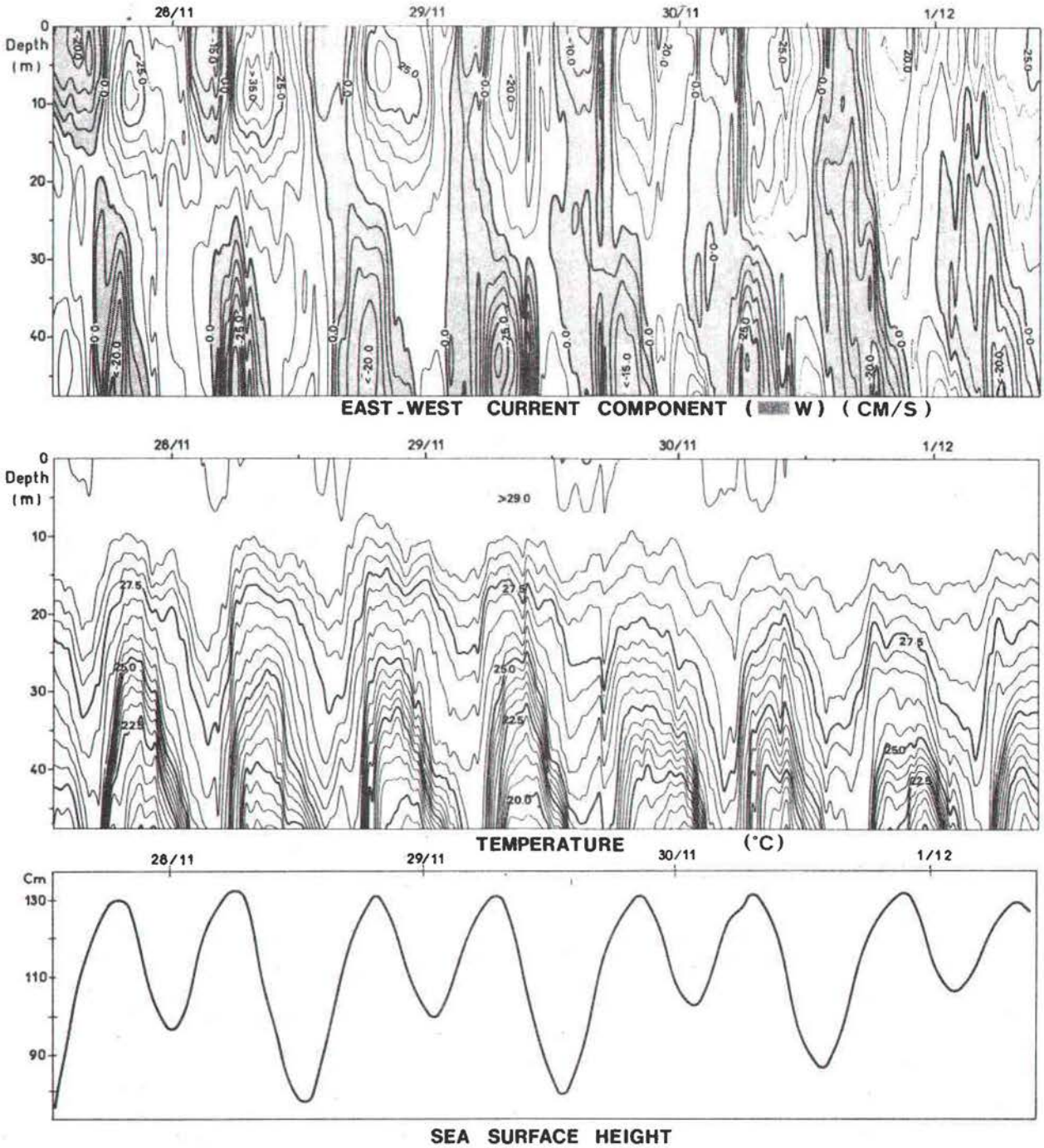

FIG. 13. High-resolution temperature and current profiles (298 profiles) in a water depth of 52 m during 4 days, off Abidjan. Sea surface height at the Abidjan tide gage.

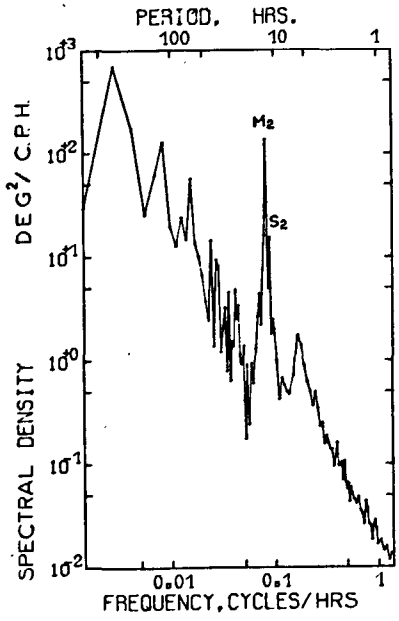

FIG. 14. Autospectrum of temperature at 45 m depth, at the thermistor chain mooring off Abidjan.

length at the Msf frequency for 45 sections between 12°W and the Gulf of Biafra. This graph shows clearly that we must take into account the alongshore variation in the shelf profile.

Nevertheless, such a simple model leads us to speculate that the observed 14.7-day wave might be a freely propagating equatorial shelf wave.

b. Locally forced waves

The period of the observed wave (14.765 days) is such that it could be due to a nonlinear interaction of the M_2 and S_2 tides. If this interaction is forcing the observed wave all along the coast then the wavenumber K_1 and K_2 of the M_2 and S_2 tides, respectively, must be related to the wavenumber K_3 of the observed wave by

$$K_1 \pm K_2 \pm K_3 = 0. \qquad (1)$$

But the wavelengths of M_2 and S_2 are approximately 10 000 km, whereas the wavelength of Msf equals about 675 km; the last wavelength is so small compared with the two others that the condition for a local forcing cannot be satisfied. It is impossible that the nonlinear interaction takes place along the coast, and we must rule out an interaction between the two barotropic waves M_2 and S_2. The remaining possibility is a nonlinear interaction between the internal M_2 and S_2 tides.

Numerous and careful experiments in the area off Abidjan give evidence of very strong semidiurnal internal waves. These internal tides were observed both in the "warm season" and in the upwelling season. For example, one experiment with an anchored ship in a water depth of 52 m for four days during the warm season, obtained high-resolution temperature and current profiles simultaneously every 20 min. Some detailed results of this experiment (Picaut and Park, unpublished manuscript) are presented in Fig. 13, which depicts typical situations observed numerous times (eight experiments in 1973). We observe a very significant coherence between the vertical oscillations of the isotherms, the east-west component of current and a sea level record from the Abidjan tide gage located nearby.

In 1977, we succeeded in maintaining an Aanderaa thermistor chain of 50 m length on the shelf off Abidjan in water 65 m deep; the mooring design was similar to that of Pillsbury *et al.*, (1969) with subsurface buoys at 12 m depth. The instruments sampled data every 20 min and were maintained from 11 February to 25 July 1977. All the autospectra of 10 thermistor time series show two important peaks at the exact frequencies of M_2 and S_2 (Fig. 14). We observe also one significant peak around 6 h, which corresponds to the compound frequencies MS_4 (6.103 h) and M_4 (6.21 h) and one other at about 15 days. It is possible that the strong baroclinic internal tides observed could interact nonlinearly and transfer energy from the M_2 and S_2 tidal periods to the periods M_4, MS_4 and Msf. Park (private communication) has shown that these oscillations are mainly of the first baroclinic mode. The stratification on the shelf is such that a first baroclinic mode semidiurnal internal tide has a theoretical wavelength between 14 and 21 km (depending whether or not it is the upwelling season). Despite the fact that the relation (1) between the wavenumbers is nearly satisfied, it seems difficult that such short waves will interact nonlinearly to give rise to 675 km wave.

Further measurements to study the generation and propagation of the internal tides are necessary to clarify relation between the internal tides and the Msf signal.

6. Concluding remarks

In this study we show that the half-monthly oscillations observed at seven tide gage stations along the northern coast of the Guinea Gulf are composed of two waves. One is the direct effect of the lunar fortnightly tide Mf. It has constant phase all along the coast and probably has a weak influence on the thermal structure. The other oscillation in the sea level has a period that corresponds exactly to that of the Msf tide. It probably results from a nonlinear interaction between the M_2, S_2 (barotropic or internal) tides. (Strong internal tides with the exact frequencies M_2 and S_2 are observed on the shelf throughout the year.) The 14.7-day wave propagates all along the coast, with a mean phase speed of 53 cm s^{-1} and a wavelength of 675 km;

this phase speed does not vary with the stratification. This wave has an important effect on the thermal structure and gives rise to strong oscillations in a broad frequency band around the original frequency Msf. The associated vertical oscillations of the subsurface isotherms are found to be present throughout the year (see Fig. 2). If this wave is coastally trapped then its presence throughout the year is consistent with the observation by Bakun, *et al.* (1973) of an offshore temperature maximum all the year round.

The amplitude of the sea surface temperature oscillations associated with this wave might reach 2.5°C in the upwelling season. This is to be compared with the 1.5°C oscillations induced by the atmospherically forced 40–50 day wave (Picaut and Verstraete, 1976).

Acknowledgments. The authors are grateful to the Ghana Fishery Research Unit, the Ghana Survey Department, the Service des Pêches in Bénin, the Services Hydrographiques of Togo and Ivory Coast in generously providing data, and to G. Philander and B. Simon for their helpful advice.

REFERENCES

Bakun, A., D. R. McLain and F. V. Mayo, 1973: Upwelling studies based on surface observations. *Coastal Upwelling Experiment Workshop Abstracts*, Dept. of Oceanography, Florida State University.

Brooks, D. A., and C. N. K. Mooers, 1977: Wind-forced continental shelf waves in the Florida current. *J. Geophys. Res.*, **82**, 2569–2576.

Cartwright, D. E., 1969: Extraordinary tidal currents near St. Kilda. *Nature*, **223**, 928–932.

——, 1971: Tides and waves in the vicinity of Saint Helena. *Phil. Trans. Roy. Soc. London*, **270**, 603–649.

Cutchin, D. L., and R. L. Smith, 1973: Continental shelf waves: low frequency variations in sea level and currents over the Oregon continental shelf. *J. Phys. Oceanogr.*, **3**, 73–82.

Demerliac, A., 1973: Calcul des niveaux moyens journaliers. *EPSHOM*, Brest, 36 pp.

Desnoës, 1975: Le bruit dans les analyses de marée. *EPSHOM*, No. 391.

Düing, W., P. Hisard, E. Katz, J. Meincke, L. Miller, V. Moroshkin, G. Philander, A. A. Ribnikov, K. Voigt and R. Weisberg, 1975: Meanders and long waves in the equatorial Atlantic. *Nature*, **257**, 280–284.

Godin, G., 1970: La résolution des ondes composantes de la marée. *Int. Hydrogr. Rev.*, **47**, 139–150.

——, 1972: *The Analysis of Tides*. Liverpool University Press, 264 pp.

Hamon, B. V., 1966: Continental shelf waves and the effects of atmosphere pressure and wind stress on sea level. *J. Geophys. Res.*, **71**, 2883–2893.

Houghton, R. W., 1976: Circulation and hydrographic structure over the Ghana continental shelf during the 1974 upwelling. *J. Phys. Oceanogr.*, **6**, 909–924.

——, and T. Beer, 1976: Wave propagation during the Ghana upwelling. *J. Geophys. Res.*, **8**, 4423–4429.

Kagan, B. A., V. Y. A. Rivkind and P. K. Chernyayev, 1976: The fortnightly lunar tides in the world ocean. *Izv. Atmos. Ocean. Phys.*, **12**, 449–452.

Lemasson, L., and J. P. Rébert, 1973: Les courants marins dans le golfe ivoirien. *Cah. ORSTOM, Sér. Océanogr.*, **11**, No. 1, 67–95.

Le Provost, C., 1976: Theoretical analysis of the structure of the tidal wave's spectrum in shallow water areas. *Mem. Soc. Roy. Sci. Liège*, 6 ème sér., **10**, 97–111.

Lisitzin, E., 1974: *Sea Level Changes*. Elsevier, 286 pp.

Longhurst, A. R., 1962: A review of the oceanography of the Gulf of Guinea. *Bull. IFAN*, **A24**, 633–663.

Maksimov, I. V., 1966: Long period lunisolar tides in the ocean. *Oceanology*, **6**, 20–30.

Marchal, E., and J. Picaut, 1977: Répartition et abondance évaluées par échointégration des poissons du plateau ivoiro-ghanéen en relation avec les upwellings locaux. *J. Rech. Oceanogr.*, **2**, No. 4.

Middleton, D., 1947: Some general results in the theory of noise through non-linear devices. *Quart. Appl. Math.*, **5**, 445–498.

Mooers, N. K., and R. L. Smith, 1968: Continental shelf waves off Oregon. *J. Geophys. Res.*, **73**, 549–557.

Moore, D. W., P. Hisard, J. McCreary, J. Merle, J. J. O'Brien, J. Picaut, J. M. Verstraete and C. Wunsch, 1978: Equatorial adjustment in the eastern Atlantic. *Geophys. Res. Lett.*, **5**, 637–640.

Morlière, A., 1970: Les saisons marines devant Abidjan. *Doc. Sci. Centre Rech. Océanogr. Abidjan*, **1**, No. 2, 1–15.

——, and J. P. Rébert, 1973: Etude hydrologique du plateau continental ivoirien. *Doc. Sci. Centre Rech. Oceanogr. Abidjan*, **3**, No. 2, 1–30.

Mysak, L. A., 1967: On the very low frequency spectrum of the sea level on a continental shelf. *J. Geophys. Res.*, **72**, 3043–3047.

——, 1968: Edge waves on a gently sloping continental shelf of finite width. *J. Mar. Res.*, **26**, 24–33.

Mysak, L., 1978a: Long-period equatorial topographic waves. *J. Phys. Oceanogr.*, **8**, 302–314.

——, 1978b: Equatorial shelf waves on an exponential shelf profile. *J. Phys. Oceanogr.*, **8**, 458–467.

——, and B. V. Hamon, 1969: Low frequency sea level behaviour and continental shelf waves off North Carolina. *J. Geophys. Res.*, **74**, 1397–1405.

O'Brien, J. J., D. Adamec and D. W. Moore, 1978: A simple model of upwelling in the gulf of Guinea. *Geophys. Res. Lett.*, **5**, 641–644.

Philander, S. G. H., 1977: The effect of coastal geometry on equatorial waves (forced waves in the Gulf of Guinea). *J. Mar. Res.*, **35**, 509–523.

——, 1978: Upwelling in the Gulf of Guinea. Submitted to *J. Mar. Res.*

Picaut, J., and J. M. Verstraete, 1975: Low-frequency oscillations of temperature and sea level along the coast of the Guinea Gulf. Paper presented at IUGG Congress, Grenoble, 25 August–6 September.

——, and ——, 1976: Mise en évidence d'une onde de 40–50 jours de période sur les côtes du Golfe de Guinée. *Cah. O.R.S.T.O.M., sér. Océanogr.*, **14**, No. 1, 3–14.

Pillsbury, D., R. L. Smith, and R. C. Tipper, 1969: A reliable low coast mooring system for oceanographic instrumentation. *Limnol. Oceanogr.*, **14**, 307–311.

Robinson, A. R., 1964: Continental shelf waves and the response of sea level to weather systems. *J. Geophys. Res.*, **69**, 367–368.

Schott, G., 1944: *Geographie des Atlantischen Ozeans*. Hambourg, 39 pp.

Simon, B., 1974: Calcul des constantes harmoniques de la marée. *EPSHOM*, Brest.

Varlet, F., 1958: Le régime de l'Atlantique près d'Abidjan (C.I.). *Études Éburnéennes*, **7**, 97–222.

Verstraete, J. M., J. P. Picaut and A. Morliere, 1978: Atmospheric and tidal forcing along the shelf of the Guinea Gulf. Paper presented at the GATE Symp., Kiel.

Wunsch, C., 1967: The long period tides. *Rev. Geophys.*, **5**, 447–475.

Cah. O.R.S.T.O.M., sér. Océanogr., vol. XIV, n° 1, 1976

MISE EN ÉVIDENCE D'UNE ONDE DE 40-50 JOURS DE PÉRIODE SUR LES CÔTES DU GOLFE DE GUINÉE

JOËL PICAUT* — JEAN-MARC VERSTRAETE**

* *Laboratoire d'Océanographie Physique. Faculté des Sciences. 29283 Brest. Cedex (France)*
** *C.R.O.-O.R.S.T.O.M. B.P. V 18. Abidjan (Côte d'Ivoire)*

RÉSUMÉ

Des mesures journalières de température de surface et de niveau moyen ont été régulièrement effectuées sur les côtes du Dahomey, Togo, Ghana et Côte d'Ivoire sur des intervalles de temps compris entre 2 et 16 ans. L'analyse spectrale détaillée de ces séries temporelles met en évidence de nombreuses oscillations de périodes comprises entre 6 et 50 jours. L'une des plus importantes, toujours présente aux différents points de mesure, a une période comprise entre 40 et 50 jours. Cette onde serait stationnaire et probablement induite par des oscillations atmosphériques de même période.

ABSTRACT

Long time series (2-16 years) of sea surface temperature and mean sea level from coastal stations located in Dahomey, Togo, Ghana and Ivory Coast have been subjected to spectral and cross-spectral analysis. The investigation detects numerous low frequency oscillations with a period range of 6-50 days. One of the most important appears at each station in the 40-50 days period range. This oscillation would be stationnary and probably induced by atmospheric oscillations in the same period range.

1. Introduction.

Depuis une vingtaine d'années l'O.R.S.T.O.M. effectue des mesures régulières de température de la mer en différents points de la côte du Golfe de Guinée. Ces données chronologiques ont été soumises pour la première fois à l'analyse spectrale; les résultats encourageants nous ont incité à étendre l'analyse aux données météorologiques et marégraphiques. Dans le domaine des basses fréquences, nous mettons en évidence une oscillation de 40 à 50 jours toujours présente aux différents points de mesure. L'utilisation d'un filtre passe-bande a permis de déterminer l'amplitude de cette onde. Les calculs de spectres croisés et des études de corrélation semblent montrer que cette onde est stationnaire.

2. Les séries chronologiques.

Les données traitées couvrent une période comprise entre 1958 et 1974. Elles ont été collectées par l'O.R.S.T.O.M. en Côte d'Ivoire et au Togo, les Services Hydrographiques de Côte d'Ivoire et du Ghana, les Services des Pêches du Ghana et du Dahomey et les Offices Météorologiques de tous ces pays. Les paramètres utilisés pour ces analyses sont : la température de la mer, le niveau de la mer moyen journalier, la pression moyenne journalière au niveau de la mer et le vent moyen. Le tableau I ci-dessous donne la liste des stations et des paramètres mesurés, la durée de chaque série et le nombre de mesures par jour. Les positions de chaque station sont présentées sur la figure 1. Le niveau moyen journalier à Téma et Takoradi est calculé à partir de 24 observations

TABLEAU I

Station	Paramètre	Durée	Nombre de mesures par jour
Cotonou	Température 0-5-10 m	1er avril 1958 - 31 juil. 1974	1
Lomé	Température surface	1er janv. 1958 - 15 fév. 1962 18 juil. 1966 - 31 déc. 1968	1
Téma	Température surface Niveau moyen	1er janv. 1969 - 31 déc. 1973 1er janv. 1969 - 31 déc. 1973	1 24
Takoradi	Température surface Niveau moyen Pression atmosphérique au niveau de la mer	1er janv. 1970 - 31 déc. 1973 1er janv. 1969 - 29 sept. 1973 1er janv. 1962 - 31 déc. 1968	1 24 24
Abidjan	Température 0-5-10-15-20 m Niveau moyen Pression atmosphérique au niveau de la mer Vent	29 mars 1966 - 29 avril 1974 1er janv. 1969 - 31 déc. 1973 1er janv. 1969 - 31 déc. 1973 1er janv. 1966 - 31 déc. 1974	Bi hebdomadaire 4 4 8
Tabou	Température de surface	1er avril 1958 - 31 mars 1960	3

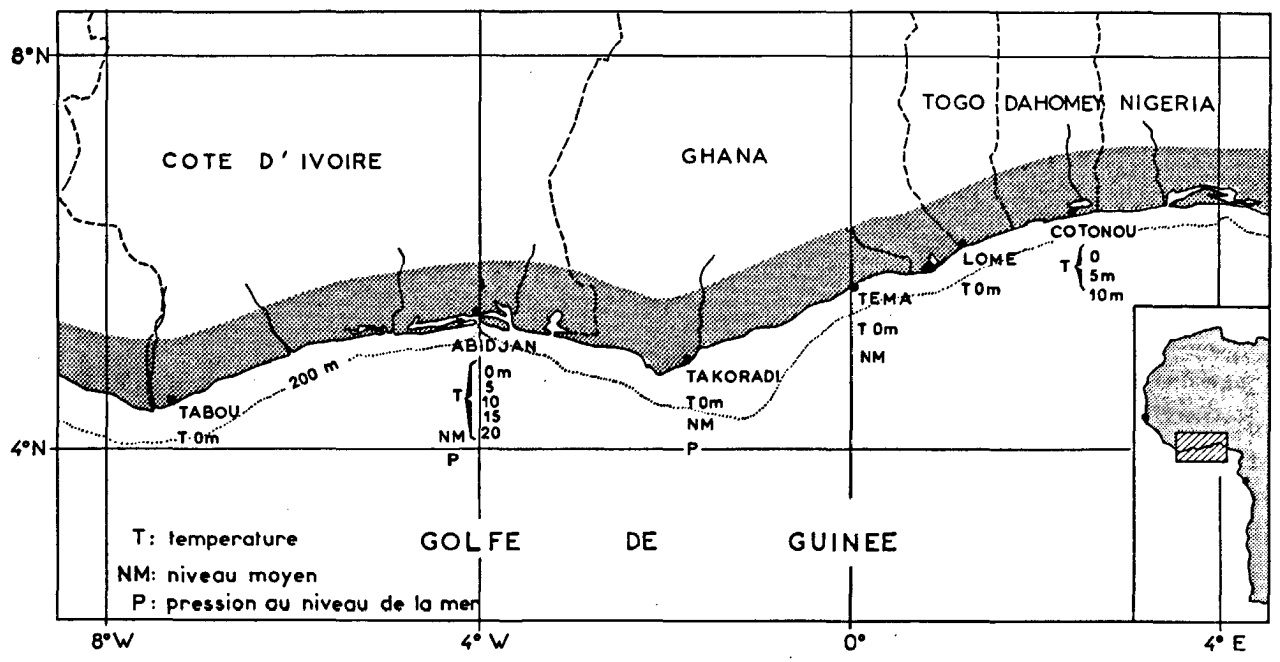

Fig. 1. — Position des stations.

horaires extraites des enregistrements continus de marégraphe; le niveau moyen à Abidjan est calculé à partir des hauteurs des pleines mers et basses mers observées chaque jour au marégraphe.

3. Rappels d'analyse spectrale.

3.1. Traitement d'une série.

Pour mettre en évidence des oscillations privilégiées dans le Golfe de Guinée à l'aide de séries de mesures de longue durée, on a calculé la fonction de densité spectrale; celle-ci est la transformée de Fourier de la fonction d'autocorrélation calculée à partir de séries rendues stationnaires. Les séries analysées sont donc transformées de sorte que leur valeur moyenne soit nulle puis filtrées pour éliminer les termes de période longue devant la série disponible (variations saisonnières). On a essayé divers types de filtres (moyenne mobile, filtrage en sinus intégral, filtrage Hanning); ce dernier a été retenu étant donné son efficacité et son faible temps de calcul.

Soit x(n Δt) la série discrète ainsi obtenue, n variant de o à N. On calcule :

— la fonction d'autocorrélation :

$$C_{xx}(k\Delta t) = \frac{1}{N-k} \sum_{i=k}^{N-k} x(i\Delta t).\, x(i\Delta t - k\Delta t) \quad o < k < M$$

M étant l'indice de décalage maximum.

— la fonction densité spectrale :

$$E_{xx}(f) = 2\,\Delta t\,\delta_k \sum_{i=O}^{M} C_{xx}(i\,\Delta t).\cos\frac{k\,\pi i}{M}.\cos^2\frac{\pi i}{2M}$$

$$\delta_k = \begin{cases} 1/2 & \text{pour } k = o \text{ et } M \\ 1 & \text{pour } k \neq o \text{ et } M \end{cases}$$

Le terme en $\cos^2 \frac{\pi i}{2M}$ correspond à l'utilisation de la fenêtre de filtrage de Tukey. Les valeurs obtenues sont relatives à des fréquences centrées autour de $f = \frac{k}{2M\ \Delta t}$, avec une largeur de bande égale à $\Delta f = \frac{2}{3\ M\Delta t}$ compte tenu de la fenêtre de Tukey. La fonction densité spectrale fournit pour chaque série les fréquences dominantes et les variations d'énergie en fonction de la fréquence.

3.2. Traitement de deux séries simultanées.

Le calcul des spectres croisés permet d'étudier la cohérence et le déphasage entre deux séries simultanées. Soient x(n Δt) et y(n Δt) les deux séries rendues stationnaires. On calcule :

— Les coefficients de corrélation croisée :

$$C_{xy}(k\Delta t) = \frac{1}{N-k} \sum_{i=k}^{N-k} x(i\Delta t).y\ (i\Delta t - k\Delta t)$$

$$C_{yx}(k\Delta t) = \frac{1}{N-k} \sum_{i=k}^{N-k} y(i\Delta t).x\ (i\Delta t - k\Delta t)$$

— Les cospectres E_{xy} et spectres de quadrature E_{yx} :

$$E_{xy}(f) = 2\Delta t\ \delta_k \sum_{i=o}^{M} [C_{xy}(i\Delta t) + C_{yx}(i\Delta t)] \cdot \cos\frac{k\,\pi i}{M} \cdot \cos^2\frac{\pi i}{2M}$$

$$E_{yx}(f) = 2\Delta t\ \delta_k \sum_{i=o}^{M} [C_{xy}(i\Delta t) - C_{yx}(i\Delta t)] \cdot \sin\frac{k\,\pi i}{M} \cdot \cos^2\frac{\pi\, i}{2M}$$

— La cohérence et le déphasage :

$$\text{Coh}(f) = \frac{E^2_{xy} + E^2_{yx}}{E_{xy} \cdot E_{yx}}$$

$$\theta(f) = \text{Arc tg}\ \frac{E_{yx}}{E_{xy}}$$

4. Résultats de l'analyse spectrale de chaque série.

Les spectres sont présentés pour les différentes stations côtières et les différents paramètres. Sur chaque spectre on indique la fréquence de coupure f_c du filtre passe-haut et l'intervalle de confiance à 90 %. La largeur de bande couramment utilisée est égale à 0.0025 cycle par jour. On observe de

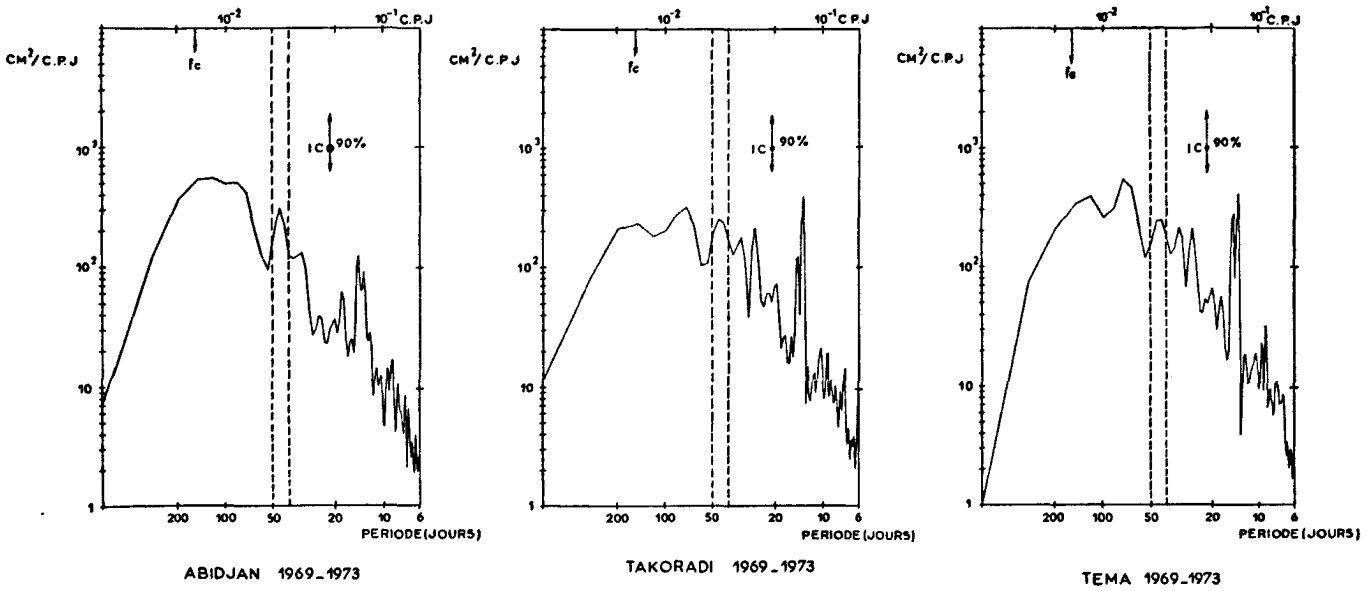

Fig. 2. — Spectres des niveaux moyens corrigés.

nombreux pics pour les périodes comprises entre 6 et 50 jours. Sur toutes les séries étudiées on trouve des pics autour des mêmes périodes : l'un se trouve dans l'intervalle de période 40-50 jours, deux autres pics apparaissent généralement entre 13,5 et 15 jours. L'un correspond à l'onde de marée semi-mensuelle lunaire Mf (13,7 jours), l'autre pourrait être la conjugaison des ondes de marées semi-diurnes M2 et S2 (14,7 jours).

Malgré le filtrage Hanning, on observe sur tous les spectres une forte densité spectrale dans les basses fréquences (variations saisonnières). Pour être certain que les pics observés ne soient pas des harmoniques de cette variation, on a moyenné les 16 années des données de température de Cotonou en une seule année type que l'on a soustrait des données brutes. Mis à part une meilleure décroissance dans les basses fréquences, le spectre ainsi obtenu demeure inchangé.

Cet article étudie plus spécialement les oscillations de périodes comprises entre 40 et 50 jours.

4.1. Niveau moyen (fig. 2).

La mer réagit comme un baromètre inversé aux variations de pressions atmosphériques. Afin de s'affranchir de cet effet direct, il convient d'utiliser le niveau moyen corrigé; celui-ci est défini comme étant le niveau moyen observé auquel on a retiré l'effet de pression barométrique (une augmentation de pression de 1 mb entraîne un abaissement de niveau moyen de 1 cm).

Les spectres d'Abidjan, Takoradi et Téma présentent un pic à 45 jours. Dans le domaine des périodes semi-mensuelles on notera les maxima d'énergie

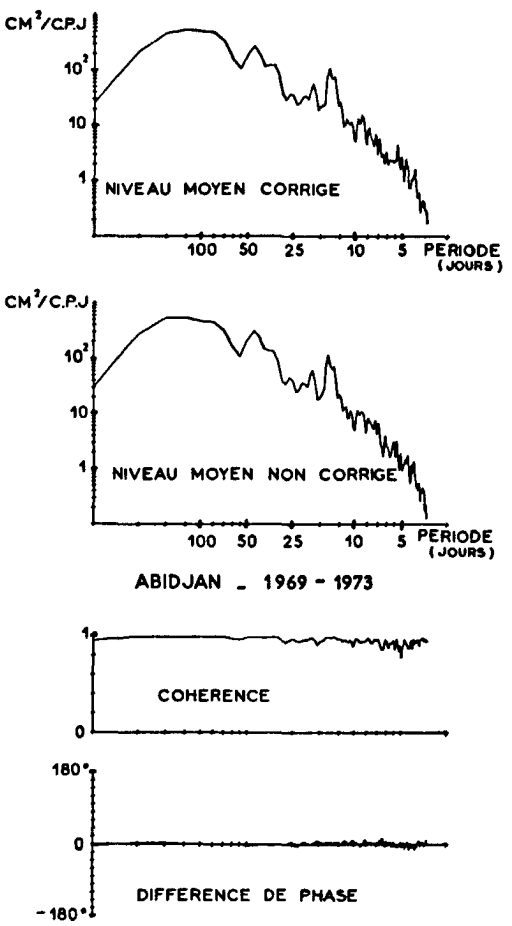

Fig. 3. — Spectres croisés des niveaux moyens corrigé et non corrigé.

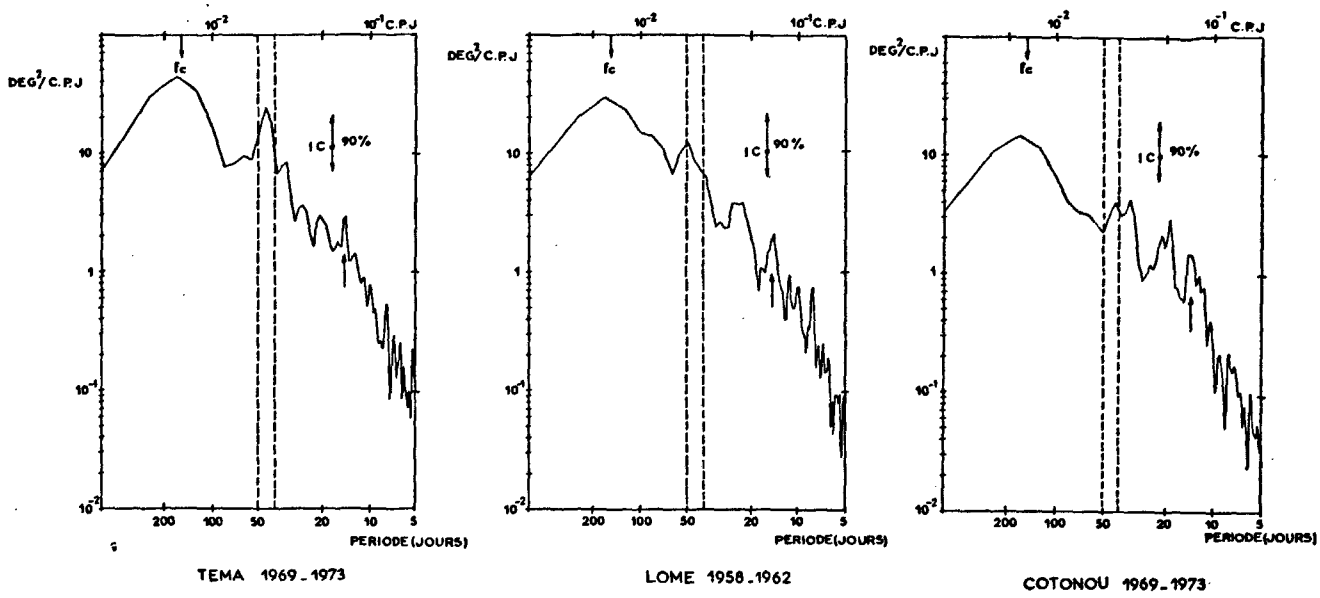

Fig. 4. — Spectres de température.

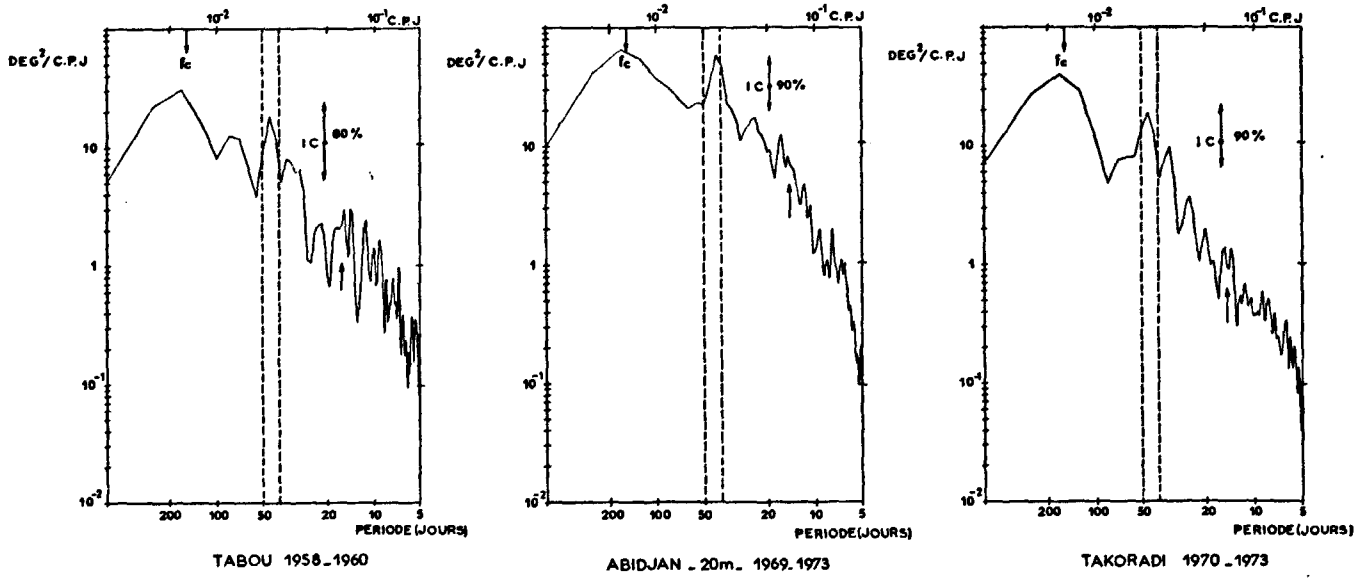

Fig. 5. — Spectres de température.

concentrées exactement à 13,7 et 14,7 jours, le pouvoir de résolution utilisé ici ($\Delta f = 0.0022$ cycle par jour) nous autorise à séparer ces deux pics. Afin d'évaluer l'importance de la pression barométrique sur le niveau moyen, nous avons effectué l'analyse spectrale croisée sur les niveaux moyens corrigé et non corrigé. La figure 3 montre la remarquable cohérence et l'absence de déphasage entre ces deux séries.

4.2. Température (fig. 4 et 5).

Les spectres de température de surface montrent qu'il y a moins de variance à Cotonou qu'aux autres stations, particulièrement dans les basses fréquences. Les oscillations ne concernent pas seulement la surface : avec les données d'Abidjan, on a trouvé environ 5 fois plus de variance à 20 mètres qu'en surface. Sur ces six stations on trouve en permanence

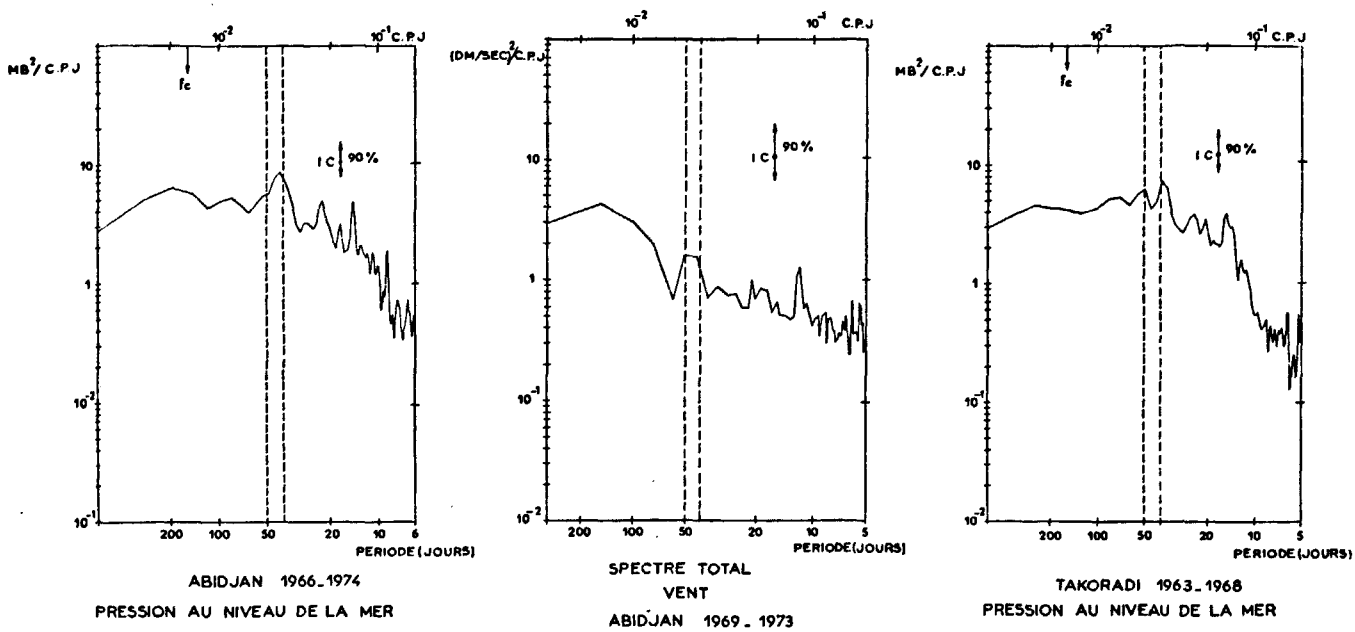

Fig. 6. — Spectres des données météorologiques.

un pic de variance entre 42 et 49 jours, significatif à 90 % à Abidjan, Takoradi, Téma. On notera que cette oscillation autour de 45 jours est observée depuis 1958; elle apparaitrait comme un phénomène permanent.

Avec les températures, il n'a pas été possible en général de séparer les deux périodes bimensuelles; les flèches sur les figures indiquent le pic commun.

4.3. Données météorologiques (fig. 6).

Les spectres de la pression barométrique au niveau de la mer à Abidjan et Takoradi présentent un pic vers 40 jours. Il est remarquable de retrouver ce même pic avec les données de vent au sol à Abidjan. Madden et Julian (1972) ont étudié les données météorologiques (pression à différents niveaux, vents en altitude) en de nombreuses stations de la zone tropicale; ils ont mis ainsi en évidence une onde atmosphérique de période 40-50 jours intéressant principalement le Pacifique et l'Océan Indien. Selon leur conclusion, cette oscillation serait le résultat d'une circulation cellulaire à grande échelle se déplaçant vers l'Est dans le plan équatorial.

5. Données filtrées.

En vue de déterminer l'amplitude de cette oscillation de 40-50 jours on a soumis toutes les séries chronologiques à un filtre passe-bande centré

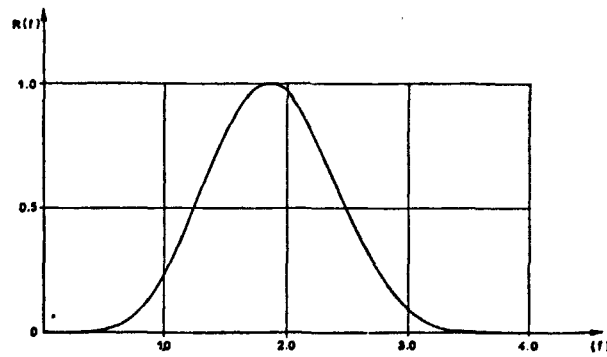

Fig. 7. — Réponse du filtre passe-bande.

à 45 jours, dont la réponse est présentée sur la figure 7. Les fréquences de coupure (réponse 1/2) correspondent aux périodes 34 et 68 jours. Les oscillations de 45 jours apparaissent nettement sur toutes les séries de données filtrées; leur amplitude pour les températures de surface est d'environ 1,5 °C; on note que l'amplitude est moins importante à Cotonou que pour toutes les autres stations ce qui confirme ce résultat déjà obtenu par l'analyse spectrale. Il existe une très remarquable concordance entre les variations de température à Tema et Takoradi bien que ces deux stations soient distantes de plus de 200 km (fig. 8).

Les amplitudes des oscillations du niveau moyen

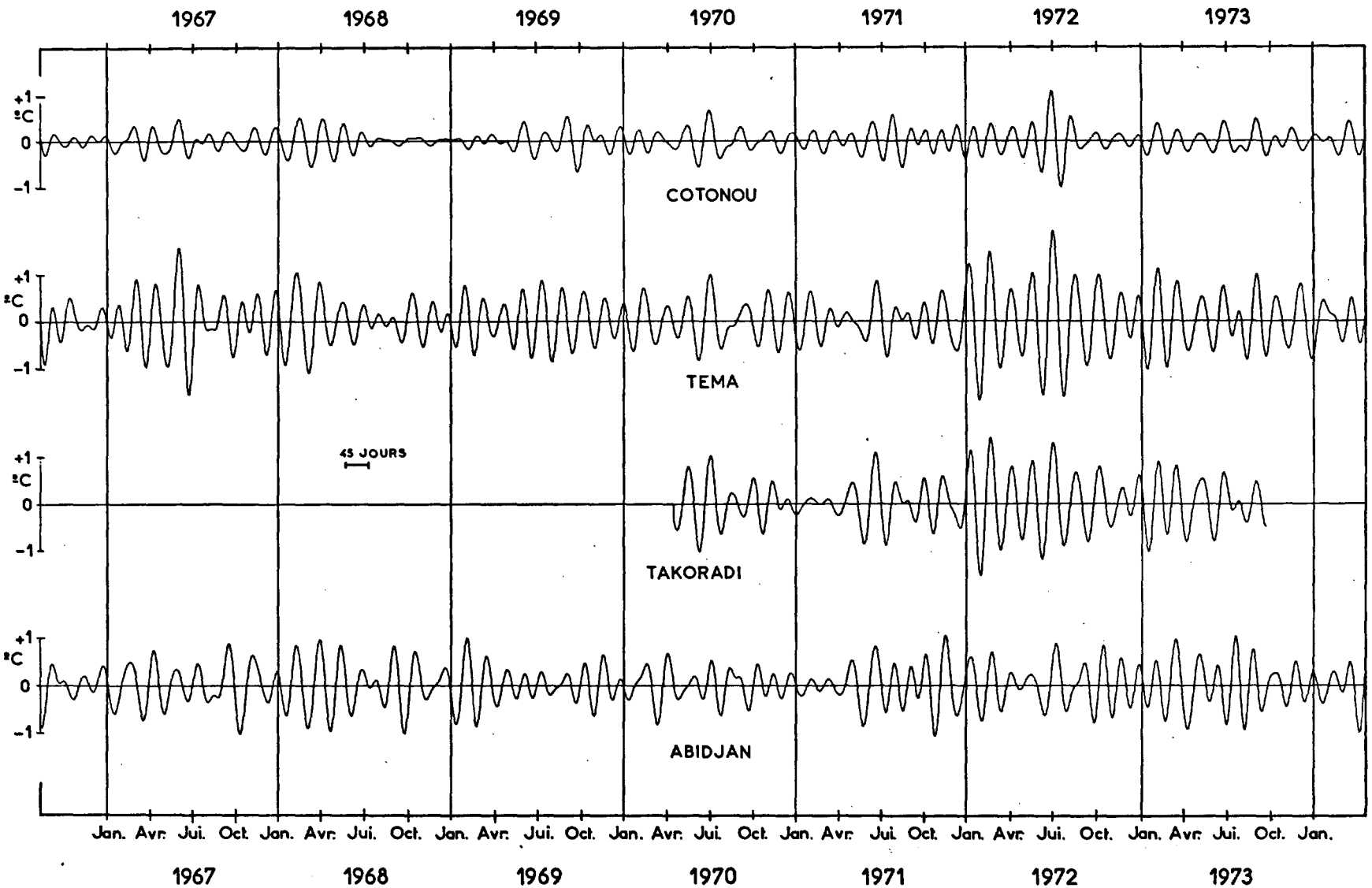

Fig. 8. — Données filtrées.

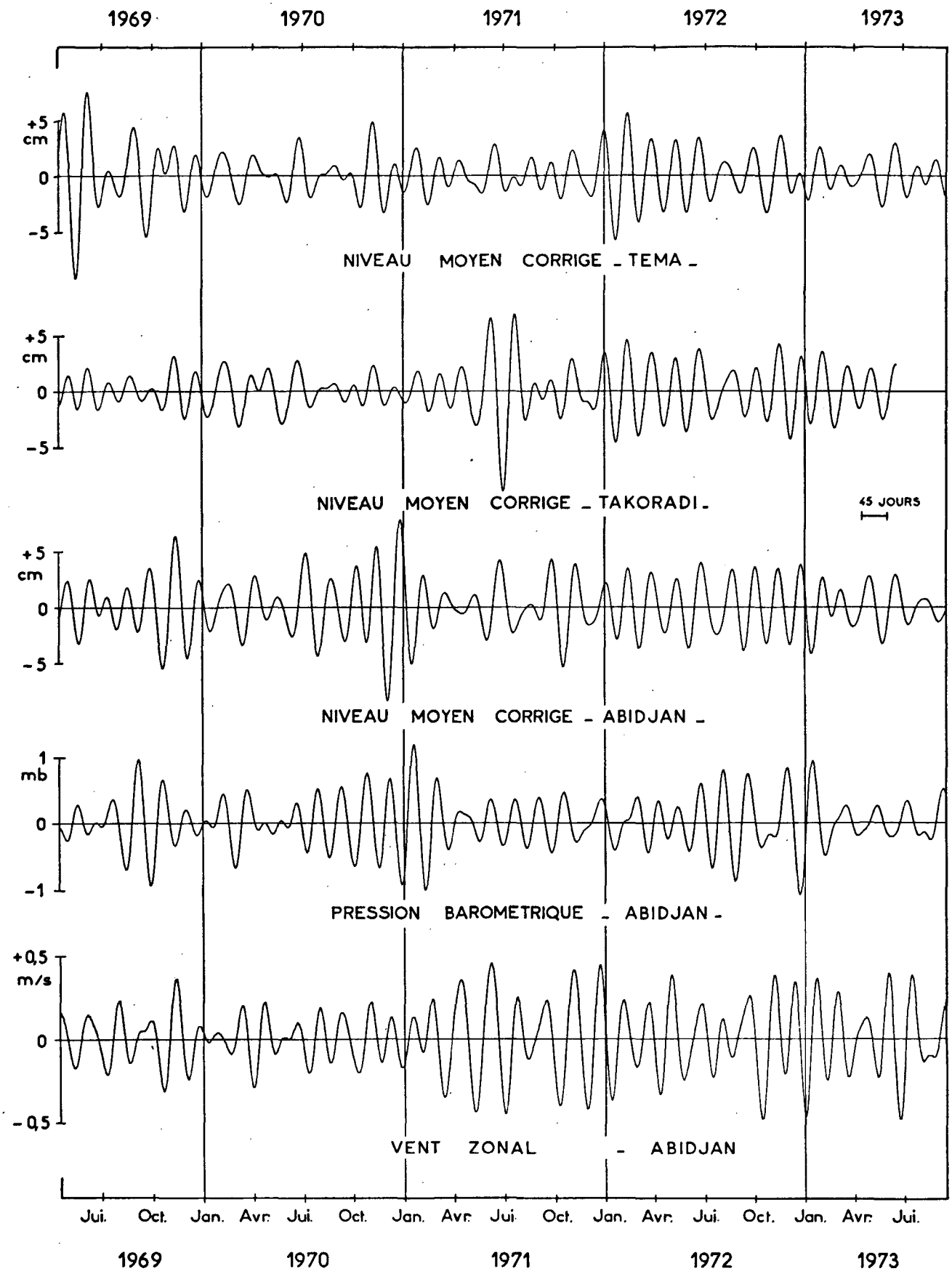

Fig. 9. — Données filtrées.

TABLEAU II

Analyse spectrale

TEMPÉRATURE : RÉFÉRENCE COTONOU

LOMÉ	TEMA	TAKORADI	ABIDJAN	TABOU
5° ± 12°	0° ± 33°	— 11° ± 35°	— 12° ± 46°	— 27° ± 70°

NIVEAU MOYEN CORRIGÉ : RÉFÉRENCE TEMA

TAKORADI	ABIDJAN
— 9° ± 38°	— 40° ± 43°

corrigé, de la pression barométrique et du vent zonal sont respectivement de 8 cm, 1,6 mb, et 0,7 m/s (fig. 9).

6. Analyse de l'oscillation de période 40-50 jours.

Afin de déterminer les caractéristiques de cette oscillation, nous avons calculé la cohérence et le déphasage par paires de stations d'une part et par paires de paramètres en une même station d'autre part.

6.1. ANALYSES ENTRE DIFFÉRENTES STATIONS.

Comme les mesures de température de surface à Cotonou recouvrent toutes les autres séries, nous avons utilisé cette série chronologique comme référence. On a donc calculé la cohérence et le déphasage entre les différentes stations côtières et Cotonou ; bien que la station de Cotonou soit moins sensible au phénomène étudié, la cohérence est toujours élevée pour cette période. S'il y a propagation, le déphasage doit croître en fonction de la distance à la station de référence.

Pour contrôler les résultats obtenus avec les températures de surface, on a fait les mêmes calculs avec les niveaux moyens corrigés disponibles aux trois stations de Téma, Takoradi et Abidjan. Le tableau II présente l'ensemble des résultats avec l'intervalle de confiance à 90 %. Compte tenu de l'incertitude sur chacun des déphasages, l'analyse

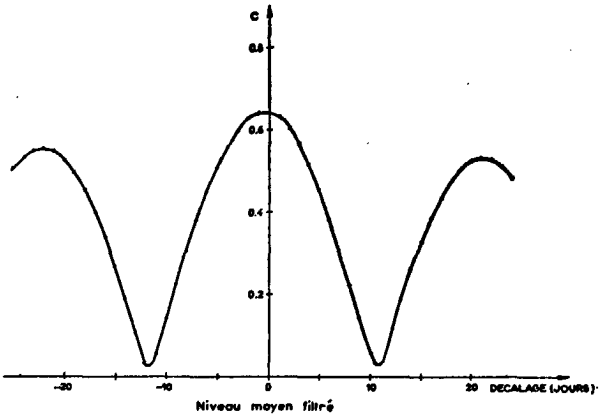

Fig. 10. — Corrélation après filtrage. Takoradi-Tema 1970-1973.

TABLEAU III

Analyse de corrélation

TEMPÉRATURE : RÉFÉRENCE COTONOU

LOMÉ	TEMA	TAKORADI	ABIDJAN	TABOU
— 1	0	+ 2	+ 1	— 2

NIVEAU MOYEN CORRIGÉ : RÉFÉRENCE TEMA

TAKORADI	ABIDJAN
0	+ 5

TABLEAU IV

NIVEAU MOYEN CORRIGÉ - TEMPÉRATURE

Type d'analyse \ Station	TEMA	TAKORADI	ABIDJAN
Spectres croisés.....	— 12° ± 25°	— 28° ± 37°	8° ± 45°
Corrélation.....	+ 2	— 4	— 1

PRESSION BAROMÉTRIQUE - ABIDJAN

Type d'analyse \ Type de données	Temp. 20 m	Niveau moyen	Vent zonal
Spectres croisés.....	— 154° ± *	— 170° ± 31°	— 16° ±*
Corrélation.....	+ 18	— 20	+ 4

* Intervalle de confiance indéterminé.

spectrale seule, ne permet pas de se prononcer sur la nature stationnaire ou progressive de cette onde.

Pour lever ce doute nous avons effectué la corrélation entre les deux séries après les avoir soumises au filtre passe-bande centré sur 45 jours. Sur la figure 10 on a représenté le coefficient de corrélation ainsi obtenu pour différents décalages de temps entre la série considérée et la série de référence. Les figures 8 et 9 montrant clairement une oscillation de 45 jours, il est logique de retrouver des maxima de corrélation voisins distants d'une demi période. Ces calculs ont été faits avec un décalage maximum de ± 60 jours. Sur le tableau III, on donne le décalage en jours correspondant au maximum absolu du coefficient de corrélation. Les données ayant été filtrées au préalable et de ce fait non indépendantes, il n'a pas été possible de faire un calcul d'erreur sur les valeurs présentées.

Sur les tableaux II et III, les signes pour les déphasages ont la même signification : un signe $> o$ correspond à une propagation vers l'Est, un signe < 0 à une propagation vers l'Ouest. Il apparaît

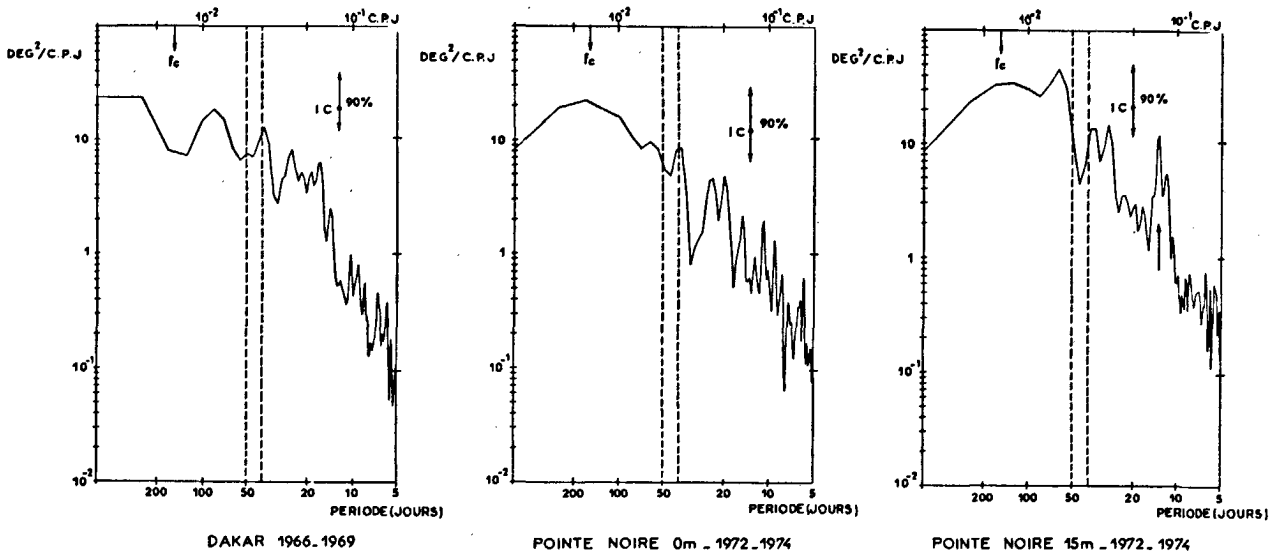

Fig. 11. — Spectres de température.

alors que les déphasages sont distribués de façon aléatoire autour de zéro, ce qui tendrait à montrer que cette onde est stationnaire.

6.2. ANALYSES À LA MÊME STATION.

Le tableau IV résume les résultats des analyses de spectres croisés et de corrélation après filtrage effectuées sur les différentes paires de paramètres :

— le niveau moyen corrigé et la température sont en phase;

— la pression barométrique est en opposition de phase avec le niveau moyen corrigé;

— la pression barométrique est en phase avec le vent zonal au niveau du sol; ce résultat est en accord avec celui trouvé par MADDEN et JULIAN (1972) dans l'île de Canton dans le Pacifique équatorial.

7. Extension à d'autres stations de la zone équatoriale.

Devant les résultats obtenus, il était intéressant de contrôler si ces phénomènes aux basses fréquences apparaissent ou non en des points éloignés de la zone comprise entre Tabou et Cotonou. Comme il n'était pas possible de reprendre une étude détaillée, nous donnons seulement les spectres de densité spectrale obtenus à l'aide des températures journalières mesurées aux stations côtières de Dakar Thiaroye (1966-1969) et de Pointe Noire (1972-1974) (fig. 11). On relève un pic d'énergie spectrale à 38,5 jours à Dakar et à Pointe Noire. Comme on l'a noté à Abidjan, la variance est beaucoup plus élevée au fond qu'en surface. Le spectre de Pointe Noire à 15 m de profondeur met en évidence un pic très important à 13,2 jours, très voisin de la période lunaire bimensuelle Mf. Il faudrait bien entendu reprendre l'étude de ces stations avec les données météorologiques et marégraphiques.

Ces résultats sont à rapprocher des observations de courant faites par BYSHEV et CHEKOTILLO (1974) pendant 198 jours par 16°30′ N et 33°30′ W en 1970. Ils mettent en évidence par l'analyse de Fourier des oscillations de courant dont les périodes sont comprises entre 36 et 68 jours sur 10 niveaux de 25 mètres à 1500 mètres.

8. Discussion.

Cette étude montre l'existence de nombreuses oscillations basses fréquences sur les côtes du Golfe de Guinée, dont une très importante de période 40-50 jours. L'extension géographique de ce phénomène doit être très importante, puisque les premiers résultats obtenus par l'analyse spectrale des données de stations aussi éloignées que Dakar et Pointe Noire présentent des oscillations de même période. Les mesures de courant faites par 33°30′ W par BISHEV et SHEKOTILLO (1974) semblent indiquer que cette oscillation concerne l'ensemble de l'Atlantique intertropical.

L'étude des déphasages tend à prouver que cette onde est stationnaire.

L'origine de cette onde semble être atmosphérique, si l'on se base sur les pics d'énergie trouvés à l'aide des données météorologiques. Il faut cependant noter que les pics d'énergie obtenus, soit avec la pression barométrique, soit avec le vent sont nettement moins accusés que ceux obtenus à l'aide des paramètres océanographiques. Cette différence se retrouve clairement sur les données filtrées. De plus les calculs de spectres croisés entre niveaux moyen corrigé et non corrigé montrent leur très forte cohérence et leur faible déphasage. Ceci nous amène à émettre l'hypothèse que cette oscillation d'environ 45 jours de période serait créée par un phénomène de résonance du bassin océanique constitué par le Golfe de Guinée sous l'excitation d'une onde atmosphérique.

Les expériences GATE faites en 1974 ont mis en évidence des oscillations de très grande longueur d'onde à l'équateur (2500 km, 16-18 jours de période). Les mesures étaient de trop courte durée pour permettre d'atteindre de plus longues périodes. On ne peut exclure que des ondes de très basses fréquences soient piégées à l'équateur et affectent les conditions hydrologiques des zones côtières avoisinantes.

Des mesures de courant de très longue durée (minimum un an) en différents points fixes le long de la côte permettraient de déterminer la nature exacte de ces ondes et leur rôle dans les variations hydrologiques importantes constatées.

Manuscrit reçu au S.C.D. de l'O.R.S.T.O.M. le 28 novembre 1975.

BIBLIOGRAPHIE

BLACKMAN (R. B.) and TUCKEY (J. W.), 1958. — The measurement of power spectra. Dover Publ., New York.

BYSHEV (V. I.) and CHEKOTILLO (K. A.), 1974. — A statistical analysis of certain current-velocity measurements in the north atlantic. Izv., *Atmospheric and Oceanic Physics*, vol. 10, n° 3 : 266-275.

DUING (W.) and EVANS (R.), 1975. — Long westward waves in the Equatorial Atlantic. GATE Report, n° 14, vol. 1 : 30-319.

MADDEN (R. A.) and JULIAN (P. R.), 1971. — Detection of a 40-50 day oscillation in the zonal wind in the tropical Pacific. *J. Atmos. Sci.*, 28 : 702-708.

MADDEN (R. A.) and JULIAN (P. R.), 1972. — Description of global - scale circulation in the tropics with a 40-50 day period. *J. Atmos. Sci.*, 29 : 1109-1123.

MAZÉ (R.), 1973. — Recherche et étude de mouvements à période propre du domaine des ondes internes dans l'Iroise. Thèse 3e cycle. Fac. Sc., Brest.

MUNK (W. H.), SNODGRASS (F. E.) and TUCKER (M. J.), 1959. — Spectra of low frequency ocean waves. *Bull. Scripps Inst. Oceanogr.*, 7 (4) : 283-362.

Deep-Sea Research GATE
Supplement II to Volume 26

ATMOSPHERIC AND TIDAL OBSERVATIONS ALONG THE SHELF OF THE GUINEA GULF

Jean-Marc Verstraete*, Jöel Picaut** and Alain Morliere*

(received 1 August 1978; revised 23 February 1979)

Abstract—In order to investigate an extensive set of large-scale ocean-atmosphere events in the Guinea Gulf, we present the following time series: sea level, daily sea surface temperature at the coast, sea temperature at a thermistor chain mooring and atmospheric pressure and wind as measured at the different coastal stations for up to 20 years. We present the mean values of the different parameters of these time series and we identify the different components of the tidal forcing in the Gulf, between the sixth diurnal and the long-period components.

INTRODUCTION

The long time series collected at different coastal stations along the coast of the Gulf of Guinea provide some useful information about the tidal and atmospheric forcing and the amplitude of the seasonal cycle in this area.

From a meteorological point of view, the Gulf of Guinea is situated between the intertropical convergence zone (ITCZ) and the high pressure of the St. Helena anticyclone in the Southern Hemisphere. The core of this anticyclone oscillates around the Tropic of Capricorn, moving northward during the southern winter and southward during the southern summer. The southeast trade winds generated by this anticyclone have a mean speed of 5 to 8 m s^{-1}, cross the equator in the Guinea Gulf and move toward the low pressure field of the Sahara. Consequently, the Gulf will have winds predominantly from the south to the southwest; during the southern winter, the winds are stronger and the Gulf is subjected to the monsoon.

* Office de la Recherche Scientifique et Technique Outre-Mer
** Laboratoire d'Océanographie Physique - Université de Bretagne Occidentale

J. -M. Verstraete, J. Picaut and A. Morliere

The ITCZ forms the frontier between the Saharan climatic zone and the monsoon area. Each year within 8 months, the ITCZ moves from 5 to 6 degrees north latitude in January to 20 or 22 degrees north in September; the southward "migration" of the ITCZ is faster, occurring within the 4 months from mid-September to January.

The most energetic disturbances along the northern coast of the Gulf are generated by easterly waves in the lower troposphere progressing westwards. These disturbances have wavelengths varying from 1500 to 4000 km and periods from 2.2 up to 5.5 days (Burpee, 1976); they are characterized by bursts of east wind of relatively short duration. These westward wave motions are observed on the northern coastline of the Gulf between March and mid-July and between October and mid-December; during the monsoon season, they increase and weaken the monsoon alternately, giving to it an intermittent character.

By comparison with the high latitudes, the atmospheric forcing in the Gulf is very regular and not subject to sudden and dramatic changes. Therefore, the tide gauge data from this meteorologically quiet area have very low background noise; they provide an adequate basis to develop further understanding of the fundamental modes of oscillation in the eastern tropical Atlantic and the possible effects of coastal geometry on equatorial waves (Philander, 1977).

The purpose of this paper is to document some characteristic features of the Guinea Gulf area, specifically the large seasonal signals observed both in the ocean (temperature and sea level) and in the atmosphere (sea-level wind and pressure).

THE DATA

We have analyzed the data collected at 27 coastal stations between 15°N and 15°S (Tables 1 and 2). The time series generally cover the period 1970-1976 and encompass the GATE period of 1974. At certain stations it was possible to obtain much longer time series. The time series used for the various analyses are: the barometric pressure, the wind, the sea temperature and the sea level. Referring to Tables 1 and 2:

a) The beach ocean temperatures are daily simultaneous observations between 8 AM and 10 AM; they are collected by the Fishery Research Unit in Ghana, the Service des Peches in Benin and the different ORSTOM Centres on the Western African Coast.

b) The sea temperature on the shelf off Abidjan (Port-Bouet) has been measured with an AANDERAA 50 m thermistor chain in water 65 m deep. The mooring was equipped with subsurface buoys 12 m deep. The mooring was maintained from February 11 to July 25, 1977.

c) The mean sea levels are extracted from continuous records obtained at the different hydrographic services of Togo, Ghana and Ivory Coast. Figure 1 shows the position of the 27 stations and the parameters collected at each station. We have also used the NOAA data (1860-1972) for the wind at sea.

Guinea Gulf Observations

TABLE I Oceanographical data.

State	Location	Parameter	Date Length	Time Origin	Remarks
ANGOLA	LOBITO	S.S.T.	5 years	1968	Bucket sample; 10.00 AM
	LUCIRA	S.S.T.	3 years	1969, August	Bucket sample; 9.00 AM
BENIN	COTONOU	S.S.T.	20 years	Apr 1, 1958	Nansen bottle; 0, 5, 8 m depths; T,S; 8.00 AM; wharf
CONGO	POINTE-NOIRE	S.S.T.	11 years	1964	Bucket sample; 9.00 AM
GABON	MAYUMBA	S.S.T.	3.5 years	1955, Feb	Bucket sample; 9.00 AM
GHANA	KETA	S.S.T.	9 years	May 1, 1968	Bucket Sample; T,S; 8.00 AM; beach
	TEMA	S.S.T.	14 years	Jan 1, 1963	Bucket sample, T,S; 8.00 AM; harbour breakwater
		S.L.	8 years	Jan 1, 1969	Mean of 24 hourly observations
		S.L.	1 year	Jan 1, 1976	Hourly observations
	WINNEBA	S.S.T.	7 years	Jan 1, 1970	Bucket sample; T,S; 8.00 AM; beach
	TAKORADI	S.S.T.	9 years	May 1, 1968	Bucket sample; T,S; 8.00 AM; beach
		S.L.	8 years	Jan 1, 1969	Mean of 24 hourly observations
	CAPE THREE POINTS	S.S.T.	3 years	Jan 1, 1974	
	PRINCESTOWN	S.S.T.	5 years	May 1, 1968	Bucket sample; T,S; 8.00 AM; beach; station closed down and replaced by CAPE THREE POINTS
	AXIM	S.S.T.	9 years	May 1, 1968	Bucket sample; T,S; 8.00 AM; beach
	HALF ASSINI	S.S.T.	8 years	Jan 1, 1969	Bucket sample; T,S; 8.00 AM; beach
IVORY COAST	ABIDJAN	T	12 years	March 29, 1966	Twice a week; Nansen bottle; 0, 5, 10, 15, 20 m depths; T,S; 9.30 AM; in 30 m water depth
		T	165 days	Feb 11, 1977	Thermistor chain; 14-59 m depths; Δt=20 mins; in 66 m water depth
		S.L.	10 years	Jan 9, 1967	High and low tides
		S.L.	1 year	Jan 1, 1971	Hourly measurements
		S.L.	27 months	Jan 1, 1974	Hourly measurements
	SASSANDRA	S.L.	304 days	Jan 5, 1965	High and low tides
	SAN PEDRO	S.L.	50 months	Apr 1, 1973	High and low tides; 10 percent of gaps
	TABOU	S.S.T.	21 months	Apr 1, 1958	Bucket sample; T; 6.00 AM; 12.00, 6.00 PM; beach
		S.S.T.	10 months	Aug 18, 1968	Bucket sample; T; 7.00 AM; beach; 20 percent of gaps
LIBERIA	MONROVIA	S.L.	338 days	Sept 22, 1953	Hourly measurements
SENEGAL	THIAROYE	S.S.T.	11 years	1966	Bucket sample; 8.00 AM
	GOREE	S.S.T.	4 years	1947	Bucket sample; 8.00 AM
			4 years	1952	Bucket sample; 8.00 AM
			4 years	1965	Bucket sample; 8.00 AM
	M'BOUR	S.S.T.	25 years	1952	Bucket sample; 8.00 AM
TOGO	KPEME	S.S.T.	6 years	Jan 1, 1970	Nansen bottle; T,S; 8.00 AM, 12.00, 4.00 PM; wharf
	LOME	S.S.T.	3 years	Jan 1, 1951	Nansen bottle; T,S; 8.00 AM, 10.00, 4.00 PM; wharf
		S.S.T.	2 years	Jan 9, 1967	Nansen bottle; T,S; 8.00 AM; wharf
		S.L.	2 years	Jan 9, 1966	High and low tides; 4 percent of gaps
		S.L.	6 years	Feb 6, 1970	High and low tides; 5 percent of gaps

d) The meteorological data were collected by the ASECNA Office and the British Meteorological Office. The sampling rate is 3 hrs at the coastal stations and 6 hrs at St. Helena.

TABLE 2 Meteorological data.

	Location	Parameter	Date Length	Time Origin	Remarks
BENIN	COTONOU	Wind	6 years	1970	Sampling rate: 3 hrs
CONGO	POINTE-NOIRE	Wind	6 years	1970	Sampling rate: 3 hrs
		Pressure	4 years	1973	Daily mean pressure
GABON	LIBREVILLE	Wind	6 years	1970	Sampling rate: 3 hrs
	PORT-GENTIL	Wind	6 years	1970	Sampling rate: 3 hrs
	MAYUMBA	Wind	6 years	1970	Sampling rate: 3 hrs
GHANA	TAKORADI	Pressure	14 years	1962	Daily mean pressure
	TEMA	Pressure	9 years	1967	Daily mean pressure
GREAT BRITAIN	St HELENA ISLAND	Wind	15 years	1961	0 hr, 6 hr, 12 hr, 18 hr
		pressure	15 years	1961	0 hr, 6 hr, 12 hr, 18 hr
	ASCENSION ISLAND	Wind	10 years	1961	0 hr, 6 hr, 12 hr, 18 hr
		Pressure	10 years	1961	0 hr, 6 hr, 12 hr, 18 hr
IVORY COAST	TABOU	Wind	6 years	1970	Sampling rate: 3 hrs
	SASSANDRA	Wind	6 years	1970	Sampling rate: 3 hrs
	ABIDJAN	Wind	9 years	1966	Sampling rate: 3 hrs
		Barometrical pressure	9 years	1966	Sampling rate: 3 hrs
	ADIAKE	Wind	6 years	1970	Sampling rate: 3 hrs
SENEGAL	DAKAR	Wind	11 years	1966	Sampling rate: 3 hrs
TOGO	LOME	Pressure	11 years	1966	Barometrical pressure at 9.00 AM
		Wind	6 years	1970	Sampling rate: 3 hrs
U.S.A.	N.O.A.A. :	Wind data 1850-1972			

Most of the time series display a large seasonal cycle. Figures 2, 3 and 10 show the mean annual curves for the longest time series: the sea-surface temperature (SST) at Tema and Cotonou (Fig. 2); the mean sea level at Tema, Takoradi and Abidjan (Fig. 3); the barometric pressure at Abidjan and St. Helena (Fig. 10). After a Fourier analysis of the "mean year," it was possible to reconstitute the seasonal cycle with only the three first harmonics (superimposed smooth curves), because the fundamental is not purely sinusoidal. The annual cycle at one station exists but is deformed by other annual events out of phase; for example, the SST variations at Tema can be explained by the superposition of annual events: the coastal upwelling (July-September) off Ghana and the Ivory Coast; the influence of advection from two hemispheres (Merle, Fieux and Hisard, 1979); and the vertical displacements of the thermocline by geostrophic adjustment as a consequence of the annual intensity changes of the Guinea Current (Bakun, 1978; Philander, 1978).

Guinea Gulf Observations

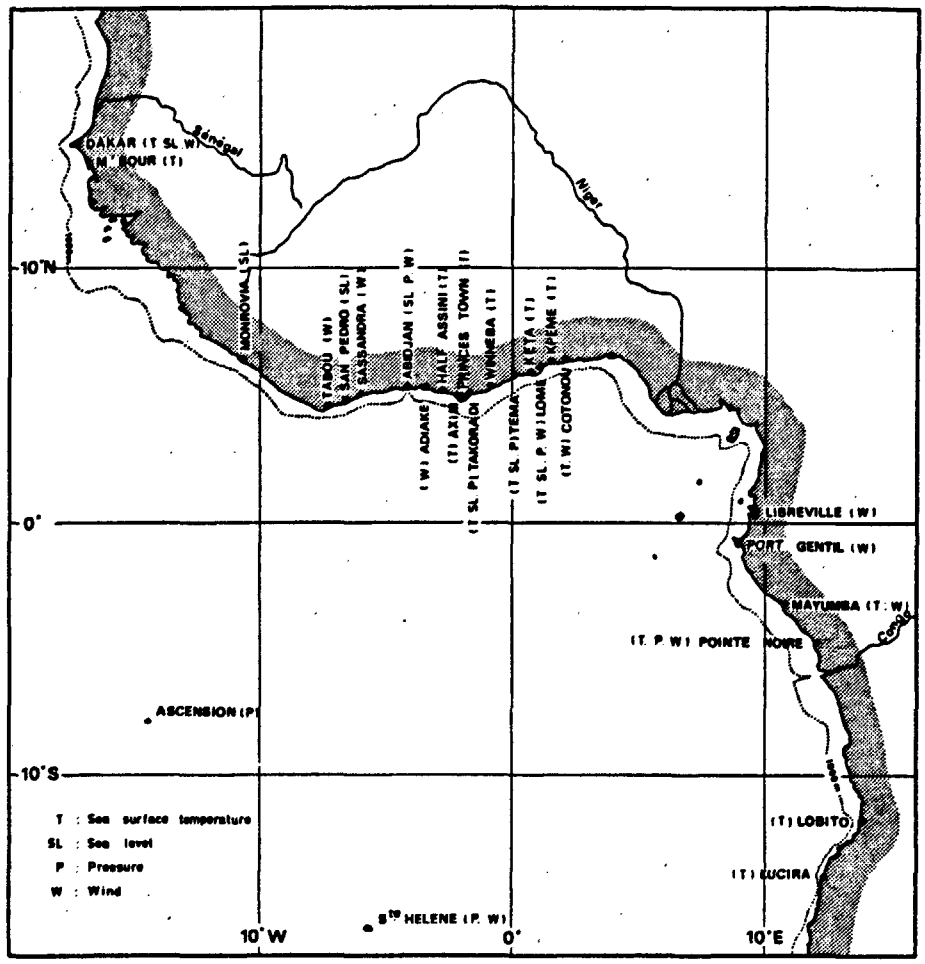

Fig. 1. Location of the coastal stations along the Western African coast.

SEASONAL VARIATION OF THE OCEAN ALONG THE COAST OF THE GULF OF GUINEA

Along the northern coast of the Gulf, the two stations where the SST time series are the longest deserve special attention. We have plotted (Fig. 2) the mean of all the SST at Cotonou (20 yrs) and Tema (14 yrs). The mean annual amplitude is 8°C at Tema and 5°C at Cotonou. At the two stations, the maximum SST occurs in April-May, the minimum in late August.

The onset of the coastal upwelling is clearly evident at Tema between 15 June and 10 July. For more than 3 months, from late June to early October, the SST is cooler than the annual mean. At the same time, we do not observe any acceleration of the coastal winds either for the meridional component or the zonal component (Fig. 8). The maximum of the

wind speed in the area between 2°E and 10°W and between 4°N and the coast occurs in mid-July (Fig. 9) after the onset of the coastal upwelling.

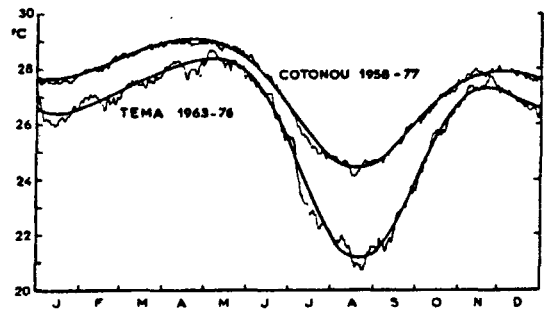

Fig. 2. Mean yearly means of the SST; the superimposed curves are the sum of the 3 first harmonics of the "mean years."

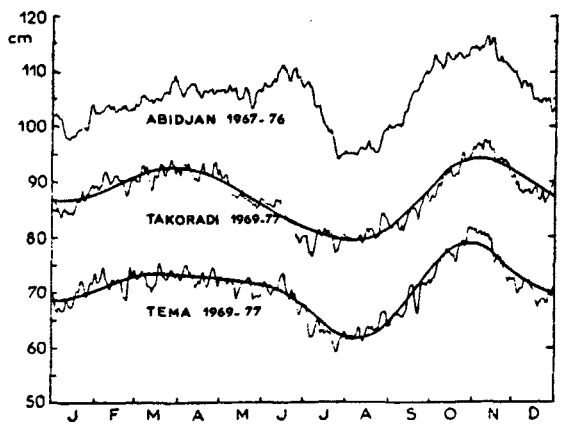

Fig. 3. Same as Figure 2, with the mean sea levels.

We have also studied the mean of the mean sea levels observed at Tema (9 yrs), Takoradi (9 yrs) and Abidjan (19 yrs) (Fig. 3). There is evidence of an annual event with a mean amplitude of about 20 cm at the three stations. The minimum lies during the upwelling season between late July and early August, about one month before the minimum

of the SST and the maximum is in nearly mid-November. Since most of the very low frequency seasonal change in coastal sea level is probably the result of isostatic adjustment, it is evident that the cooling of the deep waters on the shelf occurs about one month before the time of the observed SST minimum. The onset of the upwelling in the deep water on the shelf appears clearly in Figure 11, first in mid-June and second in mid-July. The regular oscillations of the isotherms change suddenly after mid-May, and we observe a general upward trend of all the isotherms for about one month. The same phenomenon occurs after 1 July. These observations show clearly the nonsteadiness of the upwelling and that the upwelling is not correlated with the local winds.

TIDAL ANALYSIS

To give an idea of the complexity of the tidal spectrum, we have classified (Fig. 4) the principal components observed along the northern coast of the Gulf. Each line has been calculated for four observation points (Monrovia, Abidjan, Tema and Takoradi) and is the mean of the harmonic analysis at these harbors. We note the presence of approximately 20 components of amplitude greater than 5 mm, above the background noise, and the dominance of the semi-diurnal components M2 and S2.

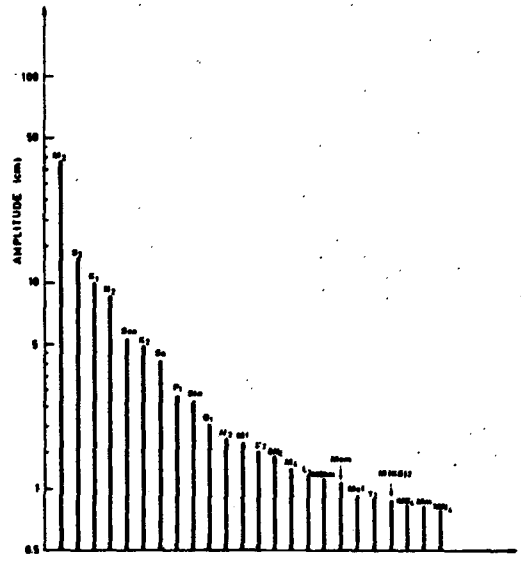

Fig. 4. Mean amplitude of the main tidal components at four harbors of the northern coast of the Guinea Gulf.

The four principal semi-diurnal components are M2, S2, N2, K2; the three principal diurnal components are K1, P1, O1. We also note the high number of nonlinear components such as M4, MS4 and Msf in the low frequency range.

The frequencies in the spectrum of the ocean tides are those of the lunar-solar potential. This spectrum is well known and is composed of a distinct combination of lines distributed in groups: long-periods, diurnals, semi-diurnals and third-diurnals. Figures 5 and 6, generously provided by B. Simon (Epshom - Brest), give a detailed graphic representation of the different groups observed at Abidjan in 1974-75. In Figure 5, we observe the diurnal, semi-diurnal, third-diurnal groups of the lunar-solar potential family.

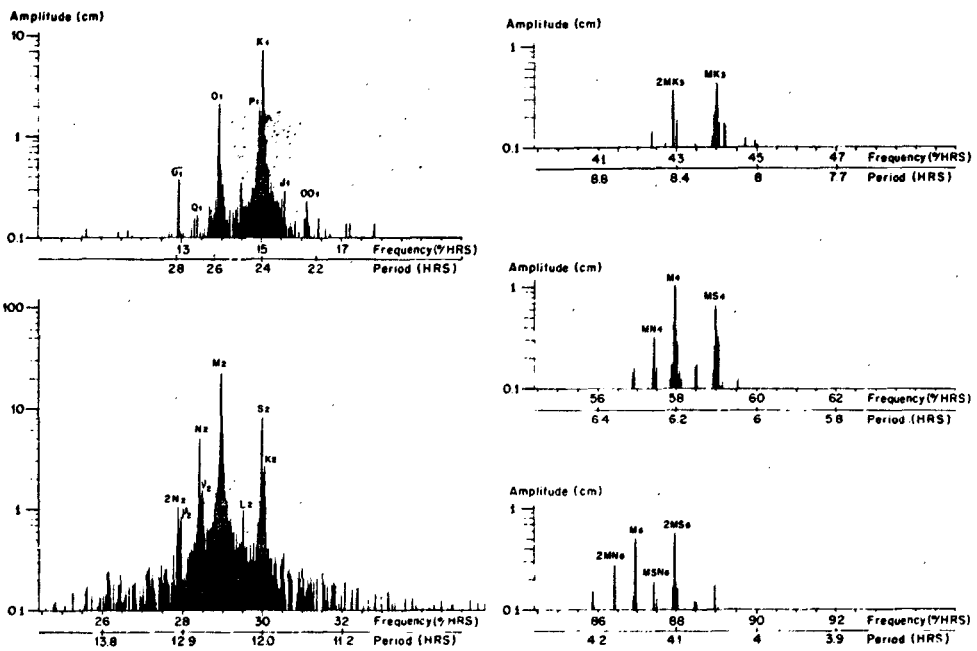

Fig. 5. Fourier analysis of two years of hourly sea level observations at Abidjan (74-75).

The fourth and sixth diurnal groups are nonlinear components which appear in shallow waters.

Figure 6 gives a detailed graphic representation of the low-frequency components; this graph is a Fourier analysis of 8 yrs of sea level observations at Abidjan. Above the background noise, we see the following peaks:

a) at 13.661 days, Mf is the lunar fortnightly tide which has a constant phase all along the coast.

b) at 14.765 days, this significant peak is at the period of the lunar-solar fort nightly tide Msf. This wave propagates westward, all along the east-west oriented coastline of the Guinea Gulf, with a mean phase speed of 53 cm s^{-1} and a wavelength of 675 km. This wave is probably a topographic shelf wave induced by some nonlinearity between the M2 and S2 tides along the coast (Picaut and Verstraete, 1979). Off-shore, Cartwright (1971 and personal communication) has analyzed one year's hourly tidal data at Ascension Island and finds the component Mf, but no significant amplitude at the Msf frequency.

c) at 31.8 days, this peak corresponds to the period of the monthly tide Msm.

d) at 45 days, we observe a standing wave induced by an atmospheric forcing at the same period (Picaut and Verstraete, 1976).

e) at four and six months, these peaks correspond to the periods of the Sta and Ssa tides. At Ascension Island, Cartwright finds an amplitude of 1.1 cm and 2.4 cm; the numerous works of Maximov (1970) and Lisitzin (1974) support the existence of a half yearly Ssa tidal component.

f) at one year, the peak corresponds to the Sa component which is mainly of atmospheric origin. Its amplitude is nearly the same in Abidjan (3.8 cm) as in Ascension Island (3.3 cm).

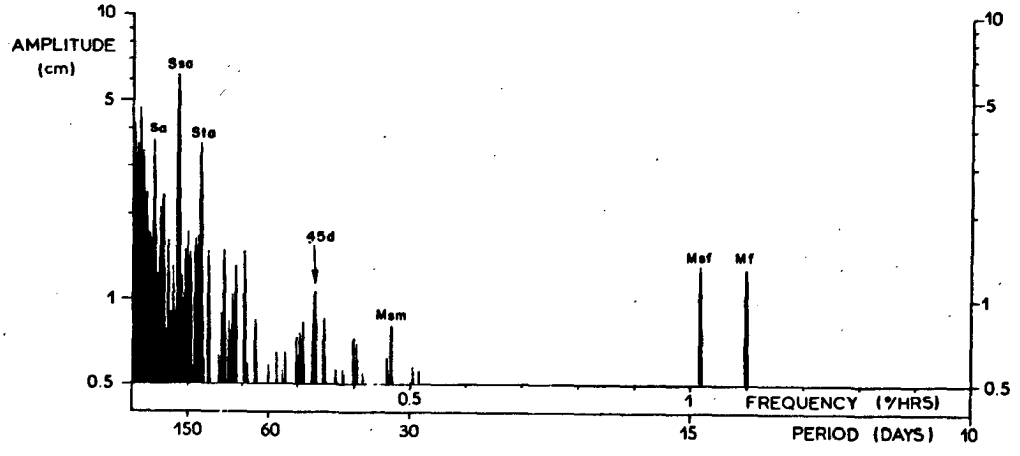

Fig. 6. Fourier analysis of 8 yrs of mid-tide sea level at Abidjan (67-74).

It is possible to compute the amplitudes of the long period equilibrium tides (Maximov, 1970) for the components Sa, Ssa, Sta, Msm, Msf, Mf. For the latitude of Abidjan, we obtain respectively (in cm): 0.10; 0.64; 0.04; 0.14; 0.12; 1.4. Except for Mf, the observed amplitudes are clearly larger than the theoretical ones, and the equilibrium theory can hardly explain the amplitudes of the long period tidal group observed either on the

coast or at Ascension Island. Some resonant phenomena or nonlinear interaction (probably the Msf case) must be involved.

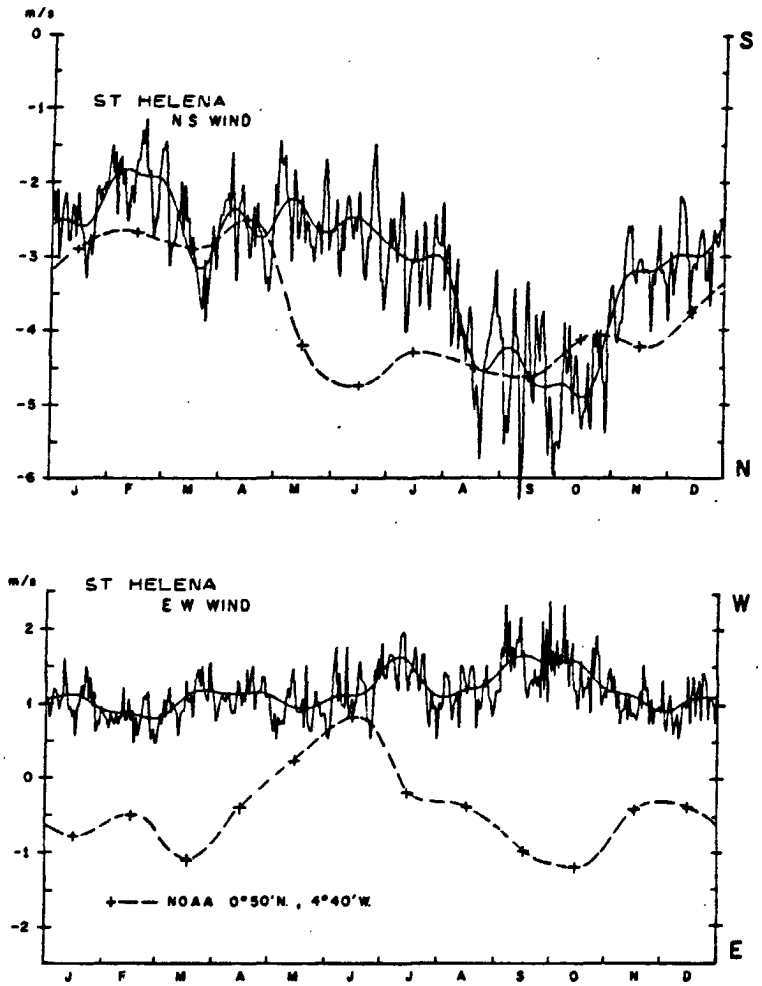

Fig. 7. Mean wind.

THE WIND AND THE BAROMETRIC PRESSURE

Figures 7 and 8 show the mean of all the data for the north and east components of the wind at St. Helena Island (1961-1975) and at Abidjan (1966-1974). The dashed lines are

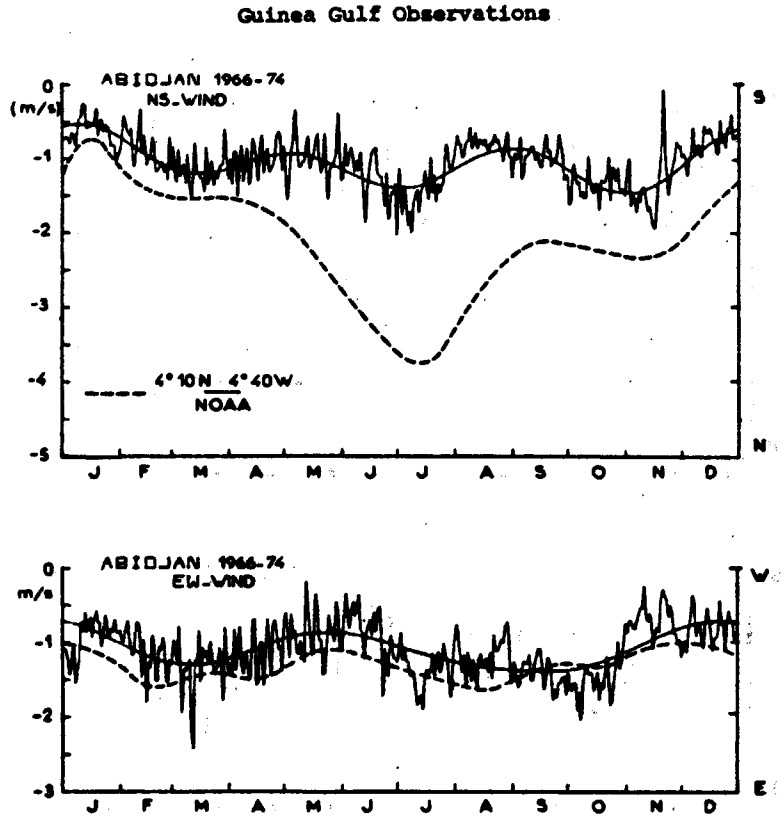

Fig. 8. Mean wind.

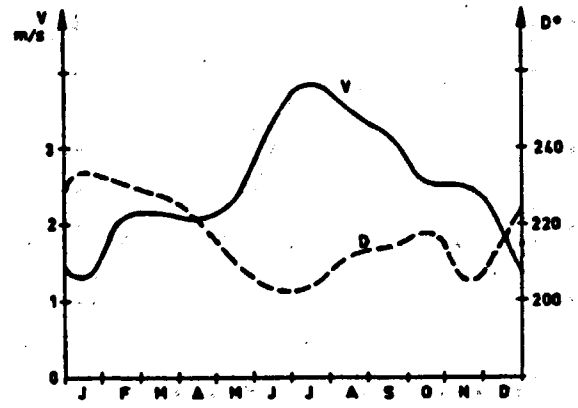

Fig. 9 Mean wind between 2°E and 10°W and between 4°N and the coast (NOAA data).

the monthly means calculated with the NOAA data near the equator at 0°50'N (Fig. 7) and near the coast at 4°10'N (Fig. 8) south of Abidjan. Figure 9 gives evidence of the annual cycle of the wind in the area between 4°N and the coast, with a maximum in July and a minimum in January.

The lack of yearly seasonal variation of the wind at Abidjan confirms the lack of correlation between the coastal winds and the yearly upwelling observed between Ghana and the Ivory Coast. We also note that the maximum of the northward component of the wind between 4°N and the coast and at the equator occurs in July whereas at St. Helena Island it occurs in September-October.

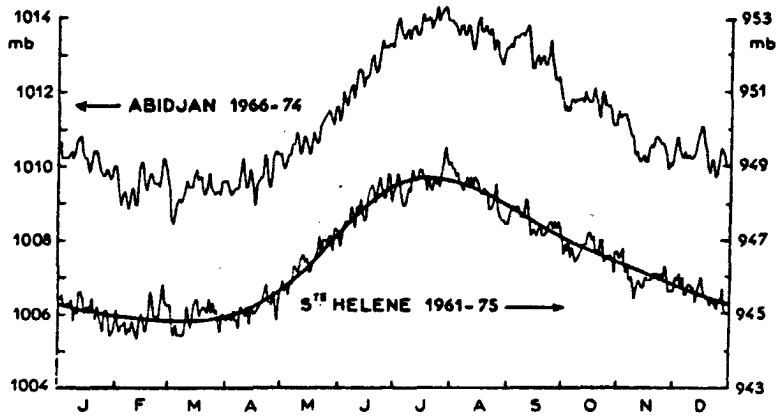

Fig. 10. Mean barometric pressure at Abidjan and St. Helena Island. The superimposed curve is the sum of the three first harmonics of the "mean year" at St. Helena.

The annual cycle of the barometric pressure at St. Helena Island (15 yrs) and at Abidjan (9 yrs) is clearly observed in Figure 10, where we have plotted the means of the pressure measured every 12 hrs for, respectively, 15 and 9 yrs. The yearly variation is about 5 mb at the two stations, with a maximum in July-August and a minimum in February-March. The synchrony of this annual cycle between the two stations is quite noteworthy.

CONCLUSION

Numerous spectral analyses of the data show that considerable low frequency variability exists among records from the coastal stations, but we really understand the physical causes only for the tide at present. The Fourier analysis of 8 yrs of sea level observations at Abidjan detects numerous low frequency oceanic oscillations. Since the periods of some of them are precisely those of the tidal forcing, their origin must be tidal.

With this time series, we have an excellent resolution equal to $(8\ yrs)^{-1}$ in frequency. It is clear that the Sta (4 months) and the Ssa (6 months) tidal components are well separated from Sa and above the background noise, so that these peaks are significant. We note that the observed amplitudes of the long period tides are larger than the theoretical ones given by equilibrium theory. The mean annual amplitude of the SST in the coastal upwelling area along the northern coast of the Gulf is $8^{\circ}C$. There is evidence of an annual cycle in mean sea level with a mean amplitude of about 20 cm at Tema, Takoradi and Abidjan. We do not observe a yearly seasonal variation of the coastal winds at Abidjan, whereas the synchrony of the annual cycle of the barometric pressure at St. Helena Island and at Abidjan is quite noteworthy. They yearly variation is of about 5 mb at these two stations.

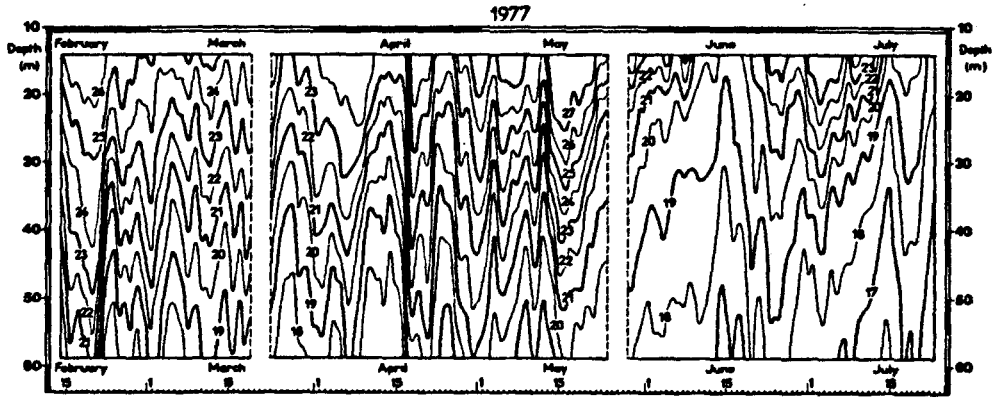

Fig. 11. Low pass filtered isotherms (Demerliac filter) at the Aanderaa thermistor chain mooring off Abidjan at a depth of 65 m, from February 11 to July 25, 1977.

REFERENCES

BAKUN A. (1978) Guinea Current upwelling. Nature, 271, 147-150.

BURPEE R.W. (1976) Structure énergétique des ondes d'Est, La Météorologie, VI série, N°6, 137-148.

CARTWRIGHT D.E. (1971) Tides and waves in the vicinity of Saint Helena. Philosophical Transactions of the Royal Society of London, Series A, 270(1210), 603-649.

LIZITZIN E. (1974) Sea Level Changes. Elsevier Oceanography Series, 286 pp.

MAXIMOV I.V. (1970) The Geophysical Forces and Water in the Oceans. Gidrometeorologickeskoie Izdatelstwo, Leningrad, 447 pp. (in Russian).

MERLE J., M. FIEUX and P. HISARD (1978) Annual signal and interannual anomalies of sea surface temperature in the eastern equatorial Atlantic ocean. Deep-Sea Research, GATE Supplement II to V. 26, 77-102.

PICAUT J. and J.M. VERSTRAETE (1976) Mise en évidence d'une onde de 40-50 jours de periode sur les côtes du Golfe de Guinee. Cahiers ORSTOM Séries Océanographique, 14(1), 3-14.

PICAUT J. and J.M. VERSTRAETE (1979) Propagation of a 14.7 day wave along the Northern Coast of the Guinea Gulf. Journal of Physical Oceanography, 9, 136-149.

PHILANDER S.G.H. (1977) The effect of coastal geometry on equatorial waves. (Forced waves in the Gulf of Guinea). Journal of Marine Research, 35(3), 509-523.

PHILANDER S.G.H. (1978) Variability of the tropical Oceans. Paper presented at the JOC/SCOR Conference on General Circulation Models of the Ocean and Their Relation to Climate; Helsinki, 23-27 May, 1977. (Revised April, 1978. Dynamics of Atmospheres and Oceans, 3, 81-82 (1979)).

VOL. 5, NO. 8 GEOPHYSICAL RESEARCH LETTERS AUGUST 1978

EQUATORIAL ADJUSTMENT IN THE EASTERN ATLANTIC

[1]Dennis Moore, [2]Philippe Hisard, [1]Julian McCreary, [3]Jacques Merle, [4]James O'Brien, [5]Joël Picaut, [6]Jean-Marc Verstraete, and [7]Carl Wunsch.

[1]Ocean Sciences Center, Nova University, Dania, Florida 33004; [2]Centre Recherches Oceanographiques, C.R.O., Abidjan, Ivory Coast Rep.; [3]CIMAS, University of Miami, Miami, Florida 33149; [4]Department of Meteorology, Florida State University, Tallahassee, Florida 32306; [5]Laboratoire d'Oceanographic Physique, Universite de Bretagne Occidentale, Brest, France; [6]Antenne Orstom C.O.B., Brest, France; [7]Department of Earth & Planetary Science, M.I.T., Cambridge, Massachusetts 02139.

Abstract. Observations suggest that the annual upwelling event in the Gulf of Guinea is not associated with changes in the local winds. A possible explanation is that a strong upwelling signal, generated by increased westward wind stress in the western Atlantic, can travel to the eastern Atlantic as an equatorially trapped Kelvin wave. This explanation is analogous to current theories of El Niño in the Pacific Ocean.

Introduction

During the FINE Workshop (FGGE/INDEX/NORPAX Equatorial Workshop, June 27-August 12, 1977) at U.C.S.D., La Jolla, California, the French participants presented data from the equatorial Atlantic and the Gulf of Guinea taken during 1974 (GATE) and 1975. The resulting discussion of these and related data in terms of simple theoretical ideas about equatorial adjustment to time-varying surface winds led to a possible explanation of many of the main features. The primary inputs to the discussion were made by the authors, with occasional comments by other workshop participants.

The data illustrated here are two N-S sections across the equator which were made from the R/V CAPRICORNE at 5°W in January and August, 1975; the time series taken at 0°N, 10°W by Rybnikov from the USSR vessel PASSAT (including moored current meter data subsequently analyzed by Duing); 1974 sea level and SST data at various coastal locations along the Gulf of Guinea (Picaut and Verstraete, personal communication); and the mean sea surface slopes along the equator based on historical data (Neumann, et al., 1975). Basic ideas about baroclinic equatorial adjustment in the ocean, in the presence of continental boundaries, are contained in Moore (1968); Lighthill (1969); O'Brien and Hurlburt (1974); Hurlburt et al. (1976); McCreary (1976); Moore and Philander (1977); and Cane and Sarachik (1976, 1977).

Observations

Figure 1 (a,b) shows the temperature and zonal velocity data obtained by Hisard at 5°W in January, 1975. Note the strong eastward undercurrent with maximum velocity in excess of 120 cm/sec at 70 meters depth. There is a marked depression of the 15°-20°C isotherms in the vicinity of the undercurrent core. The zonal velocity at the surface near the equator is westward and relatively weak (10-20 cm/sec). Figure 2 (a,b) shows the same data for August, 1975. The undercurrent is weaker and shallower, with a maximum velocity of ~80 cm/sec at 40 meters depth. The 16°-21°C isotherms now show a marked upward bowing in the vicinity of the undercurrent. The westward surface flow at the equator is much stronger (60-100 cm/sec). It is clear from comparing the January and August data that a significant change has occurred in the equatorial temperature and flow fields at 5°W during the intervening period.

Figure 3 (a) shows the time series of SST observed at 0°N, 10°W by the PASSAT during 27 June-16 July, 27 July-15 August, and 29 August-19 September, 1974. Figure 3 (b) is the time series of zonal velocity as a function of depth from moored current meters at the same location, for the entire period, 24 June-13 September. There is a marked drop (~2°C) in SST between 6 July and 9 July. There is also an upward shift in the core of the undercurrent, starting perhaps as early as 28 June. We hypothesize that the upward motion of the undercurrent and the appearance of cold water at the sea surface are associated with an upwelling event. The vertical migration of the undercurrent core begins before the

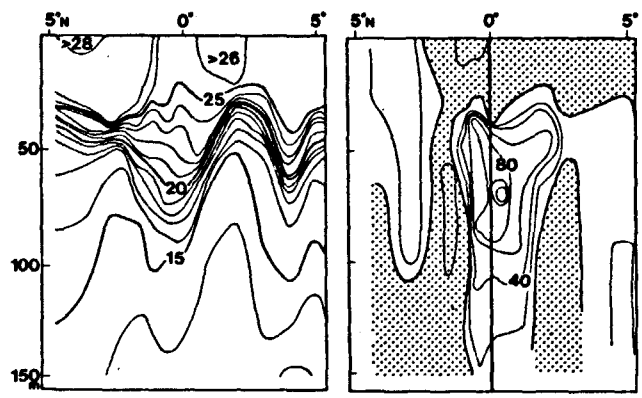

Fig. 1 (a). Temperature (°C) as a function of latitude and depth at 5°W in January, 1975.

Fig. 1 (b). Zonal velocity (cm/sec^{-1}) as a function of latitude and depth at 5°W in January, 1975. The unmarked contour at the core of the Undercurrent is 120 cm/sec^{-1}. Currents are measured relative to 300 meters.

Paper number 8L0621.
0094-8276/78/088L-0621$01.00

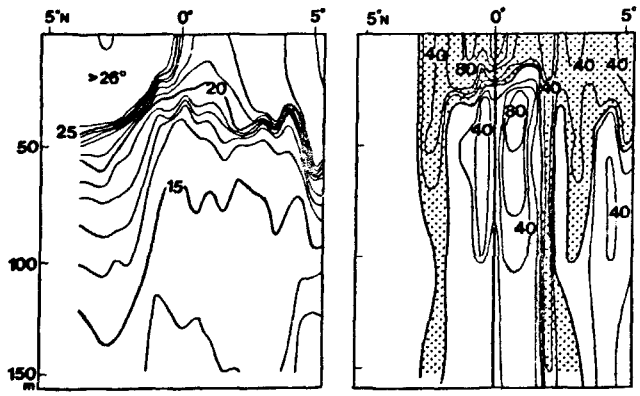

Fig. 2 (a). Temperature (°C) as a function of latitude and depth at 5°W in August, 1975.

Fig. 2 (b). Zonal velocity (cm/sec^{-1}) as a function of latitude and depth at 5°W in August, 1975. The unmarked contours in the westward surface flow at the equator are 100 cm/sec^{-1}. Currents are measured relative to 300 meters.

marked change in SST, since the mixed layer must be advected away before the cold water can appear at the surface. It is clear from the PASSAT data that the upwelling event as revealed by the cold SST was of at least two months' duration.

Figure 4 (Picaut and Verstraete, personal communication; Houghton and Beer, 1976) shows time series of daily sea surface temperature at a number of coastal stations in the Gulf of Guinea. The temperature at all locations begins a gradual decline which seems to start about 1 June; an extended Tema record, provided by Hisard, shows that this decline actually began about 20 May. There is a marked drop ($\Delta T \sim 6°$ at Tema) in SST beginning about 13 July. According to Houghton (1976) isopycnals remained relatively flat prior to 12 July to at least a depth of 100 meters. Between 12 July and 18 July, the isopycnals rose about 50 meters, the most rapid increase taking place after 15 July. A shallow thermocline at 40 meters depth was completely brought to the surface by 20 July. (The surfacing of the thermocline is evident in Figure 4 by the appearance of a 15-day baroclinic tidal oscillation. This signal occurs in corresponding sea level records throughout the year, but can exist in the SST records only when the thermocline is near the surface.) An upwelling event similar to the equatorial one has occurred along the African coast.

There is considerable evidence that upwelling events, similar to those illustrated in Figure 1-4, occur every year. Bakun (1978) has analyzed historical SST records in the Gulf of Guinea. One of his figures shows that in August a narrow band of cool ocean temperature exists all along the equator, as well as between 5°E and 10°W along the African coast. Merle (1977) has investigated seasonal variations of the deeper thermal structure in the tropical Atlantic using hydrographic data on file at NODC. According to Merle, in the eastern Atlantic cooling gradually begins in May and reaches an extreme in August or September. The cooling is identifiable to depths of 150-200 meters in some cases, but is generally confined to the upper 100 meters; it is clearly associated with an uplifting of the thermal structure of the order of 25-50 meters. Using the value of salinity at the core of the Undercurrent as a measure of the flow, he argues that from 0°-20°W the speed of the Undercurrent reaches a minimum in September, a principal maximum in April-May, and a strong secondary maximum in December-January.

The most interesting aspect of the upwelling in the Gulf of Guinea is that it is not related in an obvious way to the local winds (Houghton, 1976; Bakun, 1978). According to Hastenrath and Lamb (1977), the winds in the equatorial belt east of 10°W are primarily meridional with little variation in the zonal wind from month to month. The standard explanation of upwelling requires changes in zonal (alongshore) wind at the equator (coast), and subsequent Ekman divergence, to induce upwelling. It is not likely, then, that the marked differences in the thermal and velocity structure of the ocean discussed above are caused by changes in the local wind.

Katz et al. (1977) suggest that the upwelling signal at 10°W in the summer of 1974 (Figure 3) was dynamically related to events which took place far to the west. They report that the pressure gradient between 10°W and 35°W increased markedly between mid-June and the end of August. In fact, this increase of the zonal pressure gradient is part of an annual cycle. Figure 5, from Neumann et al. (1975), shows mean slopes of dynamic height along the equator based on historical data. It is evident in the figure that there is a substantial increase in the zonal pressure gradient between the February-March and July-September-November sections. Merle (1977) corroborates this result and finds that the pressure gradient is weakest in April (5 dynamic cm) and largest in September (30 dynamic cm).

The fluctuation of equatorial pressure gradient occurs in conjunction with large changes in the zonal wind field west of 10°W. Katz et al. (1977) show the monthly averaged

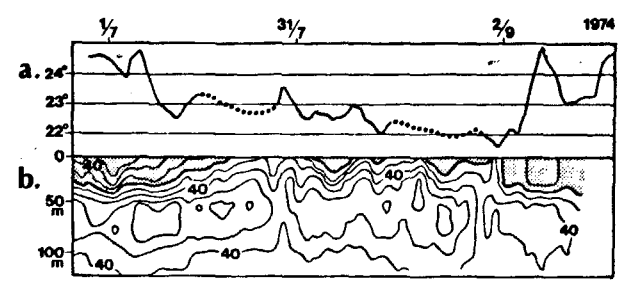

Fig. 3 (a). Time series of SST on the equator at 10°W during July-September, 1974.

Fig. 3 (b). Time-versus-depth contours of zonal velocity at the equator from moorings at 10°W during July-September, 1974. The unmarked contours at the core of the Undercurrent are 80 cm/sec^{-1}.

wind stress on the equator between 10°W and 40°W, as computed by Bunker. The westward wind stress is at its minimum value in March and increases rapidly from .25 dyne/cm^2 to .55 dyne/cm^2 during April, May and June. It remains at this high level until November. As the westward wind increases, the pressure gradient quickly follows reaching a maximum several months after that of the wind.

A Simple Explanation

We hypothesize that the above oceanic observations represent the response of the equatorial Atlantic Ocean to the strengthening of the westward zonal wind stress in the western Atlantic. Teleconnections between the eastern and western Atlantic can be simulated with simple linear models. Suppose that a wind stress confined to the western ocean is switched on at some initial time; then the models predict that:

1) In the region where the (westward) zonal wind intensifies, surface water piles up against the western boundary, and as a result a zonal pressure gradient is established which balances the applied wind stress (see Figure 5).
2) To the east of the forcing, a Kelvin wave upwelling is generated, propagating eastward at a speed $c = \sqrt{g'H}$, of the order of 250 cm/sec (Moore and Philander, 1976), where g' is reduced gravity and H is the depth of the pycnocline. Associated with the passage of this upwelling signal is a general uplifting of the thermal structure in the equatorial band and increased surface flow toward the west. This westward flow provides the source of the upper layer water which accumulates in the forcing region (see Figures 1, 2, and 3).
3) When this upwelling disturbance reaches the eastern boundary, it splits with a signal going poleward along the coast in both hemispheres (see Figure 4).

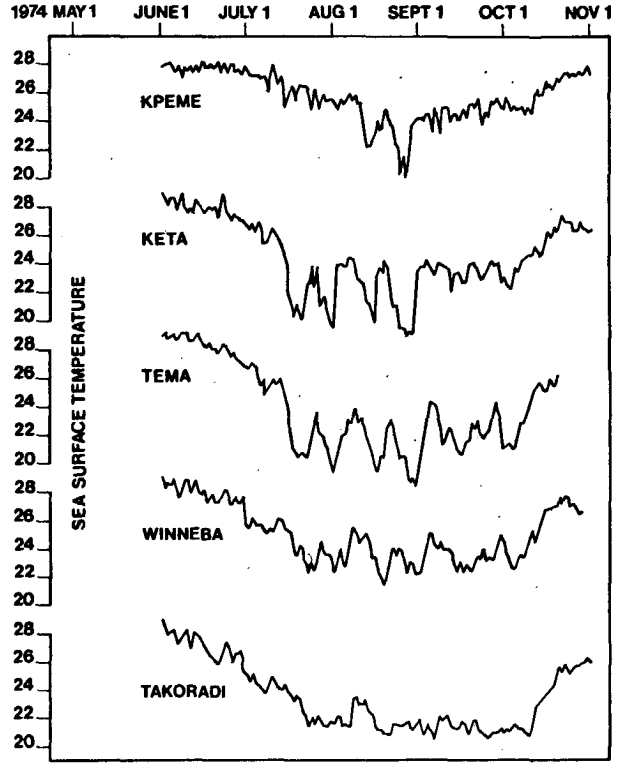

Fig. 4. Time series of SST (°C) from coastal stations in the Gulf of Guinea during 1974. The data from Ghana were kindly provided by the Ghana Fisheries Research Unit in Tema.

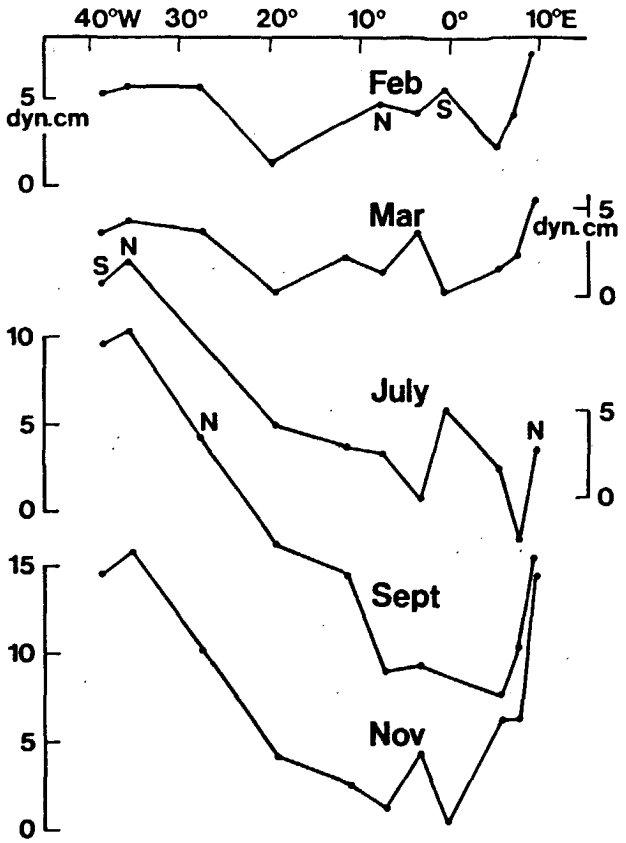

Fig. 5. Mean sea-surface slopes along the equator based on historical data.

An accompanying note by O'Brien, et al. (1978) illustrates these ideas using a model in an ocean basin which includes the African coast. This adjustment process is completely analogous to a currently proposed explanation for the El Niño phenomenon in the Pacific (Hurlburt, et al., 1976; McCreary, 1976).

Discussion

The transient model response discussed in the previous section suggests that a definite time lag must exist between the onset of equatorial and coastal upwelling. Suppose that an equatorially trapped event is originally observed at 10°W. It must travel 19° of longitude to reach the African coast. After it reflects from that boundary, in part as a coastally trapped Kelvin wave, it must travel back another 10° to reach Tema. Therefore,

the signal at Tema should lag the equatorial one by roughly 12 days. Such a lag may have existed during the 1974 upwelling event; however, it is difficult to determine a moment on the onset of upwelling in either region. Did the equatorial upwelling begin on 6 July with the rapid dropping of SST, or on 28 June with the rise of the core of the Undercurrent? Did the coastal upwelling begin on 12-15 July with the rapid rise of isopycnals, or on 1 June with the gradual cooling of SST? More observations are needed.

Hisard (personal communication) has pointed out that in 1974 a gradual lowering of SST at Pointe-Noire (4°49' south of the equator) began about 15 May, considerably before the rise of the Undercurrent at 10°W and slightly preceding the gradual drop of temperature at Tema. McCreary and Moore (personal communication) have recently been studying the response of simple models to winds oscillating at frequency ω. They find that the obvious phase relationships connecting events in the transient response are altered considerably by the reflection of Rossby waves from a meridional boundary. It may be possible to account for the early upwelling in this way.

If fluctuations of local wind are not the cause of upwelling in the Gulf of Guinea, what then is? The point of this note, and its companion, is to suggest a possible answer to this puzzle. Although the available data as yet do not allow a thorough test of our hypothesis, they do suggest the possibility that teleconnections across the Atlantic are occurring seasonally in much the same way that they are known to occur in the Pacific on interannual (El Niño) time scales.

References

Bakun, A., Guinea Current upwelling, Nature, 271, 147-150, 1978.

Cane, M., and E.S. Sarachik, Forced baroclinic ocean motions: I. The linear equatorial unbounded case, J. Mar. Res., 34, 629-665, 1976.

Cane, M., and E.S. Sarachik, Forced baroclinic ocean motions: II. The linear equatorial unbounded case, J. Mar. Res., 35(2), 395-432, 1977.

Hastenrath, S., and P.J. Lamb, Climatic Atlas of the Tropical Atlantic and Eastern Pacific Ocean, The University of Wisconsin Press, 1977.

Houghton, R.W., Circulation and hydrographic structure over the Ghana continental shelf during the 1974 upwelling, J. Phys. Oc., 6(6), 910-924, 1976.

Houghton, R.W., and T. Beer, Wave propagation during the Ghana upwelling, J. Geophys. Res., 81(24), 4423-4429, 1976.

Hurlburt, H.E., J.C. Kindle, J.J. O'Brien, A numerical simulation of the onset of El Niño, J. Phys. Oc., 6(5), 621-631, 1976.

Katz, E.J., R. Belevitsch, J. Bruce, V. Bubnov, J. Cochrane, W. Duing, P. Hisard, H.-U. Lass, J. Meincke, A. DeMesquita, L. Miller, and A. Rybnikov, Zonal pressure gradient along the equatorial Atlantic, J. Mar. Res., 35(2), 293-307, 1977.

Lighthill, M.J., Dynamic response of the Indian Ocean to the onset of the southwest monsoon, Phil. Trans. Roy. Soc. London, Ser. A., 265, 45-92, 1969.

McCreary, J., Eastern tropical ocean response to changing wind systems; with application to El Niño, J. Phys. Oc., 6(5), 632-645, 1976.

Merle, J., Seasonal variations of temperature and circulation in the upper layers of the equatorial Atlantic Ocean, unpublished manuscript, 1977.

Moore, D., Planetary-gravity waves in an equatorial ocean, Ph.D. Thesis, Harvard University, Cambridge, Mass., 1968.

Moore, D.W., and S.G.H. Philander, Modeling of the tropical oceanic circulation, The Sea, Vol. VI, John Wiley Interscience, 319-361, 1977.

Neumann, G., W.H. Beatty, and E.C. Escowitz, Seasonal changes of oceanographic and marine-climatological conditions in the equatorial Atlantic, Dept. Earth & Planetary Sci., City College of CUNY and CUNY Inst. of Mar. & Atmos. Sci., 1975.

O'Brien, J.J., D. Adamec, and D.W. Moore, A simple model of equatorial upwelling in the Gulf of Guinea, to be published in Geophysical Research Letters, 1978.

O'Brien, J.J., and H.E. Hurlburt, Equatorial jet in the Indian Ocean: Theory Science, 184, 1075-1077, 1974.

(Received March 20, 1978;
revised May 22, 1978;
accepted June 14, 1978.)

JANUARY 1983 JOURNAL OF PHYSICAL OCEANOGRAPHY VOLUME 13

Propagation of the Seasonal Upwelling in the Eastern Equatorial Atlantic

JOËL PICAUT

Laboratoire d'Océanographie Physique, Université de Bretagne Occidentale, 29200 Brest, France

(Manuscript received 2 November 1981, in final form 30 August 1982)

ABSTRACT

Several mechanisms have been proposed to explain the coastal and equatorial upwelling in the eastern Atlantic (Guinea Gulf). The most controversial is the mechanism of remote wind forcing in the western equatorial Atlantic suggested by Moore *et al.* (1978). Most of the possible explanations for the upwelling and their relative importance are discussed in view of recent observations.

Detailed analysis of daily sea surface temperature (SST) collected at 16 coastal stations along the northern coast of the Guinea Gulf reveals that the upwelling event propagates westward along this coast at a mean speed of 0.7 m s^{-1}. Similar analysis of historical monthly mean SST data shows that the coastal upwelling event propagates poleward from 1°S to at least 13°S at the same phase speed. Furthermore, the Northern Hemisphere and Southern Hemisphere coastal upwelling signals seem to start at the same time from the equator. The same kind of analysis applied to hydrographic data from a station situated 41 km off Abidjan, reveals an upward phase propagation of the upwelling event at 7 m day^{-1} from 300 m to the surface. These results and those of Servain *et al.* (1982) suggest that remote wind forcing west of the Gulf of Guinea is an important factor affecting the temperature in the Gulf.

1. Introduction

Since the early 1960's the eastern equatorial Atlantic Ocean (Guinea Gulf) has been studied intensively. A few large multinational experiments like EQUALANT, GATE and FGGE have increased our knowledge of this area, but the most important set of data is that collected regularly by the Centre de Recherches Océanographiques (ORSTOM) in Ivory Coast, Congo Republic and Senegal, and the Fishery Research Unit in Ghana. Largely due to the work of these centers the general features of the Guinea Gulf are now well documented. This area has a large seasonal signal characterized by four marine seasons (Berrit, 1958; Morlière, 1970): a warm period from February to May, a strong cold season from June through early October, a secondary warm season characterized in the surface layer by low salinity in November, and finally a secondary cold period of short duration occurring during December and January. The main upwelling event associated with cooling appears mostly along the northern and southern coasts as well as along the equator (Figs. 1 and 2). This dramatic event, first noted by Janke (1920) and Schott (1944), seems to have considerable influence both on local fisheries (Bakun, 1978; Stretta, 1977) and the climatology of the Sub-Saharan West Africa (Lamb, 1978), so the understanding of its dynamics is of fundamental interest.

One purpose of this paper is to review recent mechanisms, models and observations that have been advanced to account for the upwelling in the Guinea Gulf. The most probable mechanisms are local wind forcing and remote wind forcing west of the Gulf of Guinea. The major point of this study is to present evidence for horizontal and vertical propagation of the seasonal upwelling which supports the idea that the upwelling is remotely forced.

This paper is organized in the following manner. Section 2 presents the oceanographic and meteorological data used throughout this study, Section 3 is the review section, and Section 4 presents the new evidence of propagation. Finally, Section 5 discusses observations that support the existence of remote forcing, and reviews recent models that involve this idea.

2. The data

In this study we have used three types of data: daily coastal sea surface temperature, historical merchant ship observations, and historical hydrological data.

a. Daily sea surface temperature

The daily sea surface temperatures were measured from bucket samples taken at the beach or with Nansen bottles on a wharf at Cotonou. All the measurements used here were made around 0800 GMT. Houghton and Beer (1976) have shown that such type of records are highly representative of the temperature variations over the whole shelf. The location of the stations along the northern coast of the Guinea Gulf are given in Fig. 3. These coastal stations are

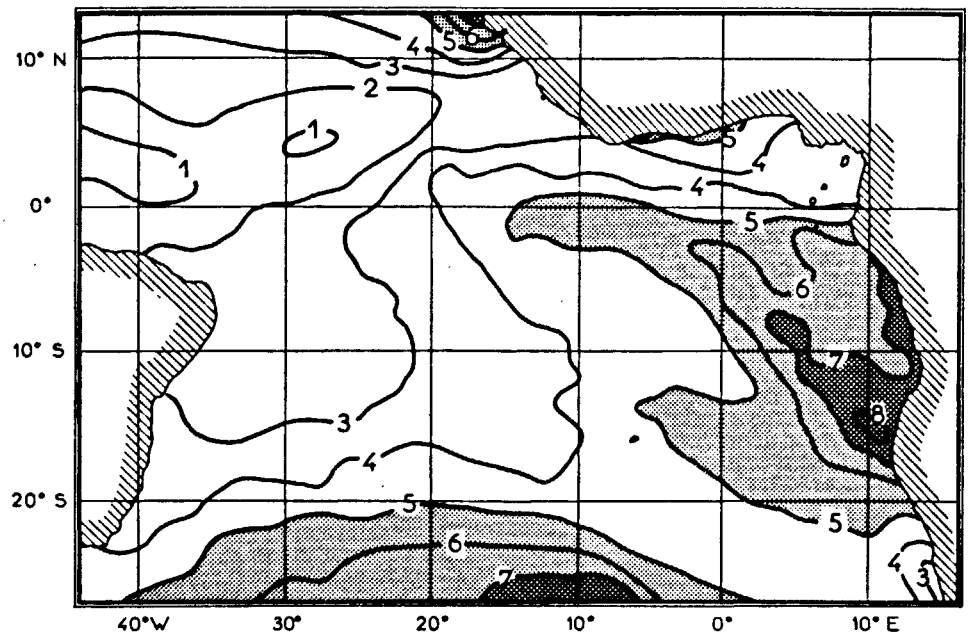

FIG. 1. Spatial distribution of the amplitude of the seasonal signal. This amplitude is defined as the difference between the maximum and minimum of sea surface temperature extracted from the "reconstituted" annual cycle within all the 1° square areas (see Fig. 2).

maintained by the Centre de Recherches Océanographiques (ORSTOM) in Ivory Coast, the Fishery Research Unit in Ghana, ORSTOM in Togo, and the Service des Pêches in Benin. Some of these stations started around 1960 but the most important data collection was initiated in 1977. Furthermore, due to some important gaps in a few of these series, we have not been able to analyze simultaneously the 16 coastal SST time series for the whole three years, 1977–79.

b. Historical merchant ship observations

Another type of data used in this study are the monthly 1° square means of winds and SST taken from merchant ships. Along the northern and southern coast of the Guinea Gulf (Fig. 4), the means for the period 1850–1970 were kindly provided by Drs. A. Bakun and W. S. Wooster. For the whole tropical Atlantic, Dr. S. Hastenrath generously sent us all his monthly means SST and winds for the period 1911–70. All these data were obtained from the National Climatic Center's file of maritime surface observations (TDF-11). For details about the preparation of these data, see Bakun *et al.* (1974) and Hastenrath and Lamb (1977). In the Guinea Gulf, which is out of the Dakar–Cape Town shipping lane, abundance is greatest near the coast. Despite the difference in length of record and probably some differences in the analysis procedures, the common means along the coast are quite similar (less than a few hundreths of a degree Celsius for the SST difference). Surface stress τ_s is calculated from the relation $|\tau_s| = \rho C_D |\mathbf{V}_s|^2$, where C_D is the drag coefficient and $\mathbf{V}_s$ the surface wind. Hastenrath and Lamb (1977) approximated $|\mathbf{V}_s|^2$ by the square of the resultant wind speed and compensated for the underestimation of $|\tau_s|$ with a large value of $C_D = 2.8 \times 10^{-3}$. On the other hand, Bunker (1976) calculated the wind stress from individual winds and a drag coefficient that is variable with both wind speed and stability of the atmosphere. The Hastenrath and

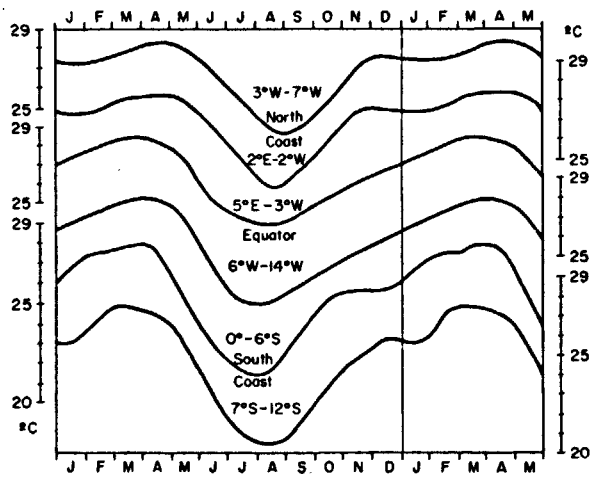

FIG. 2. Example of seasonal sea surface temperature within the 1° square areas as shown in Fig. 3. Note the absence of the secondary upwelling season with SST along the equator.

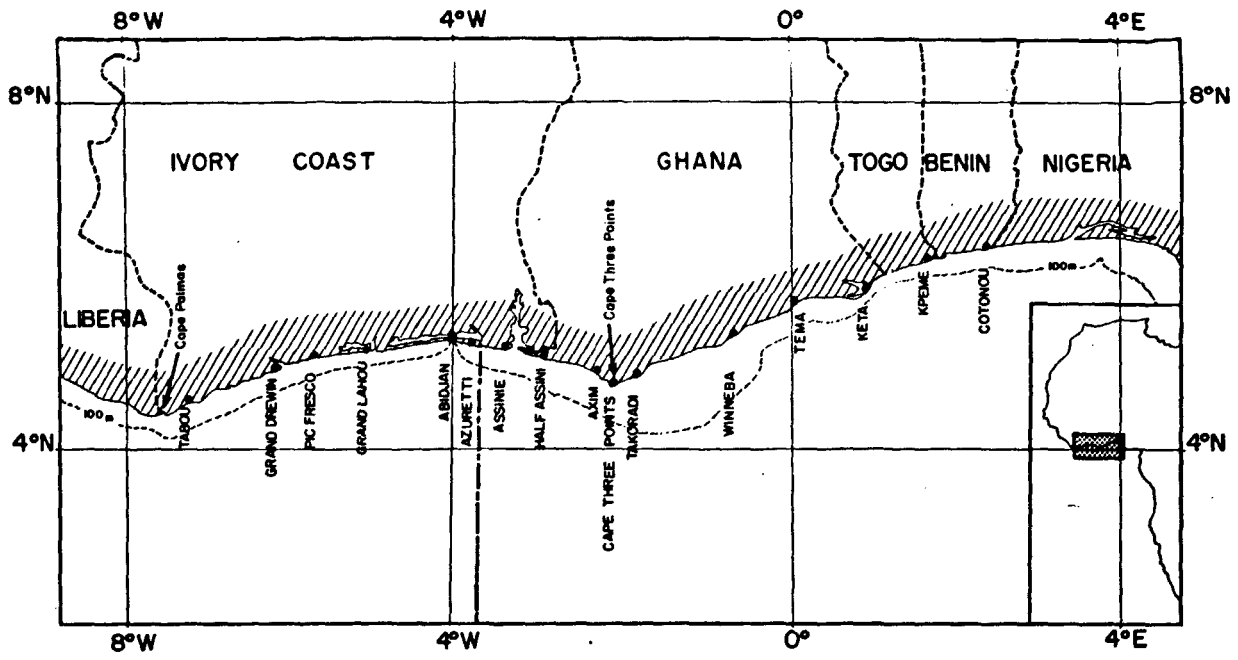

FIG. 3. Location of the coastal stations along the northern coast of the Guinea Gulf. The dotted line corresponds to the mean transect of Fig. 18.

Lamb wind stress data are very close to those of Bunker if we change the drag coefficient to 2.0 $\times 10^{-3}$, which is the value we use in this study.

c. Historical hydrological stations

Between 1957 and 1964, 217 Nansen casts were made regularly at the same station by the Centre de Recherches Océanographique of Abidjan. This hydrological station was situated 41 km off Abidjan at 4°53'N, 4°00'W in 1480 m of water on the shelf break. A maximum of 23 Nansen bottles were used from 0 to 1400 m. The upper level (0–400 m) has been visited systematically while the lower one (600–1400 m) only 80 times. Donguy and Privé (1964) have presented some results for 1960–62. For the purpose of our work we have computed monthly means after carefully checking each individual profile. Notwithstanding the fact that for the month of June the station has been visited less frequently (13 times), these monthly means are well determined.

In order to construct the mean transect during the upwelling season south of Abidjan, to be discussed in Section 5, we have compiled all the historical hydrographical data close to the section which is shown in Fig. 3. Practically all of these data have been provided by the Centre de Recherches Océanographiques from 1961 to 1971 (Donguy and Privé, 1964; Lemasson and Rébert, 1973a). Each profile is the mean of 6–12 hydrological stations and consequently is precise enough.

3. Mechanisms, models and observations related to the upwelling

Tentative general descriptions of the hydrography of the Guinea Gulf were first made by Varlet (1958) and Longhurst (1962). For more recent reviews, see Houghton (1976) for the northern part, Guillerm (1981) and Gallardo (1981) for the southern part, and Voituriez (1980) for the equatorial part. Charts of the atmospheric and oceanic fields in the equatorial Atlantic may be found in the atlases of Hastenrath and Lamb (1977) and Merle (1978). The meteorology of the Guinea Gulf is dominated by the northward winds associated with the anticyclone of Ste. Helena Island. These winds flow toward the low pressure field of the Sahara and so turn northeastward into the northern part of the Gulf. The strongest zonal winds are found in the western equatorial Atlantic. Both wind systems intensify during the Northern Hemisphere summer.

In this section we present the possible mechanisms which might account for the upwelling, some of which are illustrated by models. Recent observations have given a better idea of the relative importance of all these mechanisms.

a. Heat gain from the atmosphere through the surface

Good estimates of the various components of the net oceanic heat gain have recently been made available (Hastenrath and Lamb, 1977; Hastenrath, 1980).

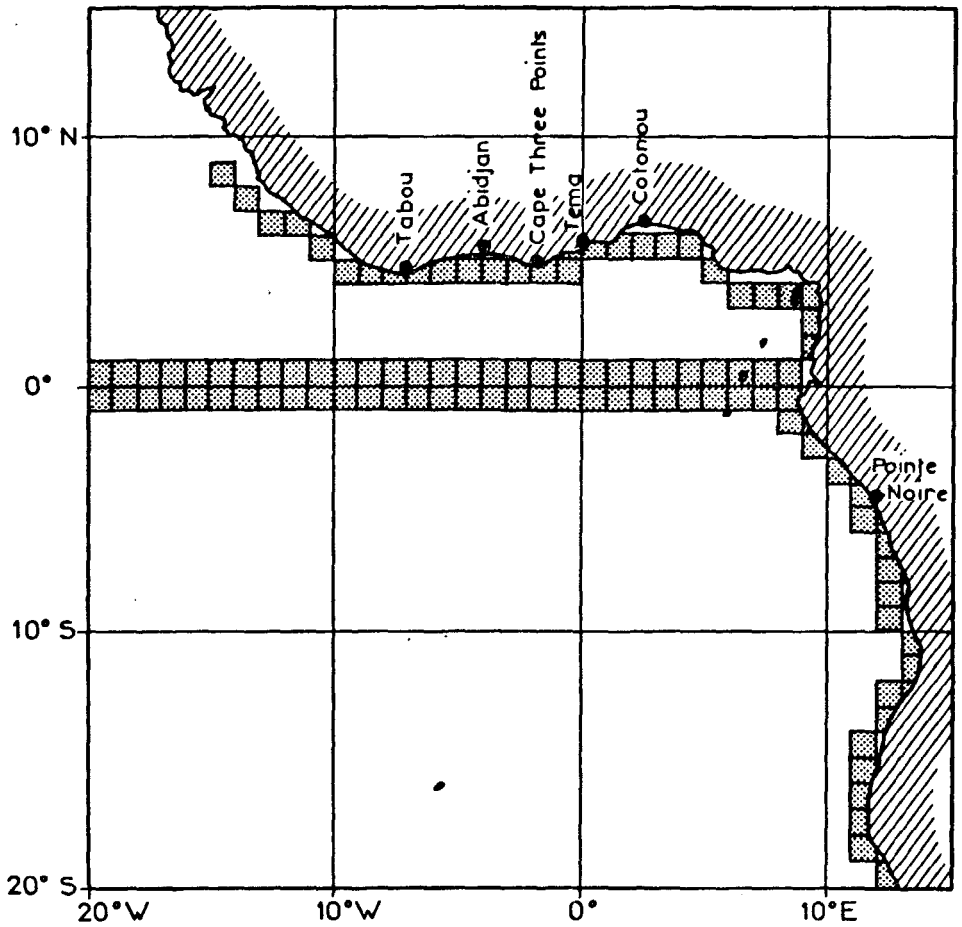

FIG. 4. Location of some coastal stations and some of the 1° square areas used.

As previously noted by Bunker (1976), the seasonal oceanic heat gain can qualitatively account for the seasonal upwelling along the northern coast of the Guinea Gulf. But recent estimates of the local seasonal variation of heat content in various parts of the equatorial Atlantic Ocean are found to be about ten times larger than the seasonal variations of the heat gain from the atmosphere through the surface, and are not confined to the upper mixed layer (Merle *et al.*, 1980). According to this last study the annual cycle of heat content appears to be due mainly to vertical movements of the thermocline by some dynamical processes.

b. Ekman divergence at the coast

1) NORTHERN COAST

Along the northern coast the cold waters appear from 2°E to 8°W (Fig. 1), where the winds blow nearly parallel to the coast, at least near Cape Three Points and Cape Palmas (see Fig. 3 for locations). With a simple steady-state model, Verstraete (1970) found that the weak mean winds along the Ivory Coast should give a maximum vertical upward movement of 0.7 m day^{-1} (8.1×10^{-6} m s^{-1}), which is smaller than that indicated by indirect observations. Furthermore, the seasonal variation of the winds are also weak at the coast and offshore (Verstraete *et al.*, 1980). Finally, with the historical records of maritime observations summarized by month and by 1° squares along the northern coast, Bakun (1978) found an offshore seasonal Ekman transport maximum off the Togo and Benin coasts (0°–4°E) and further east in the Bay of Biafra where obviously the upwelling is very poor. Thus all attempts to correlate the intensity and duration of the upwelling with local coastal winds have failed (Fishery Research Unit, 1970; Houghton, 1976).

2) SOUTHERN COAST

South of the equator the winds blow mainly parallel to the coast. In a three-dimensional numerical model of the tropical ocean, Philander and Paca-

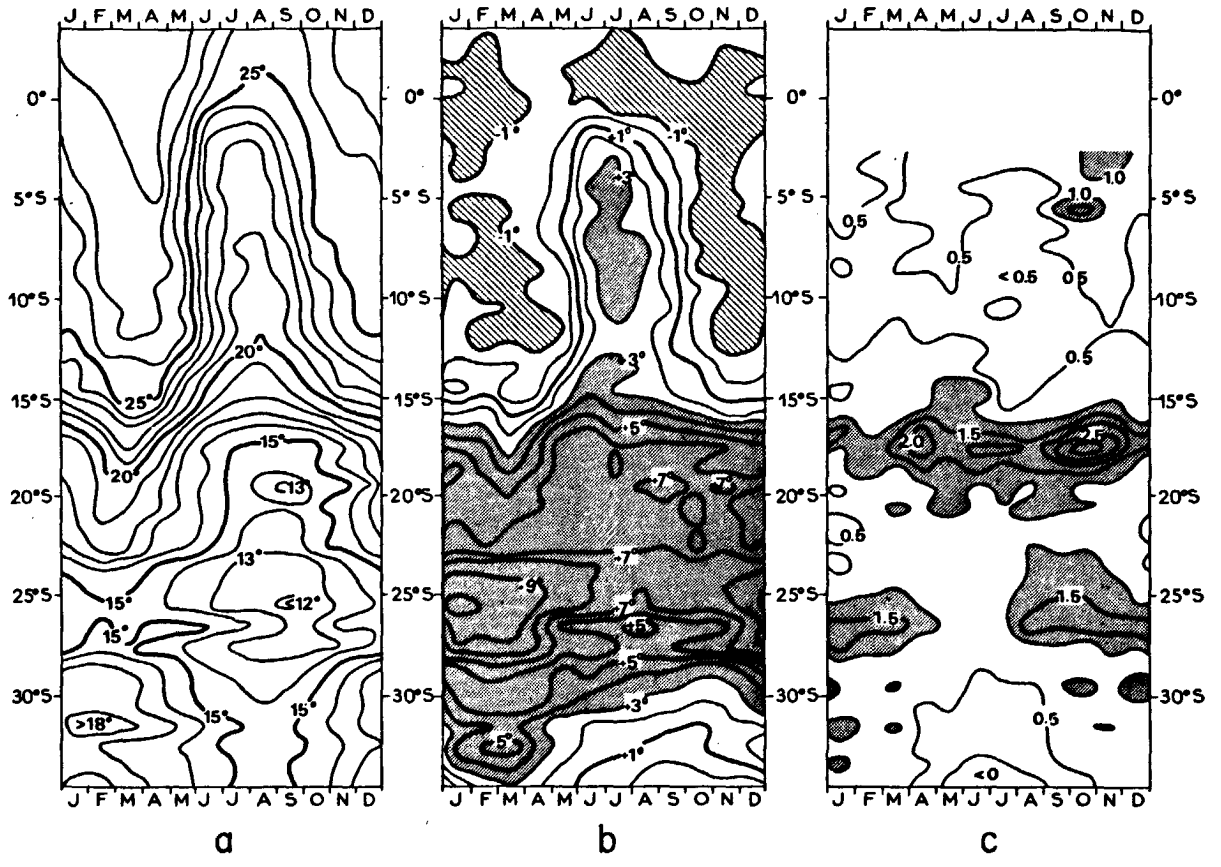

FIG. 5. (a) Sea surface temperature data by month for a long term composite year 1850–1970 by 1° square areas arranged as shown in Fig. 4. (b) Monthly deviation of the preceding data from central ocean values. (c) Offshore component of Ekman transport for the same kind of data. Units are cubic meters per second per meter of coastline. (Courtesy of Dr. W. S. Wooster)

nowski (1981a) showed that southerly winds can cause low SST throughout the southeastern part of the basin. The local coastal upwelling obtained expands offshore because of advection and propagation of Rossby waves. This theoretical study suggests that seasonal variations of the meridional winds may significantly affect sea surface temperature in the eastern equatorial Atlantic. However, the assumed wind field, limited to an idealized, gradually varying x-independent southerly wind, was inadequate for a stringent test of that idea.

Berrit (1976) tried to investigate the correlation of this upwelling with the local wind field. South of 15°S he found good agreement between strong winds and low temperature, but no correlation at all further north. His calculations, based on historical data averaged by 5° square areas, may not be able to resolve narrow coastal phenomena. Thus we are very grateful to Dr. W. S. Wooster for permission to present some unpublished results for the same area. The historical data used are similar to those of Wooster *et al.* (1976) and Bakun (1978) on the northern coast, and are summarized by month and by 1° square areas arranged along the southern coast as shown in Fig. 4. Fig. 5a shows that most of the seasonal upwelling signal appears north of 22°S, whereas further south the upwelling seems to be almost permanent (see also Fig. 1). In Fig. 5b the coastal nature of the seasonal upwelling is confirmed by the monthly variation of coastal temperature deficit defined as the difference between coastal and mid-ocean temperature in the same way as Wooster *et al.* (1976). Comparison of the field of offshore Ekman transport (Fig. 5c) with those of the coastal temperature confirm the conclusion of Berrit (1976): between 2°S and 13°S there is no correlation between local winds and nearshore temperature, but between 13°S and 20°S the correlation is good and further south the correlation decreases.

c. Ekman divergence at the equator

Along the equator, comparison of the seasonal depth variations of the 21 and 23°C isotherms (Merle, 1978; Merle *et al.*, 1980) and the SST signal (Fig. 1) shows that the equatorial upwelling is present east of

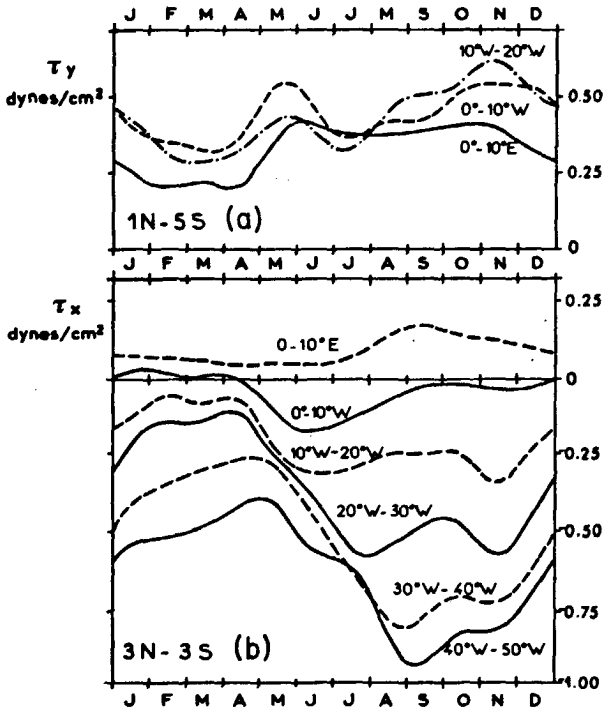

FIG. 6. Annual cycle of the wind stress: (a) south–north component in the Guinea Gulf, (b) west–east component all along the equator.

20°W. A model of local Ekman divergence based on the work of Cromwell (1953) was proposed to explain the equatorial upwelling in the Atlantic Ocean (Voituriez, 1980). It is evident from this simple model that the equatorial Ekman divergence would be more pronounced with an easterly wind than with a southerly wind. In the Guinea Gulf most of the winds are southerly with a small easterly component in the western part of the Gulf (Figs. 6a, 6b). Philander (1979) and Philander and Pacanowski (1981a), in two different models, simulate the response of the equatorial ocean to a southerly wind. They obtained an upwelling over a region of large latitudinal extent south of the equator. The poor correlation between the local nonseasonal wind stress and the nonseasonal SST in the Guinea Gulf, obtained by Servain *et al.* (1982), suggests that this local mechanism is not important. This conclusion is apparently confirmed by a direct comparison of the observed seasonal variation of the meridional wind stress at and south of the equator (Fig. 6a) with the observed SST along the equator (Fig. 2). However, as proposed by Rual and Wauthy (personal communication, 1982) the increase of the meridional wind stress in April–May could account for the beginning of the sea surface cooling during the same period. In the same way the permanent strong southerly winds can account for the permanent ridge observed by Voituriez (1981) at 2–3°S of the equator on a repeated transect along 4°W.

d. Advection by currents

Along the northern coast, the maximum offshore Ekman transport occurs east of the maximum upwelling (Bakun, 1978), which is downstream in the strong surface Guinea Current. In the subsurface layer flows a countercurrent (LeMasson and Rébert, 1973a,b) but it is too small to account for upwelling by advection of cold water from the eastern Guinea Gulf.

Along the southern coast, explaining the seasonal upwelling north of 13°S as advection of cold water by the Benguela Current appears to be inadequate. Most of this strong current turns westward off the coast around 18°S (Longhurst, 1962), leaving an area of confused currents to the north (Piton *et al.*, 1977). Hydrological and direct current observations on a long transect off Pointe Noire, visited 17 times in 1973–74, reveal that during the upwelling season the mean coastal circulation is characterized by a thin and weak northward surface current above a large countercurrent (Guillerm, 1975). Furthermore, water mass analysis shows that the upwelled waters in this area might have issued from the equatorial undercurrent in July and probably from the Benguela Current in September (Guillerm, 1981).

According to the model of Philander and Pacanowski (1981a), the equatorial upwelling may be reinforced by advection of cold water from the southern coastal upwelling. Fig. 1 suggests such advection through the Benguela Current. Detailed satellite data analysis (Citeau *et al.*, 1980; Houghton, 1981) and recent oceanographic cruises (French CIPREA experiment) reveal that the equatorial event is completely separate from the intense southwest African coastal upwelling located between 10 and 20°S. Hisard (personal communication), referring to the July chart of air-sea temperature difference of Hastenrath and Lamb (1977), argues that there is no continuity between this coastal upwelling event and the equatorial one. The distribution of nutrients (Voituriez, 1981) confirm this result. But according to Voituriez (1981), we might expect some advection of upwelled coastal water only from just south of the equator in the southern branch of the South Equatorial Current, a current that exists only during the upwelling season.

e. Current-induced upwelling

Ingham (1970) was the first to present the idea of "current-induced" upwelling along the northern coast. The Guinea Current, in geostrophic balance, is associated with an upward thermocline slope toward the coast. Therefore, an acceleration of this eastward current increases this slope and thus could give fa-

vorable conditions for a coastal upwelling. This idea has been developed by Philander (1979) with a nonlinear two-dimensional numerical model with cross equatorial winds. The linear Atlantic model of Anderson (1979) forced by realistic winds confirms one major conclusion of Philander: the Guinea Current is mainly driven by the meridional winds in the Guinea Gulf. But as pointed out by Clarke (1978), Philander's model results produce insignificant upwelling along the northern coast, because all subsurface isotherms are undisplaced at the coast. Coastal SST decreases only by vertical mixing in the Guinea Current.

Another type of current-induced upwelling along the same coast has been proposed by Marchal and Picaut (1977). They noticed the presence of shallow thermocline and cold water patches at the surface, all the year round, downstream of Cape Palmas and Cape Three Points (see Fig. 3 for location), and deep thermocline and accumulation of warm water upstream of these capes. Morlière and Rébert (1972) show that the cold water patch near Cape Palmas extends further downstream. Such local phenomena are most likely due to the dynamical effect of the capes themselves on the strong eastward Guinea Current. Though this "cape effect" seems to increase from July to September, it probably plays a secondary role in the mechanism of this dramatic coastal upwelling.

f. Vertical mixing at the equator

According to Voituriez and Herbland (1979), part of the sea surface cooling along the eastern equator could be due to the increase of vertical mixing processes in the vertical shear between the westward equatorial surface current and the eastward equatorial undercurrent. They suggested that this vertical shear might be reinforced in July–August by the acceleration of the surface current and the shallowing of the undercurrent. But the recent measurements of the French CIPREA experiment in 1978–80 in the Guinea Gulf reveal that there is no significant seasonal variation of the vertical shear or of the Richardson number (Voituriez, 1981).

g. Remote forcing mechanisms

Generally, in this paper the term "remote forcing" refers to remote forcing west of the Guinea Gulf. However, other remote forcing mechanisms have been proposed to explain part of the Guinea Gulf upwelling. This subsection discusses two of them, as well as the idea of Moore *et al.* (1978).

Clarke (1978) tried to explain the seasonal coastal upwelling along the northern coast using coastal trapped wave dynamics. He noted that the maximum values of the longshore wind stress occur to the east of the location of the most intense upwelling (Bakun, 1978). Provided that dissipation of the travelling wind-forced wave is taken into account, the theory agrees qualitatively with observations. In particular, the coastal wind causes upwelling several hundred kilometers west of the forcing region. His model, unfortunately, produces a sea level response that is too small by a factor of 3–5, the length of the forcing area being probably too small.

As noted above, Philander and Pacanowski (1981a) showed that coastal upwelling along the southern coast can extend far offshore by Rossby wave propagation on a time scale greater than a month. This idea seems to be confirmed by Guillerm (1981) who finds at 5°S that during the main upwelling season from June to October the coastal thermal structure in the upper 100 m is extended far offshore, and that the upwelling signals arrives one or two months later offshore than at the coast. Offshore propagation is even more evident during the secondary upwelling signal in December–January.

Moore *et al.* (1978) were the first to suggest that part of the equatorial and coastal upwelling in the Guinea Gulf is remotely forced by the winds in the vicinity of the northern coast of Brazil. They suggested that an increase of the easterly wind in the western equatorial Atlantic excites an internal upwelling equatorial Kelvin wave. This wave travels along the equatorial waveguide and reflects poleward and westward at the African coast in the form of coastal Kelvin waves and Rossby waves. This theoretical idea has been illustrated in the numerical, one-and-a-half layer model studies of O'Brien *et al.* (1978), Adamec and O'Brien (1978) and Bah (1981), in which the winds were switched on impulsively, and is analogous to the proposed explanation for the El Niño event in the Pacific by McCreary (1976) and Hurlburt *et al.* (1976). A number of observations support the idea. For example, it is partly justified by the equatorial zonal pressure gradient study of Neumann *et al.* (1975) and Katz *et al.* (1977) and the fact that the most pronounced seasonal variation of the wind stress is to be found in the western part of the equatorial Atlantic (Fig. 6). Servain *et al.* (1982), on a nonseasonal time scale, show a good correlation, with a one-month lag, between the zonal component of the wind stress off the northern coast of Brazil and the SST in the Guinea Gulf. The one-month lag is the time required for an equatorial Kelvin wave, with a phase speed of ~ 1 m s^{-1}, to travel from the forcing area to the Guinea Gulf. Finally, in the present study we show evidence of poleward propagation of the seasonal coastal upwelling. We will discuss this mechanism further in the last section of the paper.

4. Propagation of the seasonal upwelling

As shown by Hisard and Merle (1980), the upwelling event is substantially different from the con-

ditions during the rest of the year and is the dominant aspect of the annual signal. Our purpose was to focus on this upwelling signal itself and its space-time distribution along the northern and southern coasts and the equator. Detailed analysis of daily SST coastal measurements reveals a westward propagation of the upwelling signal along the northern coast. Further calculations allow us to extend this analysis to the historical merchant ship SST observations all along the northern coast, the southern coast and the equator and to the historical hydrological station south of Abidjan.

a. Horizontal propagation along the northern coast with daily SST data

On all the 16 coastal stations, large periodic SST fluctuations occur mainly during the upwelling season when the thermocline is close to the surface (Fig. 7). The most important of these fluctuations are found around 45- and 14.7-day periods (Picaut and Verstraete, 1976, 1979) which can be attributed to wind and tidal forcing. Such oscillations should considerably blur the mean upwelling signal. Cross-spectral analysis was first suggested to separate the upwelling signal from these oscillations. But since we wish to isolate the upwelling signal from the rest of the annual signal, such analysis was not ideal; furthermore, we have only three years of nearly complete measurements. The duration of the upwelling is roughly 3–4 months (Berrit, 1958; Morlière, 1970), so in order to suppress completely all these high-frequency oscillations, we used a cosine low-pass filter spanning 90 days with first zero lobe at a 45-day period. Small changes in the length of this filter do not alter our results at all. In Fig. 7, we have superposed on the daily raw SST data the low-pass filtered data for the three years of maximum coastal measurements. All these coastal stations show a quite similar pattern of the mean annual signal. The important difference found around Cape Three Points is due to the "cape effect" discussed previously.

From a visual inspection of these filtered data we observe that there is a shift in time of the upwelling signal from east to west. This displacement is confirmed by a time–space plot (not shown here) of the date of the minimum of filtered SST data. However, for particular years and stations (Tabou, 1978, for example) the SST minimum is not exactly centered in the middle of the upwelling signal. So, to improve the estimate of the westward phase shift, a simple lagged correlation analysis is used. The length of the time series is constant and equal to three months in order to agree with the duration of the upwelling event. For each pair of stations we calculated the maximum correlation coefficient and the corresponding lag. The maximum correlation coefficient is, of course, larger for two nearby stations than for two distant stations, and in the first case we obtain a better estimate of the phase lag. There is no special reason to choose one particular station as the reference. So we make the same type of calculation with all the stations as the reference and obtain a symmetric matrix of the maximum correlation coefficients and their corresponding lags. For each station as the reference, we plot these day lags versus the distance between the coastal stations. All these graphs are quite similar with some distortion for the farthest stations. In Fig. 8 we present the mean graph for each year. Such an average has no statistical justification but it probably reduces slightly the error obtained with the farthest stations. Unfortunately, this method of correlation on a short time scale does not permit a rigorous estimate of error. Advantages of this approach are discussed further in Section 5C.

The monthly axes of Fig. 8 have been built by the following method. We define the start of the upwelling season as the date when the temperature drops below the annual average and the end of this season as the date when the temperature becomes warmer than this average. The surface obtained by integration between these two limits is divided into two equal parts by a date line estimated as the "center of upwelling." This date is more precise than the date of minimum temperature and evident correlation with the previous mean lags allow us to add the monthly axes.

Fig. 8 shows clearly that for each year, 1977–79, the upwelling event propagates from east to west. Advective phenomena could not account for this shift of phase: in the surface layer the strong Guinea Current is eastward while in the sub-surface layer there is a countercurrent of about 20 cm s^{-1} mean speed (Lemasson and Rébert, 1973a,b). With the two lowest Fourier components of the monthly mean SST coastal measurements from Cotonou to Abidjan, Merle *et al.* (1980) found a similar propagation and related it to a semiannual oscillation of unclear origin.

It is interesting that the speed of the westward propagation varies from year to year. This variation may be related to the difference of stratification since 1977 was a normal upwelling year while 1978 was a strong one and 1979 a weak one (Fig. 9). FGGE data collected by ORSTOM in the eastern equatorial Atlantic confirm such a difference between the 1978 and 1979 upwellings (Hisard, personal communication, 1981) but this difference is probably not strong enough to cut the speed in half.

Fig. 9 shows a decrease of the seasonal amplitude east of Tema and west of Grand Drewin. These features are due to the presence of two frontal zones (Berrit, 1973), one just on the Cape Palmas, the other moving along the Togo and Benin coasts. These fronts separate the cold and saline upwelled waters from warm and fresh waters (Fig. 10). These fresh waters are provided by Guinea rivers and the Niger

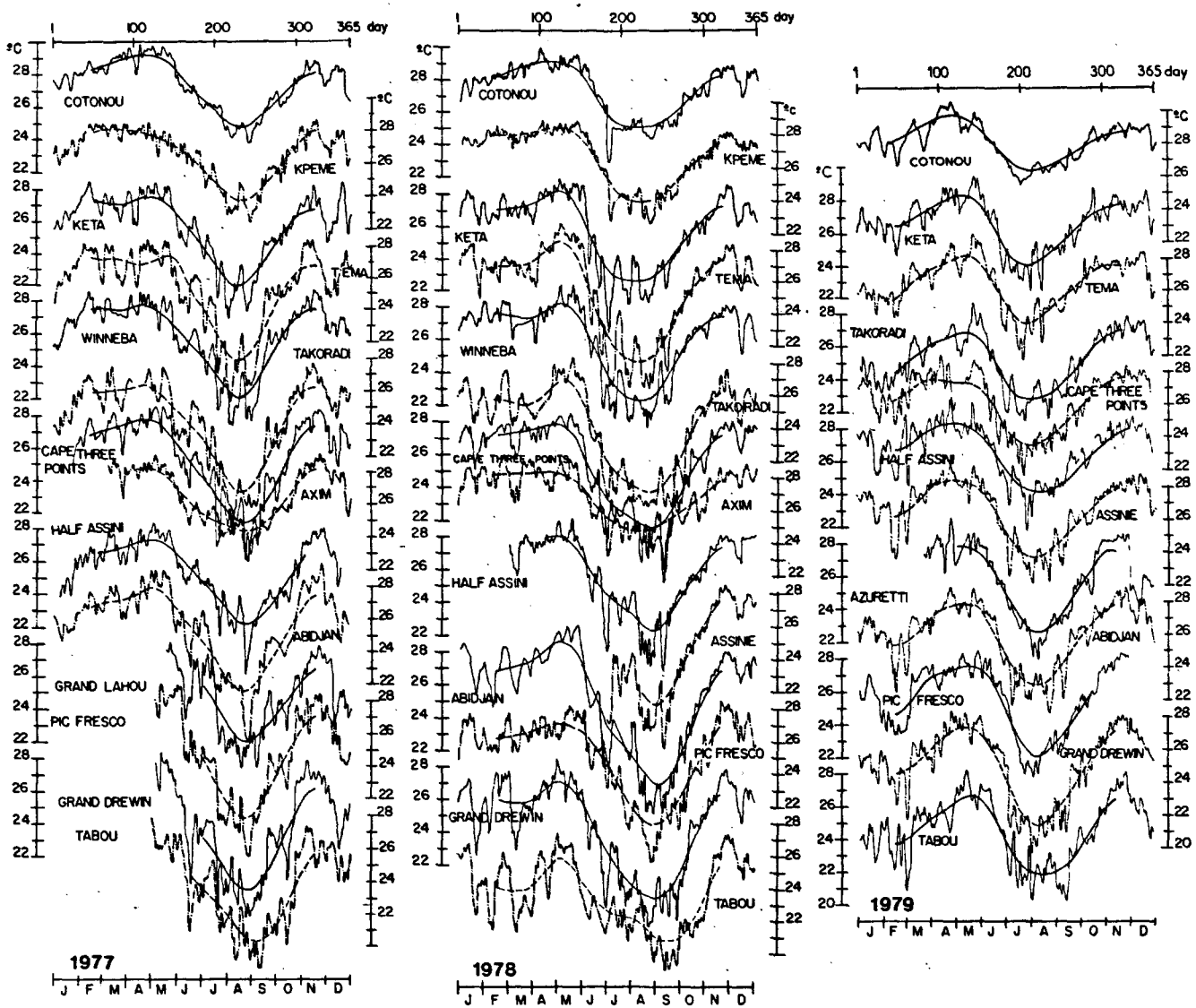

FIG. 7. Daily and low-pass filtered sea surface temperature along the northern coast of the Guinea Gulf.

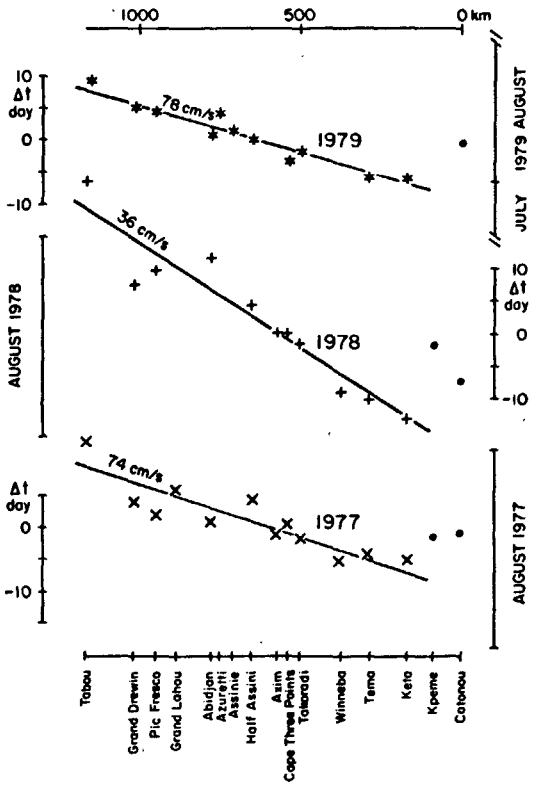

FIG. 8. Mean lag at maximum correlation between filtered sea surface temperature along the northern coast during the 1977–78 and 1979 upwelling. Solid dots represent data not used in the regression estimates of horizontal phase propagation.

River and particular heavy rainfall, and are accumulated in these two areas by favorable winds (Hastenrath and Lamb, 1977). On the other hand, along the Ivory Coast and Ghana coasts, the direction of the winds is favorable for upwelling (Verstraete, 1970). So west of Tabou (Morlière, and Rébert, 1972) and east of Keta, the thermocline is quite deep. Therefore, outside of these limits the SST signal is not closely related to the upwelling signal and for this reason the Cotonou and Kpeme reuslts are not included in the regression-line calclations of Fig. 8.

b. Horizontal propagation along the northern coast with monthly mean SST data

We have found that the upwelling signal propagates westward along the Ivory Coast, Ghana, Togo and Benin coasts. The source region has to be found further east. Unfortunately, there are no coastal stations in Nigeria and Cameroon. The only data available are the monthly 1° square SST means taken from merchant ship observations. The mean duration of the upwelling signal is around 3–4 months, so monthly data are adequate to resolve it.

In order to have a better resolution than one month in our cross correlation analysis we have built the following method: using monthly data for a Fourier analysis of the mean year, the seasonal cycle, with daily values, is reconstituted from the lowest Fourier components. This method applied to the average annual cycle of Tema shows that the best fit between the daily filtered data and the daily reconstituted data is obtained with the first 5 or 6 harmonics (Fig. 11). To test this method we have used it on the monthly mean SST of the coastal stations of the northern coast in 1978 and 1979. Despite the fact that for an individual year such Fourier analysis gives an error on the borders of the reconstituted time series, comparison of the preceding lagged cross correlation results and those obtained with this method (Fig. 12) validates it completely.

Therefore, this method was first applied on the historical records of monthly mean SST data by 1° squares arranged all along the northern coast as shown in Fig. 4. Cross correlation analysis of these reconstituted time series, identical to that applied on the daily filtered data, shows that the propagation of the upwelling signal is only evident between the Cape Palmas front and the Togo-Benin front (Fig. 13), where the thermocline shoals to the surface. Outside of this coastal area, a deep thermocline, fresh water (Fig. 10) and local thermodynamic effects probably blur the sea surface upwelling signal.

c. Horizontal propagation along the southern coast with monthly mean SST data

Similar cross correlation calculations on daily filtered data with sparse stations along the southern

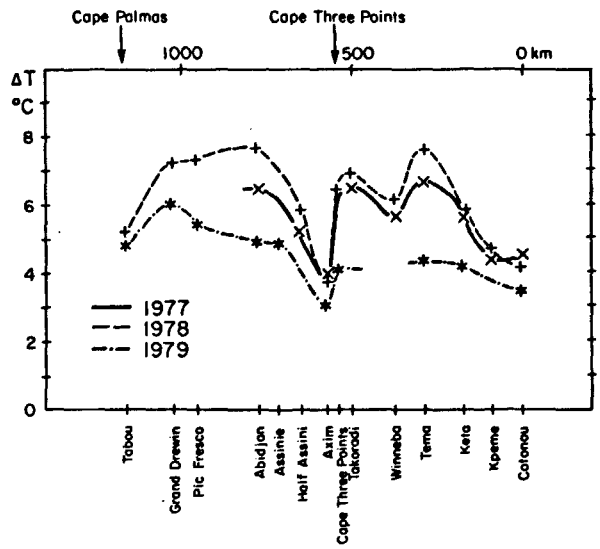

FIG. 9. Amplitude of the seasonal signal along the northern coast. This amplitude is defined as the difference between the maximum of temperature around May and the minimum of temperature around August, extracted from the low-pass filtered curves of Fig. 7.

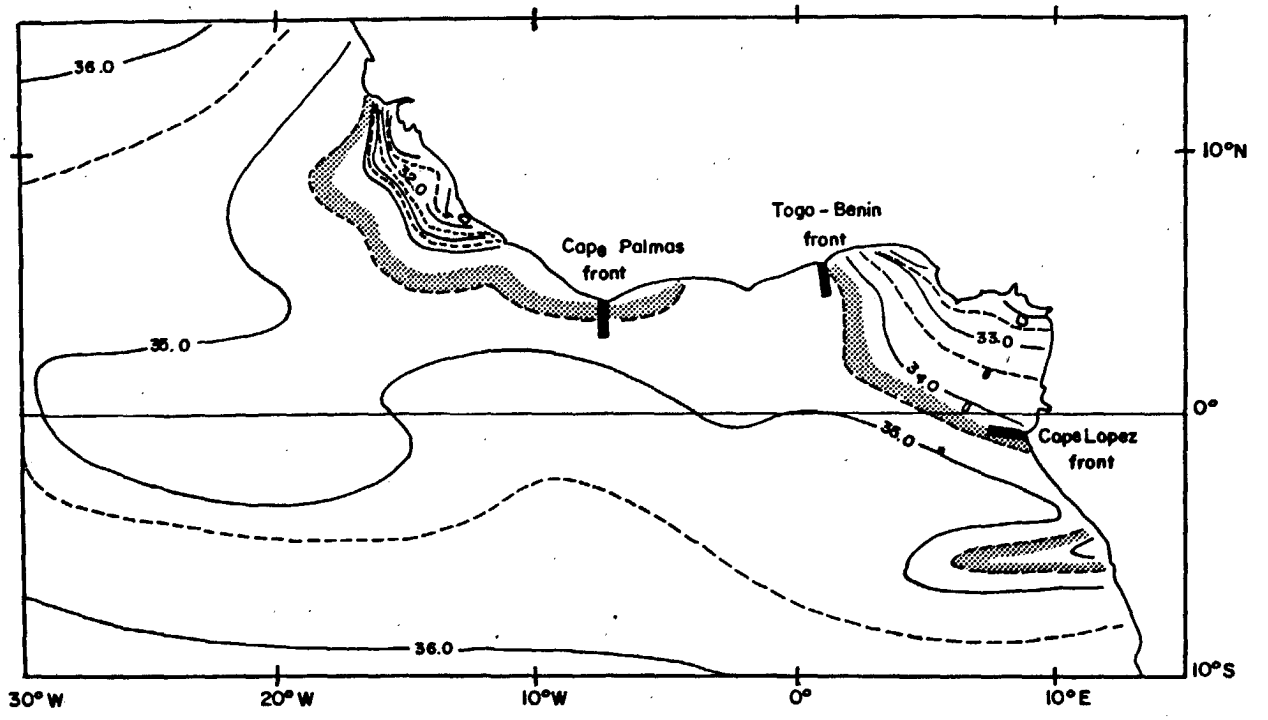

FIG. 10. Surface salinity and location of the fronts in July–August–September [composite picture from Merle (1978) and Berrit (1973)].

coast seem to indicate a poleward propagation of the coastal upwelling signal. Unfortunately, except at Pointe Noire in the Congo Republic, these few stations have not been maintained. So we were fortunate that monthly mean SST data could verify such propagation. The 1° squares chosen were arranged along the southern coast as shown in Fig. 4. The results of the cross correlation analysis, centered on the three months of upwelling, are plotted in Fig. 14. Southward propagation of the upwelling signal is evident between 1 and 13°S. Further north, there is a frontal area which sharply separates the low-salinity Guinea water to the north from high-salinity cold water (Fig. 10), probably derived from the equatorial undercurrent (Hisard *et al.*, 1975). In the same way as along the northern coast, the upwelling signal is probably masked north of 1°S. South of 13°S, Wooster (personal communication, 1980) has shown that the sea-

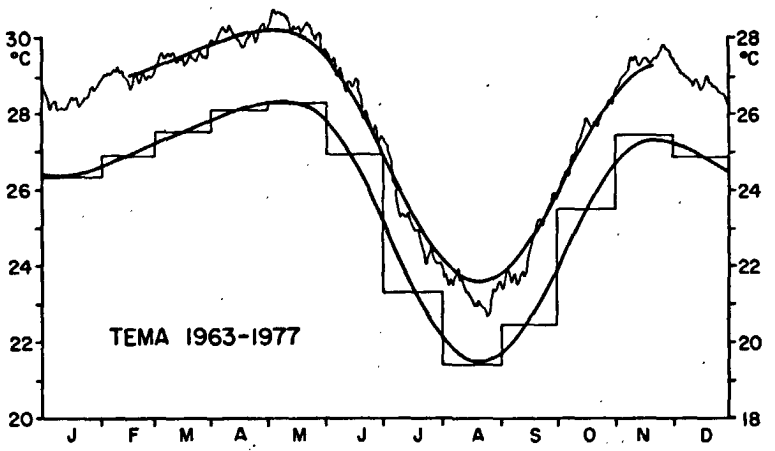

FIG. 11. Comparison of the low-pass filtered daily sea surface temperature data and the "reconstituted" sea surface temperature data at the coastal station of Tema (mean of 15 years).

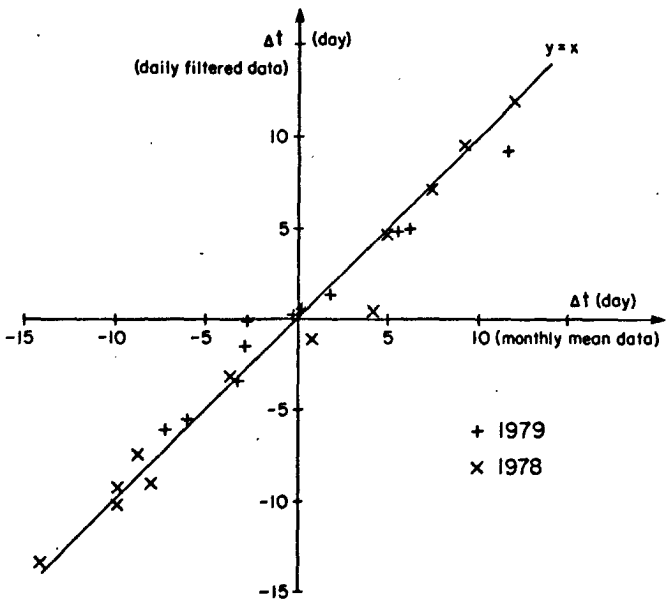

FIG. 12. Comparison of the mean lag results obtained with the daily low-pass filtered upwelling data and the "reconstituted" upwelling data from monthly mean for all the coastal stations.

sonal variation of the local offshore Ekman transport seems to fit the corresponding temperature distribution much better than in the north (Fig. 4). South of 18°S advection from the Benguela Current probably interferes with other upwelling mechanisms. These additional processes could explain the dispersion of our mean lags south of 13°S. For the interval 1–13°S a regression line has been fitted through the mean

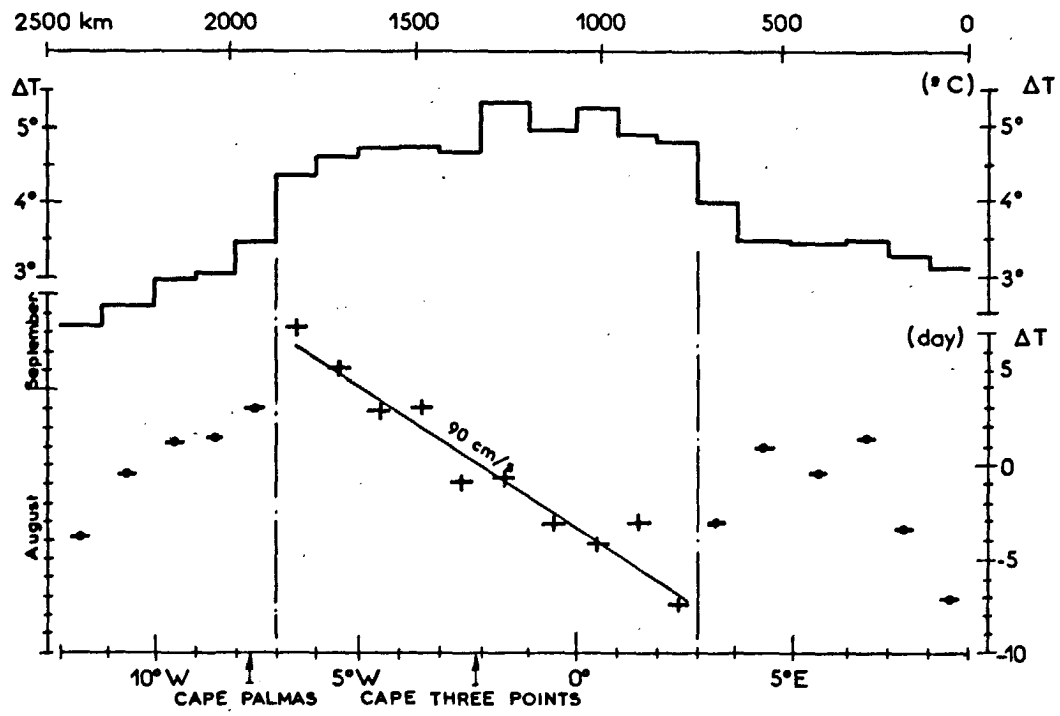

FIG. 13. Mean lag at maximum correlation between "reconstituted" sea surface upwelling temperature and amplitude of the seasonal signal within the 1° square areas arranged along the northern coast as shown in Fig. 4.

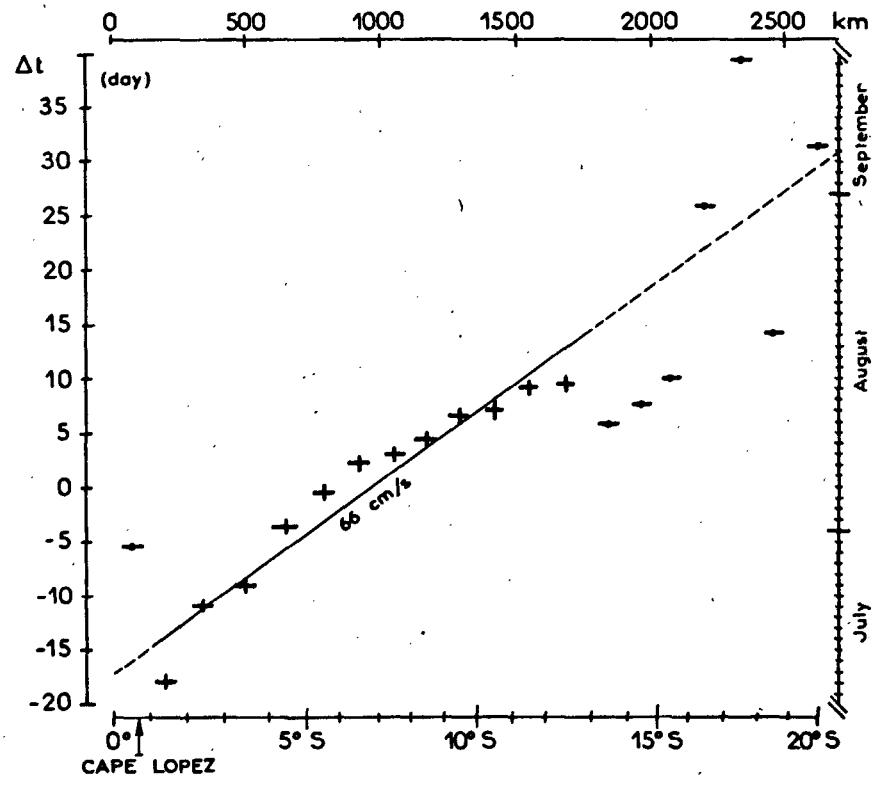

FIG. 14. Mean lag at maximum correlation between "reconstituted" sea surface upwelling temperature within the 1° square areas arranged along the southern coast as shown in Fig. 4. Only the data represented by a cross are used in the regression fit.

day-lag points (Fig. 14). The resulting mean phase speed of 66 cm s^{-1} is much greater than the speed of the southward coastal undercurrent found by the oceanographers of Pointe Noire (Guillerm, 1975). So advection could not account for this phenomenon.

d. Horizontal propagation along the equator with monthly SST data

In an attempt to account for horizontal propagation along the equator we have applied our particular correlation analysis to the SST historical data arranged along the equator by 1° squares as shown on Fig. 4. We have limited the geographical extent of our study to 20°W where the thermocline is not too far from the surface (Merle, 1978), and at 1° from the equator which is a distance smaller than the equatorial internal radius of deformation for the first vertical mode. Despite such precautions, our results are not very convincing, but at least they appear to be more favorable to an eastward propagation of the upwelling signal than to a westward one. Correlation between the equatorial and coastal upwelling signals is difficult to interpret due to the difference of shape in these signals: the coastal upwelling signal is symmetric about its minimum value, opposite to that of the equatorial upwelling signal which is asymmetric (Fig. 2). This poor evidence of horizontal propagation along the equator could be due to the difficulties of SST data to resolve the upwelling signal when the thermocline is not surfacing (Houghton, 1981). Furthermore, along the equator we expect interference between the eastward equatorial Kelvin wave and westward Rossby waves coming from the coast.

e. Vertical propagation south of Abidjan with monthly mean hydrological data

Between 1957 and 1964, 217 Nansen casts were made at a site 41 km south of Abidjan on the continental slope. The "reconstituted" seasonal cycle using monthly means from these data (Fig. 15a) has been calculated using the same method as in the previous sections. In Fig. 15b we have drawn the time-depth isotherm contours with simple linear interpolation of the time series of Fig. 15a, because such a representation gives a better idea of the vertical distribution of the upwelling event. We have limited this graph to the upper 400 m that have been sampled systematically. The amplitude of the seasonal displacement of the isotherms is minimum close to the surface, maximum between 50 and 200 m, and then decreases to 400 m. A remarkable feature of this hydrological station is the continuous linear displace-

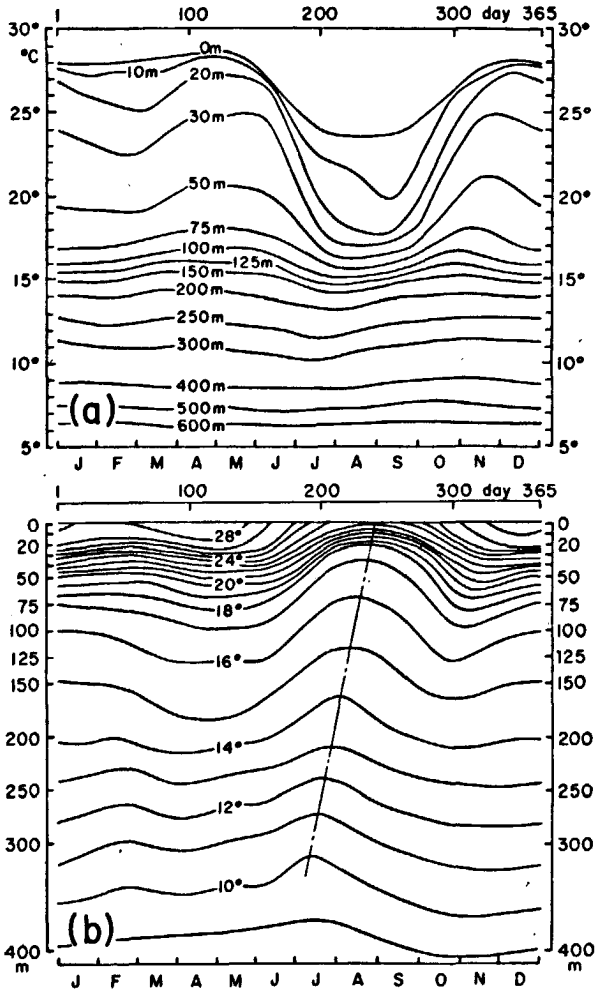

FIG. 15. (a) "Reconstituted" annual cycle of temperature at standard depths 24 miles off Abidjan. (b) Isotherm depths from the data of the preceding figure.

ment of the upwelling event from 300 m to the surface (Fig. 15b). Our cross-correlation analysis applied to this "reconstituted" time series shows an upward propagation with phase speed 7.9×10^{-5} m s^{-1} (6.8 m day^{-1}). In the surface layer the observed shift of phase might be explained by some reflection or refraction in the thermocline or by anything locally forced at the surface (Fig. 16).

5. Discussion

In the previous section we have found that in the Southern Hemisphere the upwelling signal propagates poleward, starting from the equator (Fig. 14). Along the northern coast a similar signal propagates westward from the Togo-Benin front to the Cape Palmas front (Figs. 10 and 13). Between the equator and the Togo-Benin front, there is no evidence of horizontal propagation with the SST historical data (Fig. 13). Furthermore, the upwelling signal propagates upward, at least south of Abidjan. Such features could be related to the same process, i.e., remote forcing by the winds west of the Guinea Gulf.

This section explores the possibility of this remote forcing mechanism in greater detail. First, some recent results supporting the idea are discussed. Second, similarities with the equatorial Pacific are summarized. Third, we discuss the particular method of cross correlation used throughout this study. Finally, recent models involving this remote forcing mechanism are reviewed.

a. Support for remote forcing in the equatorial Atlantic

1) POLEWARD PROPAGATION OF THE COASTAL UPWELLING SIGNAL

If the events propagating along the northern and southern coasts have the same equatorial origin, they must start from the equator at the same time. Referring to the monthly axes of Figs. 13 and 14, there is a time delay of 33 days between the starting dates of the southern upwelling signal at the equator and the northern one at the Togo-Benin front. Direct cross correlation analyses between the southern and northern coastal "reconstituted" time series reduce this delay to 28 days. This delay is the time required for a 0.6 m s^{-1} wave to travel all along the corner of the Guinea Gulf from the equator to the Togo-Benin front, and this speed is close to those observed in both hemispheres. These properties suggest that the coastal waves have a common point of origin at the equator. There is no evidence of a propagating upwelling signal in SST between the Cape Lopez front and Togo-Benin front (see Fig. 10 for location). As previously

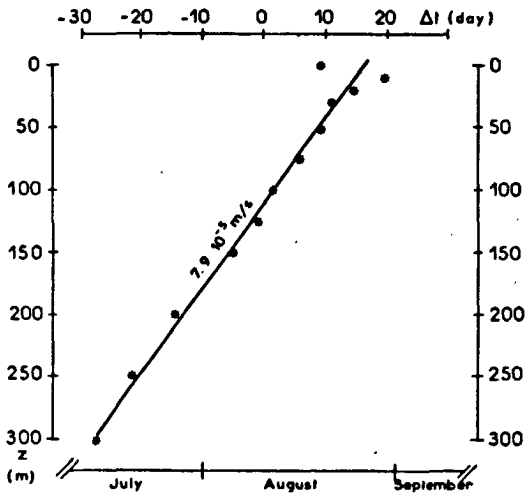

FIG. 16. Mean lag at maximum correlation between "reconstituted" upwelling temperature at different levels 41 km off Abidjan.

noted, this lack of notable propagation is probably due to the presence of a deep thermocline, as well as to fresh water and local thermodynamic effects. The Cape Lopez area has been studied intensively (see Stretta, 1977, for example). Nobody, as yet, has observed a change in the atmospheric forcing in this region that is strong enough to generate the required coastal waves. So, at the present time, the only plausible explanation for this poleward propagation is remote forcing due to wind change west of the Guinea Gulf (Moore *et al.*, 1978; McCreary *et al.*, 1982; Busalacchi and Picaut, 1982).

2) Vertical propagation of the coastal upwelling signal

According to Hickie (1977), Philander (1977) and Cane and Sarachik (1979), a zonal coast near the equator allows westward propagating, nearly non-dispersive waves that are very similar to coastally trapped Kelvin waves. In an ocean of constant Väisälä frequency, these waves, to a good approximation, satisfy the dispersion relation (Philander, 1977)

$$\sigma = -\frac{k}{m}N,$$

where σ is the wave frequency, m the vertical wavenumber, k the horizontal wavenumber, and N the Väisälä frequency. The time series of the upwelling (Figs. 7 and 11) resembles a half-sinusoid extending over three months. Furthermore, there is a secondary upwelling season around January which is more pronounced in the subsurface layer (Fig. 15) and present in all the Guinea Gulf (Merle and Le Floch, 1978). Therefore, the apparant dominant upwelling frequency is $2\pi/6$ months. With a mean westward phase speed of 0.7 m s^{-1} and an upward phase speed of 7.9 $\times 10^{-5}$ m s^{-1}, the dispersion relation is verified for a constant Väisälä frequency of 0.36×10^{-2} s^{-1}. This value is close to what we observe below the sharp and shallow thermocline (Fig. 17).

Such a vertically propagating phenomenon has been related to the remote forcing mechanism of Moore *et al.* (1978) by an extension of the linear model of McCreary (1982) to the Guinea Gulf problem (McCreary *et al.*, 1982). In this recent study the idealized winds are limited to the western equatorial Atlantic and to the annual frequency. The solutions are found as sums over the first 15 vertical modes. The energy that appears east of the wind forcing area is the result of the radiation of many equatorial Kelvin waves. They superpose to form a beam that propagates eastward and downward at the slope $-\sigma/N$. At the north–south coast of Africa this beam reflects as a packet of Rossby and Kelvin-like coastally trapped waves along the northern coast. Energy associated with the Rossby waves propagates westward and downward at a slope greater than $3\sigma/N$. This result

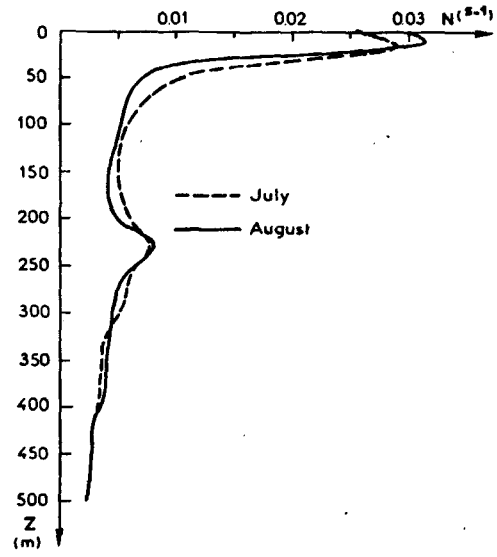

FIG. 17. Mean Väisälä frequency profiles during the upwelling season at the station south of Abidjan.

suggests that the westward and upward propagating upwelling signal south of Abidjan appears to have the characteristics of coastally trapped Kelvin waves, rather than those of reflected Rossby waves. Rossby wave energy is too deep to participate significantly in the event. Similar upward phase propagation of the seasonal upwelling signal offshore Pointe Noire at 5°S (Servain, personal communication, 1982) suggests that such a phenomenon is not exceptional in the Guinea Gulf.

3) Other results

As we have seen in the preceding subsection, the coastal upwelling signal along the northern coast has several properties of a coastally trapped Kelvin wave. A mean section south of Abidjan has been built with historical data from the upwelling season (Fig. 18) and shows an offshore exponential isotherm decay. Such a structure can be interpreted as an indication of a coastally trapped phenomenon.

The variation of surface and subsurface currents may also support the existence of such equatorial and coastal Kelvin waves. Moore *et al.* (1978) explained the decrease of the equatorial undercurrent and the increase of the South Equatorial Current from January to July by the passage of the upwelling equatorial Kelvin wave signal. This result based only on two transects made in 1975 has been confirmed by eight recent transects made, along the same meridian (4°W), during the French CIPREA experiment and FGGE. Along the northern coast, Janke (1920) noted an acceleration of the eastward Guinea current during the upwelling season, but direct measurements made by Lemasson and Rébert (1973a) on a transect close

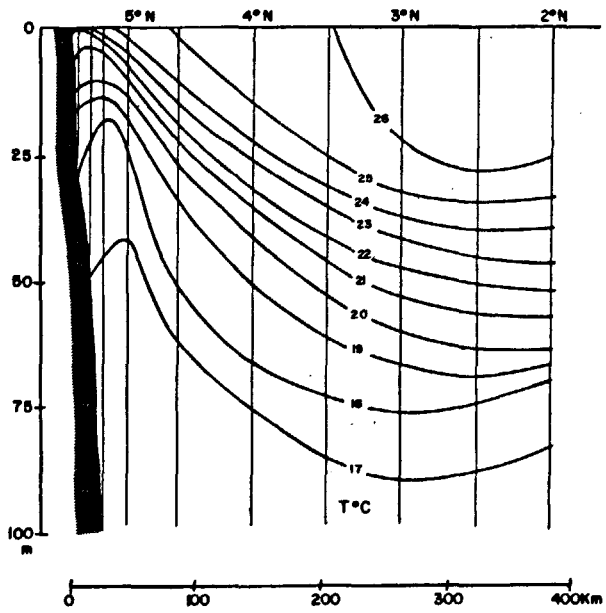

FIG. 18. Mean transect south of Abidjan during the upwelling season.

to the coast reveal that this increase arrives one or two months earlier on the shelf. This discrepancy could be due to the influence of the local meridional wind on the Guinea current (Philander, 1979; Anderson, 1979). With a transect off Pointe Noire (5°S), extended further offshore to 370 km, Guillerm (1981) observed a southward surface current which reverses during the upwelling season. The subsurface layer is characterized by a southward flow all the year round, but the mean southward transport, calculated along this transect, vanishes during the upwelling season and might reverse as the coast is approached.

Indirect evidence of an equatorial Kelvin wave has been recently found by Voituriez (1981). With *T-S* diagrams he first shows that the isopycnal surface $\sigma_t = 26.44$ is not influenced by vertical mixing with the surface layer. Comparison of the mean depth of this surface, based on all the transects made along 4°W, in the warm season (January–April) and the upwelling season (July–September), reveals that the amplitude of the difference is maximum at the equator (from 120 to 70 m) and minimum around 2°N and 2°S. This first evidence of an equatorial trapped phenomenon on a seasonal time scale at 4°W has been confirmed by recent heat content analyses and isotherm displacements by Houghton, Voituriez and Gouriou (personal communications, 1982). The results of Houghton indicate a trapping scale of 180 km, which suggests a possible 0.73 m s^{-1} horizontal propagating Kelvin wave.

The best direct evidence of the importance of remote forcing in the equatorial Atlantic has been obtained by Servain *et al.* (1982). In this study, they examined the relationship between the SST and wind stress anomalies, extracted from historical merchant ship observations. Local forcing in the Guinea Gulf appears to be very weak, while remote forcing from the western side of the basin is much more evident. The phase difference obtained is significant around the 3-month period and up to the 5-month period, and corresponds to a nearly constant lag of one month. This lag is almost the time required for the dominant (Philander and Pacanowski, 1981; McCreary *et al.*, 1982) second-mode baroclinic equatorial Kelvin wave (1.2 m s^{-1} phase speed in the eastern equatorial Atlantic) to travel from 30°W to the Guinea Gulf or probably a combination of many modes as shown by McCreary *et al.* (1982).

b. Similarities with the equatorial Pacific

In the Pacific Ocean, Wyrtki (1975) suggested that the El Niño event was caused by the relaxation of the southeast trades in the central and western Pacific which in turn results in an eastward propagation of energy along the equator. This process was later used to account for the appearance of a large semiannual variation in isotherm depth in the eastern Pacific, since wind stress forcing at the same frequency occurs predominantly in the central Pacific (Meyers, 1979). Moored upper ocean current and temperature measurements (Knox and Halpern, 1982) support the propagation of a first baroclinic Kelvin wave event from 152 to 110°W. Around the Galapagos islands, sea level variance is also compatible with the structure of such a wave (Ripa and Hayes, 1981). Close to the same area, detailed analyses of historical hydrological data on a seasonal time scale by Lukas (1981) reveal an upward phase propagation of the downwelling event from 500 to 125 m, with a mean phase speed of 6.7×10^{-5} m s^{-1}, close to our present result. Along the eastern boundary Enfield and Allen (1980) found that interannual fluctuations of sea level are coherent from northern Chile to the Canadian border and have a phase structure consistent with poleward long-wave propagation. The recent observations of upward phase propagation at the annual frequency in the subsurface layer, north and south of the equator by Lukas and Firing (1982), suggests the existence of reflected Rossby waves in the central Pacific.

Numerical and analytical models by McCreary (1976) and Hurlburt *et al.* (1976) simulated the excitation of an equatorially trapped internal Kelvin wave and its reflection on the eastern boundary. Busalacchi and O'Brien (1981) and Busalacchi *et al.* (1982), with a linear model forced by monthly estimates of the observed surface wind over the tropical Pacific for 1961–78, were able to explain a significant amount of the variability of sea level at the eastern boundary as being caused by remotely forced equatorial waves.

c. Discussion of our specific cross-correlation analysis

Our cross-correlation analysis was made only on the three months centered on the cold season. Similar analyses utilizing all the annual signal gave poor evidence of poleward propagation along the northern and southern coasts and of upward propagation south of Abidjan. There are several possible explanations for such conflicting results.

First, as pointed out in the previous sections, the SST measurements are inadequate to show horizontal propagation when the thermocline is not surfacing. The two warm seasons surrounding the main upwelling season are characterized by a deep thermocline (Morlière, 1970). Furthermore, Hisard and Merle (1980) claim that the warming during these seasons is more due to local thermohaline effects. Therefore, these seasons are probably disconnected from the main upwelling season, at least in the surface layer.

Second, model studies suggest that well-defined Kelvin wave signals exist only if the equatorial wind field changes sufficiently rapidly. Philander (1981) studied the model response to a uniform relaxation of the equatorial zonal winds. He varied the length of time T over which the relaxation occurs, and was able to detect an equatorial Kelvin wave only for $T < 4$ months. Using a simple one-and-one-half layer model of the Guinea Gulf like that of O'Brien *et al.* (1978), we found similar results related to an increase of the westward wind stress in the western part of the basin. For $T = 1$–3 months, the Kelvin wave upwelling signal is well-defined, but for $T \geq 6$ months, this signal could not be easily identified. Fig. 6b suggests that a value of T for the increase of the trades is 3–4 months. However, this figure represents the mean of 60 years of measurements and overestimates the time T. For example, a 1979 wind record from St. Paul Rocks (0°55'N, 29°21'W) reveals a sharp increase of the wind within two weeks, starting around 1 May (Katz *et al.*, 1981). In addition, detailed analyses of historical merchant ship observations for specific years (Servain *et al.*, 1982) show that in the western equatorial Atlantic such a sharp increase is not unusual. Therefore, the model results suggest that a well-defined upwelling Kelvin wave will exist. On the other hand, after a second pulse in November (which might generate part of the intringuing secondary upwelling season) the wind relaxes over a longer time (Fig. 6b), and in that case the model suggests that the downwelling Kelvin wave will not be so clearly evident. The signal-to-noise ratio of this downwelling wave is correspondingly small and neither horizontal nor vertical propagation (Fig. 15b) can be detected during the warm season. It is worth noting that the analyses of Servain *et al.* (1982) are not able to separate the upwelling and downwelling events, but the effect of the decreasing signal-to-noise ratio is compensated by the length of the time series (16 years) and the use of classical statistical methods.

Our cross-correlation method has the advantage of clearly separating each season, and is able to show evidence of horizontal and vertical propagation of the upwelling signal when the signal-to-noise ratio is large. The usefulness of a 3-months record length centered on the cold season has been confirmed in a series of additional cross-correlation calculations involving different record lengths. For longer lengths the signal-to-noise ratio decreases as previously noted. For shorter lengths, the shape of the curve about the minimum of temperature is quite different for some of the coastal stations [see Tabou (1978) on Fig. 7 for example], and this difference gives poorer evidence of horizontal and vertical propagation. Three months, which is the mean duration of the upwelling signal, gives the best evidence of propagation.

d. Models of remote forcing mechanisms

Our calculation suggests that the seasonal coastal upwelling propagates poleward in both hemispheres, starting from the equator. On a nonseasonal time scale Servain *et al.* (1982) found a good correlation between the zonal wind stress in the western equatorial Atlantic and the SST in the Guinea Gulf, with a lag of one month, the time for a Kelvin wave to travel at 1 m s^{-1} from the forcing area to the Guinea Gulf. These two results are the main features of the remote forcing mechanism proposed by Moore *et al.* (1978) and illustrated by the linear model of O'Brien *et al.* (1978). But this model involves so many simplifications that it is surprising that our observations fit its results as well as they do. So, we conclude this paper with a brief review of this model and others that involve remote forcing in the Atlantic.

O'Brien *et al.* (1978) and Adamec and O'Brien (1978) used a linear, one-and-one-half layer model, in which the wind, limited to the western part of the basin, was switched on impulsively. Equatorial and coastal Kelvin waves are evident, and phase lags in the eastern ocean are simply related to the speed of these waves. In contrast, Cane and Sarachik (1981) studied the response of a single baroclinic mode to an x-independent periodic forcing. In this model the response is a complex superposition of a locally forced response and of Kelvin and Rossby waves that make impossible the detection of a pure equatorial Kelvin wave. Moreover, at the annual frequency, coastal Kelvin waves no longer exist along north-south boundaries, equatorward of the critical latitude. Consequently, phase lags in the eastern part of the basin could not be directly related to the speed of the equatorial Kelvin wave. Busalacchi and Picaut (1982) used a similar linear model with real coastline geometry

and realistic seasonal winds. The winds used are the mean of 60 years of measurements (Hastenrath and Lamb, 1977) and are more similar to purely periodic forcing than to an impulsive one. The model simulate rather well the mean seasonal pycnocline variations in all the basin, and the seasonal variations along the equator are driven, for a significant part, by the easterly winds west of the Guinea Gulf. As in the Cane and Sarachik (1981) study, there is no obvious equatorial Kelvin wave. However, the model is able to simulate in both hemispheres the poleward propagation of the seasonal coastal upwelling signal, which appears directly related to the equatorial seasonal signal. The poleward propagation along the north-south boundaries is probably due to the presence of friction and to the higher annual harmonics used in the forcing function.

Upward phase propagation and narrow coastal and equatorial flow fields appear in the linear three-dimensional model of McCreary *et al.* (1982). As previously noted, this model is forced by an idealized annual wind that is confined west of 20°W. Its response does not remain confined to the surface but propagates downward as a beam of energy that is associated with upward phase propagation. Rossby beams all propagate in the deep ocean at a steeper angle than Kelvin beams. Therefore, along the equator and along the northern coast of the Guinea Gulf, Kelvin beams no longer completely interfere with the Rossby beam. This property accounts for the narrow coastal and equatorial phenomena in the model.

Another possibility for the presence of equatorial and coastal Kelvin waves in periodic forced models is the disappearance of Rossby waves in the upper ocean due to nonlinear effects (Philander and Pacanowski, 1981b). For an x-independent wind, these authors found that the equatorial Kelvin wave is only evident when the period is less than six months. In the same nonlinear stratified model, such limit is moved back when the forcing is confined to an area west of the eastern boundary. In the unforced region, in the same way as the McCreary *et al.* (1982) model, all the changes of the various fields are directly associated with the eastward propagating Kelvin wave.

These models suggest the following conclusions. Due to the presence of a good part of the forcing west of the Guinea Gulf, x-independent models are not very relevant to the Guinea Gulf problem. When the forcing is confined west of the Gulf, the distinction between the impulsive and the periodic forcing is no longer fundamental, because equatorial Kelvin waves can be detected in both cases. Higher order vertical modes, harmonics higher than the annual frequency, and friction are necessary for the generation of narrow coastal phenomena and their poleward propagation. But the models also indicate that a lot of questions remain to be answered. For example, what is the importance of the nonlinear terms? How much energy propagates downward? Does the upward phase propagation exist everywhere in the Guinea Gulf? What are the adjustment time scales and frictional decay time in the real ocean? Detailed analyses, in the surface and subsurface layers, on historical data and comparison with more models are needed. But real progress will depend on extensive data being available on specific years. Therefore, we expect the SEQUAL-FOCAL experiments, in the equatorial Atlantic, to provide much more information to increase greatly our knowledge of the remote forcing mechanism first suggested by Moore *et al.* (1978).

Acknowledgments. This work was begun at the Centre de Recherches Océanographiques (ORSTOM) of Ivory Coast and finished at the Université de Bretagne Occidentale. The paper was written at the University of Hawaii during my visit at JIMAR in May–October 1981 and kindly and efficiently typed by Wendy Takesono. Part of this study has been supported by CNEXO Contract 81-2437, CNRS ATP No. A15031, and a cooperative agreement (No. NA80RAH00002) from NOAA, through JIMAR. I would like to thank Warren Wooster for permission to publish Fig. 5 and Stephan Hastenrath, Andrew Bakun, the Service des Pêches in Benin, the Ghana Fishery Research Unit and the Centre de Recherches Océanographiques in Ivory Coast for generously providing data which has been efficiently managed by the BNDO (COB-BREST). I am particularly grateful for the many helpful discussions with Jay McCreary, Dennis Moore, Roger Lukas, Bruno Voituriez and Tony Busalacchi.

REFERENCES

Adamec, D., and J. J. O'Brien, 1978: The seasonal upwelling in the Gulf of Guinea due to remote forcing. *J. Phys. Oceangr.*, **8**, 1050–1060.

Anderson, D., 1979: Low-latitude seasonal adjustment in the Atlantic. (Unpublished manuscript).

Bah, A., 1981: Upwelling in the Gulf of Guinea. *Echohydrodynamics*, J. C. J. Nihoul, Ed., Elsevier, Amsterdam, 99–140.

Bakun, A., 1978: Guinea current upwelling. *Nature*, **271**, 147–150.

——, D. R. McLain and F. V. Mayo, 1974: The mean annual cycle of coastal upwelling off western North America as observed from surface measurements. *Fish. Bull.*, **72**, 843–844.

Berrit, G. R., 1958: Les saisons marines à Pointe Noire. *Bull. Inf. C.O.E.C.*, **6**, 335–360.

——, 1973: Recherches hydroclimatiques dans les régions côtieres de l'Atlantique tropical oriental. Etat des connaissances et perspectives. *Bull. Mus. Nat. Hist. Nal. Paris*, **148**, *Ecologie Générale*, **4**, 85–99.

——, 1976: Les eaux froides côtières du Gabon à l'Angola sont-elles dues a un upwelling d'Ekman? *Cah. ORSTOM, Sér. Océanogr.*, **14**, 273–278.

Bunker, A. F., 1976: Computations of surface energy flux and annual air-sea interaction cycles in the North Altantic Ocean. *Mon. Wea. Rev.*, **104**, 1122–1139.

Busalacchi, A. J., and J. J. O'Brien, 1981: Interannual variability of the equatorial Pacific in the 1960's. *J. Geophys. Res.*, **86**, 10901–10907.

——, and J. Picaut, 1983: Seasonal variation from a model of the tropical Atlantic. Submitted to *J. Phys. Oceanogr.*

——, K. Takeuchi and J. J. O'Brien, 1982: Interannual variability of the equatorial Pacific—Revisited (Manuscript in preparation).

Cane, M. A., and E. S. Sarachik, 1979: Forced baroclinic ocean motions, III: The linear equatorial basin case. *J. Mar. Res.* **37**, 355–398.

——, and ——, 1981: The response of linear equatorial ocean to periodic forcing. *J. Mar. Res.*, **39**, 651–693.

Citeau, J., G. R. Berrit and L. Verseci, 1980: The upwelling in the Guinea Gulf as observed by Meteosat. *Proc. Workshop Applications of Existing Satellite Data to the Study of the Ocean Surface Energies.* University of Wisconsin Press, 233–237.

Clarke, A. J., 1978: On the generation of the seasonal coastal upwelling in the Gulf of Guinea. *J. Geophys. Res.*, **84**, 3743–3751.

Cromwell, T., 1958: Circulation in a meridional plane in the central equatorial Pacific. *J. Mar. Res.*, **12**, 196–213.

Donguy, J. R., and M. Privé, 1964: Les conditions de l'Atlantique entre Abidjan et l'équateur. *Bull. Inf. C.O.E.C.*, **16**, 193–204.

Enfield, D. B., and J. S. Allen, 1980: On the structure and dynamics of monthly sea level anomalies along the Pacific coast of North and South America. *J. Phys. Oceanogr.*, **10**, 557–578.

Fishery Research Unit, Tema, Ghana, 1970: The N.C.O.R. report of the mechanism of the upwelling of Ghana's coastal waters. *Mar. Fish. Rep.*, No. 3.

Gallardo, Y., 1981: Milieu marin et ressources halieutiques de la République Populaire de Congo: Océanographie Physique. *Trav. Doc. ORSTOM*, **138**, 47–73.

Guillerm, J. M., 1975: Variation saisonnières des transports côtiers dans le sud-est de Golfe de Guinée. *Bull. Union Océanogr. France*, **7**, 55–67.

——, 1981: Contribution a l' océanographie physique du Golfe de Guinée: hydrologie et circulation saisonnières sur une radiale au large de Pointe-Noire (Congo). Thèse d' Université, Université de Bretagne Occidentale, 203 pp.

Hastenrath, S., 1980: Heat budget of tropical ocean and atmosphere. *J. Phys. Oceanogr.*, **10**, 159–170.

——, and P. Lamb, 1977: *Climatic Atlas of the Tropical Atlantic and Eastern Pacific Oceans.* University of Wisconsin Press, 112 pp.

Hickie, P. B., 1977: The effects of coastal geometry on equatorially trapped planetary waves: Free oscillations in the Gulf of Guinea. (Unpublished manuscript).

Hisard, P., J. Citeau and A. Morliere, 1975: Le courant de Lomonossov et la formation de la zone frontale du Cap Lopez (Baie de biafra, Golfe de Guinée). *Cah. ORSTOM, Sér. Océanogr.*, **13**, 107–116.

——, and J. Merle, 1980: Onset of summers surface cooling in the Gulf of Guinea during GATE. *Deep Sea Res.*, **26** (Suppl. II), 325–341.

Houghton, R. W., 1976: Circulation and hydrographie structure over the Ghana Continental Shelf during the 1974 upwelling. *J. Phys. Oceangr.*, **6**, 909–924.

——, 1981: Temperature variations in the Gulf of Guinea. *Trop. Ocean. Atmos. News.*, **8**, 1–3. (Unpublished manuscript).

Hurlburt, H. E., J. C. Kindle and J. J. O'Brien, 1976: A numerical simulation of the onset of El Niño. *J. Phys. Oceanogr.*, **6**, 621–631.

Ingham, M. C., 1970: Coastal upwelling in the northwestern of Gulf of Guinea. *Bull. Mar. Sci.*, **20**, 2–34.

Janke, J., 1920: Strömungen und Oberflächentemperaturen im Golfe von Guinea. *Arch. Dtsch. Seewarte*, **6**, 1–68.

Katz, E. J., and Collaborators, 1977: Zonal pressure gradient along the equatorial Atlantic. *J. Mar. Res.*, **35**, 293–307.

——, D. Cartwright, P. Hisard, H. Lass, A. Mesquita and R. Molinari, 1981: The seasonal transport of the equatorial undercurrent in the western Atlantic (during FGGE). *Océan. Acta*, **4**, 445–450.

Knox, R. A., and D. Halpern, 1982: Observation of an equatorial Kelvin wave in the central Pacific. *J. Mar. Res.* (in press).

Lamb, P. J., 1978: Case studies of tropical Atlantic surface circulation pattern during recent sub-Saharan weather anomalies, 1967–1968. *Mon. Wea. Rev.*, **106**, 482–491.

Lemasson, L., and J. P. Rébert, 1973a: Les courants marins dans le Golfe ivoirien. *Cah. ORSTOM, Sér. Océanogr.*, **11**, 67–95.

——, and ——, 1973b: Circulation dans le Golfe de Guinée. Etude de la région d'origine du sous-courant ivoirien. *Cah. ORSTOM. Sér. Océanogr.*, **11**, 303–316.

Longhurst, A. R., 1962: A review of the oceanography of the Gulf of Guinea. *Bull. IFAN*, Sér. **A24**, 633–663.

Lukas, R. B., 1981: The termination of the Equatorial Undercurrent in the eastern Pacific. Ph.D. dissertation, University of Hawaii, 127 pp.

——, and E. Firing, 1982: An annual equatorial Rossby wave in the central Pacific. *Trop. Ocean. Atmos. News*, **12**, 3–4 (Unpublished manuscript).

McCreary, J. P., 1976: Eastern tropical response to changing wind systems with application to El Niño. *J. Phys. Oceanogr.*, **6**, 632–645.

——, 1982: Equatorial beams. (Manuscript in preparation).

——, J. Picaut and D. W. Moore, 1982: Effect of annual remote forcing in the eastern tropical Atlantic. (Manuscript in preparation).

Marchal, E., and J. Picaut, 1977: Répartition et abondance évaluées par échointegration des poissons du plateau ivoiro-ghanéen en relation avec les upwellings locaux. *J. Res. Océanogr.*, **2**, 39–57.

Merle, J., 1978: Atlas hydrologique saisonnier de l'océan Atlantique intertropical. *Trav. Doc. ORSTOM*, **82**, 184 pp.

——, and J. F. Le Floch, 1978: Cycle annual moyen de la température dans les couches supérieures de l' Océan Atlantique intertropical. *Océan. Acta*, **1**, 271–276.

——, M. Fieux and P. Hisard, 1980: Annual signal and interannual anomalies of sea surface temperature in the eastern equatorial Atlantic ocean. *Deep Sea Res.*, **26**(Suppl. II), 77–101.

Moore, D. W., P. Hisard, J. P. McCreary, J. Merle, J. J. O'Brien, J. Picaut, J. M. Verstraete and C. Wunsch, 1978: Equatorial adjustment in the eastern Atlantic. *Geophys. Res. Lett.*, **5**, 637–640.

Morlière, A., 1970: Les saisons marines devant Abidjan. *Doc. Sci. Centre Rech. Océanogr. Abidjan*, **1**, 1–15.

——, and J. P. Rébert, 1972: Etude hydrologique du plateau continental ivoirien. *Doc. Sci. Centre Rech. Océanogr. Abidjan*, **3**, 1–30.

Neumann, G., W. H. Beatty and E. C. Ecowitz, 1975: Seasonal changes of oceanographic and marine-climatological conditions in the equatorial Atlantic. Dept. Earth Planet Sci., City College of CUNY. 211 pp.

O'Brien, J. J., D. Adamec and D. W. Moore, 1978: A simple model of equatorial upwelling in the Gulf of Guinea. *Geophys. Res. Lett.*, **5**, 641–644.

Philander, S. G. H., 1977: The effect of coastal geometry on equatorial waves (forced waves on the Gulf of Guinea) *J. Mar. Res.*, **35**, 509–523.

——, 1979: Upwelling in the Gulf of Guinea. *J. Mar. Res.*, **37**, 23–33.

——, 1981: The response of equatorial oceans to a relaxation of the trade winds. *J. Phys. Oceanogr.*, **11**, 176–189.

——, and R. C. Pacanowski, 1980: The generation of equatorial currents. *J. Geophys. Res.*, **85**, 1123–1136.

——, and ——, 1981a: The oceanic response to cross-equatorial winds (with application to coastal upwelling in low latitudes). *Tellus*, **33**, 204–210.

——, and ——, 1981b: Response of equatorial oceans to periodic forcing. *J. Geophys. Res.*, **86**, 1903–1916.

Picaut, J., and J. M. Verstraete, 1976: Mise en évidence d'une onde de 40–50 jours de période sur les côtes du Golfe de Guinée. *Cah. ORSTOM Sér. Océanogr.*, **14**, 3–14.

——, and ——, 1979: Propagation of a 14.7 day wave along the northern coast of the Guinea Gulf. *J. Phys. Oceanogr.*, **9**, 136–149.

Piton, B., R. Perrin and J. P. Gausi, 1977: Nouvelles considérations sur les saisons marines et la circulation superficielle dans le Golfe de Guinée. *Doc. ORSTOM Pointe-Noire NS*, **49**.

Ripa, P., and S. P. Hayes, 1981: Evidence for equatorial trapped waves at the Galapagos Islands. *J. Geophys. Res.*, **86**, 6509–6516.

Schott, G., 1944: Geographie des Atlantischen Ozeans. Hamburg, 39 pp.

Servain, J., J. Picaut and J. Merle, 1982: Evidence of remote forcing in the equatorial Atlantic ocean. *J. Phys. Oceanogr.*, **12**, 457–463.

Stretta, J. M., 1977: Température de surface et pêche thonière dans la zone frontale du Cap Lopez (Atlantique tropical oriental) en juin et juillet 1972, 1974 et 1975. *Cah. ORSTOM, Sér. Océanogr.*, **15**, 163–180.

Varlet, F., 1958: Le régime de l'Atlantique pres d'Abidjan (Côte d' Ivoire). *Etud. Eburné.*, **7**, 97–222.

Verstraete, J. M., 1970: Etude quantitative de l'upwelling sur le plateau continental ivoirien. *Doc. Sci. Centre Rech. Océanogr. Abidjan*, **1**, 1–17.

——, J. Picaut and A. Morlière, 1980: Atmospheric and tidal observations along the shelf of the Guinea Gulf. *Deep Sea Res.*, **26**(Suppl. II), 343–356.

Voituriez, B., 1980: The equatorial upwelling in the eastern Atlantic: problem and paradoxes. *Coastal Upwelling*, F. A. Richards, Ed., Amer. Geophys. Union, 95–106.

——, 1981: The equatorial upwelling in the eastern Atlantic ocean. *Report of the Final Meeting of SCOR WG 47*. Nova University Press, 229–247.

——, and A. Herbland, 1979: The use of the salinity maximum of the Equatorial Undercurrent for estimating nutrient enrichment and primary production in the Gulf of Guinea. *Deep Sea Res.*, **26A**, 77–83.

Wooster, W. S., A. Bakun and D. R. McLain, 1976: The seasonal upwelling cycle along the eastern boundary of the North Atlantic. *J. Mar. Res.*, **34**, 131–141.

Wyrtki, K., 1975: El Niño. The dynamic response of the equatorial Pacific ocean to atmospheric forcing. *J. Phys. Oceanogr.*, **5**, 572–584.

Evidence of Remote Forcing in the Equatorial Atlantic Ocean

JACQUES SERVAIN AND JOËL PICAUT

Laboratoire d'Océanographie Physique-Université de Bretagne Occidentale, 29200 Brest, France

JACQUES MERLE

ORSTOM-Laboratoire d'Océanographie Physique-Muséum, 75005 Paris, France

(Manuscript received 22 September 1981, in final form 5 February 1982)

ABSTRACT

An analysis of sea-surface temperature (SST) and surface winds in selected areas of the tropical Atlantic indicates that the nonseasonal variability of SST in the eastern equatorial Atlantic (Gulf of Guinea) is highly correlated with the nonseasonal variability of the zonal wind stress in the western equatorial Atlantic. A negative (positive) anomaly of the zonal wind stress near the north Brazilian coast is followed by a positive (negative) SST anomaly in the Gulf of Guinea about one month later. Furthermore, the correlation between the local wind stress anomaly and SST anomaly in the Gulf of Guinea is considerably smaller. These preliminary results indicate that remote forcing in the western equatorial Atlantic Ocean is an important factor affecting the eastern equatorial Atlantic sea-surface temperature. Recent equatorial theories are consistent with these observations.

1. Introduction

The variations of temperature in the eastern equatorial Atlantic (Gulf of Guinea) have a significant effect on the abundance of fish (Bakun, 1978; A. Fonteneau, pers. comm., 1981) and on the rainfall distribution along the western African coast and the sub-Saharan countries (Lamb, 1978). For this reason, understanding the dynamics of this region is of great interest to both meteorologists and oceanographers. Several ideas have recently been proposed to explain these fluctuations of temperature. Philander (1978, 1981) argues that the local wind forcing may account for this variability. Moore *et al.* (1978) suggested that remote forcing by winds in the western Atlantic may provide an alternate explanation. In this study we present evidence, based on historical SST and wind data, that supports the latter idea.

2. Data and processing

Merchant ship data are routinely collected at the U.S. National Climate Center at Ashville, NC. There they are put in the form of individual monthly averages of various meteorological parameters for 1° latitude × 1° longitude squares in the tropical Atlantic. Full details of this data set are given in Hastenrath and Lamb (1977). These authors have further processed this data to produce 60-year time series (1911–1972) of the field of wind and SST averaged over 5° squares, and have kindly offered us this derived data set.

Fig. 1a shows selected areas of relevance to our study: a Brazilian region (BR) 5°N–5°S, 35–25°W, a north Guinea region (GN) 5°N–0°, 10°W–10°E, a west Guinea region (GW) 5°N–5°S, 10–5°W, a northeastern region (NE) 30–25°N, 20–15°W, and a southeastern region (SE) 30–25°S, 10–15°E. These regions have been chosen to test, in the most simple way, the effect of remote or local wind forcing on sea-surface temperature in areas where the distribution of the data along shipping lanes are the most favorable. Fig. 1b indicates the temporal distribution of wind data in a part of the BR area. According to this graph there are two periods of extensive data coverage: from 1923 to 1938 (between the two world wars), and from 1964 to 1969. For this reason, our analysis is limited to these two time periods.

Because the annual cycle is strong in all the data sets, we expect to have a high correlation between all the variables. If we remove the monthly mean, any significant correlations we find between the resulting nonseasonal data sets will be a more sensitive indicator of the dynamical processes involved in the response. However, removing the monthly mean does not imply that we have completely suppressed the annual cycle. The anomalous years are due, in part to an increase or decrease in amplitude, or to a shift of phase, of the normal seasonal cycle. This property is clearly illustrated in Fig. 2. An alternate method of suppressing the annual cycle is to low-pass filter the time series. However, this method will also elim-

0022-3670/82/050457-07$05.75

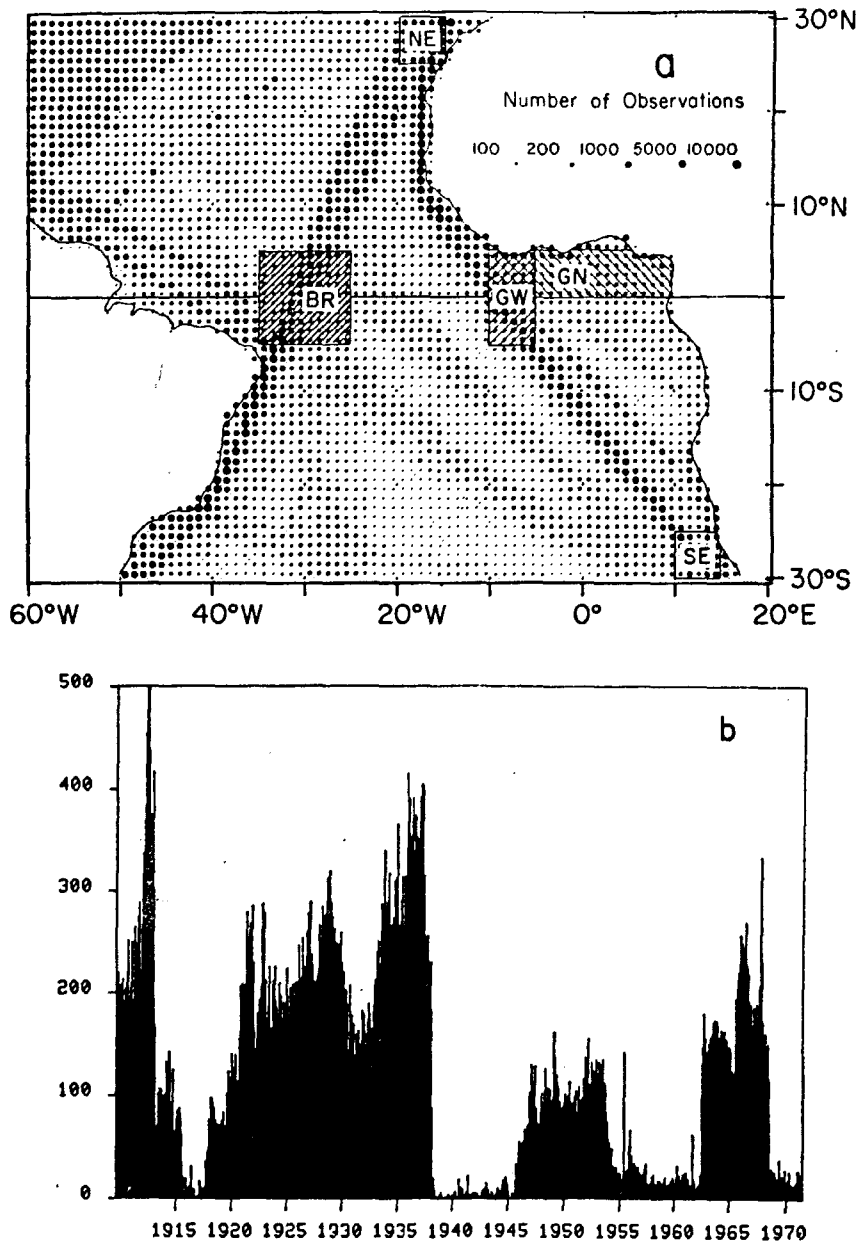

FIG. 1. (a) Position of the studied areas (composite picture from Hastenrath and Lamb, 1977). (b) Number of observations by month in a part of the BR area (0-5°S, 30-35°W).

inate the short time-scale anomalous events evident in Fig. 2. Therefore, the commonly used method of nonseasonal decomposition is preferable in the present case, and so is used here.

The nonseasonal variations of the zonal (τ^x) and meridional (τ^y) components of the wind stress and SST were computed for the 5° square areas by subtracting out the monthly mean values. The monthly means were found by averaging over the whole 1911-1972 period, excepting those months where less than 10 observations are available. A drag coefficient of 2.0×10^{-3} was used for the calculation of the wind stress. To find the mean in each of the selected regions (BR, GN, GW, NE, SE), individual 5° square mean values were weighted according to the mean number of observations in these areas.

3. Results

Fig. 3 shows the interannual anomalies of SST in the NE, SE, GN and GW regions. The Gulf of Guinea areas (GN, GW) appear to share a common

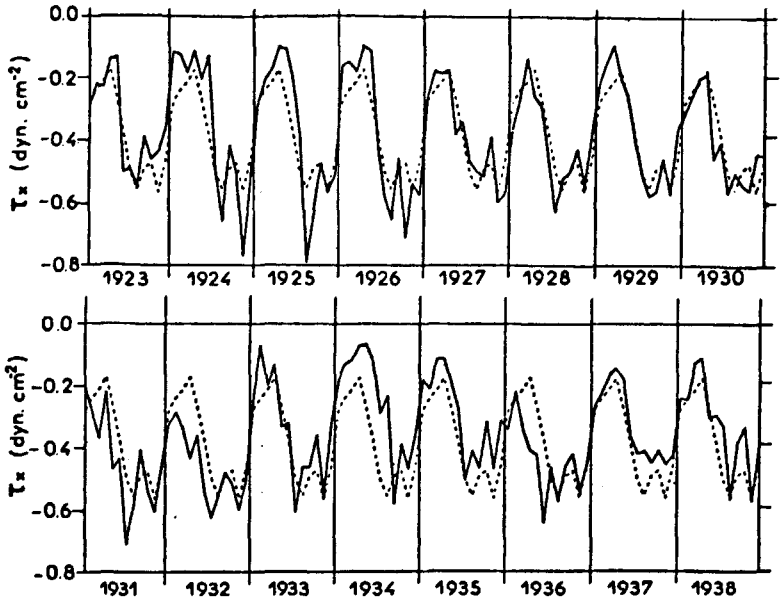

FIG. 2. Monthly mean of τ^x in BR area. Solid line: individual years from 1923–1938. Dotted line: mean year on the period 1911–72.

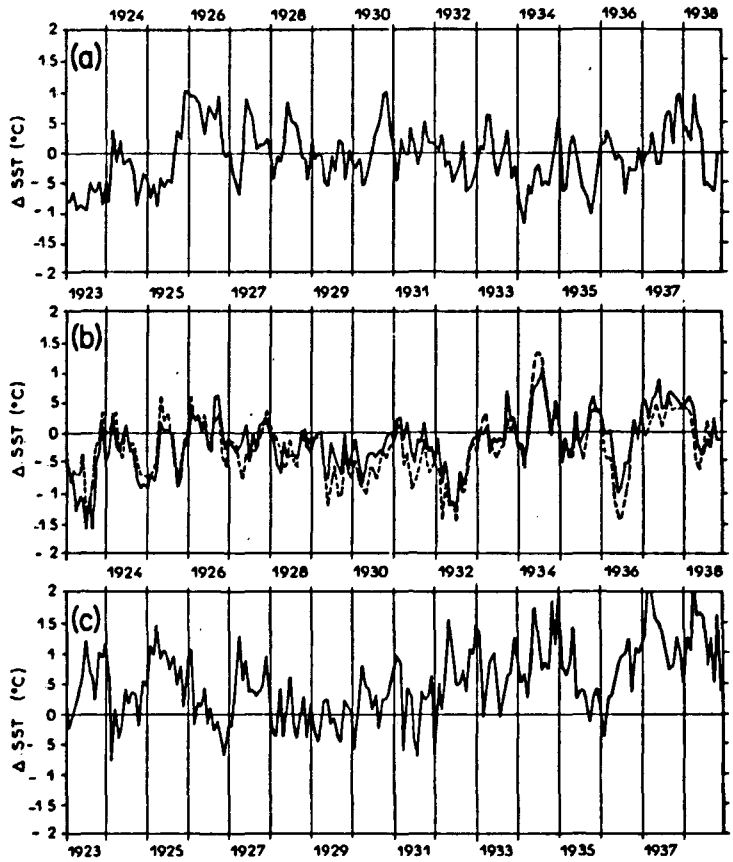

FIG. 3. Monthly anomalies of SST from 1923 to 1938. (a) Northeastern area (NE). (b) Guinea Gulf (dashed line GW, solid line GN). (c) Southeastern area (SE).

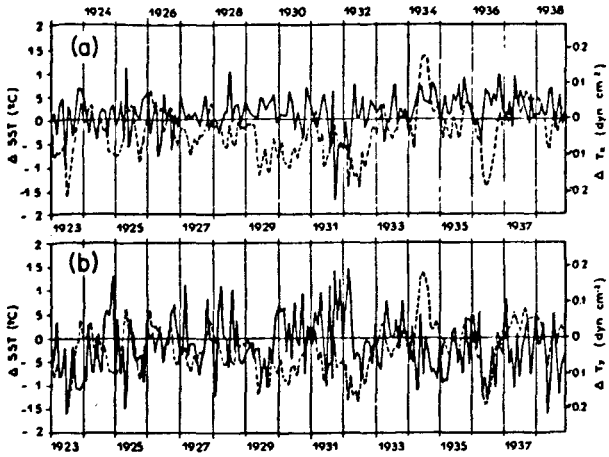

FIG. 4. Monthly anomalies from 1923 to 1938 in the western Guinea Gulf (GW area). (a) Solid line τ^x, dotted line SST. (b) Solid line τ^y, dotted line SST.

interannual variability of SST (Merle *et al.*, 1980). On the contrary, the anomalies of SST in the north and southeast tropical regions (NE, SE) are very different (Fig. 3), and are both different from those of the Gulf of Guinea. Thus, we can consider the SST anomalies to have a spatial extent affecting the whole eastern equatorial basin and to be characteristic of this region.

According to the qualitative model of Cromwell (1953), variations in the northward and westward wind stress near the equator should induce local temperature fluctuations there. Furthermore, according to Philander (1978) the northward equatorial wind can affect SST along the northern coast of the Guinea Gulf. So, following these authors, we might expect to have a good correlation between the τ^x and τ^y anomalies in the western Guinea region (GW) and the corresponding SST anomalies. In Fig. 4a a positive (negative) peak in the τ^x anomaly corresponds to a decrease (increase) in the westward wind stress, and for local forcing we should expect an increase (decrease) in SST anomaly. In Fig. 4b a positive (negative) peak in the τ^y anomaly corresponds to an increase (decrease) in the northward wind stress and for local forcing we should expect a decrease (increase) in the SST anomalies. Therefore the two curves in Fig. 4a would be in-phase and the two curves in Fig. 4b would be out-of-phase. The poor visual agreement between these curves is confirmed by a lagged regression correlation analysis (Fig. 5). For zero lag the correlation coefficient is on the order of the noise level. However, notice a surprising maximum of correlation coefficient at roughly three months lag. We will comment on this feature in the last section.

According to the remote forcing idea of Moore *et al.* (1978), variations in the westward wind stress in the western equatorial Atlantic should induce temperature fluctuations in the eastern equatorial Atlantic. So, we expect to have a good correlation between the τ^x anomaly in the Brazilian region (BR) and the SST anomaly in the Guinea Gulf (GW or GN). In Fig. 6 a positive (negative) peak in the τ^x anomaly of BR corresponds to a decrease (increase) in the westward wind stress anomaly, and for remote forcing we should expect an increase (decrease) in

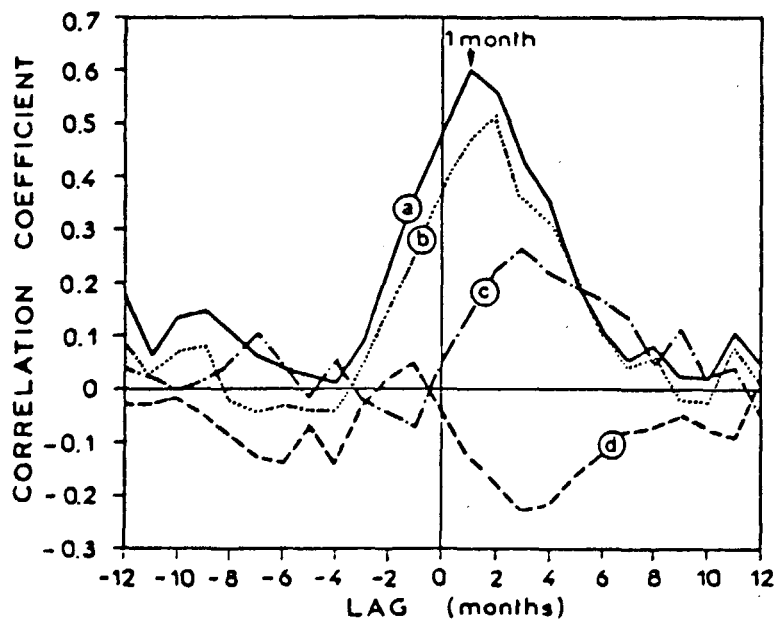

FIG. 5. Correlation with time lag. Curve a: τ^x-BR with SST-GW. Curve b: τ^x-BR with SST-GN. Curve c: τ^y-GW with SST-GW. Curve d: τ^y-GW with SST-GW.

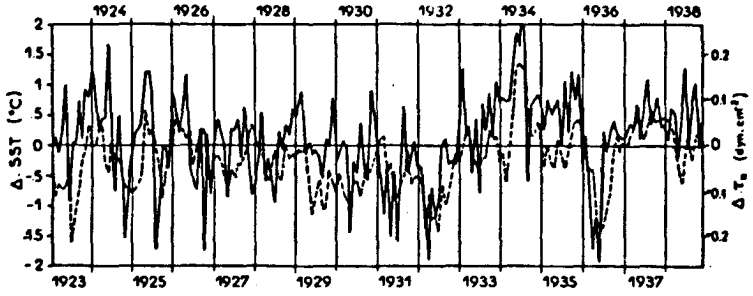

FIG. 6. Comparison of monthly anomalies from 1923 to 1938 of τ^x in BR area (solid line) and SST in GW area (dotted line).

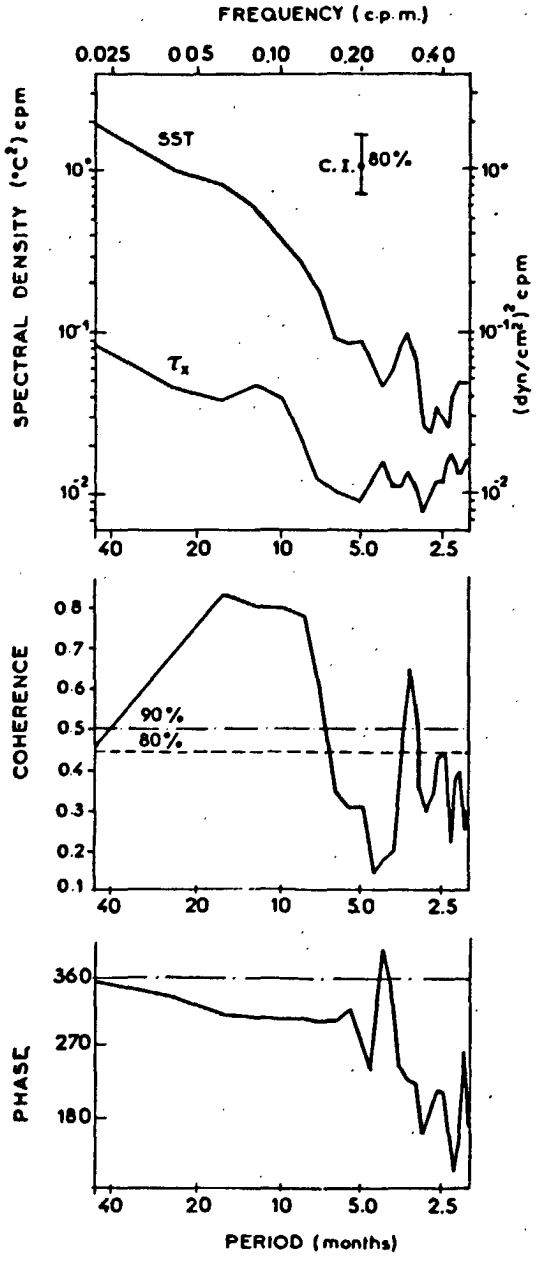

FIG. 7. Cross spectrum of τ^x in BR area and SST in GW area.

SST anomaly of GW. Therefore these two curves would be in-phase. The lagged correlation analysis confirms the good visual agreement between these two curves (Fig. 5). A highly significant maximum of correlation coefficient is obtained with a one month lag, the wind stress anomaly preceding the SST anomaly.

These last results are supported by a cross-spectral analysis of the same data set (τ^x – BR and SST-GW, 1923–38). Despite the absence of marked peaks in the power spectral densities, the coherence is characterized by maxima around a 3-month period and from 7 to 24-month periods (Fig. 7). For this high coherence we have plotted the phase difference in months versus the frequency and added the corresponding error bar for the 80% confidence level (Fig. 8). It is clear from this figure that a phase lag of one to two months occurs over a broad frequency range, and so justifies *a posteriori* our lagged correlation analysis.

4. Discussion and conclusion

This analysis shows that the SST anomaly in the eastern equatorial Atlantic is dominated by remote

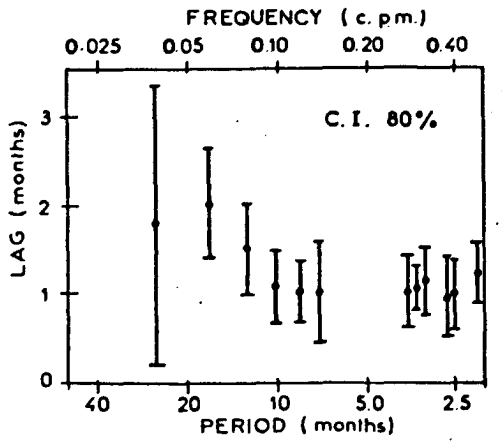

FIG. 8. Time lag versus frequency of the cross-spectrum of τ^x in BR area and SST in GW area (Fig. 7). Only frequencies where coherence is high are considered. The confidence interval is for probability of 0.8.

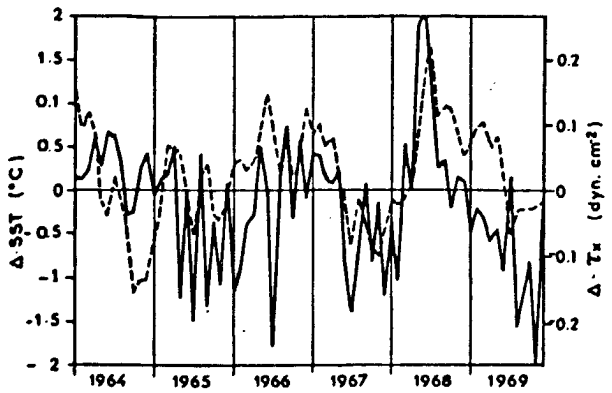

FIG. 9. Comparison of monthly anomalies from 1964 to 1969 of τ^x in BR area (solid line) and SST in GW area (dotted line).

wind forcing in the western equatorial Atlantic. The nonseasonal variability of SST in the Guinea Gulf is poorly correlated with the nonseasonal local wind forcing and highly correlated with the nonseasonal variability of the wind forcing off Brazil. Furthermore, a time lag of roughly one month exists between this remote forcing and its response in the Guinea Gulf.

Moore *et al.* (1978) proposed a simple remote-forcing mechanism to account for the Guinea Gulf upwelling. According to this hypothesis an increase of the easterly wind in the western equatorial Atlantic excites an internal upwelling equatorial Kelvin wave that propagates into the eastern equatorial Atlantic. When this disturbance reaches the eastern boundary it splits into Kelvin waves propagating poleward along the coasts in both hemispheres and a large number of westward propagating equatorial Rossby waves. Thus, the lag between the response in the Gulf of Guinea and the winds off Brazil is simply related to the speed of Kelvin waves. This theoretical idea has been illustrated in the numerical, one-and-a-half layer model studies of O'Brien *et al.* (1978) and of Adamec and O'Brien (1978), in which the wind in the western Atlantic was switched on impulsively. In contrast, Cane and Sarachik (1981) studied the response of a single baroclinic mode to periodic forcing, and found that the equatorial Kelvin wave, and associated time lag, was completely masked by reflected Rossby waves. However, in three-dimensional models remotely forced by periodic winds the equatorial Kelvin wave is again clearly evident (Philander and Pacanowski, 1981; McCreary *et al.*, 1982). In any case, the rapid increase of the easterly wind in spring 1979 at St. Paul Rocks (0°55'N, 29°21'W) (Katz *et al.*, 1981), which is not unusual (Fig. 2), seems to indicate that impulsive forcing is most relevant to the present study.

The mean lag observed here implies a wave propagation speed of ~ 1 m s^{-1}, which is slower than the phase speed of the first baroclinic mode Kelvin wave. It compares better to the speed of the second mode or to a combination of several low-order modes. An interesting aspect of Fig. 8 is that there is an apparent increase of this lag with the period of the forcing. In a recent model, which includes many baroclinic modes, J. P. McCreary (pers. comm., 1981) has shown that lower-frequency forcing excites higher-order modes in the Kelvin wave and so decreases the apparent horizontal phase speed, in agreement with our observations.

Similar results hold for the mean seasonal signal as well. Picaut (1982) shows poleward propagation of the mean seasonal coastal upwelling at speeds slower than the first baroclinic mode. In addition, south of Abidjan there is a vertical propagation of the upwelling signal. This upward phase shift is clear evidence that the coastal signal is a combination of modes, and is also a feature of the model of McCreary *et al.* (1982).

A correlation analysis, not shown here, reveals that the anomalies of the wind stress in the western equatorial Atlantic are highly correlated with the wind stress anomalies in the Guinea Gulf with a lag of two months. This property could explain the intriguing 3-month lag obtained for the maximum of correlation between the SST anomalies in the Gulf of Guinea and the local wind stress anomalies (Fig. 5). Consider the following scenario. A wind anomaly appears first in the Gulf of Guinea, but apparently does not always significantly affect the ocean there. Two months later a similar wind anomaly appears in the western equatorial Atlantic. Only after a delay of one more month is the ocean in the Guinea Gulf affected by the remote forcing.

Finally, it should be pointed out that there is a similarity between the temperature variability of the eastern equatorial Atlantic and Pacific Oceans. The "El Niño" phenomenon in the eastern equatorial Pacific is probably another dramatic example of the response of the equatorial ocean to remote wind forcing (Wyrtki, 1975; McCreary, 1976; Hurlburt *et al.*, 1976; Busalacchi and O'Brien, 1981). A striking example of such warming in the Gulf of Guinea was particularly evident during the summer of 1968 (Hisard, 1980; Merle, 1980) and can be explained by abnormal wind stress forcing off the northern Brazil coast (Fig. 9).

Acknowledgments. We would like to thank Stefan Hastenrath for giving us his Atlantic marine surface data set. This study has been supported by a CNEXO contract N° 81-2437, a CNRS ATP A15031 and, for one of the authors (J. P.), partly by the Joint Institute of Marine and Atmospheric Research, Hawaii. This study has also greatly benefited from an efficient management of the data by the Bureau National des Données Océanologiques (Centre Oceanologique de Bretagne-BREST).

REFERENCES

Adamec, D., and J. J. O'Brien, 1978: The seasonal upwelling in the Gulf of Guinea due to remote forcing. *J. Phys. Oceanogr.*, **8**, 1050-1060.

Bakun, A., 1978: Guinea current upwelling. *Nature*, **271**, 147-150.

Busalacchi, A. J., and J. J. O'Brien, 1981: Interannual variability of the equatorial Pacific in the 1960's. *J. Geophys. Res.*, **86**, 10901-10907.

Cane, M. A., and E. S. Sarachik, 1981: The response of a linear baroclinic equatorial ocean to periodic forcing. *J. Mar. Res.*, **39**, 651-693.

Cromwell, T., 1953: Circulation in a meridional plane in the central equatorial Pacific. *J. Mar. Res.*, **12**, 196-213.

Hastenrath, S., and P. Lamb, 1977: *Climatic Atlas of the Tropical Atlantic and Eastern Pacific Oceans.* University of Wisconsin Press, 112 pp.

Hisard, P., 1980: Observation de réponses de type "El Niño" dans l'Atlantique tropical oriental-Golfe de Guinée. *Ocean. Acta*, **3**, 69-78.

Hurlburt, H. E., J. C. Kindle and J. J. O'Brien, 1976: A numerical simulation of the onset of El Niño. *J. Phys. Oceanogr.*, **6**, 621-631.

Katz, E. J., D. Cartwright, P. Hisard, H. Lass, A. Mesquitta and R. Molinari, 1981: The seasonal transport of the equatorial undercurrent in the western Atlantic (during FGGE). *Ocean. Acta*, **4**, 445-450.

Lamb, P. J., 1978: Case studies of Tropical Atlantic surface circulation patterns during recent Sub-Saharan weather anomalies. 1967-1968. *Mon. Wea. Rev.*, **106**, 482-491.

McCreary, J. P., 1976: Eastern tropical ocean response to changing wind systems with application to El Niño. *J. Phys. Oceanogr.*, **6**, 632-645.

——, D. W. Moore and J. Picaut, 1982: Effect of annual remote forcing in the eastern tropical Atlantic. (Manuscript in preparation.)

Merle, J., 1980: Variabilité thermique annuelle et interannuelle de l'océan Atlantique équatorial Est. L'hypothèse d'un "El Niño" Atlantique. *Ocean. Acta*, **3**, 209-220.

Merle, J., M. Fieux and P. Hisard, 1980: Annual signal and interannual anomalies of sea-surface temperatures in the eastern equatorial Atlantic ocean. *Deep-Sea Res.*, GATE Suppl. II to V, **26**, 77-102.

Moore, D. W., P. Hisard, J. McCreary, J. Merle, J. J. O'Brien, J. Picaut, J. M. Verstraete and C. Wunsch, 1978: Equatorial adjustment in the eastern Atlantic. *Geophys. Res. Lett.*, **5**, 637-640.

O'Brien, J. J., D. Adamec and D. W. Moore, 1978: A simple model of upwelling in the Gulf of Guinea. *Geophys. Res. Lett.*, **5**, 641-644.

Philander, S. G. H., 1978: Upwelling in the Gulf of Guinea. *J. Mar. Res.*, **37**, 23-33.

——, 1981: The oceanic response to cross-equatorial winds (with application to coastal upwelling in low latitudes). *Tellus*, **33**, 204-210.

——, and R. C. Pacanowski, 1981: Response of equatorial oceans to periodic forcing. *J. Geophys. Res.*, **86**, 1903-1916.

Picaut, J., 1982: Propagation of the seasonal upwelling in the eastern equatorial Atlantic. Submitted to *J. Phys. Oceanogr.*

Wyrtki, K., 1975: El Niño—The dynamic response of the equatorial Pacific ocean to atmospheric forcing. *J. Phys. Oceanogr.*, **5**, 572-584.

VOLUME 13 JOURNAL OF PHYSICAL OCEANOGRAPHY SEPTEMBER 1983

Seasonal Variability from a Model of the Tropical Atlantic Ocean[1]

ANTONIO J. BUSALACCHI[2]

Mesoscale Air-Sea Interaction Group, Florida State University, Tallahassee 32306

JOËL PICAUT

Laboratoire d'Oceanographie Physique, Universite de Bretagne Occidentale, 29200 Brest, France

(Manuscript received 13 December 1982, in final form 3 June 1983)

ABSTRACT

A numerical model incorporating a single baroclinic mode and realistic coastline geometry is used to analyze the linear, dynamic response to estimates of the seasonal wind field over the tropical Atlantic Ocean. The forced periodic response consists of a spatially dependent combination of a locally forced response, Kelvin waves, Rossby waves and multiple wave reflections. The seasonal displacements of the model pycnocline are compared with observed dynamic height. Annual and semiannual fluctuations dominate the seasonal signal throughout the basin. In general, the distribution of amplitude and phase are similar for annual changes in dynamic height and pycnocline depth. Major features of the seasonal response are reproduced, e.g., east-west changes in pycnocline depth about a nodal point at the equator, the seasonal pycnocline movement along the northern and southern coast of the Guinea Gulf, and a significant change of phase in the ocean variability north and south of the ITCZ. The relative importance between local and remote forcing is determined for several parts of the model basin. The wind-driven annual signal in the idealized Gulf of Guinea is due to equatorial zonal wind stress fluctuations west of the Gulf. The semiannual response in the Gulf of Guinea is a result of zonal and meridional wind stress fluctuations in the eastern half of the tropical Atlantic. The seasonal response in the western equatorial and northernmost parts of the model basin are primarily local.

1. Introduction

In the upper tropical Atlantic Ocean, the seasonal variations of heat content are approximately ten times larger than that which can be explained by the seasonal variations of the heat gain from the atmosphere through the surface (Merle, 1980a). This annual cycle of the heat content is mainly caused by the horizontal redistribution of heat associated with wind-induced changes in the topography of the thermocline. Therefore, knowledge of the dynamic response of the upper tropical Atlantic to the seasonal surface winds is fundamental to our understanding of this tropical ocean–atmosphere interaction. Studies of the wind-driven response allow a basis to be formed from which to analyze this complex system with the future implementation of sophisticated, thermodynamic and coupled, tropical, ocean–atmosphere models.

The Atlantic Ocean is a prime region to study the seasonal response of a tropical ocean because of the strong seasonal cycle present. Merle *et al.* (1980) determined that the annual sea surface temperature (SST) signal in the Gulf of Guinea was several times greater than the interannual variability. Katz *et al.* (1977) and Lass *et al.* (1982) have shown that the zonal pressure gradient in the western and central equatorial Atlantic varies almost in phase with the seasonally varying winds. These findings are in contrast to the tropical Pacific where interannual fluctuations often associated with El Niño dominate (Wyrtki, 1975; Hickey, 1975). Studying the seasonal variability may also help in understanding nonseasonal events since interannual changes are frequently perturbations to the seasonal cycle.

The Gulf of Guinea is characterized by a shallow thermocline associated with the eastward shoaling of the thermal structure at low latitudes. This is also the region of the tropical Atlantic where the seasonal variability of SST has the largest amplitude (5–7°C compared to 1–2°C further west). Anomalous SST variability in this area has been linked with extreme climatic events such as droughts and excessive rainfall along the coast of the Gulf of Guinea, in sub-Sahara Africa, and possibly in northeastern Brazil (Hastenrath, 1976; Markham and McLain, 1977; Lamb, 1978; Bakun, 1978). The presence of abnormal SST

[1] Contribution No. 192, Geophysical Fluid Dynamics Institute, The Florida State University, and Contribution No. 17 of the PEQUOD Program.

[2] Present affiliation: Goddard Laboratory for Atmospheric Sciences, NASA/Goddard Space Flight Center, Greenbelt, MD 20771.

in the tropical Atlantic may also have an important effect on cyclogenesis (Namias, 1969). Moreover, this surface and associated subsurface variability appear to have a significant effect on the coastal and pelagic fisheries (Hisard and Piton, 1981).

Seasonal equatorial and coastal upwelling episodes and coincident cold water outbreaks in this region have never been convincingly explained by forcing due to the local winds or local currents (Houghton, 1976; Berrit, 1976; Bakun, 1978; Voituriez, 1981a,b). Moore *et al.* (1978) suggested that a strong upwelling signal, generated by a significant increase of the easterlies in the western Atlantic, can be transmitted to the eastern Atlantic as an equatorially trapped Kelvin wave. When this disturbance reaches the African coast, part of the energy splits poleward as coastal Kelvin waves and the remainder is reflected westward as equatorial Rossby waves. Following this remote-forcing concept, Servain *et al.* (1982) found that the nonseasonal variability of SST in the Gulf of Guinea is highly correlated with the nonseasonal variability of the zonal wind stress in the western equatorial Atlantic. The correlation between the local wind stress anomaly and SST anomaly in the Gulf of Guinea was considerably smaller. In a study of the seasonal SST signal, Picaut (1983) found poleward propagation of the mean seasonal coastal upwelling. Thus, there is a need to understand the relation between the equatorial wind forcing and this upwelling in the Gulf of Guinea. For a more detailed review of this Gulf-of-Guinea problem see Picaut (1983).

Other prominent features of the subsurface thermal structure in the eastern tropical Atlantic are the shallow thermocline regions of the Guinea and Angola Domes (Mazeika, 1967; Voituriez, 1981c). Although observations and modelling studies have been used to provide an understanding of the Costa Rica Dome in the eastern tropical Pacific Ocean (Wyrtki, 1964; Hofmann *et al.*, 1981), little is known about the counterparts in the tropical Atlantic.

The northwestern part of the equatorial Atlantic is characterized by a north–south tilting of the thermocline near the mean position of the Inter-Tropical Convergence Zone (ITCZ) (Merle, 1983). This pivot line is situated at latitudes where equatorial waves and Ekman pumping may play an important role in determining the variability. Due to the location, the presence of this feature may influence the variability of the North Equatorial Current and Countercurrent. Hence, an explanation is desired for such an important oscillation.

Within the last five years several modelling efforts have been directed toward studying certain aspects of the wind-driven response in the tropical Atlantic. O'Brien *et al.* (1978) and Adamec and O'Brien (1978) demonstrated the remote forcing mechanism of Moore *et al.* (1978) with a linear, 1½-layer model, in which the wind in the western part of the basin was switched on impulsively. Cane and Sarachik (1981) examined the linear, inviscid response of a meridionally infinite but zonally bounded equatorial basin to periodic zonal forcings, with some implications for the Atlantic Ocean. Philander and Pacanowski (1981a,b), with a three-dimensional, nonlinear model, studied the response to various x-independent and y-independent periodic wind forcings in a rectangular basin comparable to the width of the equatorial Atlantic. In all of these studies the wind forcing and the coastline geometry had limited resemblance to those of the tropical Atlantic.

McCreary *et al.* (1983) investigated the effect of remote forcing in the eastern tropical Atlantic with a three-dimensional, linear model forced by an annual periodic wind. Despite the fact that the coastal geometry was an approximation of the Brazilian and African coasts and the wind stress forcing was a simple representation of the annual zonal wind stress west of 20°W, this model succeeded in simulating several important features of the vertical structure in the Gulf of Guinea, e.g., the annual variation of the equatorial and coastal undercurrents and the upward phase propagation of the upwelling signal. Another three-dimensional numerical calculation has been performed by Anderson (1979) with realistic mean seasonal winds and coastlines. The variability of the resultant current fields were compared with the few observations available. The discussion of upwelling features was limited by constraints imposed by the surface boundary condition. Patton (1981) used a single baroclinic mode to study the seasonal cycle in the Gulf of Guinea. The model was forced by an analytical approximation of the real wind field. The influence of the winds in the eastern and western halves of the basin was examined. A subsequent extension of this calculation with the Atlantic wind data of Hellerman (1980) simulated rather well the mean seasonal sea level variation in the Gulf of Guinea (M. Cane, personal communication, 1982). Both these studies represented the Brazil coast by a north–south boundary at 50°W.

In the present work a more detailed calculation is used to study the wind-driven seasonal cycle of the upper tropical Atlantic. We seek to understand the linear response of the gravest baroclinic mode to periodic wind forcing based on the climatology throughout the basin. This approach will entail using a single-mode model of the tropical Atlantic, with realistic coastline geometry forced by the mean seasonal wind stress. Regions of important variability in the model domain and the dynamics responsible for these features will be discussed. Dynamic heights derived from observations will be used to identify areas of important variability in the tropical Atlantic, and thereby determine if the features of the model have any relevance to the real ocean. The results of a similar calculation for the tropical Pacific Ocean (Busalacchi

and O'Brien, 1980) indicate such a study may provide useful information pertaining to the low-latitude, seasonal Atlantic Ocean response. Furthermore, it is hoped that the results of such a simple model will provide the groundwork enabling the influence of additional physics to be determined when future models including nonlinearities, stratification, or thermodynamics are forced by estimates of the real wind field.

A description of the tropical Atlantic model is presented next. This is followed by a discussion of the climatological wind stress data which is used to form a periodic forcing function for the model. The basin-wide response to the seasonal forcing is then compared with the available dynamic height data to determine key features of interest. The important seasonal responses in the western tropical, equatorial and eastern tropical Atlantic are subsequently analyzed in more detail.

2. The numerical model

A linear, single baroclinic mode, numerical model on an equatorial β-plane will be used to study the oceanic response to an applied wind stress forcing. A similar approach was used by Busalacchi and O'Brien (1980) to study the wind-driven seasonal variability in the tropical Pacific Ocean. The linear governing equations for the horizontal dependency of a single baroclinic mode on an equatorial β-plane are as follows:

$$\frac{\partial \mathbf{V}}{\partial t} = -\beta y \hat{\mathbf{k}} \times \mathbf{V} - c^2 \nabla h + \frac{\tau}{\rho} + A\nabla^2 \mathbf{V}, \quad \text{(1a)}$$

$$\frac{\partial h}{\partial t} = -\nabla \cdot \mathbf{V}, \quad \text{(1b)}$$

$$\mathbf{V} = U_i + V_j, \quad \text{(1c)}$$

$$U = uH, \quad V = vH, \quad \text{(1d)}$$

where U, V are the respective x, y components of the horizontal transport, c is the baroclinic phase speed, and the wind stress τ is included as a body force. The pycnocline depth anomaly is denoted by h. The initial depth of the pycnocline is H. The diffusive terms, $A = 10^6$ cm^2 s^{-1}, are included to bring the horizontal flow to zero along closed boundaries and reduce high-wavenumber numerical noise. Bottom topography, thermohaline and thermodynamic effects have been neglected.

Philander and Pacanowski (1980) pointed out that the presence of a shallow tropical thermocline in a continuously stratified fluid, will result in the largest projection of the surface wind stress onto the second baroclinic mode. McCreary *et al.* (1983) found that the second baroclinic mode provided the dominant sea level response in a linear, three-dimensional model of remote forcing in the Gulf of Guinea. The vertical structure for their model was based on many observed density profiles at the equator. The amplitude of large-scale sea level changes corresponding to the second baroclinic mode was three times larger than that for the first or third modes. The sum of the sea level responses for the first three modes accounted for nearly all of the total (15 modes) sea level signal. Hence, the approach taken in the present study involves a single baroclinic mode with an equivalent depth corresponding to a second baroclinic mode.

The mean equatorial density profile used by McCreary *et al.* implied a 1.34 m s^{-1} (18.3 cm equivalent depth) phase speed for the second baroclinic mode. An equivalent depth of 20 cm was suggested by Moore and Philander (1977) as being typical of the second baroclinic mode in the equatorial Atlantic. A phase speed of $c = 1.37$ m s^{-1} was chosen for the single mode of the model presented here which corresponds to a 19 cm equivalent depth. Parameter tests performed with an invariant projection of seasonally varying wind data indicate the qualitative character of the modelled oceanic response is relatively insensitive to changes in the phase speed of ± 0.35 m s^{-1}. For discussions of current magnitudes and the mean pycnocline displacement, values of $H = 75$ m and a density contrast across the pycnocline of approximately $\Delta\rho/\rho = 2.5 \times 10^{-3}$ were chosen. In this type of calculation the amplitude of the pycnocline variability is influenced by the magnitude of c^2 or the equivalent depth, whereas the upper-layer thickness and perturbations to sea level elevation also depend on the chosen values of H and $\Delta\rho/\rho$, respectively. Since c^2 can be kept constant while changing H and $\Delta\rho/\rho$, we will only consider fluctuations about the mean depth of the pycnocline, not the upper layer thickness or sea level elevation. Nonetheless, if one wishes to convert from pycnocline variability to that of sea level, the amplitude of the pycnocline signal should be multiplied by the desired value of $\Delta\rho/\rho$.

The model basin extends from 20°N to 20°S and 61°W to 12°E. It is important that the model basin approximate the coastline geometry of the Atlantic Ocean since the wind stress forcing is derived from wind observations over the Atlantic. No regions of the wind field will be ignored nor will the ocean wind field be extended over the continents as in studies with rectangular-type geometries. Boundary effects present in the wind field will also influence the ocean in a corresponding location. The coastline idealization chosen is shown in Fig. 1. Meridional boundaries are taken to be solid walls. An open boundary condition (Camerlengo and O'Brien, 1980) is applied at the northern and southern boundaries permitting the passage of coastal Kelvin waves, thus preventing contamination of the interior solution.

A staggered grid with a 40 km mesh size in both x and y is employed to reduce computer storage. A 2 h time step is incorporated for the integration of

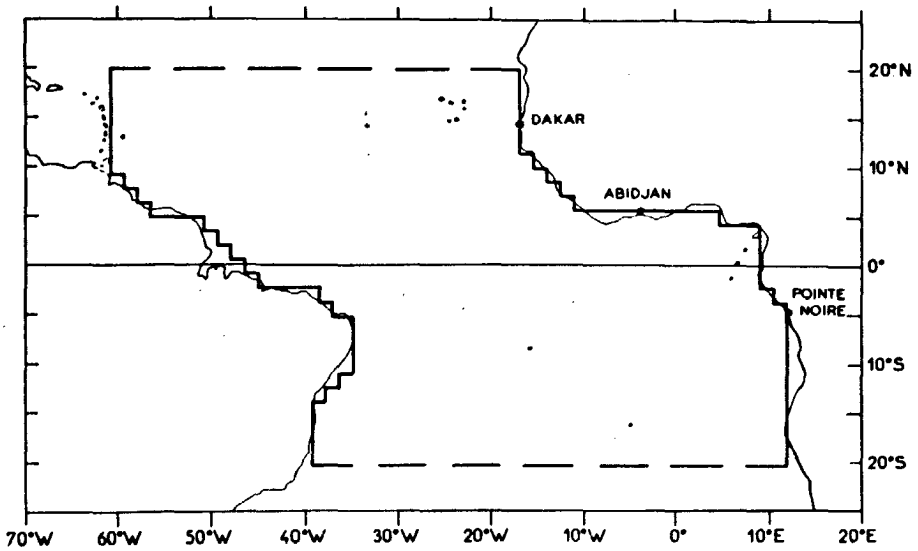

FIG. 1. Comparison of the model geometry with the tropical Atlantic Ocean basin. The dashed line represents an open boundary; all remaining boundaries are solid walls.

the model equations over five years. This provides sufficient time for the initial transients to die out and for a seasonal signal to develop. All the results to be presented are from the fifth year of integration. Hereafter, all references to pycnocline variability pertain to the model results.

3. The wind field

The seasonal forcing for this study is based on monthly mean shipboard estimates of the surface wind field compiled by Hastenrath and Lamb (1977) for a climatological atlas of the tropical Atlantic. The observations for each calendar month were averaged in time from 1911 to 1970 and averaged in space within a 1° square. Conspicuously incorrect observations were deleted. The area of interest, 20°N–20°S, is covered by a substantial number of ship tracks. Despite the high density of observations (~2 million) there are still a few 1° squares with little or no data for a particular month. Regions with the lowest number of observations are along the southern limit of the model basin.

Each monthly mean wind estimate was converted to wind stress using the relation $\tau = \rho_a C_D |\mathbf{W}| \mathbf{W}$, where τ is the wind stress, ρ_a the air density, C_D the drag coefficient and W the wind velocity. When converting the monthly mean wind data to stress, Hastenrath and Lamb (1977) used a rather large value of $C_D = 2.8 \times 10^{-3}$ to compensate for underestimating the square of the resultant wind speed. Bunker (1976) created an alternate wind stress product in which each individual wind observation was converted to stress using a drag coefficient that was dependent on wind speed and atmospheric stability. Hellerman (1980) interpolated this irregularly spaced, coarse resolution data onto a 1° mesh. Comparison between the Hastenrath and Lamb monthly stress fields and those of Hellerman indicates that both analyses are similar if the drag coefficient used by Hastenrath and Lamb is reduced to 2.0×10^{-3} (Picaut, 1983).

For this study, as in Busalacchi and O'Brien (1980), the air density was assumed to be constant at 1.2 kg m^{-3} and a constant drag coefficient of 1.5×10^{-3} was chosen. The precise value of C_D is not critically important in this linear calculation since we will not focus on the absolute magnitudes of the oceanic response. The phase and relative amplitude of the response between one part of the basin and another is more important. If a different constant drag coefficient is chosen the model results would change in proportion with C_D.

The 12 monthly means at each point were decomposed into the first five Fourier harmonics in time, 12 month, 6 month, 4 month, 3 month, 2.4 month, to provide a continuous time series for the model integration. This resulted in a smoother profile of the seasonal cycle than would linear interpolating from month to month. The possibility of high-frequency noise being generated in the model by rapid wind stress changes at mid-month has thus been reduced. The implementation of this harmonic forcing also allows the total ocean response at any point to be analyzed and described in terms of five harmonics.

Fourier decomposition of the wind stress data also helped in editing the monthly means. The wind stress amplitude fields for the five harmonics were used to locate 1° squares with anomalous data. The higher harmonics were very good indicators of those isolated 1° squares where the wind signal was considerably

different than the surrounding data points. The monthly mean time series for each 1° square in question was adjusted to provide continuity in time and space by eliminating the spurious datum point and replacing it with a spatially and temporally averaged value. All the points needing correction were in regions where the monthly means were determined by a small number of observations. Less than 0.5% of the monthly means were corrected following this procedure. Next, the zonal and meridional wind stress monthly means were interpolated from the 1° grid to the finer model grid. A two-dimensional Hanning filter was used to suppress small spatial scale variability in each monthly stress field. These adjusted monthly means were once again Fourier decomposed into their final form to be used as input for the model calculation.

Representation of the climatological seasonal cycle by five harmonics provides a reasonable fit with climatological daily mean data (Picaut, 1983). This is primarily due to the large influence of the lower harmonics. Spectral analysis and Fourier decomposition of wind time series of up to 15 years at 10 coastal stations in the Gulf of Guinea and at St. Helena Island (16°S, 6°W) indicate that the annual and semiannual harmonics dominate the seasonal cycle with some contribution from the third harmonic (Picaut *et al.*, 1978). This is confirmed for the entire tropical Atlantic by the Fourier decomposition of the wind stress data in this study. Basin-wide, the largest harmonic amplitudes are for the annual and semiannual signals.

The spatial distribution of the annual mean, annual harmonic amplitudes, and the semiannual harmonic amplitudes for the zonal and meridional wind stress are depicted in Fig. 2. The mean stress field is characterized by the northeast and southeast trade wind systems associated with the Azores and St. Helena anticyclones. The trade systems flow toward South America and converge north of the equator to form the ITCZ. West of the Gulf of Guinea the mean zonal wind stress (Fig. 2a) is easterly and maximum near the Brazil coast. Since the ITCZ is located north of the equator the low-latitude meridional wind field (Fig. 2b) is predominantly southerly. In the Gulf of Guinea there is an eastward veering of the southerly wind toward the low pressure of the Sahara. This forms the basis for the West African monsoon.

Annual variations in both stress fields (Fig. 2) are most pronounced in the western tropical Atlantic. The core regions of the northeast trades are strongest from January to March and the southeast trades are strongest from July to September. This is also reflected in the seasonal excursion of the ITCZ which is near the equator in March and reaches its northernmost extent in August. The semiannual variability of the trades, particularly in the west, is much smaller than the annual. Strong semiannual wind variability has been detected in the Caribbean Sea by Hellerman (1980) and Cochrane (personal communication, 1981) but this is northwest of our area of interest. The effect of semiannual forcing must not be dismissed. Studies of sea level (Verstraete *et al.*, 1980) and subsurface thermal structure (Merle and LeFloch, 1978) in the Gulf of Guinea indicate the semiannual variability is almost as large as the annual signal. A four-month sea level oscillation was also detected by Verstraete *et al.* (1980). At the four-month period the amplitude of the tropical Atlantic wind stress is still notable (roughly half that of the semiannual) but the physical meaning of such an atmospheric oscillation is unclear. The higher harmonics of the wind stress decomposition account for small differences between the monthly means and the low-order harmonics at time scales of two to three months.

4. Tropical Atlantic response to the seasonal wind field

The seasonal variability of the model height field will be our primary concern in this study. The model results will be examined in terms of deviations about the local mean depth of the pycnocline. Analysis of the height field variability will provide some insight into the processes responsible for observed fluctuations in sea level and dynamic height since these quantities are determined by the gravest baroclinic modes. The effect of wind stress curl, alongshore wind, zonal equatorial wind, and remotely forced Kelvin waves and Rossby waves at various points in the basin will be addressed. Analysis of the current variability is of lesser importance in this calculation since the current fields are only described by a single baroclinic mode and nonlinear influences have been neglected.

An overview of the pycnocline response to the tropical Atlantic wind field will be presented first. This will consist of a discussion of the mean and seasonal fluctuations of the pycnocline topography for the entire model basin. Comparison with observed variations of dynamic height will be provided. A closer scrutiny of the response in the western Atlantic, along the equator, and in the eastern Atlantic will follow.

a. Basin-wide response

The model pycnocline response to the mean wind field over the tropical Atlantic is presented in Fig. 3 as the mean displacement of the pycnocline from a level surface. The mean height field is characterized by a shallow pycnocline in the east and a deep pycnocline in the west. Superimposed upon this east–west gradient are a zonal equatorial trough and a low-latitude ridge in each hemisphere terminating at an upwelled dome-like feature. The zonal slope at the equator is induced by the mean zonal wind stress, $\tau^x/\rho = c^2 h_x$. The meridional pycnocline topography

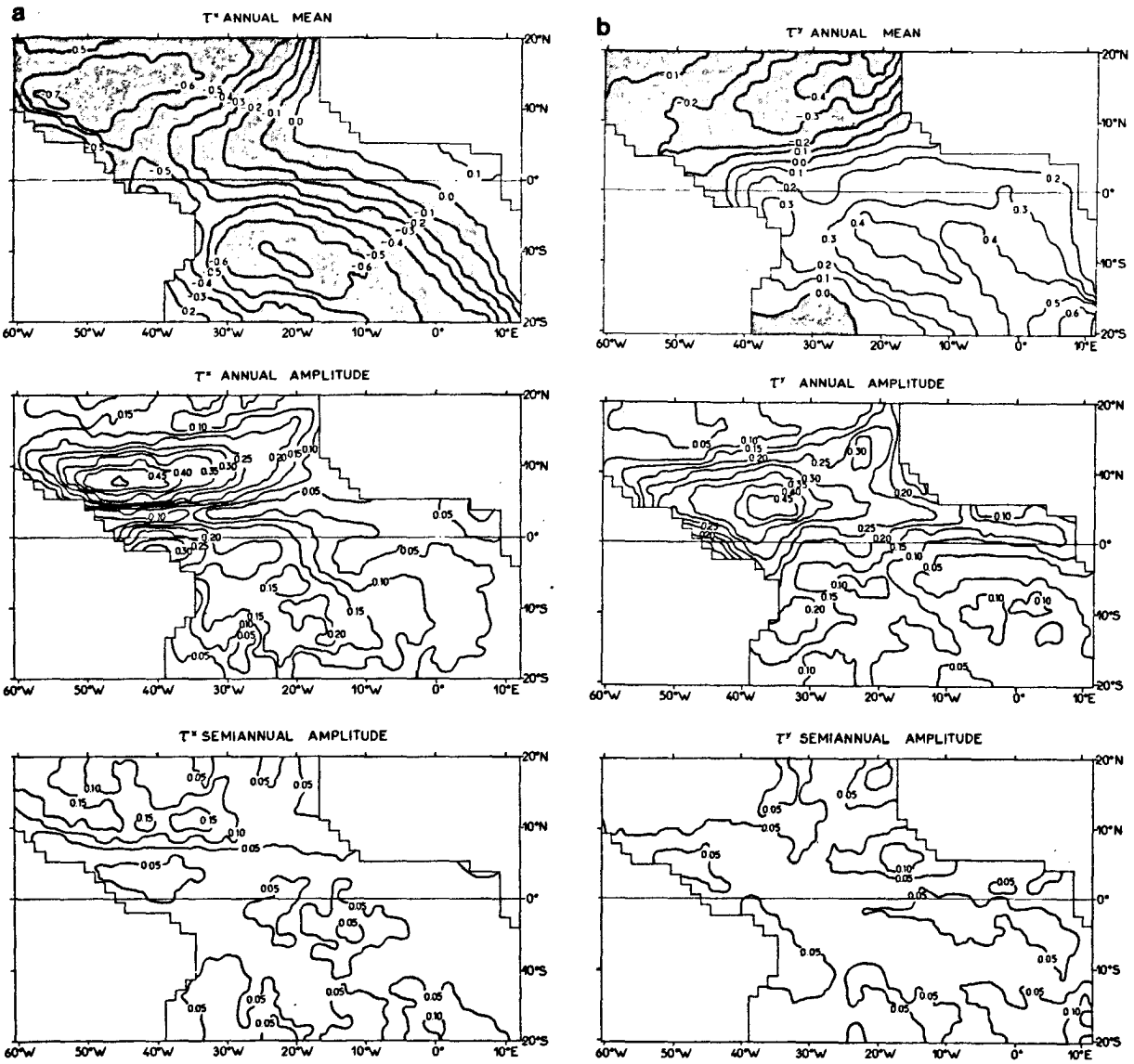

FIG. 2. Mean, amplitude distribution for the first harmonic, and amplitude distribution of the second harmonic for (a) the zonal wind stress and (b) the meridional wind stress (dyn cm^{-2}).

is determined by the wind-stress curl distribution, primarily $\partial\tau^x/\partial y$ [see Fig. 7 of Hellerman (1980)], and the influence of cross-equatorial winds. The shallow region in the northeastern part of the basin is in the vicinity of the Guinea Dome. This formation is well defined by observations and has been described by Rossignol and Meyrueis (1964) and Mazeika (1967). The Angola Dome in the Southern Hemisphere is not as clearly defined by observations. Mazeika (1967) noted the existence of a subsurface dome structure located near 10°S, 9°E during the austral summer but Bogorov *et al.* (1973) described a larger cyclonic vortex centered at 13°S, 3°E.

All historical Nansen, CTD, MBT and XBT data available have recently been used by Merle and Arnault (1983) to update a computation of the mean dynamic height field relative to 300 db for the tropical Atlantic from 20°N to 16°S. The MBT and XBT data were used to obtain salinity information via the *T–S* relation following Stommel (1947) and Emery (1975). The updated dynamic height data are more precise than the previous calculation by Merle (1978) which only included Nansen data up through 1972. The monthly mean dynamic height data (surface/300 db), generously provided by S. Arnault and J. Merle, were subjected to a weighted least squares method (Bloomfield, 1976; Draper and Smith, 1981) to extract the mean, annual harmonic, and semiannual harmonic on a 2° latitude by 4° longitude grid.

The mean dynamic height field (Fig. 4) and the

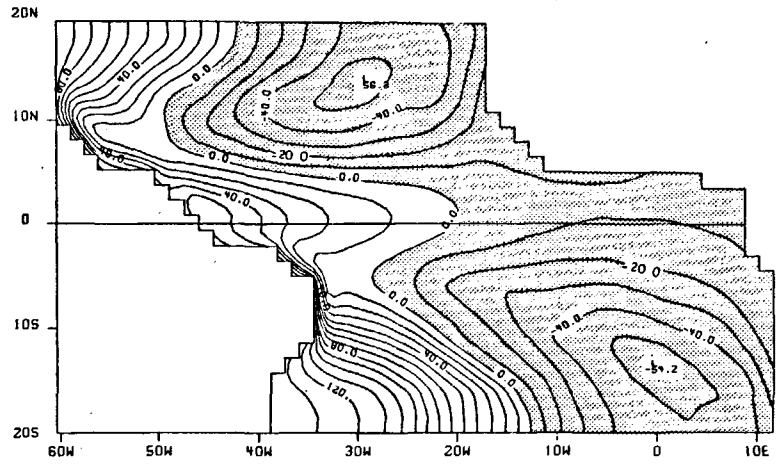

FIG. 3. Annual mean perturbation (m) to the upper layer thickness. Shaded regions indicate where the pycnocline is shallower than the initial state of no motion.

model pycnocline topography (Fig. 3) compare favorably, provided one notes that these two fields are inversely related. A system of troughs and ridges delineates several equatorial currents (Katz, 1981) as in the tropical Pacific (Wyrtki, 1974a,b). Based on the distribution of dynamic height, the North Equatorial Current is located between 20°N and the trough near 10°N. The North Equatorial Countercurrent (NECC) is bounded by the trough at 10°N and the ridge at 3°N. In the model the expression of this ridge as a pycnocline trough is closer to the equator as was the location of the Equatorial Ridge in the Pacific Ocean model by Busalacchi and O'Brien (1980). The sparse data in the Southern Hemisphere indicate a poorly defined ridge in dynamic height at 8°S which may form the northern boundary of the South Equatorial Countercurrent (Merle, 1977). A corresponding feature is not present in the annual mean of the model pycnocline topography. A seasonal pycnocline trough is present south of the equator in the central and eastern sections of the model basin from June to August. Note also the large dynamic height in the corner of the Gulf of Guinea caused by Niger River outflow.

The major thrust of this study will deal with the seasonal variations about the mean state. Merle and LeFloch (1978) have shown that the seasonal cycle of the surface and subsurface thermal structure in the tropical Atlantic is mainly described by the annual and semiannual harmonics. This is also true of the wind field. Fourier decomposition in time of the linear, periodic model solution provides a straightforward method of assessing the basin-wide spatial and temporal variability. The seasonal signals of both the model pycnocline and dynamic height deduced from observations are governed by annual and semiannual fluctuations (Figs. 5–7). The phase of the response should be overlooked in regions where the amplitude is very small. Due to errors inherent in dynamic height calculations only amplitudes greater than 2 dynamic cm are significant.

The largest annual model pycnocline and dynamic

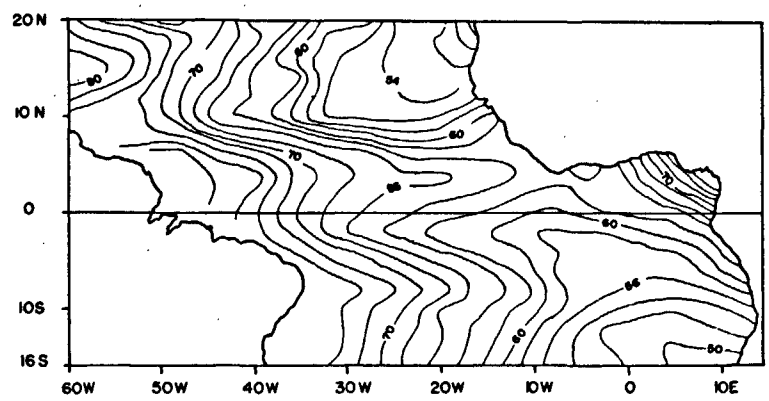

FIG. 4. Annual mean of dynamic height (dynamic cm) at 0/300 db.

height changes (Figs. 5, 6) are in the western half of the basin north of the equator and south of a band of rapid phase change. This area of large amplitudes is associated with a north–south pivoting of the northern tropical Atlantic about a line roughly parallel to the ITCZ. North of the pivot line, near 10°N, a secondary amplitude maximum is present in the model. The pivot line also indicates the location of the smallest seasonal SST variations for the tropical Atlantic (Merle and LeFloch, 1978). Along the equator the largest amplitudes in the model and observations are near the eastern and western boundaries. An amplitude minimum and a large phase gradient in the central equatorial Atlantic represent a nodal or pivot point for the east–west tilting of the pycnocline at the equator (Merle, 1980a). In the eastern Atlantic, an area of notable amplitude is along the southern coast of the Gulf of Guinea extending northwestward toward the equator. The modelled and observed phase differ by less than 40°. Near the equator between the eastern boundary and 4°W, there is a very small westward increase in phase. Between 4°W and the pivot point the phase increases eastward. An area of major discrepancy between the model and observations is along the coasts of Mauritania and Senegal. In this region the amplitudes of dynamic height increase northward, but the model height field amplitudes decrease northward. For the remainder of the basin, near the northern and southern extremes, the modelled and observed amplitudes are small and phase lines indicate the pycnocline is deeper in the summer–fall of each hemisphere.

The distribution of the semiannual amplitudes for the model and observations are presented in Fig. 7.

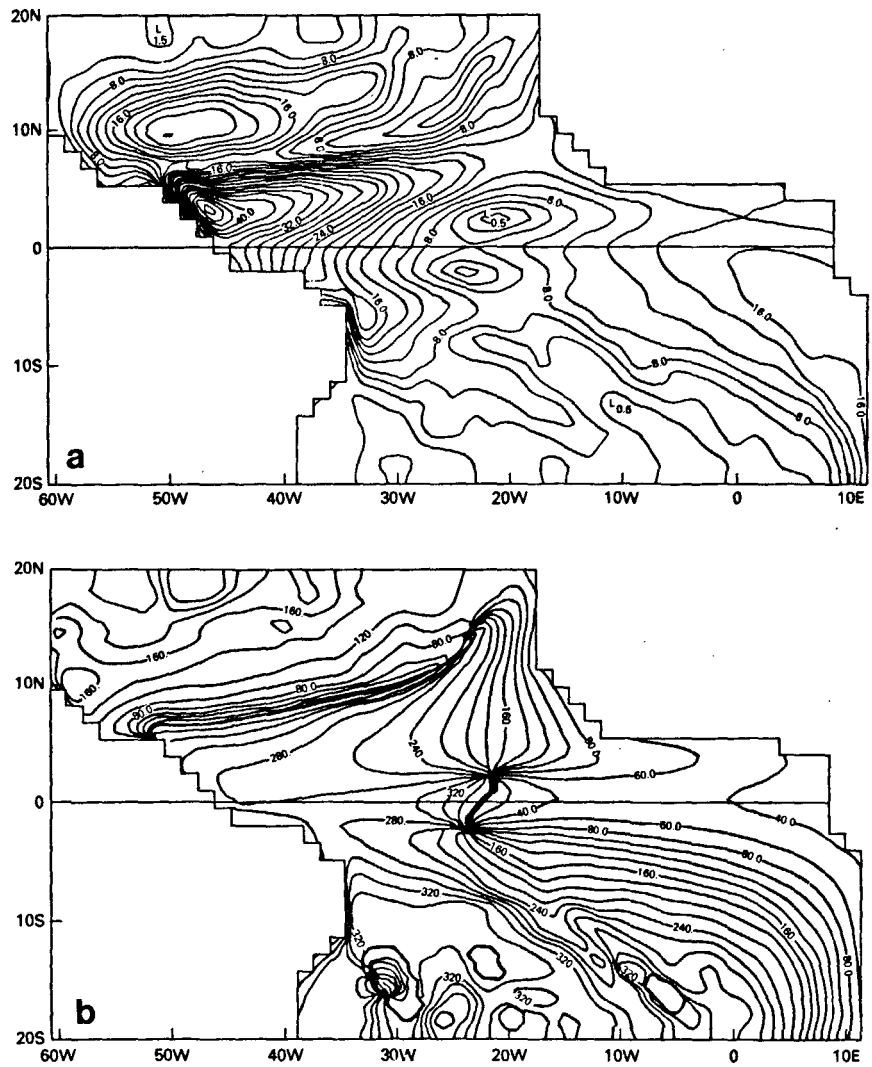

FIG. 5. (a) Amplitude (m) and (b) phase (deg) of the annual variability of the model pycnocline depth. The phase map indicates when the pycnocline is deepest.

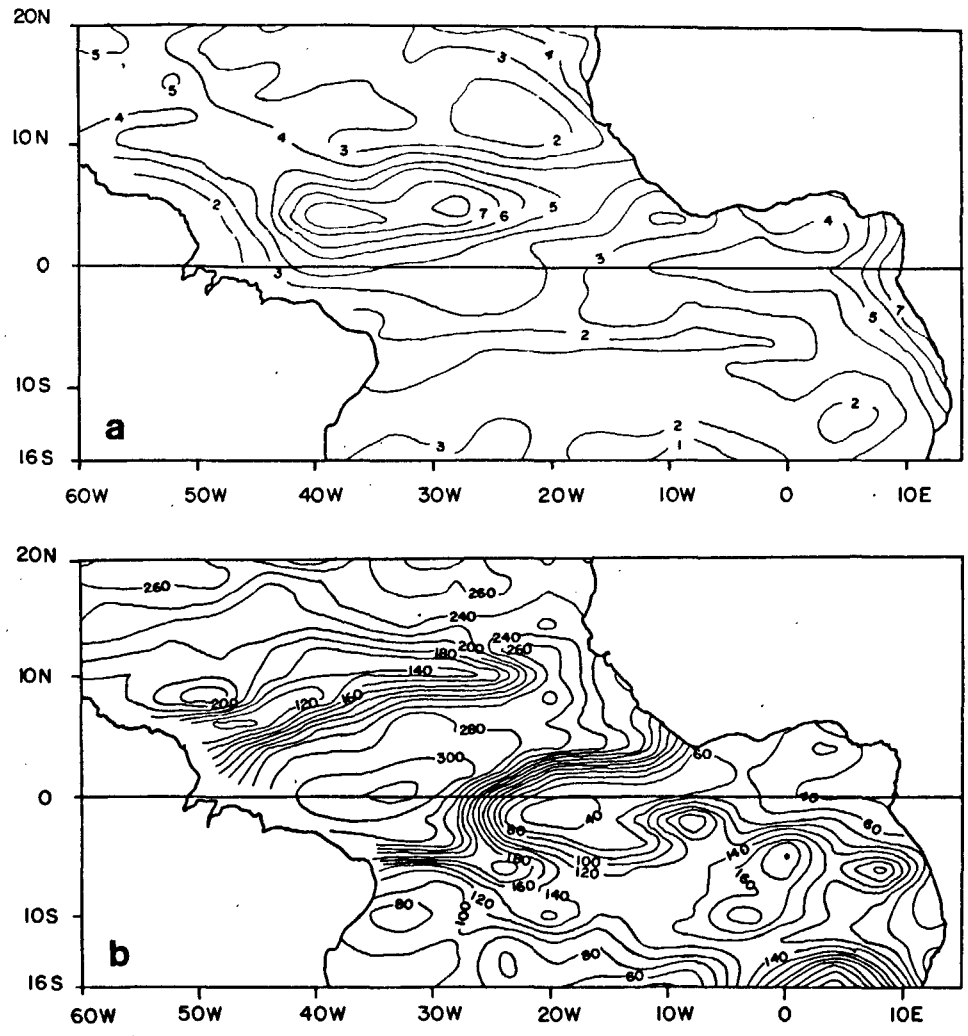

FIG. 6. (a) Amplitude (dynamic cm) and (b) phase (deg) of the annual variability of the dynamic height at the surface relative to 300 db.

The major areas of variability are similar to those of the annual period. Regions of maximum amplitude are along the eastern boundary, and north of the equator in the central and western Atlantic. In contrast with the annual signal, there is no significant semiannual variability near the western boundary at 10°N. At the equator in the central model basin there is little semiannual change. The phase lines (not shown) indicate this area corresponds to a pivot point for a 6-month period east–west tilting of the equatorial pycnocline. The smallest dynamic height changes along the equator occur near the western boundary as opposed to a more central location in the model. An important feature of the semiannual response is that the largest amplitudes are in the east, opposite to that for the annual response. The semiannual response in the Gulf of Guinea is roughly one-half of the annual signal. Variations in subsurface thermal structure (Merle and LeFloch, 1978) and sea level (Verstraete *et al.*, 1980) also indicate a strong semiannual component in the eastern Atlantic in agreement with Fig. 7. Inspection of the wind stress fields (Fig. 2) does not offer any explanation of these relations.

Several case studies were performed in order to understand the interesting features reproduced by the model. These entailed integrating the model equations with parametric wind distributions representing portions of the total wind stress field. The separate influences of the zonal and meridional wind stress were isolated by repeating the model calculations with only zonal wind stress forcing, i.e., the meridional wind stress was set identically equal to zero (Fig. 8). By comparing the annual and semiannual response to zonal winds with the total forcing solution (Figs. 5a, 7b, 8) it is evident that the variations in the central and western parts of the model basin are due to the variability of the zonal wind stress component. The

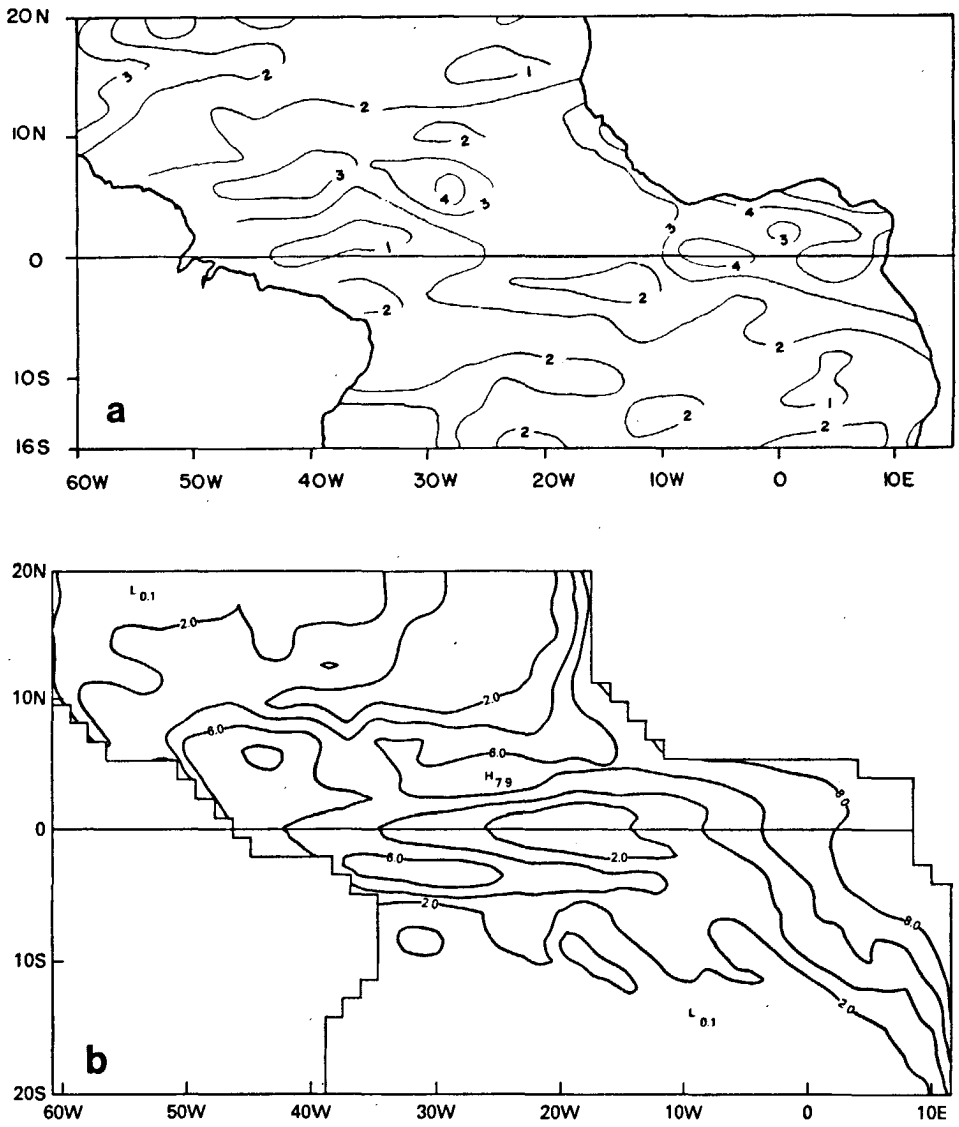

FIG. 7. Semiannual amplitudes of (a) dynamic height (dynamic cm) at 0/300 db and (b) model pycnocline depth (m).

only notable influence of the meridional wind variability is along the eastern boundary. The coastal signal along Mauritania and Senegal is much larger when alongshore winds are neglected. The annual response to τ^x forcing along the zonal coast of the Gulf of Guinea is also weakened by the addition of meridional wind forcing. Though the large pycnocline changes are still present in the Gulf of Guinea, the tongue-like pattern of the pycnocline amplitudes is not well defined when annual zonal forcing is employed. The influence of the southerly wind at the coast is to increase the amplitude of the pycnocline signal south of the equator and decrease the total response north of the equator. The importance of meridional winds near the equator and along the southern coast have been discussed by Voituriez (1981a) and Philander and Pacanowski (1981a). In the present linear model nearly all of the annual and 75% of the semiannual pycnocline fluctuations in the Gulf of Guinea are driven by changes in the zonal component of the wind field.

Additional calculations were performed whereby the zonal wind stress was limited to being either inside or outside the Gulf of Guinea, or was limited to the eastern or western sides of the basin. Since the meridional stress was neglected, no erroneous wind stress curl was produced by this fractional suppression of the wind stress. These calculations will aid in determining the processes responsible for seasonal changes in the western, equatorial and eastern Atlantic. The

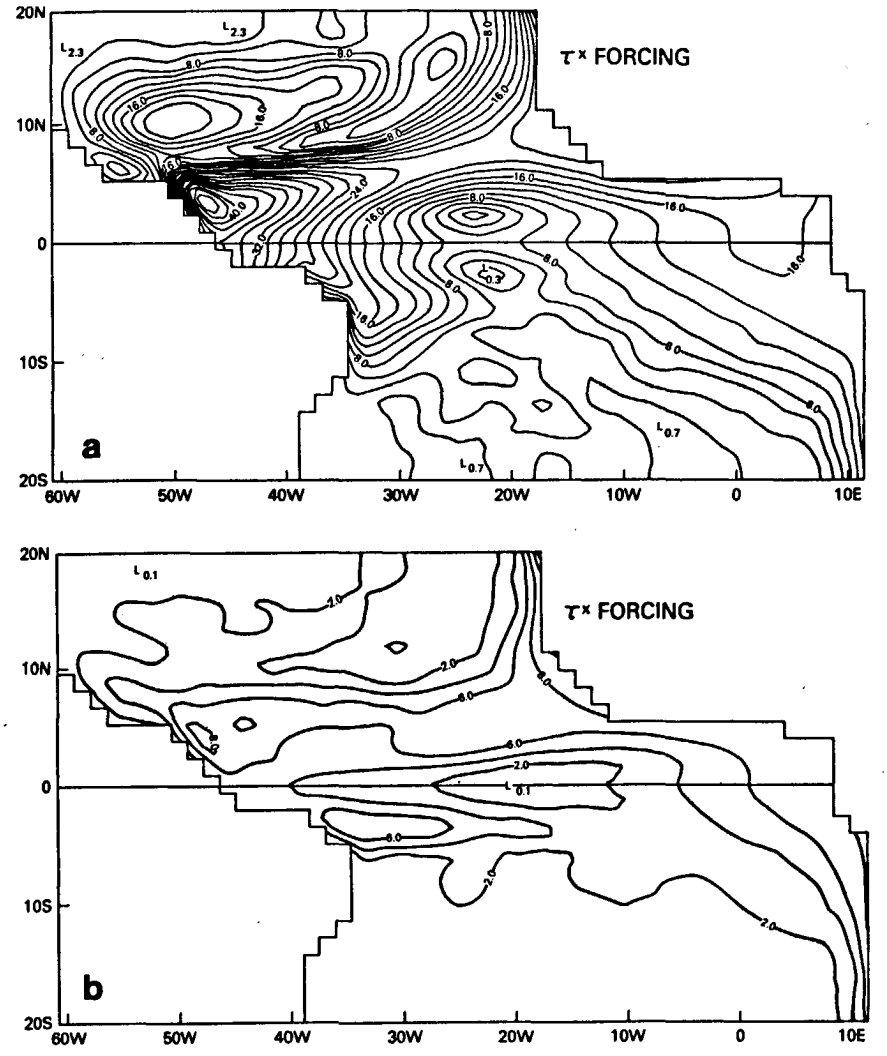

FIG. 8. Amplitude distributions for the pycnocline response to (a) annual τ^x forcing and (b) semiannual τ^x forcing. The differences from Fig. 5a and 7b indicate the influence of τ^y forcing.

results will provide a simple determination of whether the seasonal response in a particular region of the model basin is dominated by local or remote forcing.

b. Western tropical response

The model results and observations (Figs. 5–7) demonstrate that the seasonal variability in the western tropical North Atlantic is characterized by a north–south tilting of the sea surface/pycnocline topography. A pivot line extending northeastward from the western boundary at 5°N, parallel to the mean position of the ITCZ, separates two regions of large, out-of-phase variability. The seasonal displacements of the pycnocline are dominated by annual processes (Figs. 9 and 10). Semiannual fluctuations are considerably smaller as they are in the local wind field. North of the pivot line the annual signal is driven by zonal wind stress changes in the western part of the basin (Figs. 8a and 10a). In the region to the south there is a contribution from the wind stress east of 25°W (Fig. 10b) implying the influence of Rossby waves.

Analysis of the vertical displacement of the pycnocline can be pursued further by forming the vorticity equation from the inviscid version of (1a), and then substituting for the divergence and βV terms. The pycnocline fluctuations are then described by

$$h_t = \frac{1}{\beta y}\left(V_{xt} - U_{yt} + \frac{1}{y}U_t\right) - \hat{\mathbf{k}}\cdot\nabla\times\frac{\tau}{\rho\beta y} + \frac{c^2}{\beta y^2}h_x. \tag{2}$$

The magnitudes of the terms in (2) are calculated in

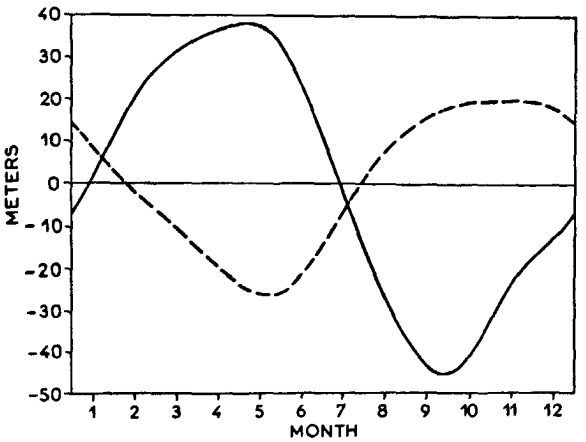

FIG. 9. Seasonal pycnocline displacements for 2° squares centered at 10°N, 48°W (dashed line) and 3°N, 43°W (solid line). These variations are indicative of a north–south tilting about a pivot line which separates the two areas. Negative values indicate the model pycnocline is deeper than the annual mean.

order to isolate the mechanisms responsible for the large-amplitude variability in the western tropical Atlantic. Theory and observations indicate that at extra-equatorial latitudes Ekman pumping and Rossby waves (last two terms respectively) may be important on seasonal time scales (Yoshida, 1955; Meyers, 1979). The acceleration terms have been included because the region south of the pivot line is close enough to the equator to be influenced by equatorial waves.

The major contribution in (2) representing the model pycnocline displacements centered at 10°N, 48°W is Ekman pumping (Fig. 11), primarily $\partial(\tau^x/\rho\beta y)/\partial y$. This holds true for the entire region of large-amplitude pycnocline changes north of the pivot line. The seasonal deepening of the pycnocline during the first half of the year is a local response to an increase in the easterly wind stress and an anticyclonic perturbation to the wind stress curl. These wind stress changes are related to the southward displacement of the ITCZ. All other terms in the vorticity equation are insignificant. This is consistent with the case studies incorporating partial forcing (Fig. 10) which demonstrate that the variability north of the pivot line is locally forced. During parameter range tests this region north of the pivot line was the only part of the model basin in which the magnitude of the pycnocline variations was independent of the phase speed c. This also implied the relative importance of Ekman pumping with respect to the Rossby wave influence at this location.

The case studies indicate remote and local effects are present south of the pivot line (Fig. 10). Ekman pumping and Rossby waves are the dominant mechanisms (Fig. 12a). The seasonal displacement of the pycnocline is determined by the phase relation between the two processes. The effects of the acceleration terms are small but only the V_{xt} term can be ignored. The contributions from U_t and U_{yt} (Fig. 12b) are not negligible because of the proximity to the equator. Rossby waves emanating from the east are downwelling favorable from March to August. The sign of the Ekman pumping in this area is governed by the changes in the wind stress curl. From June to November the ITCZ is shifted north of its mean position. The associated influx of the southeast trades results in an anticyclonic perturbation to the wind stress curl. The combination of the two effects causes a seasonal deepening of the pycnocline from May through September. The pycnocline deepens at the equator during the same period in response to strengthening equatorial easterlies.

These large model pycnocline displacements are in locations where seasonal variations to the current field are produced. The mean position of a simulated NECC in the western model basin is between a pycnocline ridge near 8°N and an equatorial pycnocline trough (Fig. 3). The pycnocline displacements at 10°N determine the seasonal depth and location of the pycnocline ridge forming the north flank of the NECC. Similarly, the large annual changes near 3°N influence the location and strength of the low-latitude trough south of the NECC. Since the two regions are out of phase there are large seasonal changes in the meridional pressure gradient. The pycnocline ridge is most shallow and the equatorial trough is deepest from July through December (Fig. 9). Both features are north of their mean position at this time. During the first part of the year the ridge and trough are weak and not well defined.

The simulated NECC undergoes significant spatial and temporal variations in response to the pressure field changes in the model. Early in the year the current is weak and close to the equator. From May to September the NECC progresses northward and becomes well formed between 5–8°N. This displacement of the NECC is similar to the observations at 35–50°W compiled by Boisvert (1967). The zonal current within the rectangle from 3–9°N and 30–42°W has been averaged to provide an indication of the seasonal variability of the NECC (Fig. 13). Within this region the averaged NECC is strongest in August and is nonexistent in April. From February to August the southern boundary of a simulated North Equatorial Current (NEC) is situated south of 10°N and results in a reversal of the zonal flow in the northern portion of this rectangle. West of 35°W the NEC reaches 5°N in March–April and contributes to the current minimum depicted in Fig. 13. Dynamic height differences across the NECC at 5/500 db averaged between 20–40°W imply that the current is weakest from February to June and strongest from July to November (Merle, 1977). Ship drift data averaged between 5–8°N and 25–30°W indicate a maximum eastward current (29 cm s^{-1}) in August re-

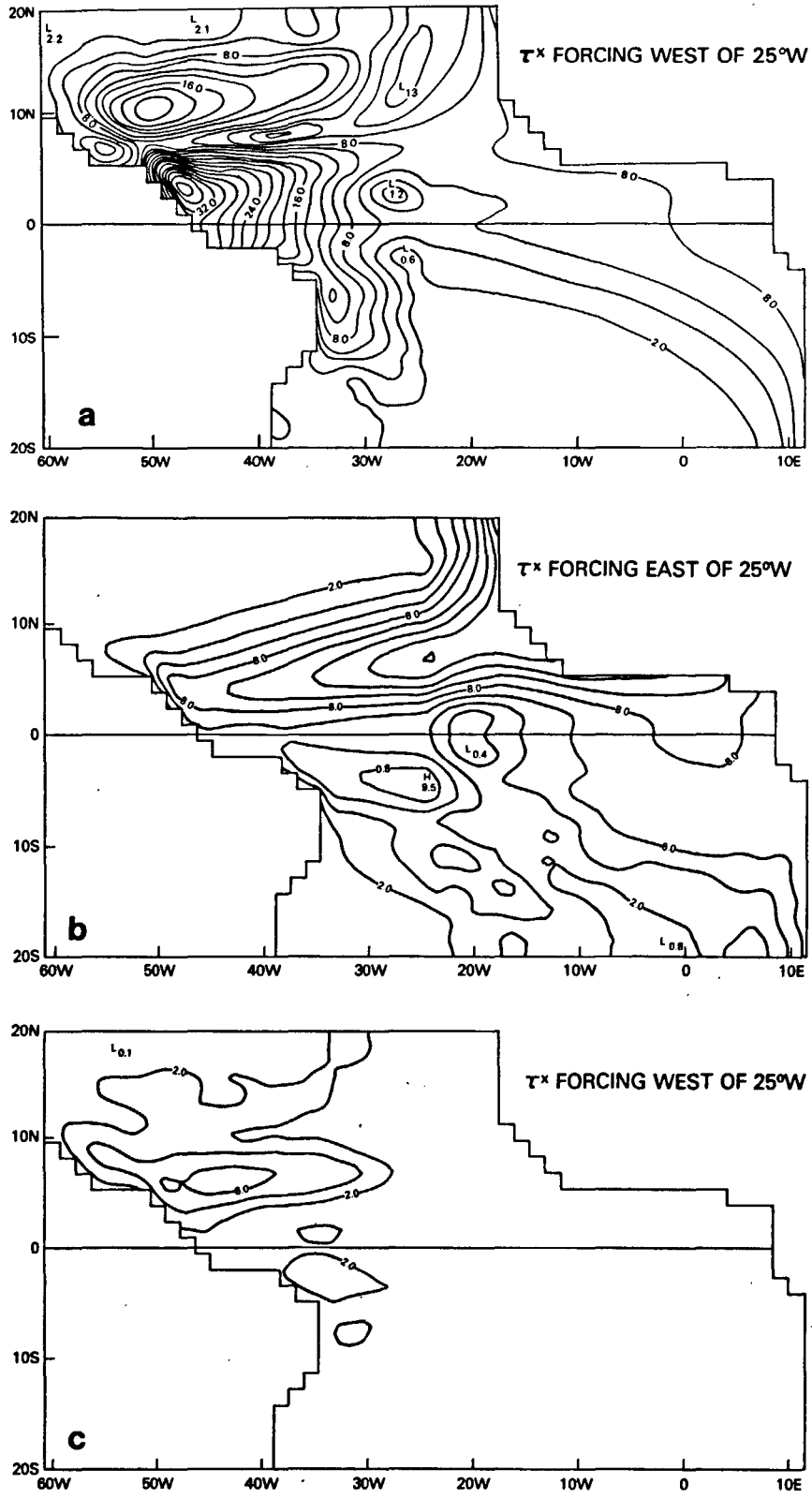

FIG. 10. Amplitude distributions for the pycnocline response to (a) annual τ^x forcing west of 25°W, (b) annual τ^x forcing east of 25°W, (c) semiannual τ^x forcing west of 25°W, and (d) semiannual τ^x forcing east of 25°W.

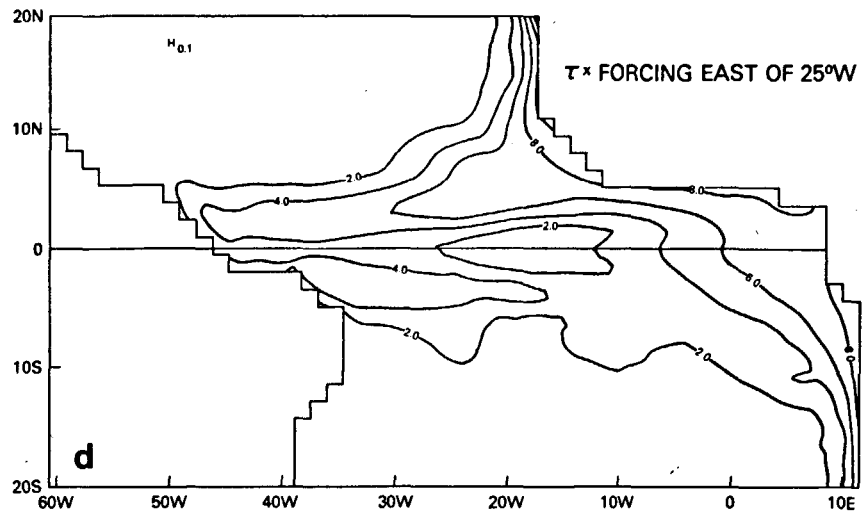

FIG. 10 (*Continued*)

versing to a maximum westward flow (-12 cm s^{-1}) in April (P. Richardson, personal communication, 1983).

In the Southern Hemisphere there is no well-formed convergence zone in the atmosphere. The western South Atlantic is always under the influence of a single trade wind system. Therefore, there is only one area of large pycnocline displacements south of the equator. Off the coast of Brazil at 6°S the seasonal pycnocline displacements are produced by Ekman pumping and Rossby waves. The Ekman pumping contribution is downwelling favorable from July through January due to a seasonal increase in the southeast trades. The Rossby wave influence has the same phase as north of the equator. The combined effect of the two processes is a downward displacement of the pycnocline from June through November.

c. *Equatorial response*

The seasonal changes in the model height field along the equator are presented in Fig. 14a. The mean zonal tilt of the pycnocline has been included to aid in discussing the pressure gradient variations. The western side of the model ocean is characterized by a deep pycnocline which has a minimum depth in April–May and maximum depth in September–October. The seasonal variation is dominantly annual. The eastern side is characterized by a shallow pyc-

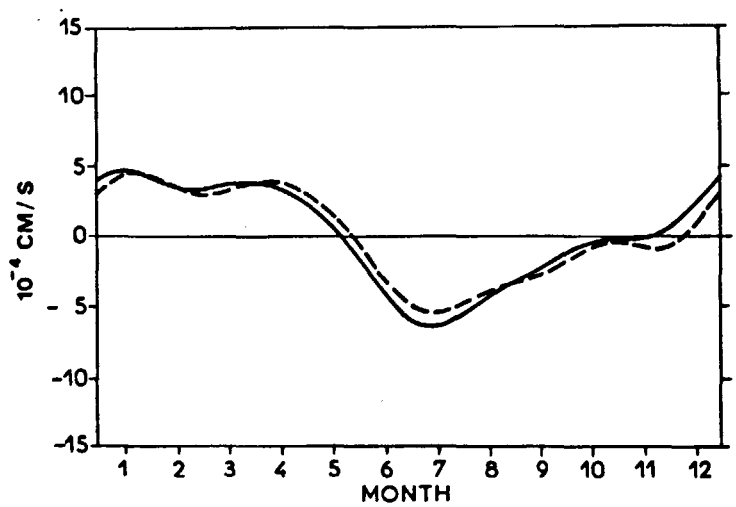

FIG. 11. Comparison of the time rate of change of the model pycnocline depth: $\partial h/\partial t$ (solid), and the contribution due to Ekman pumping: $\hat{\mathbf{k}} \cdot \nabla \times \tau/(\rho\beta y)$ (dashed) for the 2° square centered at 10°N, 48°W. Positive values indicate the model pycnocline is deepening.

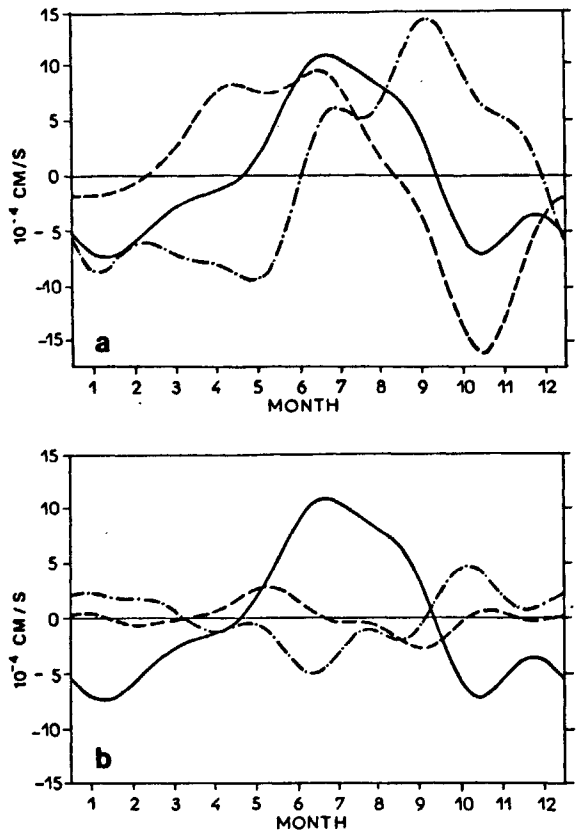

FIG. 12. Comparison among the model results at 3°N, 43°W for (a) $\partial h/\partial t$ (solid) and the contributions to this from Ekman pumping (dashed-dotted), and Rossby waves: $(c^2/\beta y^2)h_x$ (dashed); and (b) $\partial h/\partial t$ (solid) and the contributions to this from $-(1/\beta y)(\partial^2 U/\partial y \partial t)$ (dashed-dotted) and $(1/\beta y^2)(\partial U/\partial t)$ (dashed).

nocline which attains a maximum depth in February–March and minimum depth in July. A secondary maximum is present in October–November followed by a secondary minimum. The timing of the shallow model pycnocline in July is very close to that of the observed minima of thermocline depth and SST in July and August. The small upwelling episode later in the year has also been observed. These seasonal pycnocline displacements on each side of the basin are separated by a nodal point between 20–30°W. The oscillation along the equator is not a simple east–west tilting or "seesaw" because the phase difference between opposite ends is closer to 90° than 180°.

Katz *et al.* (1977) studied the seasonal change in slope of the dynamic topography along the equator from 10 to 40°W. It was noted that the zonal pressure gradient was weak in spring and maximum in summer. A reasonable agreement was found between the vertically integrated pressure gradient and the zonal wind stress. Additional calculations by Lass *et al.* (1982) also indicated the zonal pressure gradient was weak in March–April and maximum in September–October. The east–west slope of the model pycnocline undergoes a similar seasonal cycle. A comparison of the zonal wind stress along the equator (Fig. 15a) and the equatorial height field (Fig. 14a) suggests this simple equilibrium response, with the ocean lagging slightly, holds true in the western half of the basin. In the east, changes in pycnocline depth do not appear to be consistent with local wind stress changes.

Analysis of the pycnocline and zonal wind stress variability is simplified if the annual mean at each point in space is removed. It is now more evident (Fig. 14b) that the height field change is not a rigid oscillation about a fulcrum in the mid-Atlantic. The amplitude of the variability is largest in the west as are the winds. The annual and semiannual pycnocline displacements in the eastern Atlantic are significant, but the overlying wind changes are small. The response at each boundary is in phase for roughly one-third of the basin width. There is also a lag between the minimum pycnocline depth in the east (July) and the maximum depth in the west (September–October). A similar lag appeared in the heat content calculations by Merle (1980a) and has recently been detected in thermocline depth variations (Houghton and Garzoli, personal communication, 1982).

The seasonal cycle of the equatorial model pycnocline indicates that the upwelling season at the eastern boundary is not associated with any explicit eastward phase propagation. Based on climatology, the largest intensification of the equatorial easterlies (Fig. 15b) is in the western Atlantic from April to September. In terms of a single train of impulsive Kelvin waves, this would result in remotely forced upwelling at the eastern boundary on into October. Hence, there is no indication in this periodic solution that the shallow pycnocline in July is induced by an eastward-propagating Kelvin wave front.

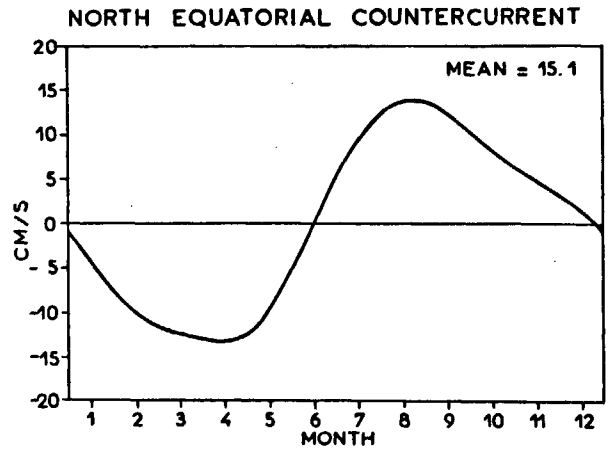

FIG. 13. Zonal velocity corresponding to a simulated North Equatorial Countercurrent averaged between 3–9°N and 30–42°W.

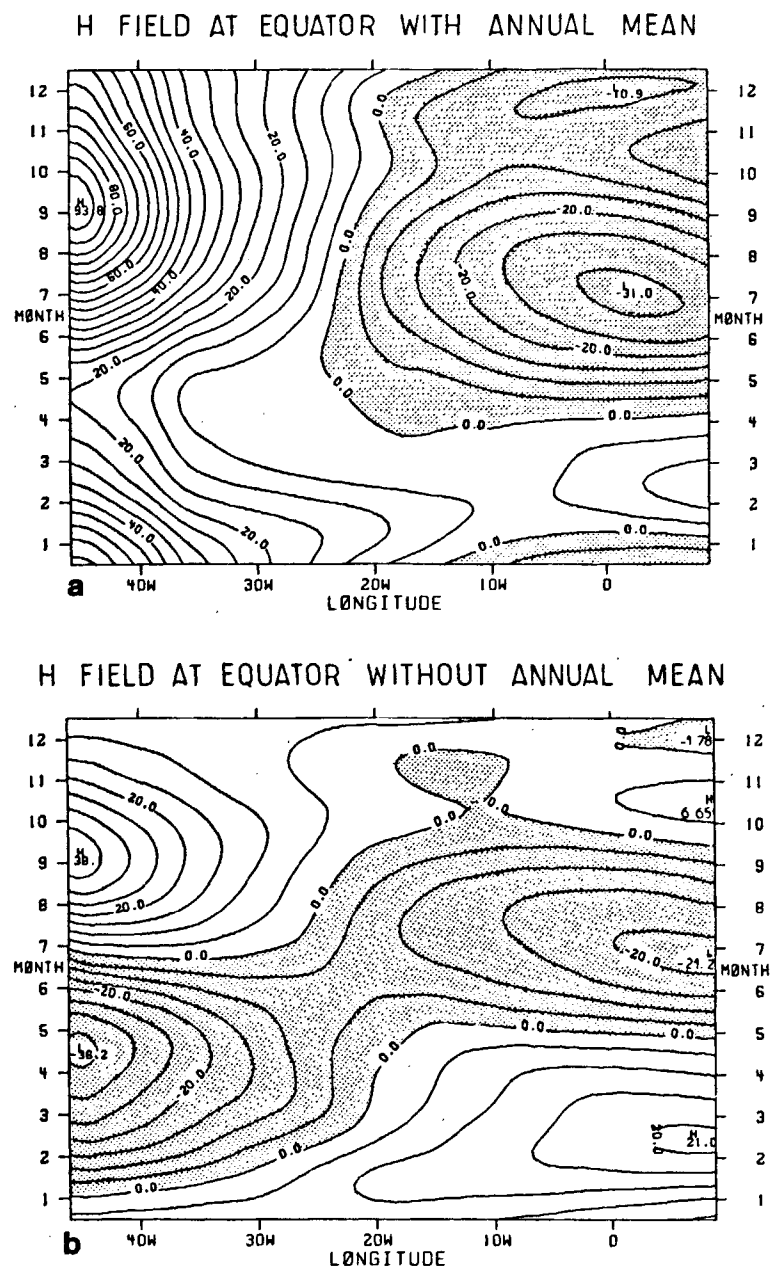

FIG. 14. Temporal variability of the model pycnocline (meters) along the equator. (a) Shaded regions indicate the pycnocline is shallower than the initial state of no motion. The annual mean east-west pycnocline tilt is included in this plot. (b) The annual mean east–west pycnocline tilt has been removed. Shaded regions indicate the pycnocline is shallower than the annual mean.

Kindle (1979) and Cane and Sarachik (1981) have studied the linear response of a zonally bounded equatorial ocean to periodic zonal forcing. The resulting solution is a complex superposition of a locally forced response, equatorial Kelvin waves, Rossby waves, and multiple wave reflections. The phase and amplitude of the total periodic response depend on the Kelvin wave speed, the frequency of the forcing, and the width of the basin. These in turn determine the interference pattern set up by the various waves. Zonal phase gradients are therefore not necessarily indicative of any single propagating wave.

The importance of the local response and remotely-forced equatorial waves will vary across the basin because there is a definite zonal structure to the equatorial wind field. Observations suggest that an

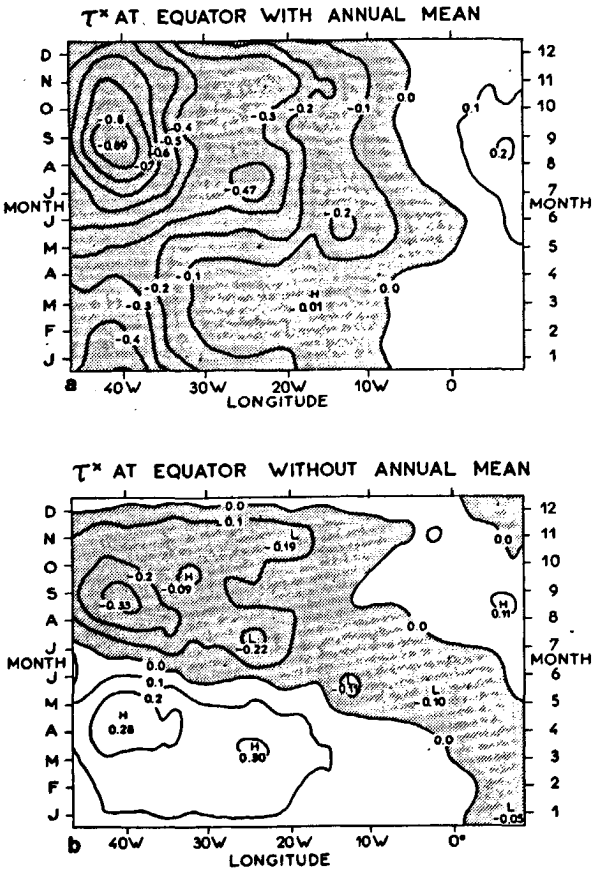

FIG. 15. Temporal variability of the zonal wind stress (dyn cm^{-2}) along the equator. (a) The annual mean has been included. Shaded regions indicate easterly wind stress. (b) The annual mean has been removed. Shaded regions indicate an easterly wind stress perturbation.

equilibrium response exists between the zonal wind stress and the pressure gradient between 10 and 40°W. In the western part of the model basin the height field changes appear to be in qualitative agreement with zonal wind stress fluctuations (Figs. 14 and 15). The time history of each term in the x-momentum equation has been analyzed for several intervals along the equator. The seasonal cycles of c^2h_x and τ^x/ρ in the western equatorial region of the model are large in amplitude and nearly in phase. Most of the annual model pycnocline variability in the western equatorial Atlantic is therefore associated with the overlying zonal wind stress changes. The influence of remote effects is small when compared with the magnitude of the locally forced signal. The pressure gradient lags the wind by about 10 days. This slight time delay produces a seasonal acceleration of the equatorial current. Lass *et al.* (1982) reported that the observed pressure gradient lags the wind stress by approximately one month. The seasonal amplitudes of the model pressure gradient and wind stress terms in the eastern Atlantic are smaller than in the western Atlantic. The amplitude of the pressure gradient variation in the Gulf of Guinea is larger than the local wind stress amplitude. The seasonal cycles of the two are not in phase. It appears the modelled response in the western equatorial Atlantic is predominantly local, but not in the Gulf of Guinea.

The case studies incorporating partial forcing show that the annual equatorial variability in the idealized western Atlantic is dominated by the local wind (Fig. 10a). Annual fluctuations of the zonal wind stress east of 25°W (Fig. 10b) have a measurable effect on the pycnocline depth in the west, but the amplitude is much smaller than the locally forced response. The remote effects from the semiannual wind changes in the east are more important than the local 6-month period wind oscillations in the west (Figs. 10c,d). However, the total amplitude of the semiannual pycnocline displacements is much smaller than the annual cycle.

The annual pycnocline motion in the eastern equatorial Atlantic is comprised of equal contributions from zonal wind stress changes east and west of 25°W (Figs. 10a,b). The amplitude of the semiannual pycnocline displacement is half of the annual signal. This relatively large semiannual variation may be responsible for the intriguing secondary upwelling season that is observed. The entire semiannual response induced by the zonal wind stress (Fig. 8) is a result of the forcing east of 25°W (Fig. 10d); there is no contribution from the semiannual wind field of the western Atlantic.

d. Eastern tropical response

Several mechanisms have been proposed in theoretical and observational studies to explain the coastal and equatorial variability in the eastern tropical Atlantic. A detailed review is provided by Picaut (1983). Philander and Pacanowski (1981a) modelled the relation between southerly winds, Rossby waves, advection, and coastal upwelling south of the equator. Berrit (1976) correlated SST with the local wind field along the southern coast of the Guinea Gulf. South of 15°S there was good agreement between strong southerly winds and low SST, but there was no correlation at all further north. Comparisons of offshore Ekman transports and coastal SST, provided by W. Wooster, yield the same conclusion (Picaut, 1983).

Along the northern coast of the Gulf of Guinea, Houghton (1976) determined there was no significant correlation between the coastal wind and observed upwelling. Clarke (1978) tried to explain the seasonal coastal upwelling off Ghana and the Ivory Coast using coastally trapped wave dynamics since the maximum alongshore wind stress (Fig. 2a) occurs to the east. Philander (1979) proposed that the seasonal variations of the cross-equatorial wind contribute to the intensification of the Guinea Current. An associated

shoaling of the pycnocline, needed to satisfy the geostrophic balance, would result in low SST.

Since there was a lack of evidence throughout the Gulf of Guinea in support of locally forced coastal upwelling, a remote forcing mechanism was offered by Moore *et al.* (1978). As illustrated by O'Brien *et al.* (1978) and Adamec and O'Brien (1978), a rapid increase of the zonal wind observed in the western Atlantic would excite an equatorially trapped Kelvin wave. The eastward-propagating wave front would reflect at the eastern boundary and induce a coastally trapped, poleward-propagating upwelling response symmetric about the equator. For nonseasonal events, Servain *et al.* (1982) found a good correlation between the zonal wind stress in the west and SST in the Gulf of Guinea. The correlation between local wind stress and SST was small. Picaut (1983) noted a southward propagation of the primary low SST episodes along the coast south of 1°S, westward propagation along the coasts of Benin-Togo-Ghana-Ivory Coast (3°E to 8°W), and a one-month delay between the upwelling events at the equator and the Benin coast (5°N). An upward propagation of phase was detected for the summer upwelling event south of Abidjan and has recently been studied using a three-dimensional, remote-forcing model (McCreary *et al.*, 1983). The secondary upwelling event observed later in the year has never been explained satisfactorily. This event has also been observed to propagate west along the northern coast (Roy, 1981).

The seasonal displacement of the model pycnocline along the eastern boundary is presented in Fig. 16. Annual and semiannual coastal upwelling/downwelling events are symmetric about the equator. Poleward propagation of the seasonal signal is evident in both hemispheres. The amplitude of the coastal response decreases offshore while the phase increases. The variability along the northern and southern coasts is a symmetric response to equatorial Kelvin waves impinging on the boundary. Upon reflection, the zonal velocity associated with the incoming Kelvin waves must be eliminated to satisfy the no-flux condition at the coast. Thus, a finite number of Rossby waves and an infinite series of Hermite modes which asymptote to coastal Kelvin waves are generated to satisfy the boundary condition (Moore, 1968).

The most extensive monitoring of the thermal structure in the Gulf of Guinea has been performed by the Oceanographic Research Centers (ORSTOM) off of Abidjan, Ivory Coast and Pointe Noire, Congo. The seasonal movements of the model pycnocline are compared with the mean seasonal cycles of dynamic height (surface/300 db) at Abidjan and Pointe Noire in Fig. 17. Four marine seasons are simulated by the

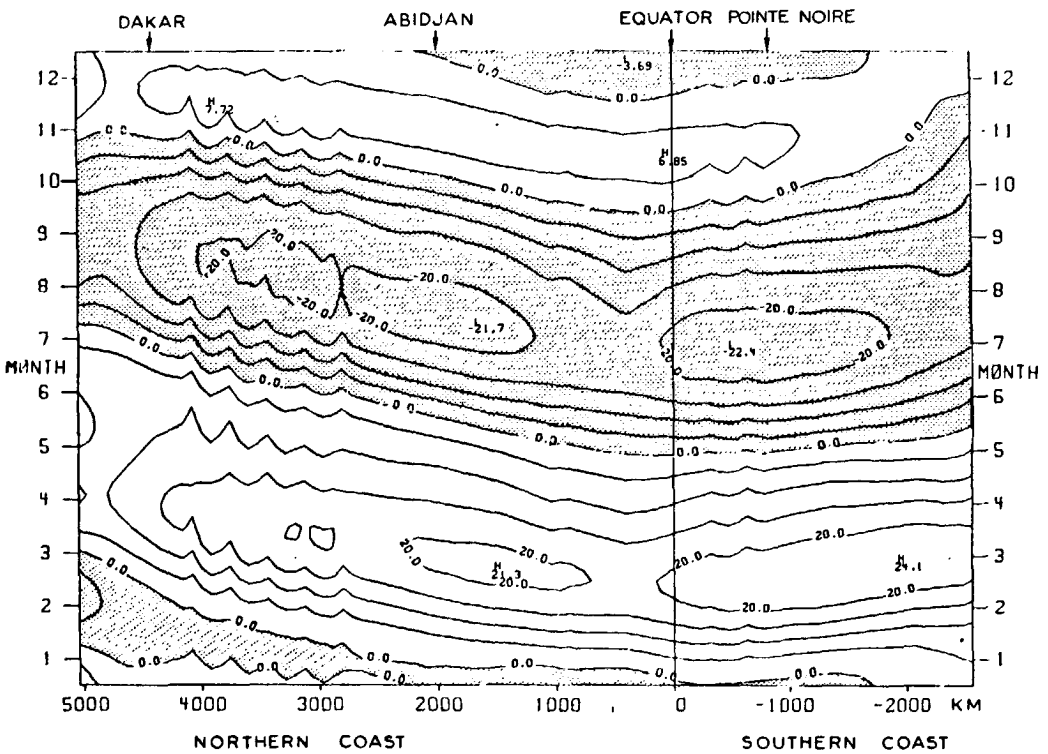

FIG. 16. Seasonal pycnocline displacements (m) north and south along the eastern boundary. Shaded regions indicate the pycnocline is shallower than the annual mean. The zonal coast in the Guinea Gulf extends from +500 km to +2800 km.

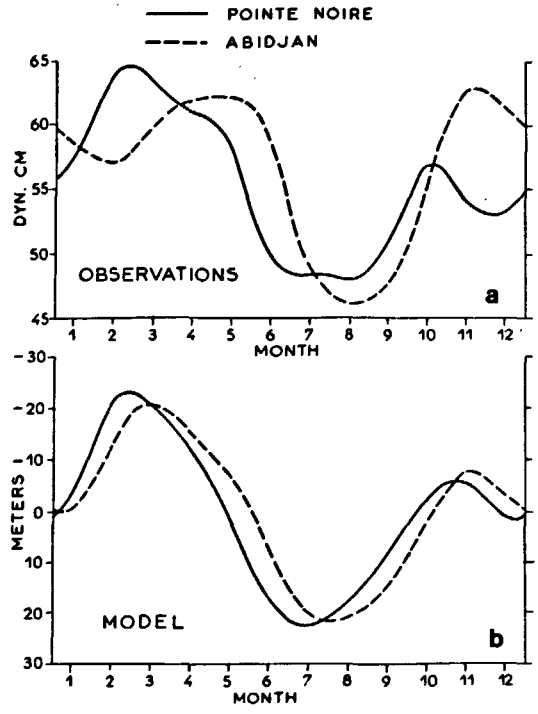

FIG. 17. Comparison of (a) dynamic height for 0/300 db and (b) model pycnocline depth at Abidjan (dashed) and Pte. Noire (solid). Negative values indicate the pycnocline is deeper than the annual mean. (Dynamic height analysis at Pte. Noire courtesy of J. Servain.)

model with similar phase. The seasonal cycle of SST in these areas consists of a secondary cold season in December–January, a primary warm season from February to May, a major cold season from June to mid-October, and a secondary warm season around November (Berrit, 1961, 1962). Annual and semiannual contributions dominate the model pycnocline, observed thermocline depth, SST, and dynamic height records. Temperature measurements at a depth of 15 m indicate the seasonal variability at Pointe Noire leads the comparable signal at Abidjan by one and a half months (Morlière, 1970). A similar lag is evident in the dynamic height signal (Fig. 17). The model pycnocline deviations at Pointe Noire have the same amplitude as at Abidjan but lead by 2–3 weeks.

The main region of low summer SST (22–24°C) extends along the northern coast of the Guinea Gulf west to 8°W, ~2500 km from the equator in Fig. 16 (Morlière and Rébert, 1972). The outbreak of low SST follows a dramatic upwelling of the thermal structure from April to August. In the model there is a notable diminution of this main upwelling signal 1000 km north of the observed limit (Fig. 16). Northward along the coasts of Senegal and Mauritania the surface waters are warm from July to October (Rossignol, 1972; Wooster *et al.*, 1976); at this time atmospheric heating is maximum and the deviation from the mean coastal winds is downwelling favorable. Off Dakar a subsurface upwelling is present in late summer–early fall (Rossignol, 1972; Servain, personal communication, 1982). This upwelling signal is strong enough to result in a sea level minimum at Dakar in September (Portolano, 1981); one month later than the sea level minimum at Abidjan. This apparent sinking of the upwelling event has been studied by McCreary *et al.* (1983) with a three-dimensional model that allows the downward propagation of energy to occur. In the present model we sacrifice vertical resolution in order to treat the wind field and horizontal structure more realistically than in McCreary *et al.* Thus, for this solution the main upwelling event along the coast of the Guinea Gulf, though weaker, is still present along the Senegal–Mauritania coasts.

Observations and the model results indicate an upwelling event along the coasts of Senegal and Mauritania early in the year. A large part of this event in the model is locally forced. The largest response to alongshore winds occurs in this region of the model basin. The local meridional wind stress is predominantly annual. The prevailing northerly wind is maximum in February and March. As suggested by Wooster *et al.* (1976) and Speth and Detlefsen (1983), the February upwelling along Senegal and Mauritania is mainly driven by the local winds.

A large proportion of the current measurements in the Gulf of Guinea have been taken on the continental shelf of the Ivory Coast within the Guinea Current. Observations by Lemasson and Rébert (1973) indicate the current is strongest in early summer, and weakest in fall and again in late winter. The zonal coastal current from the model has been averaged between 4°E and 11°W (Fig. 18). The seasonal variations for this single-mode solution compare favorably with the observations: the maximum east-

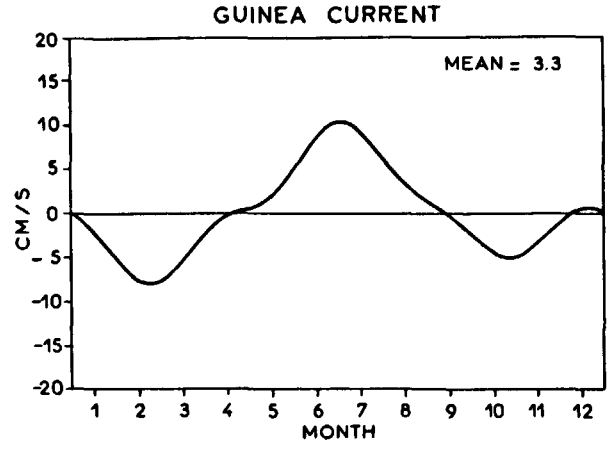

FIG. 18. Zonal velocity corresponding to a simulated Guinea Current averaged along the coast between 4°E and 11°W.

ward current is in June–July and is near zero or reverses in February–March and October–November. The majority of this Guinea Current signal is associated with the basin-wide response to the zonal wind field. The meridional wind stress induces seasonal Guinea Current fluctuations one-fourth the size of the total response. As indicated by McCreary *et al.* (1983) a more complete description of this current would involve the contributions from several vertical modes.

Away from the coastal regions much less is known about the seasonal variability in the eastern Atlantic. The model results indicate that the pycnocline displacements near the Guinea Dome are small compared with the pycnocline excursions in the western and southeastern parts of the basin (Fig. 5). The pycnocline is deepest from March through May and shallow from August through October. The terms in (2) indicate the pycnocline movement north of the pivot line is governed by Ekman pumping. A cyclonic perturbation to the wind stress curl causes upwelling from May to September. The upwelling favorable wind stress curl is due to an increase in the meridional gradient of the zonal wind stress as the ITCZ migrates northward. Rossby wave effects are not important north of the pivot line. The Guinea Dome in this model is therefore more stationary than the Costa Rica Dome in a numerical calculation for the eastern Pacific discussed by Hofmann *et al.* (1981).

Near the eastern terminus of the pivot line (24°W, 13°N) the pycnocline deviations are small (Fig. 5). The pycnocline is slightly deeper during the first six months of the year. There is little seasonal change in this area because the Ekman pumping and Rossby wave contributions are out of phase and have similar amplitudes. The pycnocline displacements are much larger to the south in a region of westward increasing phase. At 20°W, 7°N the pycnocline is deepest in June and shallow in October–November. The seasonal signal is determined by Rossby waves which radiate away from the boundary throughout the year. Ekman pumping is second order. Observations in this area during GATE suggest that the local summer upwelling is not related to Ekman pumping (Perkins, 1981). The Rossby waves are upwelling favorable from June to November. The zonal phase gradient represents the phase speed of the nondispersive, westward-propagating Rossby waves at this latitude. As evidenced by the phase distribution, the pivot line in the northeastern model basin separates regions influenced by the wind stress curl from regions influenced by Rossby waves.

In the Southern Hemisphere the pycnocline movement at the center of the Angola Dome is smaller than and out of phase with the pycnocline motion within the Guinea Dome. Small contributions from the wind stress curl and Rossby waves produce the pycnocline deviations. The wind stress curl variability is several times smaller than in the Northern Hemisphere. Northeast of the Angola Dome the influence of Ekman pumping is still small, but the seasonal response is much larger. The phase lines (Fig. 5b) and the vorticity equation imply that Rossby waves determine the seasonal cycle there.

In the previous subsection it was demonstrated that the annual equatorial variability within the idealized Gulf of Guinea was formed by equal contributions from the zonal wind stress on either side of 25°W. The entire semiannual pycnocline response was caused by wind forcing east of 25°W. The choice of 25°W as a dividing line had no *a priori* geographical significance because it is difficult to choose a mid-line for such a non-rectangular basin. It did, however, prove *a posteriori* to be a good choice for isolating the wind stress effects of different regions. Yet, the case studies did little to answer the question of whether the annual and semiannual variability in the Gulf of Guinea are locally or remotely forced.

A convenient definition of the Gulf of Guinea for the model geometry chosen is the region between the eastern boundary and approximately 10°W. Additional case studies were performed in which the model ocean was driven by the zonal wind stress west of the Gulf of Guinea and another with the zonal forcing limited within the Guinea Gulf (Fig. 19). Comparison with Figs. 5a and 8a indicates that almost all of the annual variability in the Gulf of Guinea is remotely forced. This remotely forced periodic response is formed by the superposition of equatorial Kelvin waves and their reflections as Rossby waves. The influences of annual zonal and meridional winds within the interior of the Gulf of Guinea are much smaller than the influence of the zonal wind stress west of 10°W. There is, however, a notable annual pycnocline response along the zonal coast driven by the zonal component of the southwesterly wind within the gulf (Figs. 8a, 19b), but this coastal signal is cancelled in the total forcing solution (Fig. 5a) by the effects of the meridional wind stress fluctuations at the eastern boundary (0–4°N).

The response to semiannual forcing is somewhat different (Figs. 7b, 8b, 19c, d). Only half of the semiannual pycnocline signal is remotely forced by the zonal wind stress. The remaining half of the response is formed by equal contributions from zonal and meridional wind stress fluctuations within the Gulf of Guinea.

5. Summary and conclusions

The objective of this work was to study the linear, dynamic, oceanic response to the seasonally varying wind field of the tropical Atlantic. A linear, single baroclinic mode model driven by the climatological seasonal wind stress was incorporated. Based on previous studies implying the dominance of the second

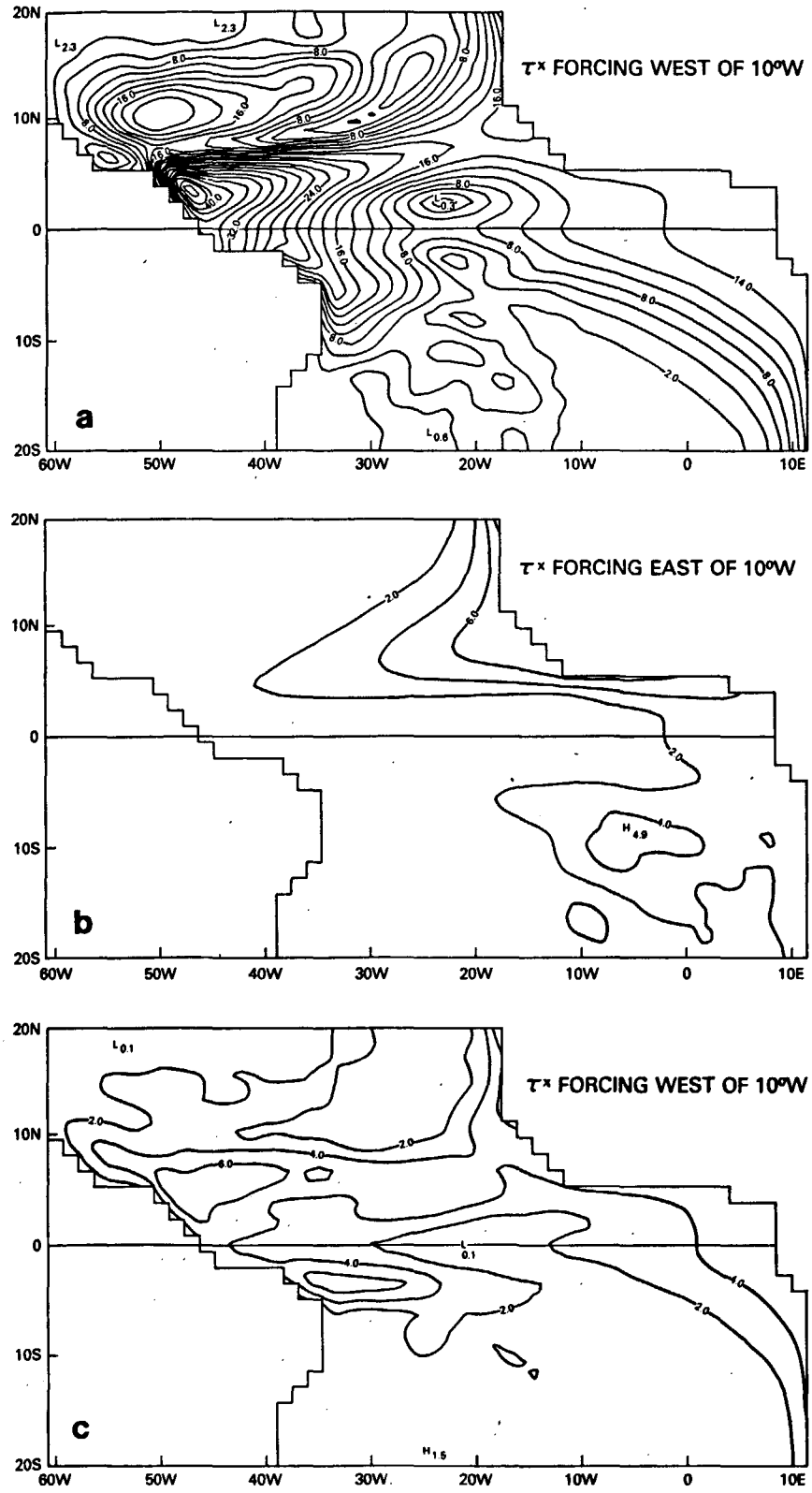

FIG. 19. Amplitude distributions for the pycnocline response to (a) annual τ^x forcing west of 10°W, (b) annual τ^x forcing east of 10°W, (c) semiannual τ^x forcing west of 10°W, and (d) semiannual τ^x forcing east of 10°W.

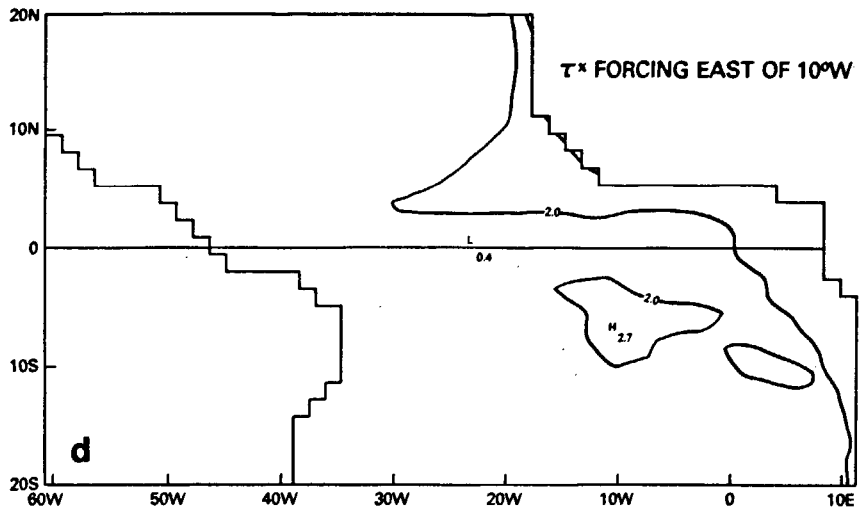

FIG. 19 (*Continued*)

baroclinic mode in the tropical Atlantic, an equivalent depth of 19 cm (c = 1.37 m s^{-1}) was chosen for the gravest mode of this calculation. The coastline geometry of the model was an idealization of the tropical Atlantic basin from 20°N to 20°S. Monthly estimates of the Atlantic surface wind field on a 1° × 1° mesh averaged over 60 years (Hastenrath and Lamb, 1977) provided the basis for the seasonal periodic forcing function. Important regions of variability were identified for the atmosphere and ocean. Of interest were the physical mechanisms responsible for the seasonal signal of key features such as the meridional topography in the western Atlantic, the equatorial pressure gradient, and the response within the Gulf of Guinea. Observations of the seasonal cycle throughout the tropical Atlantic were compared with the results of the simple model to ascertain whether the simulated response had any relevance.

The modelled seasonal response to the Atlantic wind field, depending on the location, consists of a combination of a locally forced response, Kelvin waves, Rossby waves, and multiple wave reflections. Throughout the tropical Atlantic basin the seasonal cycles of the atmospheric forcing, the observed dynamic height, and the model pycnocline depth are largely annual and semiannual. In general, there is a reasonable comparison between the phase and amplitude distributions of the observed dynamic height and the model pycnocline depth. The northwest part of the model basin is characterized by a north–south tilting of the pycnocline about a pivot line which roughly parallels the mean position of the ITCZ. North of the pivot line (~10°N) wind stress curl and divergence of the Ekman transport govern the annual response. The model pycnocline response south of the pivot line is a combination of local and remote effects, i.e., wind stress curl and westward propagating Rossby waves. At the equator, there is a non-rigid east–west tilting of the model pycnocline in which the minimum pycnocline depth in the east (July) leads the maximum depth in the west (September–October). Large model pycnocline displacements in the western equatorial region are a locally forced near-equilibrium response between the annual zonal wind stress and the zonal pressure gradient. The equatorial zonal pressure gradient in the eastern part of the basin is not balanced by the local wind stress. Case studies in which the model was forced by various partitions of the wind field indicate the annual wind-driven variability in the Gulf of Guinea may be remotely forced. Fluctuations of the zonal wind stress west of 10°W are responsible for a majority of the simulated annual pycnocline displacements in the Gulf of Guinea. The annual zonal wind east of 10°W has a secondary influence along the zonally oriented coast, but is cancelled by meridional wind stress variations at the eastern boundary. Thus, the major summer upwelling is implied to be a response to changes in the equatorial easterlies remote from the Gulf of Guinea. Half of the semiannual pycnocline signal in the Gulf of Guinea is forced by 6-month period zonal wind stress oscillations west of 10°W. The remaining portion of the model pycnocline signal comes from the zonal and meridional winds within the gulf. This suggests the secondary winter upwelling season is an expression of the wind variability remote from and within the Gulf of Guinea.

Even though there was some agreement between observations and the results of the model, there were several limitations to this work. The model was constrained to be linear and consisted of a single baroclinic mode. The vertical resolution was therefore

poor and wind-induced changes to features such as the undercurrent could not be studied. In addition, the effects of downward energy propagation could not be determined. It is not known whether nonlinearities or the vertical propagation of Kelvin waves and Rossby waves will significantly alter the superposition constituting this forced periodic response. McCreary (1981) and McCreary *et al.* (1983) demonstrated the importance of contributions to the equatorial and coastal velocity fields by high-order vertical modes. According to the results from McCreary *et al.* the subsurface signal in the interior of the Gulf of Guinea is mainly due to the first horizontal mode of reflected Rossby beams. As the downward-directed beams are no deeper than 300 m in the gulf, the single-mode results presented here should still be relevant to the 0/300 db dynamic height field of the Gulf of Guinea. Philander and Pacanowski (1981b) suggest that the solution from a nonlinear stratified model will differ from a single-mode solution if Rossby waves are severely impeded by the current field. Recently, the nonlinear, hydrodynamic and thermodynamic model of Schopf and Harrison (1983) was adapted to the tropical Atlantic basin and driven by the Hellerman (1980) wind data. The total sea level response formed by the gravest baroclinic mode and a shear mode based on stratification has some similarity to the single-mode solution presented here (P. Schopf, personal communication, 1983). A logical extension of the present study would use the climatological wind data in calculations involving several vertical modes with and without nonlinear effects. Subsequent comparisons with the results of this single-mode linear model would provide a better understanding of the role of additional physics.

The lack of any thermodynamics precluded any firm understanding of the SST variability in regions where pycnocline depth and SST are uncorrelated. A prime example is the Senegal and Mauritania coasts where there are important differences between the surface and subsurface thermal structure. The application of thermodynamic models to the seasonal Atlantic problem should provide some insight into the questions involving SST.

Another limitation of this study was the use of climatological wind data to represent the seasonal cycle. Averaging the wind field over many decades results in smaller temporal variations than may occur in a particular year. This approach was chosen rather than having to make a subjective judgement of which year had "typical" seasonal variations. This was not a severe limitation to this work since most descriptions of the seasonal cycle in the tropical Atlantic Ocean are based on time-averaged observations. The results from the numerical calculation were dependent on this wind field having the same periodicity from one year to the next. A periodic solution was thereby allowed to develop.

In contrast to this periodic solution, the response of an equatorial ocean to impulsive forcing is a single eastward-traveling Kelvin wave front which reflects at an eastern boundary as a train of westward-propagating Rossby waves. This was the premise used by Moore *et al.* (1978), O'Brien *et al.* (1978) and Adamec and O'Brien (1978) as a possible explanation of the seasonal upwelling in the Gulf of Guinea. For example, a rapid seasonal increase of the easterlies in the western equatorial Atlantic would excite an upwelling Kelvin wave front. The impulsive remote forcing hypothesis assumes that the upwelling at the eastern boundary lags the wind change in the west by the time required for a Kelvin wave to travel from the forcing region to the eastern boundary. Climatology indicates the initial strengthening of the easterlies takes place in the mid-Atlantic and then progresses westward (Fig. 6). The most dramatic wind changes are in the western Atlantic where the easterlies continue to increase after the peak upwelling in the Gulf of Guinea. This suggests the timing may not be correct for the impulsively excited Kelvin wave concept. However, a rapid increase of the easterly wind in spring 1979 at St. Peter and St. Paul rocks (0°55'N, 29°21'W) (Garzoli *et al.*, 1982), which is not unusual (Servain *et al.*, 1982), indicates that the impulsive forcing idea might still be relevant for specific years. Servain *et al.* also found a good correlation between nonseasonal perturbations of the zonal wind stress in the western Atlantic and nonseasonal SST in the Gulf of Guinea. The SST lagged the remote winds by one month; the time it would take a 1 m s^{-1} phase speed Kelvin wave to travel from the forcing area to the Gulf of Guinea. Interannual short time scale events observed in the Gulf of Guinea thermal structure have also been compared with the El Niño phenomena of the eastern Pacific (Hisard, 1980; Merle, 1980b). It has been suggested that these episodes may have important implications for fisheries, coastal rainfall and cyclogenesis. An interannual calculation similar to the Pacific Ocean study by Busalacchi and O'Brien (1981) could help determine the difference between the forced periodic response to the climatological seasonal cycle and the response to the seasonal signal of several consecutive years of Atlantic wind data.

This study has demonstrated that a significant part of the seasonal dynamic height signal can be analyzed in the context of linear, periodic, wind-driven processes. As previous modelling studies of the seasonal and interannual variability of the tropical Pacific have shown, the oceanic response can be studied with some degree of skill if a realistic estimate of the wind field variability is provided. The wind-driven response in this study was a combination of local and remote forcing effects which were strongly dependent on location. Only the northernmost and western equatorial parts of the basin were totally dominated by local

forcing. Therefore, continuous monitoring of the entire tropical Atlantic surface wind field at small time and space scales in conjunction with intensive measurements of the ocean variability such as the SEQUAL (Seasonal Equatorial Atlantic) and FOCAL (Francais-Ocean-Climat-Atlantique-Equatorial) experiments, are vital to our understanding of this seasonal oceanic response.

Acknowledgments. This work was supported by the National Science Foundation under Grant OCE8119052, the Centre National d'Exploitation des Oceans under Contract 82-2651 and the Centre National de la Recherche Scientifique. Partial support was provided to both authors by a NOAA cooperative agreement NA80RAH00002 during a visit to the Joint Institute for Marine and Atmospheric Research (JIMAR) at the University of Hawaii in the summer of 1981. Computations were performed at the Florida State University Computing Center and the Hawaii Institute of Geophysics. We wish to express our gratitude to Stefan Hastenrath for graciously providing the wind stress data and to Jacques Merle and Sabine Arnault for kindly providing the dynamic height data. We also would like to thank Dennis Moore for providing the opportunity to visit JIMAR. Special thanks to James J. O'Brien and Julian P. McCreary for many stimulating discussions. The support provided to one of us (AJB) by J. J. O'Brien is gratefully acknowledged. The many hours of assistance rendered by Roger Lukas and Sharon Yokogawa is deeply appreciated. Manuscript preparation was kindly provided by Pat Teaf. Valuable comments on the manuscript were made by J. McCreary, Benoît Cushman-Roisin, and two reviewers.

REFERENCES

Adamec, D., and J. J. O'Brien, 1978: The seasonal upwelling in the Gulf of Guinea due to remote forcing. *J. Phys. Oceanogr.*, **8**, 1050–1060.

Anderson, D., 1979: Low latitude seasonal adjustment in the Atlantic (unpublished manuscript). [Available from the author.]

Bakun, A., 1978: Guinea current upwelling. *Nature*, **271**, 147–150.

Berrit, G. R., 1961: Contribution à la connaissance des variations saisonnières dans le Golfe de Guinée. Observations le long des lignes de navigation. *Cah. ORSTOM, Sér. Océanogr.*, **13**, 715–727.

——, 1962: Contribution à la connaissance des variations saisonnières dans le Golfe de Guinée. Observations le long des lignes de navigation. *Cah. ORSTOM, Sér. Océanogr.*, **14**, 663–673.

——, 1976: Les eaux froides côtières du Gabon a l'Angola sont-elles dues à un upwelling d'Ekman? *Cah. ORSTOM, Sér. Oceanogr.*, **14**, 273–278.

Bloomfield, P., 1976: *Fourier Analysis of Time Series: An Introduction.* Wiley, 258 pp.

Bogorov, V. G., and collaborators, 1973: Tropical cyclonic macrocirculation systems and their role in the formation of the ocean structure. Formation of Biological Productivity and Bottom Sediments as Related to Ocean Circulation in the South-Eastern Atlantic, *Trans. P. P. Shirsov Inst. Oceanol.*, **95**, 1–13.

Boisvert, W. E., 1967: Major currents in the North and South Atlantic Oceans between 64°N and 60°S. Naval Oceanogr. Office, Tech. Rep. No. 193, 92 pp.

Bunker, A. F., 1976: Computations of surface energy flux and annual air-sea interaction cycles of the North Atlantic Ocean. *Mon. Wea. Rev.*, **104**, 1122–1140.

Busalacchi, A. J., and J. J. O'Brien, 1980: The seasonal variability in a model of the tropical Pacific. *J. Phys. Oceanogr.*, **10**, 1929–1951.

——, and ——, 1981: Interannual variability of the equatorial Pacific in the 1960's. *J. Geophys. Res.*, **86**, 10901–10907.

Camerlengo, A. L., and J. J. O'Brien, 1980: Open boundary conditions in rotating fluids. *J. Comput. Phys.*, **35**, 12–35.

Cane, M. A., and E. S. Sarachik, 1981: The response of a linear equatorial ocean to periodic forcing. *J. Mar. Res.*, **39**, 651–693.

Clarke, A. J., 1978: On the generation of the seasonal coastal upwelling in the Gulf of Guinea. *J. Geophys. Res.*, **84**, 3743–3751.

Draper, N. R., and H. Smith, 1981: *Applied Regression Analysis.* Wiley, 709 pp.

Emery, W. J., 1975: Dynamic height from temperature profiles. *J. Phys. Oceanogr.*, **5**, 369–375.

Garzoli, S., E. J. Katz, H. J. Panitz and P. Speth, 1982: *In situ* wind measurements in the equatorial Atlantic during 1979. *Oceanol. Acta*, **5**, 281–288.

Hastenrath, S., 1976: Variations in low-latitude circulation and extreme climatic events in the tropical Americas. *J. Atmos. Sci.*, **33**, 202–215.

——, and P. J. Lamb, 1977: *Climatic Atlas of the Tropical Atlantic and Eastern Pacific Oceans.* University of Wisconsin Press, Madison, 97 charts.

Hellerman, S., 1980: Charts of the variability of the wind stress over the tropical Atlantic. GATE Sup. II. *Deep-Sea Res.*, **26**, 63–75.

Hickey, B., 1975: The relationship between fluctuations in sea level, wind stress and sea surface temperature in the equatorial Pacific. *J. Phys. Oceanogr.*, **5**, 460–475.

Hisard, P., 1980: Observation de réponses de type ⟨⟨El Niño⟩⟩ dans l'Atlantique tropical oriental Golfe de Guinée. *Oceanol. Acta*, **3**, 69–78.

——, and B. Piton, 1981: Interannual variability in the eastern tropical Atlantic during the last decades. *Recent Progress in Equatorial Oceanography*, Nova University Press, 297–306.

Hofmann, E. E., A. J. Busalacchi and J. J. O'Brien, 1981: Wind generation of the Costa Rica Dome. *Science*, **214**, 552–554.

Houghton, R. W., 1976: Circulation and hydrographic structure over the Ghana continental shelf during the 1976 upwelling. *J. Phys. Oceanogr.*, **6**, 909–924.

Katz, J., 1981: Dynamic topography of the sea surface in the equatorial Atlantic. *J. Mar. Res.*, **39**, 53–63.

——, R. Belevitsch, J. Bruce, V. Bubnov, J. Cochrane, W. Duing, P. Hisard, H. U. Lass, J. Miencke, A. deMesquita, L. Miller and A. Rybnikov, 1977: Zonal pressure gradient along the equatorial Atlantic. *J. Mar. Res.*, **35**, 293–307.

Kindle, J. C., 1979: Equatorial Pacific Ocean variability—seasonal and El Niño time scales. Ph.D. dissertation, Florida State University, 134 pp.

Lamb, P. J., 1978: Case studies of tropical Atlantic surface circulation pattern during recent sub-Sahara weather anomalies, 1967–1968. *Mon. Wea. Rev.*, **106**, 282–291.

Lass, H. U., V. Bubnov, J. M. Huthance, E. J. Katz, J. Meincke, A. deMesquita, F. Ostapoff and B. Voituriez, 1982: Seasonal changes of the zonal pressure gradient in the equatorial Atlantic west of 10°W during the FGGE year. *Oceanol. Acta*, **6**, 3–11.

Lemasson, L., and J.-P. Rébert, 1973: Les courants marins dans le Golfe Ivoirien. *Cah. ORSTOM, Sér. Océanogr.*, **11**, 67–95.

Markham, C. G., and D. R. McLain, 1977: Sea surface temperature related to rain in Ceara, northeastern Brazil. *Nature*, **265**, 320–323.

Mazeika, P. A., 1967: Thermal domes in the eastern tropical Atlantic Ocean. *Limnol. Oceanogr.*, **12**, 537–539.

McCreary, J. P., 1981: A linear stratified ocean model of the Equatorial Undercurrent. *Phil. Trans. Roy. Soc. London*, **A298**, 603–635.

——, J. Picaut and D. W. Moore, 1983: Effect of annual remote forcing in the eastern tropical Atlantic. *J. Mar. Res.* (in press).

Merle, J., 1977: Seasonal variations of temperature and circulation in the upper layers of the equatorial Atlantic Ocean. Paper presented at the GATE workshop, Miami, 28 February–10 March 1977 (unpublished manuscript).

——, 1978: Atlas hydrologique saisonnier de l'ocean Atlantique intertropical. Travaux et documents de ORSTROM, No. 82.

——, 1980a: Seasonal heat budget in the equatorial Atlantic Ocean. *J. Phys. Oceanogr.*, **10**, 464–469.

——, 1980b: Variabilité thermique annuelle et interannuelle de l'océan Atlantique équatorial Est. L'hypothèse d'un ⟨⟨El Niño⟩⟩ Atlantique. *Oceanol. Acta*, **3**, 209–220.

——, 1983: Seasonal variability of subsurface thermal structure in the tropical Atlantic Ocean. *Proc. 14th Int. Liege Colloquium Ocean Hydrodynamics*, Elsevier, 31–49.

——, and J. F. LeFloch, 1978: Cycle annual moyen de la temperature dans les couches superieures de l'océan Atlantique intertropical. *Oceanol. Acta*, **1**, 271–276.

——, and S. Arnault, 1983: Seasonal variability of dynamic topography in the tropical Atlantic Ocean. (manuscript in preparation).

——, M. Fieux and P. Hisard, 1980: Annual signal and interannual anomalies of sea surface temperature in the eastern equatorial Atlantic. *Deep-Sea Res.* (GATE Supp. II), **26**, 77–101.

Meyers, G., 1979: Annual variation in the slope of the 14°C isotherm along the equator in the Pacific Ocean. *J. Phys. Oceanogr.*, **9**, 885–891.

Moore, D. W., 1968: Planetary-gravity waves in an equatorial ocean. Ph.D. thesis, Harvard University, 201 pp.

——, and S. G. H. Philander, 1977: Modeling of the tropical oceanic circulation. *The Sea*, Vol. 6, E. Goldberg *et al.*, Eds., Wiley-Interscience, 319–361.

——, P. Hisard, J. P. McCreary, J. Merle, J. J. O'Brien, J. Picaut, J. M. Verstraete and C. Wunsch, 1978: Equatorial adjustment in the eastern Atlantic. *Geophys. Res. Lett.*, **5**, 637–640.

Morlière, A., 1970: Les saisons marines devant Abidjan. *Doc. Sci. Centre Rech. Océanogr. Abidjan*, **1**, 1–15.

——, and J. P. Rébert, 1972: Etude hydrologique du plateau continental ivoirien. *Doc. Sci. Centre Rech. Oceanogr. Abidjan*, **3**, 1–30.

Namias, J., 1969: On the causes of the small number of Atlantic hurricanes in 1968. *Mon. Wea. Rev.*, **97**, 346–348.

O'Brien, J. J., D. Adamec and D. W. Moore, 1978: A simple model of equatorial upwelling in the Gulf of Guinea. *Geophys. Res. Lett.*, **5**, 641–644.

Patton, R. J., 1981: A numerical model of equatorial waves with application to the seasonal upwelling in the Gulf of Guinea. M.S. thesis, Massachusetts Institute of Technology, 120 pp.

Perkins, H., 1981: Low-frequency forcing of the tropical Atlantic Ocean under the ITCZ during GATE. *Deep-Sea Res.* (GATE Suppl. I), **26**, 225–236.

Philander, S. G. H., 1979: Upwelling in the Gulf of Guinea. *J. Mar. Res.*, **37**, 23–33.

——, and R. C. Pacanowski, 1980: The generation and decay of equatorial currents. *J. Geophys. Res.*, **85**, 1123–1136.

——, and ——, 1981a: The oceanic response to cross-equatorial winds (with application to coastal upwelling in low latitudes). *Tellus*, **33**, 204–210.

——, and ——, 1981b: Response of equatorial oceans to periodic forcing. *J. Geophys. Res.*, **86**, 1903–1916.

Picaut, J., 1983: Propagation of the seasonal upwelling in the eastern equatorial Atlantic. *J. Phys. Oceanogr.*, **13**, 18–37.

——, J. M. Verstraete and A. Morlière, 1978: Ondes forcées par la marée et l'atmosphère le long des cotes du Golfe de Guinée. CNEXO Report, Université de Bretagne Occidentale, 78 pp.

Portolano, P., 1981: Contribution a l'étude de l'hydroclimat des cotes Sénégalaises. ORSTOM, Centre Océanogr. Dakar-Thiaroye, 69 pp.

Rossignol, M., 1972: Contribution à l'étude du "complexe guinéen". Doc. Sci. ORSTOM, Rép. Sénégal Serv. Océanogr. Pêches, 143 pp.

——, and M. Meyrueis, 1964: Campagne oceanographique de Gerard-Treca. ORSTOM, Centre Oceanogr., Dakar-Thiaroye, 53 pp.

Roy, C., 1981: Sur le phénomene de la petite saison froide dans le Golfe de Guinée. D.E.A. Report, Université de Bretagne, Occidentale, France, 38 pp.

Schopf, P. S., and D. E. Harrison, 1983: On equatorial Kelvin waves and El Niño. I: Influence of initial states on wave-induced currents and warming. *J. Phys. Oceanogr.*, **13**, 936–948.

Servain, J., J. Picaut and J. Merle, 1982: Evidence of remote forcing in the equatorial Atlantic Ocean. *J. Phys. Oceanogr.*, **12**, 457–463.

Speth, P., and H. Detlefsen, 1983: The relationship between sea surface temperatures and winds off Northwest Africa and Portugal *Oceanogr. Tropicale* (in press).

Stommel, H. S., 1947: Note on the use of the *T–S* correlation for dynamic height anomaly computations. *J. Mar. Res.*, **5**, 85–92.

Verstraete, J. M., J. Picaut and A. Morlière, 1980: Atmospheric and tidal observations along the shelf of the Guinea Gulf. *Deep-Sea Res.* (GATE Suppl. II), **26**, 343–356.

Voituriez, B., 1981a: The equatorial upwelling in the eastern Atlantic: Problem and paradoxes. *Coastal Upwelling*, F. A. Richard, Ed., Amer. Geophys. Union, Washington, DC, 95–106.

——, 1981b: The equatorial upwelling in the eastern Atlantic Ocean. *Recent Progress in Equatorial Oceanography*, Nova University Press, 229–247.

——, 1981c: Les sous-courants equatoriaux nord et sud et la formation des domes thermiques tropicaux. *Oceanol. Acta*, **4**, 497–506.

Wooster, W. S., A. Bakun and D. R. McClain, 1976: The seasonal upwelling cycle along the eastern boundary of the North Atlantic. *J. Mar. Res.*, **34**, 131–141.

Wyrtki, K., 1964: Upwelling in the Costa Rica Dome. *Fish. Bull.*, **63**, 355–372.

——, 1974a: Sea level and the seasonal fluctuations in the western Pacific Ocean. *J. Phys. Oceanogr.*, **4**, 91–103.

——, 1974b: Equatorial currents in the Pacific 1950 to 1970 and their relations to the trade winds. *J. Phys. Oceanogr.*, **4**, 372–380.

——, 1975: El Niño—the dynamic response of the equatorial Pacific Ocean to atmospheric forcing. *J. Phys. Oceanogr.*, **5**, 572–584.

Yoshida, K., 1955: Coastal upwelling off the California Coast. *Rec. Oceanogr. Works Japan*, **2**, 8–20.

Journal of Marine Research, 42, 45–81, 1984

Effects of remote annual forcing in the eastern tropical Atlantic Ocean

by Julian P. McCreary, Jr.,[1] Joël Picaut[2] and Dennis W. Moore[3]

ABSTRACT

An ocean model is used to study the effects of remote annual forcing in the eastern tropical Atlantic. The model is linear, viscid and continuously stratified. The ocean basin is an idealized version of that of the tropical Atlantic, and the wind stress forcing the model is an idealized representation of the annual variation of the equatorial trades in the western Atlantic. Solutions are represented as expansions of the baroclinic modes of the system. The response of each mode is found numerically, not by integrating the equations of motion forward in time, but at a fixed frequency (2π year^{-1}) using techniques that are typically used in models of the tides.

Prominent features of the solution are the following. When the remote trades strengthen, sea level drops and the pycnocline rises markedly throughout the Gulf of Guinea. At 4W the annual response is tightly trapped to the equator and to the coast of Africa near 5N. In contrast, the response propagates offshore along the southern coast of Africa near 10E. Events propagate upward everywhere in the Gulf of Guinea and poleward (nearly) everywhere along the coast of Africa. These features compare favorably with observations.

A single baroclinic mode does not dominate the response. Instead, waves associated with several modes superpose to form beams that propagate energy vertically as well as horizontally (McCreary, 1984). Along the equator the response is predominantly a combination of a beam of equatorial Kelvin waves and a lowest order ($\ell = 1$) Rossby beam. Along the coast of Africa at 5N it is primarily a beam of coastal Kelvin waves.

1. Introduction

The annual variability of the ocean circulation in the eastern equatorial Atlantic (Gulf of Guinea) is striking. Most notably, during the northern hemisphere, summer sea-surface temperature (SST) cools by about 5°C along and to the south of the equator, as well as along the western coast of Africa both north and south of the equator. At the same time the pycnocline rises markedly over a broad area throughout the region, and there are significant changes in the strength of the surface and subsurface currents.

Presumably this variability is driven by the seasonal cycle of the trade wind field

1. Nova University Oceanographic Center, 8000 N. Ocean Drive, Dania, Florida, 33004, U.S.A.
2. Laboratoire d'Océanographie Physique, Université de Bretagne Occidentale, 29200 Brest, France.
3. JIMAR (Joint Institute for Marine and Atmospheric Research), University of Hawaii, 1000 Pope Road, Honolulu, Hawaii, 96822, U.S.A.

over the tropical Atlantic. Bunker (1976), Hastenrath and Lamb (1977), Hellerman (1980) and Busalacchi and Picaut (1983) describe this cycle in detail. In the eastern Atlantic and south of the equator the mean winds are southeasterly with a magnitude of about .5 dyn/cm^2. At 5N they have a slight westerly component. The winds are weakest in March and strongest in August, typically varying only by about .2 dyn/cm^2 or less. The seasonal variability of alongshore winds along the coast of Africa is very weak everywhere except south of 10S. In the western Atlantic the mean winds at the equator have a strong easterly component with a magnitude of about .75 dyn/cm^2. The winds are weakest in April and strongest in September, and vary by about .5 dyn/cm^2 near 40W.

a. Theoretical background. A number of models have already studied the effect of the tropical wind field on the Atlantic Ocean. They involve essentially three different processes for the wind to force the ocean. The processes are equatorial Ekman divergence driven by meridional winds in the eastern Atlantic, coastal Ekman divergence forced by alongshore winds at the coast of Africa, and equatorially trapped Kelvin waves generated by equatorial zonal winds.

Cromwell (1953) first suggested how a southerly wind will effect the equatorial ocean. Sufficiently south of the equator there is a westward Ekman drift, but near the equator the flow bends to the north. As a result, there is a divergence of water somewhat south of the equator, and upwelling occurs there. Similarly, sufficiently north of the equator there is an eastward flow, a convergence of water, and downwelling. Philander (1979) studied this process in detail using a zonally-independent, stratified, nonlinear model. His solutions exhibit all the features described by Cromwell. In addition, nonlinear effects strengthen upwelling south of the equator and the eastward flow north of the equator. Analogous phenomena are also present in the similar, but three-dimensional, models of Cane (1979) and of Philander and Pacanowski (1981). Anderson (1979) also concludes that the zonal current generated just north of the equator in his linear model is driven by the local meridional winds. These results suggest that the summertime increase in the southerly wind field in the Gulf of Guinea can account for the appearance of cool water south of the equator and the strengthening of the eastward Guinea Current just north of the equator. This increase, however, cannot explain either the observed upwelling along the northern coast of the Gulf of Guinea (where the process causes downwelling), or the general uplifting of the pycnocline throughout the region.

Clarke (1978) suggested that coastal upwelling driven by alongshore winds is the primary cause of the seasonal upwelling event along the northern coast of the Gulf of Guinea. He noted that beginning in June of 1974 the alongshore winds there became more upwelling favorable (eastward). He forced a reduced-gravity model (that is, a system consisting of a single, low-order baroclinic mode) with the observed winds, and compared its sea level response with observations from Tema, Ghana. There was

qualitative agreement between the observed and predicted sea level curves in that both drop in the month of June, but the predicted drop was somewhat weaker than that observed. Reduced-gravity models involve the choice of a pycnocline depth, H, and H^{-1} measures how efficiently wind stress couples to the ocean. It is worth noting that Clarke's choice of H to be 20 m is considerably smaller than commonly used values. [For example, in the present model the smallest coupling coefficient for any baroclinic mode has a value of 100 m. See Eq. (10) and Table 1.] If Clarke had selected a more realistic value for H his response would have been far too weak to provide an adequate explanation for the observed sea level change. In a similar way the model of Philander and Pacanowski (1981) suggests that the summertime increase of alongshore winds south of the equator could be the primary cause of the upwelling there. Picaut (1983), however, points out that the annual variability of the alongshore wind north of 15S is small, and bears little resemblance to the variability of coastal SST. For these reasons, it is not likely that changes in alongshore winds, and in the resulting coastal Ekman divergence, can explain a significant fraction of the annual variability of upwelling anywhere in the Gulf of Guinea.

Moore *et al.* (1978) first suggested that upwelling in the Gulf of Guinea could be caused by zonal wind changes along the equator, particularly the large changes in the western Atlantic. They noted that this remote forcing will generate an equatorially trapped Kelvin wave that propagates into the eastern ocean, and reflects initially poleward along the coast of Africa as coastal Kelvin waves and subsequently westward as Rossby waves. In this way, remote equatorial winds affect the state of the ocean throughout the Gulf of Guinea. Adamec and O'Brien (1978) and O'Brien *et al.* (1978) illustrated the probable importance of this process with reduced-gravity models. In both studies a strengthening of the wind stress field in the western Atlantic by .25 dyn/cm^2 lowers sea level in the eastern ocean by nearly 9 cm, a value consistent with observations (Verstraete *et al.*, 1980).

The importance of this remote-forcing mechanism has been demonstrated even more clearly in two recent studies. Servain *et al.* (1982) correlated the nonseasonal variability of SST in the Gulf of Guinea with wind stress variability from various regions of the tropical Atlantic. They found that the highest correlations occurred with zonal winds from the western equatorial Atlantic, with SST lagging the wind by about one month. Correlations with the winds from the Gulf of Guinea were considerably smaller. Busalacchi and Picaut (1983) forced a reduced-gravity model with realistic winds from the tropical Atlantic. They found that the annual sea level response along the coast of Africa is most strongly influenced by zonal winds west of 10W. The alongshore component of the wind does affect coastal sea level, but not nearly as much as the remote zonal winds do.

b. The present approach. Picaut (1983) pointed out a remarkable feature of the upwelling signal at Abidjan (located near point C in Fig. 1): the event propagates

vertically, as well as horizontally. The peak of the upwelling event arrives first at 300 m, but does not appear at the surface until 1½ months later (see the discussion in Section 4). Reduced-gravity models are not capable of generating this vertical phase propagation, but continuously stratified models are. For example, McCreary (1984) forced a continuously stratified model with periodic zonal winds at the equator. The wind excites a beam of equatorially trapped Kelvin waves that slopes downward into the eastern ocean and reflects from the eastern boundary as a set of beams of Rossby waves. Phase propagates vertically across each of the beams.

This paper continues to study the effects of remote equatorial wind forcing on ocean circulation in the Gulf of Guinea. The ocean model is linear, continuously stratified, and includes both vertical and horizontal mixing. Solutions are represented as expansions in vertical normal modes. The ocean basin is an idealized version of that of the tropical Atlantic, with open boundary conditions imposed at the north and the south. The wind stress forcing the model is specified to be entirely remote from the Gulf of Guinea and is an idealized representation of the annual variation of the zonal component of the trades in the western Atlantic. Because the boundary conditions are complicated, it is necessary to find the solutions for each mode numerically. Solutions are *not* found by integrating the equations of motion forward in time as is usually done; instead, the frequency of the wind is fixed throughout to be 2π year^{-1}. Solutions compare favorably with many aspects of the observations; in particular, there is vertical phase propagation throughout the Gulf of Guinea. As in the McCreary (1984) study, it is possible to interpret the response as a superposition of beams. At the equator the response is predominantly a beam of equatorially trapped Kelvin waves and the lowest-order Rossby beam. Along the northern coast it is primarily a beam of coastal Kelvin waves.

2. The model ocean

a. Equations. In a state of no motion the model ocean has a stably stratified background density structure $\rho_b(z)$ and an associated Väisälä frequency $N_b(z)$. Equations of motion linearized about this background state are

$$\begin{aligned} &u_t - f_v + p_x = (\nu u_z)_z + \nu_h \nabla^2 u, \\ &v_t + f u + p_y = (\nu v_z)_z + \nu_h \nabla^2 v, \\ &u_x + v_y + w_z = 0, \\ &\rho_t + g^{-1} N_b^2 w = (\kappa \rho)_{zz}, \\ &p_z = -\rho g, \end{aligned} \tag{1}$$

where u, v and w are the zonal, meridional and vertical velocity fields, p and ρ are the pressure and density perturbations, g is the acceleration due to gravity, and f is the Coriolis parameter. Coefficients of vertical eddy viscosity and eddy diffusivity are

given by

$$\nu = \kappa = \frac{A}{N_b^2}. \tag{2}$$

The coefficient of horizontal eddy viscosity is ν_h. Constant factors of $\bar{\rho}$, the average density of the water column, are everywhere ignored. The x-axis is oriented eastward, the y-axis is oriented northward with $y = 0$ at the equator, and the z-axis is positive upward with $z = 0$ at the ocean surface. Finally, the equatorial β-plane is adopted, so that $f = \beta y$.

Surface boundary conditions are

$$\nu u_z = \tau^x, \qquad \nu v_z = \tau^y, \qquad w = \kappa\rho = 0, \tag{3}$$

where τ^x and τ^y are the zonal and meridional components of the wind stress at the ocean surface. The ocean bottom, at $z = -D$, is assumed to be flat. Boundary conditions there are

$$\nu u_z = \nu v_z = w = \kappa\rho = 0. \tag{4}$$

Eqs. (1)–(4) involve several unconventional or physically unrealistic assumptions. For example, in (1) the vertical mixing of heat and momentum have slightly different forms. According to (2), vertical mixing coefficients are inversely proportional to the square of the Väisälä frequency. The last condition in (3) prohibits the ocean from ever generating any sea-surface temperature variations. Finally, in (4) the no-stress condition means that the ocean bottom is slippery. These assumptions are all crucial to the method of solution adopted here. Only in this way is it possible to find solutions simply (and economically) as expansions of vertical normal modes. McCreary (1980, 1981) discusses these assumptions in greater detail.

The eigenfunctions

$$\left(\frac{\psi_{nz}}{N_b^2}\right)_z = -\frac{1}{c_n^2}\psi_n \tag{5}$$

subject to the boundary conditions

$$\psi_{nz}(-D) = 0, \qquad \frac{1}{c_n^2}\int_{-D}^{o}\psi_n dz = 0, \tag{6}$$

are the vertical normal modes of the model ocean. They are commonly normalized so that

$$\psi_n(0) = 1, \tag{7}$$

and it is convenient to order them so that the eigenvalues, c_n, decrease monotonically. The $n = 0$ eigenfunction is unique in that $c_o = \infty$; this eigenfunction is the barotropic

mode of the ocean. The remaining eigenfunctions form an infinite set of baroclinic modes.

Solutions to (1), subject to boundary conditions (3) and (4), are then given by

$$\begin{aligned} u &= \sum_{n=1}^{N} u_n \psi_n, \qquad v = \sum_{n=1}^{N} v_n \psi_n, \qquad p = \sum_{n=1}^{N} p_n \psi_n, \\ w &= \sum_{n=1}^{N} w_n \int_{-D}^{z} \psi_n \, dz, \qquad \rho = \sum_{n=1}^{N} \rho_n \psi_{nz}, \end{aligned} \tag{8}$$

where the expansion coefficients are functions only of x, y and t. The barotropic mode is not included in the sums of (8). At the annual frequency the barotropic mode is essentially in a state of Sverdrup balance with the wind field. For this reason, it is easy to verify that the barotropic response is dominated by the baroclinic response described in the next section. In addition, the sums over the infinite number of baroclinic modes are necessarily truncated at a finite value, N. As we shall see, for the choices of $\rho_b(z)$ and ν made here, solutions converge rapidly enough with n that N need not be large.

The equations governing the expansion coefficients are

$$\begin{aligned} &(\partial_t + A/c_n^2)u_n - fv_n + p_{nx} = F_n + \nu_h \nabla^2 u_n, \\ &(\partial_t + A/c_n^2)v_n + fu_n + p_{ny} = G_n + \nu_h \nabla^2 v_n, \\ &(\partial_t + A/c_n^2)\frac{p_n}{c_n^2} + u_{nx} + v_{ny} = 0, \end{aligned} \tag{9a}$$

and also

$$w_n = (\partial_t + A/c_n^2)\frac{p_n}{c_n^2}, \qquad \rho_n = -\frac{p_n}{g}. \tag{9b}$$

The forcing of each mode is given by

$$F_n = \tau^x \Big/ \int_{-D}^{o} \psi_n^2 \, dz, \qquad G_n = \tau^y \Big/ \int_{-D}^{o} \psi_n^2 \, dz, \tag{10}$$

and the integral in the denominator defines a coupling coefficient ($C = \int_{-D}^{o} \psi_n^2 \, dz$) that measures how effectively each mode is forced by the wind. Note that a small value of C means relatively strong excitation of the mode in question, whereas a large value means weak excitation. Eqs. (9a) can be solved for the three unknowns u_n, v_n and p_n, and then Eqs. (9b) give w_n and ρ_n in terms of p_n.

It is possible to include a constant thickness, surface mixed layer in the model simply by assuming that $N_b(z) = 0$ for $z \geq -H$. The eigenfunction problem, defined in (5)–(7), is still well posed, and so the eigenfunctions as well as the solutions (8) remain well behaved. An important effect of the mixed layer is that $\psi_{nz}(z) = 0$ within it. As a result, in the mixed layer u, v and p are independent of z, w varies linearly with z, and ρ is identically zero. Other properties and limitations of this mixed-layer formulation are discussed in greater detail in McCreary (1980, 1981).

Two other useful quantities are sea level, $d(x, y)$, and isopycnal displacement, $\zeta(x, y, z)$. It is possible to replace the rigid-lid restriction in (3) with a free-surface condition, and Eqs. (8)–(10) still hold to the level of the Boussinesq approximation. It follows that

$$d = \frac{p(x, y, o)}{g}, \tag{11}$$

where $p(x, y, o)$ is the surface pressure field. A convenient measure of isopycnal displacement is

$$\zeta = -\rho/\rho_{bz}. \tag{12}$$

This definition is valid only where the vertical mixing of heat is small, and so is most accurate in the deeper ocean.

b. Basin boundary conditions. Eqs. (9a) are solved in an ocean basin that is an idealization of the tropical Atlantic. The thick lines of Figure 1 show the eastern and western boundaries of the model basin. For most solutions the basin has artificial open boundaries adjacent to 10S and 10N; one solution is obtained in a wider basin that extends from 20S to 20N.

Horizontal mixing is necessary in the model to ensure that the numerical solution of Eqs. (9a) remains computationally stable (see the discussion at the end of Section 2c). As a result, two boundary conditions are required at each boundary. No-slip conditions are adopted at the western boundary, where

$$u = v = 0. \tag{13}$$

Slip conditions are imposed at the eastern boundary. For the sections of the boundary at 10E and at 16W,

$$v_x = 0, \qquad u = 0, \tag{14a}$$

and along the section at 5N,

$$v = 0, \qquad u_y = 0. \tag{14b}$$

The use of slip conditions at the eastern boundary is desirable because they reduce the importance of horizontal mixing in the dynamics of the coastal currents. Open boundary conditions at the northern and southern boundaries are

$$u_y = v_y = p_y = 0. \tag{15}$$

(The effects of the slip and open boundary conditions on the solution are discussed further in Section 4c.)

c. The numerical solution. This paper is concerned with finding the model response to a wind field that oscillates at the annual frequency. Because the basin boundaries are

not sufficiently simple, it is necessary to evaluate this response numerically. A common method of solution is to switch the wind stress on at some initial time, and then to integrate Eqs. (9a) forward in time until initial transients have passed through the system, necessarily for a period of several years. An alternate approach, and the one used here, avoids the generation of any transients. It assumes from the outset that the wind has the time dependence $e^{-i\sigma t}$. As a result, all fields also have this time dependence, the operator ∂_t in (9) is just the imaginary number $-i\sigma$, and Eqs. (9a) reduce to a set of elliptic equations in the spatial coordinates x and y. This approach has been successfully used in models of barotropic tides (Hendershott, 1978), and our numerical scheme is related to several of these earlier studies. Details of the method are discussed in the Appendix.

A numerical instability occurs in the model if ν_h is not sufficiently large. At the annual frequency solutions to (9a) involve narrow boundary currents adjacent to meridionally oriented, western ocean boundaries (the boundaries at 60W and 40W in Fig. 1). For low-order baroclinic modes, the correct offshore structure of these currents is $e^{-\alpha x}\sin kx$ where $\alpha = (\beta/\nu_h)^{1/3}/2$ and $k = \sqrt{3/2}\,(\beta/\nu_h)^{1/3} = 2\pi/\lambda$, a boundary layer first described by Munk (1950). The numerical model, however, does not always reproduce this boundary layer. In a series of tests involving only the $n = 2$ mode, numerical solutions were found and compared for a range of values of ν_h. When ν_h is large enough so that $\lambda > 2\Delta x$ ($\nu_h = 10^8$ cm^2/sec), the structure of the numerical boundary layer does closely approximate that of the Munk layer. When ν_h is small enough so that $\lambda < 2\Delta x$ ($\nu_h = 10^6$ cm^2/sec), there is no western boundary layer at all; instead, large-amplitude $2\Delta x$-noise spreads from the western boundary nearly across the ocean basin.

d. Phase relations. Let q represent any of the fields u, v, p, w, ρ, d or h in Eqs. (8), (11) and (12). Each q is a complex number that can be expressed as

$$q = |q|e^{i\phi}e^{-i\sigma t}, \tag{16}$$

where $|q|$ is the amplitude of q, and ϕ is a phase lag. Note that the real part of q reaches a maximum value at a time ϕ/σ, and a minimum value at the time $\phi/\sigma + \pi/\sigma$. Generally ϕ varies in space, and in that case q describes a propagating disturbance. Local values of the zonal, meridional, and vertical components of wavenumber are ϕ_x, ϕ_y and ϕ_z, respectively, and corresponding values of phase speeds are $c_x = \sigma/\phi_x$, $c_y = \sigma/\phi_y$, and $c_z = \sigma/\phi_z$. Finite-difference forms of these speeds at point P in the grid are

$$c_x = \frac{2\sigma\Delta x}{\phi_E - \phi_W}, \qquad c_y = \frac{2\sigma\Delta y}{\phi_N - \phi_S}, \qquad c_z = \frac{2\sigma\Delta z}{\phi_A - \phi_B}, \tag{17}$$

where the subscripts indicate the directions of nearest-neighbor grid points from point P (E, W, N, S, A and B are east, west, north, south, above and below, respectively). In the next section Δz is always equal to 25 m. By definition, lines of constant phase in the

x-z plane have the slope $-c_z/c_x$. A convenient measure of this slope at point P is

$$\gamma = -\frac{c_z/c_x}{\sigma/N_b} \tag{18}$$

As we shall see in the next section, the quantities defined in (17) and (18) help to identify the types of waves that are present at any point P.

3. Dynamics

The radiation field in the Gulf of Guinea is a complex superposition of many different types of waves. What types of waves exist there, and what are their identifying characteristics? Do certain types of waves dominate the model response in specific regions of the ocean? What waves create the current structures apparent in Figures 4–6? Hickie (1977), Philander (1977) and Cane and Sarachik (1979) discuss in detail the types of waves that are associated with individual baroclinic modes. Schopf *et al.* (1981), Cane and Sarachik (1981) and Cane and Moore (1982) describe the response of a single baroclinic mode to periodic forcing. McCreary (1984) points out that superpositions of several periodically forced modes produce beams that propagate vertically as well as horizontally. This section briefly reviews pertinent aspects of these studies and others.

a. Modes. An equatorial Kelvin wave is associated with each baroclinic mode. This wave has the meridional structure $e^{-1/2(y/r_n)^2}$ where $r_n = (c_n/\beta)^{1/2}$, and is therefore equatorially trapped in the region $|y| < \sqrt{2}r_n$. It has the simple dispersion relation

$$\sigma = kc_n, \tag{19}$$

and an eastward phase speed c_n. The quantity, r_n, is the equatorial Rossby radius of deformation, and Table 1 lists values for several of the modes used here.

There are an infinite number of possible Rossby waves, designated below by the index ℓ. The v-field associated with each Rossby wave has a meridional structure given by one of the parabolic cylinder functions $\phi_{\mu_{n\ell}}(y/r_n)$. The eigenvalues $\mu_{n\ell}$ are fixed so that each function vanishes at $y = -\infty$ and at $y = y_n$, and they are ordered so that they increase monotonically. The Rossby waves for $\ell \geq 1$ are equatorially trapped in the region $|y| < (2\mu_{n\ell} + 1)^{1/2} r_n$. The $\ell = 0$ Rossby wave exists only because there is northern boundary at y_N, and is trapped to that coast. Its trapping scale is measured by the smaller of $(2\mu_{n0} + 1)^{1/2} r_n$ and c_n/f.

The coast at $y = y_N$ affects the eigenvalues in a complicated way. However, if the $\ell \geq 1$ Rossby waves are sufficiently trapped to the equator that they do not "feel" the coast, (that is, they have a small v-field there), then the eigenvalues have very nearly the values they do in an unbounded ocean. Similarly, if an $\ell = 0$ Rossby wave does not "feel" the equator its eigenvalue approaches zero. In other words, if $(2\mu_{n\ell} + 1)^{1/2} r_n$

$< y_N$ then

$$\mu_{n\ell} = \ell. \tag{20}$$

Cane and Sarachik (1979) develop various approximations for estimating the eigenvalues. With the aid of one of them [their Eq. (5)], it is possible to verify that (20) holds quite well for nearly all the $\ell = 0$ and $\ell = 1$ Rossby waves in the model. The sole exception is the $n = 1, \ell = 1$ wave for which the estimated eigenvalue is 1.3.

The dispersion relation for Rossby waves is

$$-\frac{\sigma^2}{c_n^2} + k^2 + \frac{k}{\sigma}\beta + \frac{\beta}{c_n}(2\mu_{n\ell} + 1) = 0. \tag{21}$$

Because the frequency of the forcing here is so low, the first term of (21) is always negligible. For low values of ℓ (such that $2\mu_{n\ell} + 1 < \beta c_n/4\sigma^2$) the second term is also small, and (21) reduces to

$$\sigma = -\frac{kc_n}{2\ell + 1} \tag{22}$$

where, according to (20), $\mu_{n\ell}$ has been replaced by ℓ. These Rossby waves have a westward phase speed $-c_n/(2\ell + 1)$. Values of $\beta c_n/4\sigma^2$ are listed in Table 1, and it is easy to verify that (22) is valid for all of the $\ell = 0$ and $\ell = 1$ Rossby waves in the Gulf of Guinea.

For sufficiently large values of ℓ (such that $2\mu_{n\ell} + 1 > \beta c_n/4\sigma^2$) values of k in (21) are complex, and so corresponding Rossby waves remain trapped to the eastern boundary. Moore (1968) showed that these waves sum to form a β-plane coastal Kelvin wave that exists only poleward of the latitude $y_n = c_n/(2\sigma)$. According to Table 1, $y >$ 550 km only for $n > 10$, and so coastal Kelvin waves along 10E exist in the Gulf of Guinea only for the high-order baroclinic modes. Coastal Kelvin waves are therefore *not* an important part of the model response along 10E.

On the other hand, the $\ell = 0$ Rossby waves along the boundary at $y_N = 5$N closely resemble coastal Kelvin waves. First, the offshore structures of their zonal velocity and pressure fields have a form $e^{-(y-y_N)/(c_n/f)}$ for nearly all the vertical modes; the sole exception is the structure of the $n = 1$ wave that extends across the equator (as in Figure 4b of Cane and Sarachik, 1979). The quantity, c_n/f, is the Rossby radius of deformation appropriate at midlatitudes, and several values at 5N are listed in Table 1. Second, their westward phase speed is about c_n. Finally, at the annual frequency their north-south velocity field is insignificant. Because of these similarities, we refer to these waves as coastal Kelvin waves in the rest of this paper.

b. Beams. Solutions to (1) exhibit vertical, as well as horizontal, propagation of phase and energy (Figs. 4–6), even though the contributions from individual baroclinic modes necessarily do not. WKB theory (Bender and Orszag, 1978) provides an elegant way to understand why superpositions of baroclinic modes *must* have this property.

Using this technique, we look for approximate solutions to (5) that have the exponential form

$$\psi(c, z) = A(z)\, e^{i\phi(z)}, \tag{23}$$

and so entirely avoid the expansion into modes. Because the boundary conditions (6) are not imposed, c does not have discrete values, and so subscripts n are not necessary. Let $m \equiv \phi_z$ be the local vertical wavenumber of ψ, and $b = N_b/N_{bz}$ measure the vertical scale of $N_b(z)$. Then, the WKB solution that is valid to order $(mb)^{-2}$ has

$$A(z) = N_b^{1/2}, \qquad \phi(z) = \int^z \frac{N_b}{c} dz', \tag{24}$$

and $m = N_b/c$. It follows that the amplitudes of free waves proportional to $\psi(c, z)$ satisfy the homogeneous form of (9a) with replacement $c_n \rightarrow N_b/|m|$. So, equatorial Kelvin waves satisfy the dispersion relation

$$\sigma = k \frac{N_b}{|m|}, \tag{25}$$

and, according to (22), the $\ell = 0$ and $\ell = 1$ Rossby waves satisfy

$$\sigma = -\frac{kN_b/|m|}{2\ell + 1}. \tag{26}$$

By definition, lines of constant phase in the x-z plane have the slope $\tan\theta_p = c_z/c_x = -k/m$. Values of $\tan\theta_p$ obtained from (25) and (26) are $-|m|\sigma/(mN_b)$ and $(2\ell + 1)|m|\sigma/(mN_b)$, respectively. Thus, when $m > 0$ so that phase propagates upward ($c_z > 0$), lines of constant phase slope downward toward the east for equatorial Kelvin waves, and downward to the west for Rossby waves. The slopes are quite gradual. At the annual frequency and with $N_b = .005$ sec^{-1} (a typical value below 100 m in Fig. 2) $\sigma/N_b = 40$ m/1000 km; with $N_b = .02$ sec^{-1} (roughly the maximum value of N_b in Fig. 2) $\sigma/N_b = 10$ m/1000 km. Note that when $m > 0$ values of γ [defined in (18)] for the equatorial Kelvin wave and for the $\ell = 0$ and 1 Rossby waves are -1, 1 and 3, respectively.

Energy associated with packets of waves travels along ray paths. Let the zonal and vertical components of group velocity be c_{gx} and c_{gz}. The slope of ray paths is $\tan\theta_e = c_{gz}/c_{gx} = \sigma_k/\sigma_m$, and it is easy to verify that $\theta_e = \theta_p$. Thus, the direction of energy propagation is everywhere parallel to lines of constant phase.

A zonal wind patch in the ocean interior oscillating at the annual frequency is an efficient source of Kelvin waves. With no vertical mixing wave energy is confined primarily between ray paths that originate at the western and eastern edges of the patch. Thus, the Kelvin radiation forms a thin beam that slopes downward into the eastern ocean at the gradual slope $-\sigma/N_b$. The presence of vertical mixing acts to broaden the beam considerably away from the forcing region. At the eastern boundary it reflects as a set of Rossby beams that slope downward toward the west at the slope

$(2\ell + 1)\sigma/N_b$. Along the equator the $\ell = 1$ Rossby beam dominates the other reflected beams. The $\ell = 0$ Rossby beam is also involved in the reflection, and the results of this paper indicate that it is an important part of the model response along the coast at y_N.

The meridional structures of the equatorial Kelvin beam and the reflected $\ell = 1$ Rossby beam differ significantly. Both u and p for the Kelvin beam are concentrated on the equator. The u-field for the $\ell = 1$ Rossby beam is even more narrowly confined to the equator. However, its p-field is concentrated several degrees north and south of the equator, and is relatively weak at the equator. This difference provides another useful way of distinguishing the two types of beams.

c. The radiation field. In the Gulf of Guinea, where there is no (model) wind field, any dynamical field q is entirely a superposition of the free waves allowed by Eqs. (1). For example, if $c_x > 0$ near the equator, then q must be strongly influenced by equatorial Kelvin waves, since at the annual frequency they are the only waves with eastward phase speed that are significantly excited by the wind; however, if $c_x < 0$ near the equator, q is dominated by Rossby waves. If $c_z > 0$, so that phase propagates upward, then q is affected by a beam of Kelvin or Rossby waves that propagates downward from the ocean surface; conversely, if $c_z < 0$ q is affected by a beam that has certainly reflected somewhere from the ocean bottom. Finally, the value of γ defined in Eq. (18) is a particularly sensitive indicator of beam type. If $\gamma = -1$ near the equator, q is caused by a beam of equatorial Kelvin waves; if $\gamma = 3$ there then q is caused by a beam of $\ell = 1$ Rossby waves. If $\gamma = 1$ along the coast of Africa at 5N then q is caused by a beam of coastal Kelvin waves.

Phase propagation is not always a conclusive indicator of wave type. A combination of several different waves can lead to values of phase speed or γ that bear little relationship to those of the component waves. There are several instances of this phenomenon in the present study. For example, phase speeds greater than $c_1 = 225$ cm/s, the fastest possible individual wave in the system, often occur. In addition, above the pycnocline and almost everywhere along the coast of Africa, phase associated with ρ propagates in a direction opposite to any of the component waves.

4. Results

The wind field that drives the model is an idealization of the annual component of the equatorial trade winds in the western Atlantic. It has the separable form

$$\tau^x = \tau_o X(x)\, Y(y) e^{-i\sigma t}, \qquad \tau^y = 0, \tag{27}$$

where

$$X(x) = \begin{cases} \cos\,[\pi(x - 35°)/30°], & 20\text{W} \le x \le 50\text{W}, \\ 0, \quad \text{otherwise}, \end{cases} \tag{28a}$$

$$Y(y) = \begin{cases} \frac{1}{2}[1 + \cos(\pi y/10°)], & 10S \le y \le 10N, \\ 0, & \text{otherwise}, \end{cases} \tag{28b}$$

$\tau_o = .25$ dyne/cm, $\sigma = 2\pi$/year, and x and y are expressed in degrees. The shaded region of Figure 1 indicates the extent of the wind patch, and the thin lines the profiles of $X(x)$ and $Y(y)$. Both the forcing and the solution, (27) and (16), are complex numbers, and we adopt the convention that only their real parts are relevant. In that case, the model trade winds are maximum westward at $t = \pi/\sigma$ sec = 6 months, and they are a minimum (that is, maximum eastward) at $t = 0$.

Figure 2 shows the structure of the background density field, $\rho_b(z)$, used throughout this study. There is a surface mixed layer with a thickness of 25 m, a sharp near-surface pycnocline, and an ocean depth of 4000 m. This choice is representative of the mean density field in the equatorial Atlantic, although in the real ocean the pycnocline is somewhat deeper in the western ocean and shallower in the eastern ocean (Merle, 1980a). The figure also shows the structure of the square of the Väisälä frequency $N_b^2(z)$, that is associated with $\rho_b(z)$. Table 1 lists values of c_n and of the coupling coefficients C defined in (10) that are associated with this density field. Note that the coupling coefficient of the $n = 2$ mode is smaller by a factor of 2.5 than that of any other mode, indicating that this mode is the most strongly excited.

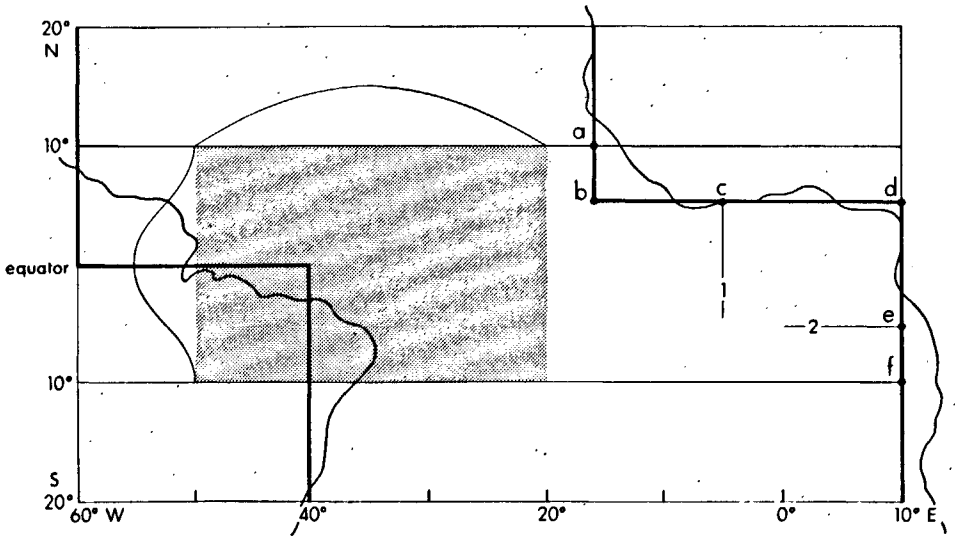

Figure 1. A schematic diagram showing the location of the ocean basin and the wind field, points a–f, and Sections 1 and 2. The thick lines indicate model continental boundaries, and the wiggly lines the actual coastlines of South America and Africa. Most solutions are found in a basin with open boundaries at ±10°; one solution has open boundaries at ±20°. The shaded region indicates the extent of the wind field, and the thin lines its zonal and meridional profiles. The wind stress oscillates at a frequency of 2π/year and reaches a maximum of 0.5 dyn/cm^2 in the center of the wind patch.

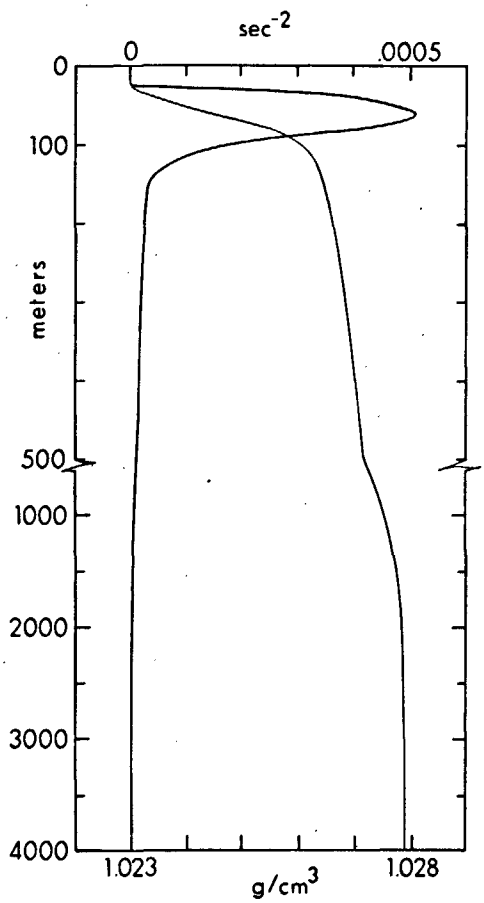

Figure 2. Profiles of background density structure, $\rho_b(z)$, and of the square of the Väisälä frequency, $N_b^2(z)$ (thicker curve).

Table 1. Values of various quantities associated with individual baroclinic modes. Associated units are in parentheses. $r_n = (c_n/\beta)^{1/2}$ is the equatorial Rossby radius of deformation, and $y_n = c_n/(2\sigma)$ is the turning latitude. Values of c_n/f are evaluated at 5N.

n	1	2	3	4	5	6	8	10	15
c_n (cm/sec)	225	134	89.5	62.6	48.6	40.9	30.7	24.3	16.1
$\int_D^o \psi_n^2\, dz$ (m)	251	105	399	899	710	473	1125	1100	2363
r_n (km)	314	242	198	165	146	134	116	103	84
c_n/f (km)	179	107	71	50	39	33	25	19	13
$\beta c_n/4\sigma^2$	321	191	128	89	69	58	44	35	23
y_n (km)	5625	3350	2238	1565	1215	1023	768	608	403

Values for the other model parameters are $g = 981$ cm/sec^2, $\beta = 2.28 \times 10^{-13}$ cm^{-1}sec^{-1}, $\nu_h = 10^7$ cm^2/sec, and $N = 15$. The horizontal viscosity, ν_h is taken to be as small as possible, and yet still to be sufficiently large to prevent the development and spreading of $2\Delta x$-noise from the western boundary. A final parameter, A, measures the size of ν throughout the water column. According to (2) and Figure 2, ν is infinitely large in the surface mixed layer, it reaches a minimum value, ν_{min}, just beneath the mixed layer where N_b^2 reaches a maximum value, and it increases monotonically at greater depths. In order that $\nu_{min} = .25$ cm/sec, A is set equal to .00013 cm^2/sec^3; in that case, $\nu = 5$ cm^2/sec at $z = -200$ m and $\nu = 12$ cm^2/sec at $z = -500$ m.

The choices for ν_{min} and N were not made arbitrarily. In two series of tests, solutions to the analytic (and economical) model of McCreary (1981, 1984) were found for a wide range of values of ν_{min} and N. In both of these tests the ocean basin was confined between meridional barriers separated by 6000 km, the background density field was that of Figure 2, and a wind field very similar to (22) forced the ocean. In the first, N was fixed at 50 and ν_{min} was varied. With $\nu_{min} = .25$ cm^2/sec the amplitudes of the equatorial currents in the central and eastern ocean had physically realistic values, with $\nu_{min} = 1$ cm^2/sec their amplitudes were a bit weak, and with $\nu_{min} = 0$ they were far too large. In the second, ν_{min} was fixed at .25 cm^2/sec and N was varied. With $N = 15$ the solution was well converged nearly everywhere in the ocean basin; only in the forced region in the western ocean were there any significant differences from another case with $N = 50$.

a. The annual response. Table 2 lists values of the amplitude and phase of various fields that are useful in the discussions of Figures 3, 4 and 5. Also listed are c_x, c_y, c_z, and γ whenever it is appropriate. The table is divided into three parts. The upper, middle and lower portions correspond to values taken from Figures 3, 4 and 5, respectively.

Figure 3 shows the fields of sea level and surface velocity at 2, 4 and 6 months. Significant changes in ocean circulation occur throughout the ocean basin. Perhaps most striking is the shift of surface water from the eastern to the western ocean. At 2 months, sea level is high in the eastern ocean and low in the western ocean. At 4 months, after the wind shifts from eastward to westward, a strong westward jet develops at the equator and drains water from the eastern ocean. As a result, sea level drops throughout the Gulf of Guinea. At 6 months, when the wind stress reaches its maximum value, sea level is low in the eastern ocean and high in the western ocean.

The response in the wind-forced region has expected features. Sea level tilts along the equator to balance approximately the wind. A measure of this tilt is the difference in sea level between 20W and 40W. This difference reaches a minimum value of -8.5 cm at 6.6 months. Sea level has a minimum amplitude at 34W, and equatorial sea level tends to pivot about this point; however, because the minimum value is not identically zero the pivot point is not fixed in space (compare the three panels of Fig. 3), as in the model of Cane and Sarachik (1981). Ekman pumping due to the wind stress curl in the model generates the extrema at 50W, 3N and 40W, 3S.

Table 2. Values of sea level (cm), isopycnal displacement (m), and currents (cm/sec) at various points in the Gulf of Guinea. Also listed are phase speeds (cm/sec) and γ whenever it is appropriate. Locations are indicated in parentheses, and the third coordinate measures depth (m). The table is divided into three sections corresponding to values taken from Figures 3, 4 and 5.

q	$\lvert q \rvert$	ϕ	c_x	c_y	c_z	γ
d (5W, 5N)	3.7	.4	−293			
d (10E, 5S)	4.1	.3		−1058		
d (5W, 0°)	4.4	.2	758			
d (20W, 0°)	4.6	0	147			
d (34W, 0°)	1.9	9.7	7			
d (40W, 0°)	4.2	7.4	16			
u (5W, 0°, 0)	17.5	.2	54			
u (5W, 0°, −75)	47	8.2	195		.0008	−.2
ζ (5W, 0°, −50)	23.8	.7.7	79			
ζ (5W, 0°, −75)	18.3	5.9	52		.0006	−1.2
ζ (5W, 0°, −450)	13.9	2.4	−52		.0096	3.3
ζ (5W, 2.5S, −450)	21.9	3.8	−26		.0065	4.5
ζ (5W, 2.5N, −450)	19.8	3.9	−33		.0062	3.3
u (5W, 5N, 0)	11	5.7	−100			
u (5W, 5N, −75)	14	4.5	−61		.0009	1.6
ζ (5W, 5N, −50)	8.1	8.1	210			
ζ (5W, 5N, −75)	14.9	7.1	−151		.0012	.9
ζ (5W, 5N, −250)	24.9	4.3	−68		.0065	1.4
v (10E, 5S, 0)	2.1	6.6		+29		
v (10E, 5S, −75)	7.9	2.6		−22	.0008	
ζ (10E, 5S, −50)	13.4	8.4		+85		
ζ (10E, 5S, −75)	19.4	6.7		−74	.0007	
ζ (10E, 5S, −175)	30.4	4.3		−28	.0025	

Phase associated with sea level propagates eastward near the equator in the Gulf of Guinea, indicating the presence of equatorial Kelvin waves there. However, east of 14W the eastward phase speed is everywhere considerably greater than c_1 (225 cm/sec), the speed of the fastest possible equatorial Kelvin wave. A phase speed of this magnitude is possible only if reflected Rossby waves also contribute significantly to the equatorial signal. Phase propagates westward elsewhere in the Gulf, indicating the presence of Rossby waves. At 5S the westward phase speed is roughly −30 cm/sec, consistent with expected phase speeds for Rossby waves at that latitude. In contrast, along the coast at 5N the westward phase speed approaches −300 cm/sec. Such a large value is possible only if coastal Kelvin waves contribute strongly to the solution there. Again, because its magnitude is greater than c_1 other waves must also affect the coastal signal. Phase propagates poleward south of the equator along 10E. Equator-

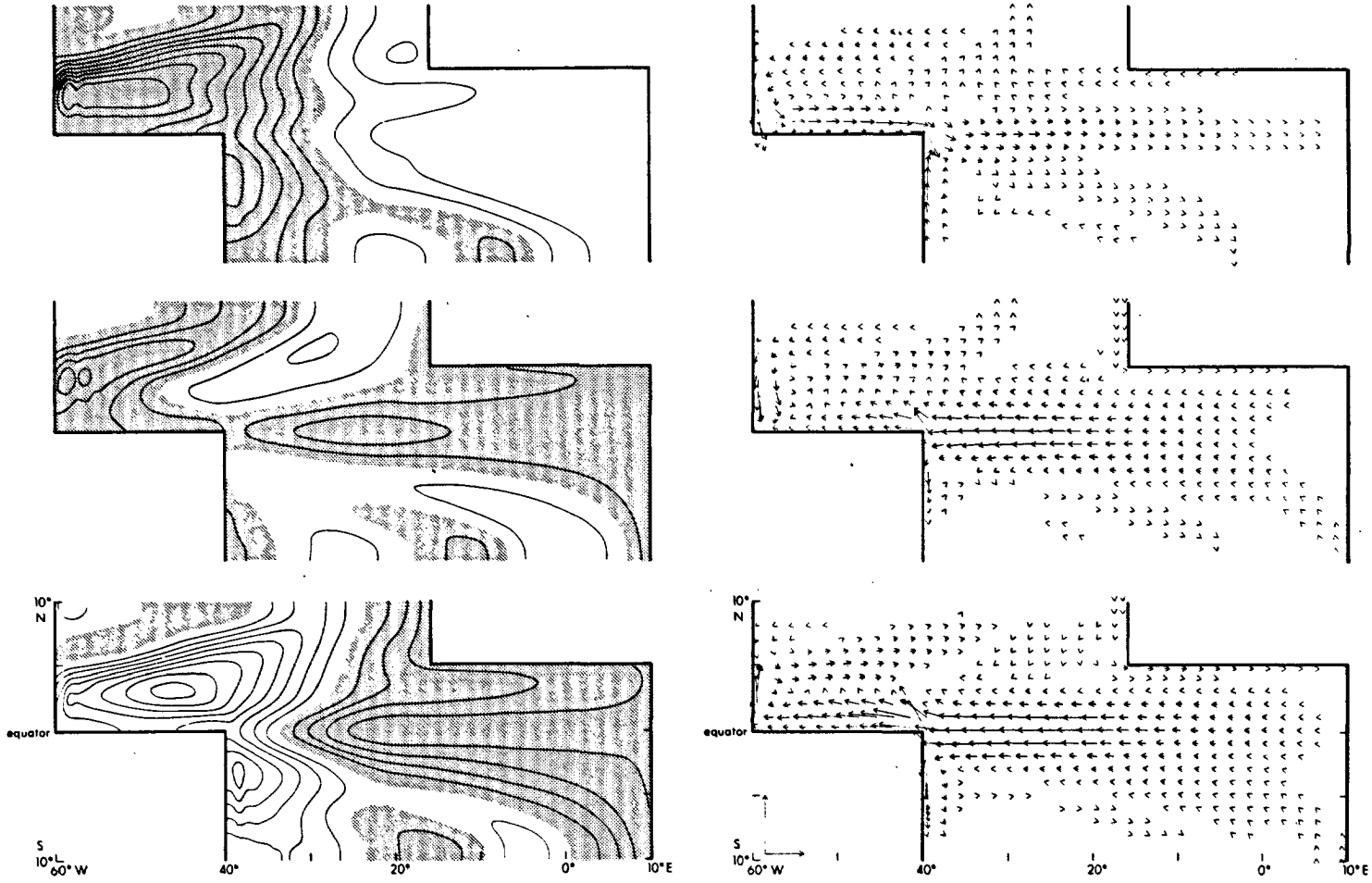

Figure 3. Sea level (left panels) and the surface velocity field (right panels) for t = 2, 4 and 6 months in the upper, middle and lower panels, respectively. The contour interval is 1 cm, shaded regions indicate negative values, and there is no zero contour. Calibration arrows in the lower right panel are 100 cm/sec. The sequence shows the onset of upwelling in the Gulf of Guinea.

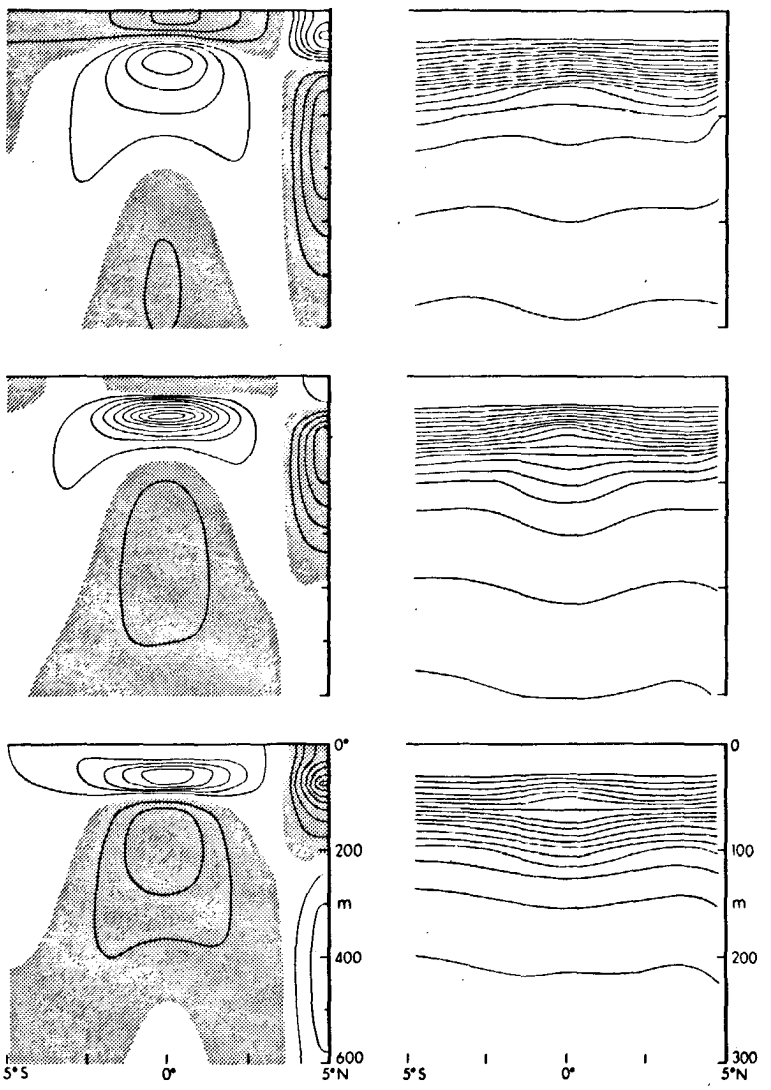

Figure 4. Vertical sections of zonal velocity and of the density field along Section 1 of Figure 1 for t = 6, 8, and 10 months in the upper, middle and lower panels, respectively. The velocity contour interval is 2 cm/sec for the coastal current, but is 5 cm/sec for all other flows. Shaded regions indicate westward flow, and there is no zero velocity contour. The density contour interval is .0002 gm/cm^3, and the uppermost contour is 1.0002 gm/cm^3. The depth range in the left panels is 600 m, whereas in the right panels it is 300 m. As time progresses the currents move upward, and eventually surface. Coastal currents are tightly trapped to the coast.

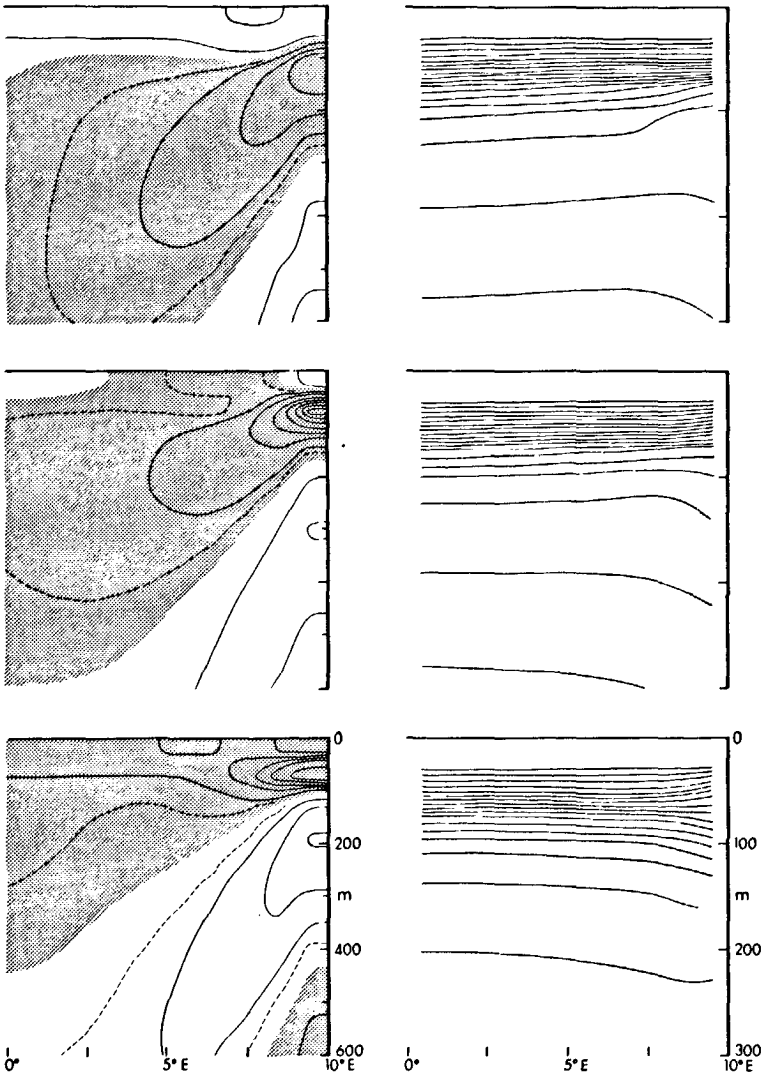

Figure 5. Vertical sections of meridional velocity and the density field along Section 2 of Figure 1 for t = 6, 8 and 10 months in the upper, middle and lower panels, respectively. The velocity contour interval is 1 cm/sec, and the dashed contour is ±.5 cm/sec. Shaded regions indicate southward flow, and there is no zero velocity contour. The density contour interval is .0002 gm/cm^3, and the uppermost contour is 1.0002 gm/cm^3. The depth range in the left panels is 600 m, whereas in the right panels it is 300 m. As time progresses the currents move upward, eventually surface, and spread well offshore.

ward of 5S the southward phase speed is faster than -1000 cm/sec; poleward of 5S the phase speed slows to about -200 cm/sec at 9S. This signal is not a coastal Kelvin wave since the turning latitudes at this frequency are poleward of this region for most of the modes making up the solution.

Figure 4 shows the fields of zonal velocity and total density, $\rho + \rho_b(z)$, along Section 1 of Figure 1 at $t = 6$, 8, and 10 months. For purposes of display, the contour intervals of the equatorial and coastal currents are not the same, and the vertical scale in the right panel is expanded by a factor of 2. There are distinctive surface and subsurface currents that are strongly trapped to the equator and to the coast. These features are also evident in the structure of the density field, as required by geostrophy; note that isopycnals spread apart in regions of eastward flow at the equator and in regions of westward flow at the coast. It is also apparent that both the current and density signals propagate upward in time. The eastward current maximum and isotherm-spreading region at 100 meters depth at $t = 6$ months moves up to 75 meters depth at $t = 8$ months and to 50 meters depth at $t = 10$ months. Vertical phase speeds are quite similar at the equator and at the coast. Speeds associated with the density field gradually decrease from about .008 cm/sec at 600 m to .001 cm/sec at 75 m. Speeds associated with the zonal velocity field decrease from roughly .005 cm/sec at 600 m to .001 cm/sec at 75 m.

At the surface the equatorial current is maximum westward (-17 cm/sec) at 6.3 months, and the coastal current at 5N is maximum eastward ($+11$ cm/sec) at 5.7 months. Because phase changes so rapidly in the upper 100 meters of the ocean (see Tables 2 and 4), it is difficult to establish a precise phase for the subsurface currents. At a depth of 75 m the equatorial flow is maximum eastward ($+45$ cm/sec) at 8.2 months and the coastal flow is maximum westward (-15 cm/sec) at 10.5 months, whereas at a depth of 50 m (100 m) maxima occur roughly one month later (earlier).

Since $\rho = 0$ in the surface mixed layer the model cannot provide direct information about the annual cycle of sea-surface temperature. However, the displacement of subsurface isopycnals in Figure 4 suggests when upwelling is most likely to appear at the ocean surface. Again, because phase changes rapidly it is difficult to establish a precise date for maximum upwelling. At a depth of 50 m isopycnal displacement (ζ) at the equator is maximum upward ($+24$ m) at 7.7 months, and at the coast is maximum upward ($+8$ m) at 8.1 months, whereas at 75 m maxima occur more than a month earlier. Although the largest isopycnal displacements at the equator occur near the surface, in other regions they occur at depth. There are relative maxima near a depth of 450 m and at 2.5S and 2.5N (20 m and 22 m amplitude, respectively). The largest isopycnal displacement anywhere in Figure 4 occurs at a depth of 250 m at the coast (25 m amplitude).

Near the equator phase associated with the density field propagates eastward above 250 m and westward below that level. Above 200 m the eastward phase speed is about 40 cm/sec, and below 300 m it is about -50 cm/sec. Values of γ vary gradually from

-1.2 at 75 m to 3.3 at 450 m. All of these properties indicate that the near-surface and deeper responses are due predominantly to an equatorial Kelvin beam and an $\ell = 1$ Rossby beam, respectively. This interpretation is also consistent with the patterns of $|\zeta|$ described in the previous paragraph; the equatorial Kelvin beam displaces isopycnals most strongly on the equator near the surface, whereas the $\ell = 1$ Rossby beam displaces isopycnals weakly on the equator and strongly off the equator at greater depths.

At the coast phase associated with the density field propagates westward everywhere below the pycnocline ($z < -65$ m) at a speed of the order of -70 cm/sec, and values of γ are 1.4 or less. These properties suggest that the response there is due predominantly to a coastal Kelvin beam. Again, this interpretation is supported by the occurrence of a relative maximum of $|\zeta|$ at the coast at depth, and by the fact that the coastal disturbance is narrowly trapped to the coast. Curiously, phase propagates eastward above the pycnocline, a property that holds all along the coast at 5N.

Figure 5 shows the fields of meridional velocity and total density along Section 2 of Figure 1. As in Figure 4, the vertical scale in the right panel is expanded by a factor of 2. Although surface and subsurface currents are still trapped to the coast, they extend much farther offshore than the coastal currents do in Figure 4. In a similar way the isopycnal variability also extends much farther offshore. This difference between the two coastal flows is due to the fact that reflected Rossby waves propagate offshore from the southern coast. Again, upward propagation of both the current and density fields is apparent; moreover, the upward phase speed has roughly the same magnitude and characteristics as in Figure 4 (see Table 2).

Because the coastal currents spread offshore, they have a smaller amplitude than they do at 5N. The surface current is maximum northward (+2.1 cm/sec) at 6.6 months, and the subsurface flow at a depth of 75 m is maximum southward (-7.9 cm/s) at 8.6 months. At the coast at a depth of 50 m isopycnal displacement is maximum upward (+13 m) at 3.3 months. Again, because phase changes so rapidly in the upper 100 m, it is difficult to identify a precise phase for any of the subsurface fields. The largest isopycnal displacement at the coast (30 m amplitude) occurs near a depth of 175 m.

Below the pycnocline both the alongshore current and density fields propagate poleward at the coast. Propagation speeds associated with ρ are -74 cm/s at 75 m, -34 cm/s at 100 m, and about -25 cm/s at greater depths. These low speeds indicate that the response along the southern coast cannot be due to a beam of coastal Kelvin waves. Above the pycnocline phase propagates equatorward, a property that holds everywhere south of 4S.

Figure 6 shows a vertical section of the coastal flow field all along the African coast. The figure illustrates the continuity of surface and subsurface currents everywhere in the Gulf of Guinea, and indicates that the currents are all caused by the reflection of the equatorial Kelvin beam from the African coast. Note that during the time of

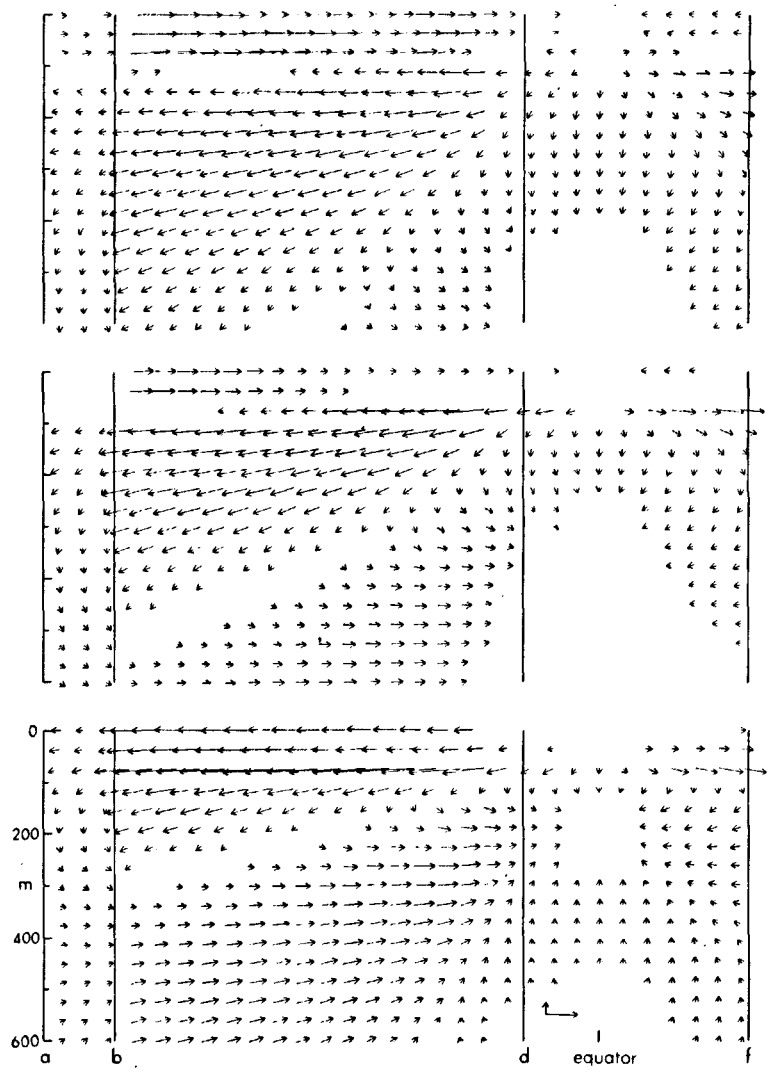

Figure 6. Vertical section of alongshore flow at the African coast from points a–f in Figure 1 for t = 6, 8 and 10 months in the upper, middle and lower panels, respectively. The calibration arrows in the lower panel are .001 cm/sec and 10 cm/sec in the vertical and horizontal directions, respectively. Currents spread poleward from the equator. As time progresses they move upward and eventually surface. There is a distinct change in the structure of the flow field between Sections a–b and b–d.

Table 3. Values of the amplitudes of sea level (cm) and currents (cm/sec), and of phase speeds (cm/sec) associated with ρ_n, at three points in the Gulf of Guinea. Locations are indicated in parentheses.

n	1	2	3	4	5	6	8	10
$\lvert d_n \rvert$(5W, 0°)	9.2	28	9.2	2.0	1.5	1.2	.5	.2
$\lvert u_n \rvert$(5W, 0°)	1.4	12.5	10.8	6.2	7.1	8.3	1.6	.5
c_x(5W, 0°)	−35,700	2310	246	37	28	30	31	24
$\lvert d_n \rvert$(5W, 5N)	9.3	29	9.3	2.3	2.2	2.8	.06	.05
$\lvert u_n \rvert$(5W, 5N)	1.4	11.2	7.8	2.9	2.2	1.9	1.2	.01
c_x(5W, 5N)	−397	−158	−93	−78	−44	−34	−26	−22
$\lvert d_n \rvert$(10E, 5S)	9.4	30	11	3.3	2.6	2.4	.2	.02
$\lvert v_n \rvert$(10E, 5S)	.2	1.8	1.5	.9	1.3	1.7	2.4	.3
c_y(10E, 5S)	−385	−136	−60	−30	−22	−21	−24	−24

maximum upwelling favorable winds (6 months), the surface currents move water equatorward while the subsurface currents flow poleward. All the currents propagate vertically. This propagation is most noticeable in the subsurface poleward flow which surfaces from 6 to 10 months. Upward phase speeds are similar all along the coast, decreasing gradually from .005 cm/s at 600 m to .001 cm/s at 100 m with a more rapid decrease just below the pycnocline. Horizontal phase propagation is also evident, and virtually everywhere in the figure there is poleward propagation. Finally, note that there is a marked decrease in the flow from Section bd to Section ab. This reduction occurs because Section ab is along a north-south oriented coast, and just as at 5S (Fig. 5) the current there extends much farther offshore.

b. Contributions from individual modes. The existence of vertical propagation in Figures 4, 5 and 6 clearly demonstrates that the solution is not dominated by a single baroclinic mode. Which modes contribute significantly to the model response? To help to answer this question, Table 3 lists the values of the amplitudes of various fields at three different points in the Gulf of Guinea, and Figure 7 compares the response of several different modes. The figure shows the horizontal structure of the surface pressure field at 6 months for the $n = 2$, 4 and 6 modes in the upper, middle and lower panels, respectively; note that the contour interval is an order of magnitude less in the middle and lower panels. It is evident in both Table 3 and Figure 7 that the pressure field is most strongly influenced by the $n = 2$ mode, and that nearly all of its variability is accounted for by the first three modes. On the other hand, the equatorial and coastal currents are strongly affected by higher order modes, and only very weakly affected by the $n = 1$ mode.

Why do the higher-order modes contribute so strongly to the currents? The reason is that the horizontal structure of the pressure field varies considerably with n. As n increases the equatorial and coastal Rossby radii of deformation decrease (see Table

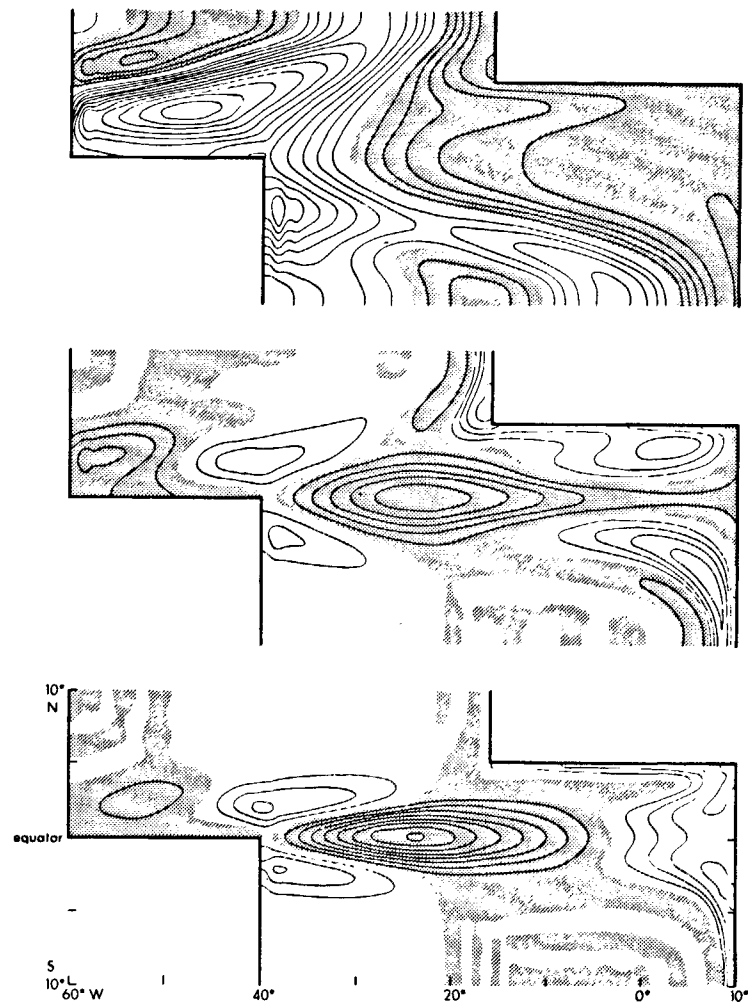

Figure 7. Sea level at t = 6 months for modes 2, 4 and 6 in the upper, middle and lower panels, respectively. The contour interval is .5 cm in the upper panel, and is .05 cm in the lower panels. Shaded regions indicate negative values and there is no zero contour. Mode 2 dominates the sea level field, but does not dominate the velocity field. It is apparent that coastal Kelvin-like waves play an important role in the responses of modes 4 and 6.

1), as does the wavelength of annual-frequency Rossby waves, and so currents are increasingly confined to the equator and the coast. These changes in structure are evident in Figure 7; note that lines of constant sea level are tightly trapped to the coast of Africa for the n = 6 mode, are trapped less for the n = 4 mode, and are hardly confined at all for the n = 2 mode. It follows from geostrophy that the equatorial and coastal currents do not decrease as rapidly with n as the pressure field does. This

property has a precise expression in the analytic solutions of similar remotely forced problems; for low-order modes the pressure field is proportional to F_n, but the current and density fields are proportional to F_n/c_n (McCreary, 1980, 1981, 1984).

Phase speeds corresponding to individual modes provide additional evidence of the types of waves that affect the flow field in the Gulf of Guinea, and Table 3 also lists several values associated with the ρ_n-fields. At (5W, 0°) phase speeds shift from westward to eastward and approach c_n as n increases. Thus, along the equator low-order modes are strongly affected by reflected Rossby waves, but higher-order modes are not. At (5W, 5N) phase speeds are all westward, and have values that are close to $-c_n$. This property indicates that all the ρ_n-fields in this region are dominated by coastal Kelvin waves. It is for this reason that values of γ associated with ρ are so close to 1 along the coast at 5N. At (10E, 5S) meridional phase speeds are generally not related to Kelvin wave speeds; on the other hand, zonal phase speeds are very close to values expected for Rossby waves at that latitude.

Recall that above the pycnocline phase speeds associated with ρ are eastward at 5N along the northern coast and equatorward south of 4S along the southern coast. Note in Table 3, however, that phase speeds associated with the individual modes (that sum to produce ρ) are all westward at 5N and poleward at 4S. So, here is a situation in which component waves all propagating in one direction produce a signal propagating in the opposite direction.

c. The effect of boundary conditions. How does the use of free slip conditions affect the solution? To answer this question, we repeated the calculation with no-slip conditions along the coast of Africa. The two solutions are virtually identical everywhere in the basin except along the coast at 5N. Along this boundary the use of no-slip conditions decreases the amplitude of the coastal currents by a factor of 2, with little effect on its phase. Horizontal mixing is required in the model in order to be able to resolve the western boundary currents. The use of slip conditions minimizes frictional effects on the eastern boundary flow.

According to the discussion in the Appendix, the numerical scheme is most efficient when $N_y < N_x$, so that ab^2 is as small as possible. For this reason the ocean basin was made as narrow as possible, and open boundary conditions were imposed on the northern and southern boundaries. To investigate the effect of these conditions, we found the response of several baroclinic modes in a somewhat wider ocean basin. For example, Figure 8 shows the horizontal structure of the surface pressure field of the $n = 2$ mode at 6 months when the open boundaries are extended to 20N and 20S. A comparison with the upper panel of Figure 7 shows the fields to be very nearly the same. Similar comparisons for the $n > 2$ modes are even closer. The comparison is not quite as good for the $n = 1$ mode, but that mode contributes very little to the highly baroclinic flows of interest here. So, the open conditions have very little effect on the response in the Gulf of Guinea.

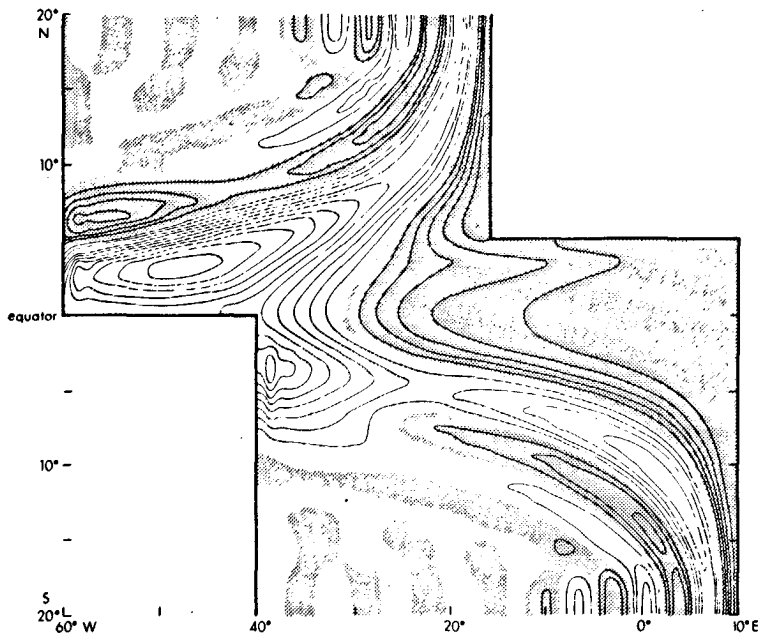

Figure 8. Sea level at t = 6 months for mode 2 in a basin that extends to ±20°. The contour interval is .5 cm, shaded regions indicate negative values, and there is no zero contour. Compare this response to that in the upper panel of Figure 7. The similarity between the two figures demonstrates that solutions are insensitive to the position of open boundaries.

5. Comparison with observations

The model suggests how annual remote forcing affects the circulation in the Guinea Gulf both in the surface and subsurface layers. Prominent figures of the response are the existence of horizontal and vertical phase propagation throughout the region, and the continuity of the equatorial and of the north and south coastal currents. The purpose of this section is to discuss some observations from the eastern Atlantic that are relevant to the model. Most of the data have been collected by the ORSTOM Centers at Pointe-Noire, Abidjan and Dakar and by the Fishery Research Unit at Tema, and the general hydrography in the vicinity of these Centers is quite well known. In addition, the quasi-permanence of the French research vessel *Capricorne* in the Guinea Gulf since 1970, as well as the additional cruises during the EQUALANT, GATE and FGGE experiments, have given us some idea of the seasonal variability elsewhere in the Gulf, especially along the 4W meridian.

The mean seasonal cycle in the region is characterized by a primary upwelling season from July to September and a secondary one during December–January (Berrit, 1961, 1962). The relatively short duration of the primary upwelling season (3 months), combined with the secondary upwelling season, results in a strong semi-

annual cycle with an amplitude that is only a bit less than that of the annual cycle (Merle and Le Floch, 1978). Assuming that equatorial dynamics are linear, a harmonic decomposition of the mean seasonal cycle can separate the annual cycle from this strong semi-annual cycle. Unfortunately, although there are many subsurface observations from the Guinea Gulf, they are not usually sufficient to provide an accurate estimate of the annual component. The only exception comes from a deep hydrographic station south of Abidjan repeated 217 times (see the discussion below). Primarily because of this difficulty our comparison is necessarily qualitative.

For convenience, the discussion in this section follows as closely as possible that of the various figures. The general variation of sea level in the entire basin is first discussed. Then the coastal and equatorial transects south of Abidjan (4W) and the zonal section west of Pointe-Noire (5S) are discussed. Finally, evidence for poleward propagation is presented. According to Busalacchi and Picaut (1983) the annual component of the zonal wind stress in the western part of the basin reaches a minimum at the beginning of March. Therefore, in the following discussion March 1 is assumed to be the time origin for our model. In other words, $t = 3$, 6 and 9 months in the model correspond to June 1, September 1 and December 1, respectively, and so on.

a. Variations of sea level: Figure 3. In several studies of all the historical hydrographic data collected in the tropical Atlantic, Merle (1978, 1980a, b) finds that most of the variations of heat content are directly related to vertical displacements of the thermocline. In addition, the subsurface layers to a depth of 300 m have a seasonal cycle with a phase close to that in the surface layers. Therefore, the sea level field of Figure 3 can be usefully compared to the annual cycle of surface dynamic height relative to the 300 db calculated by Merle and Arnault (1983).

The model simulates correctly the seasonal displacement of dynamic height along the equator. This displacement is characterized by a tilt about a pivot point that seems not to be fixed (Merle, 1980a), and has been directly related to the zonal wind stress variations in the western part of the equatorial basin (Katz *et al.*, 1977). Dynamic height is lowest during August–September ($t \simeq 6$ months) in the eastern part of the equatorial basin and highest in September–October ($t \simeq 8$ months) in the western part, very close to the phase values noted in the previous section. In the Guinea Gulf the observed amplitude of surface dynamic height along the northern coast is 4 cm, along the southern coast is 7 cm, and south of the equator is 4.5 cm. The model gives 3.7, 4.2 and 4.5 cm, respectively, for the same regions. The larger amplitude along the southern coast is probably related to the annual meridional wind in the eastern basin. In the western basin the amplitude of the observed dynamic height field reaches a maximum of 8 cm at 4N, also in good agreement with the model values.

b. Equatorial transect: Figure 4. The South Equatorial Current increases as the upwelling season approaches, and reaches its maximum around August ($t \simeq 5$ months)

in agreement with the model. The current also splits into two branches: a northern one that remains as an equatorial jet, and a southern one that has been related to the intensification of oceanic divergence south of the equator by Voituriez (1981). Voituriez suggested that this divergence is induced by southerly winds which increase at the beginning of the upwelling season. Separation of this current also occurs in the model (see the lower panel of Fig. 3 and the middle panel of Fig. 4), but is caused by Rossby waves radiating from the southern coast of Africa.

Hisard (1973) first noticed that the Equatorial Undercurrent weakens during the upwelling season in the Guinea Gulf. This weakening also appears in recent data from 4W (Voituriez, 1981). Its speed reaches a maximum of about 100 cm/sec in January–March ($t \simeq 10$–12 months) and reaches a minimum somewhat greater than 50 cm/sec in June–July ($t \simeq 4$ months). Corresponding phase values from the model at a depth of 75 m are 8.2 months and 2.2 months, but as noted in the last section it is difficult to compare the model with observations because phase changes so rapidly with depth in the pycnocline. Recent measurements do not show any upward movement of the Equatorial Undercurrent during the upwelling season. Rather, it appears to stay at the same level all year round (Voituriez, 1981), contrary to model predictions.

At 4W and on the equator, SST is minimum near the end of August ($t \simeq 6$ months). The seasonal variation of isopycnal displacement in the pycnocline and below is also obvious (Voituriez, 1981). For example, the mean isopycnal surface $\sigma_t = 26.44$, which is not influenced by vertical mixing with the surface layer, is at a depth of 145 m in April and 95 m in August ($t \simeq 5$ months), in good agreement with the response in Figure 4. In addition, the amplitude of this displacement is maximum at the equator and nearly zero at 2N and 2S. This property suggests the existence of an equatorially trapped phenomenon, and it has been confirmed in recent analyses of isotherm displacements by Gouriou (1982) and by Houghton (1983). Houghton's results indicate a radius of deformation of 180 km, in agreement with Figure 4.

c. Abidjan transect: Figure 4. At the coast the surface flow is dominated by the eastward Guinea Current which transports low salinity water from the coasts of Guinea and Liberia. This current flows above two distinct westward undercurrents. One appears trapped on the shelf (trapping scale $\simeq$40 km) at a mean depth of 50 m, whereas the other is deeper and farther offshore (Lemasson and Rébert, 1973a, b).

The seasonal variation of the Guinea Current differs between the coastal and offshore region. The coastal current reaches a maximum speed of about 50 cm/sec in June–July ($t \simeq 3$–4 months), and reverses weakly in October and again sometime in January–February (Lemasson and Rébert, 1973b; Bakun, 1978). Farther offshore between 3N and 4N the Guinea Current never reverses; its mean velocity approaches 100 cm/sec in August and weakens to 30 cm/s in December (Janke, 1920). Coastal flow at a depth of 75 m in the model has an amplitude of 14 cm/sec and reaches its eastward maximum at 4.5 months, in fair agreement with the observations. There is no analog of the offshore variability in the model. As mentioned in the Introduction, the

Table 4. Observed and predicted values of phase (months) at various depths (m) just offshore from Abidjan (roughly point c in Fig. 1).

Depth	50	75	100	125	150	200	250	300	400	500
ϕ (observed)	5.6	6.0	6.4	6.3	6.2	5.5	4.2	3.5	2.9	2.7
ϕ (model)	8.0	7.2	6.5	6.1	5.7	5.0	4.4	3.9	3.1	2.5

offshore part of the Guinea Current is probably driven by meridional winds in the Gulf of Guinea (Philander, 1979; Anderson, 1979).

Due to the small number of subsurface current measurements off the shelf, there is almost no information on the seasonal variation of the undercurrent there. However, there is some information about the coastal undercurrent, especially near Abidjan (Lemasson and Rébert, 1968, 1973b, c). Its seasonal variation appears to be smaller than that of the surface current, with a dominant semi-annual component. An interesting characteristic is its apparent upward movement from May to October; according to Lemasson and Rébert (1973b) the zero velocity contour is displaced by roughly 50 m during this time. A similar feature is evident in Figure 4.

There is considerable information about the temperature field on the shelf (Morlière, 1970; Morlière and Rébert, 1972). A precise analysis of its variability has been recently made by Picaut (1983), based on a hydrographic station at a site 24 miles south of Abidjan in 1480 m of water just off the shelf break. This station consists of 217 Nansen casts regularly made by the Centre de Recherches Océanographiques of Abidjan between 1957 and 1964. With this large amount of data it was possible to calculate precisely the mean seasonal cycle by a Fourier decomposition of monthly means. Table 4 compares observed values with those predicted by the model. Recall that in the model there is no phase information of the density field in the mixed layer, so the comparison is only possible below this level.

The observed and predicted values of phase in Table 4 agree remarkably well below 75 m. However, note that the observed annual phase actually decreases upward above 100 m. This decrease probably indicates the effects of near-surface thermodynamic processes that are not present in the model. Assuming that the deviations from the mean observed temperature profile reflect vertical displacements (which is a sensible approximation below the thermocline), the amplitude of the observed displacements is 17 m from 50 m to 500 m, and thus is very similar to the displacements produced by the model over the same depth range. This observed isotherm displacement and the corresponding regular shift of phase from 500 m to 100 m are clear evidence of vertical phase propagation at a mean speed of 4×10^{-3} cm/s. As we have seen such propagation is a dominant feature of the model throughout the Guinea Gulf, and the good agreement between the observations and the model south of Abidjan suggests that vertical propagation may be present throughout the Guinea Gulf. The remote forcing mechanism is at present the only explanation of this phenomenon.

Another interesting similarity between the model and observations along this

transect is the evidence of a seasonal temperature signal trapped at the coast (Gouriou, 1982; Houghton, 1983). This fact and the evidence for vertical propagation discussed in the preceding paragraph strongly support the idea that the coastal upwelling signal is predominantly due to a remotely forced beam of coastal Kelvin waves.

d. Pointe-Noire transect: Figure 5. For more than 20 years oceanographic observations have been collected near Pointe-Noire. The most complete and regular set of data comes from a section extending 370 km off Pointe-Noire that was repeated 23 times from 1973 to 1976 (Guillerm, 1981). Unfortunately, the data are not sufficient to provide an accurate estimate of the mean seasonal cycle of temperature, salinity and circulation in the area.

Guillerm (1975) compiled most of the current measurements to provide an estimate of the mean circulation along this transect during the two important marine seasons: the warm season from January to May ($t \simeq 10$ months—2 months) and the cold season from June to September ($t \simeq 3$–6 months). During the warm season there is a well-defined southward current in the surface layer (0–100 m) with northward flow in the 100–250 m layer and weak southward flow at depth. In contrast during the cool season there is evidence of northward flow in the upper 40 m. In the model the flow is maximum southward at 9.7 months at a depth of 50 m and at 0.6 months at the surface, in rough agreement with the observations. It should be noted, however, that the dynamics of the surface flow in the region are complicated by a large amount of fresh water coming from the Congo estuary at 6S (Piton *et al.*, 1977; Wauthy, 1977). The resulting low-density surface layer in the top few meters appears to respond directly to the local southerly winds (Gallardo, 1981), and thereby distorts the remote signal.

At the coast there is precise information of the seasonal variation of hydrographic parameters. Data have been collected from the wharf station since 1969 at a depth of 17 m, and temperature there reaches a minimum during the first week of August. On the self break there are only scattered hydrographic data. These data have been averaged in a 30-mile square box (Picaut *et al.*, 1983) and give an indication of upward phase propagation of the primary upwelling event from 250 m to 50 m, similar to that found at Abidjan. Unfortunately, the large dispersion in space and the relatively small number of stations so far compiled (124) does not allow as precise an analysis as that for the station offshore from Abidjan.

In contrast to the Abidjan transect the currents and thermal structure on the Pointe-Noire transect are not highly trapped to the coast (Guillerm, 1981); instead, they spread a considerable distance offshore. In the model this spreading is due to the propagation of Rossby waves from the coast, and there is some evidence that this process is the cause in the real ocean as well. In the 370 km-section off Pointe-Noire the primary upwelling signal arrives in the subsurface layers one or two months later offshore than at the coast (Guillerm, 1981). This delay corresponds to an offshore propagation speed of 7–14 cm/s, a range of values consistent with that produced in our

model. A similar delay is even more evident with the secondary upwelling signal in December–January.

e. Poleward propagation. A detailed analysis of daily SST, collected from 1977 to 1979 at 15 coastal stations along the northern coast of the Guinea Gulf, reveals that the primary upwelling signal propagates westward along this coast; propagation speeds associated with the three events are −74, −37, and −78 cm/s. A complementary analysis of historical SST data collected by merchant ships also shows westward propagation in this region at a speed of −90 cm/s. Model phase speeds below the pycnocline are about −70 cm/s along this coast, in good agreement with these observations. Along the southern coast, again based upon data collection by merchant ships, there is a poleward propagation of the upwelling signal between 1S and 13S at a mean speed of 66 cm/s (Picaut, 1983). Below the pycnocline and south of 1S model phase speeds are typically −80 cm/sec at 75 m, decreasing to −25 cm/sec at greater depths.

At Dakar (15N) SST is mostly driven by local wind and thermodynamic effects. It is minimum in February and maximum in July–August, and so is out-of-phase with the SST variability in the Guinea Gulf. However, the thermal structure between 50 m and 250 m rises to a minimum depth in September–October (Rossignol, 1972; Picaut *et al.*, 1983). The roughly one-month delay between the minimum depth of the 14–18° isotherms (just below the thermocline) during the late summer–early fall at Abidjan and Dakar suggests a 90 cm/sec poleward propagation speed between these two points, of the same order as the corresponding one in the model. This, it may be that the subsurface annual signal at Dakar is remotely driven by the wind in the western Atlantic.

6. Summary and discussion

This paper investigates the wind-driven response of the tropical Atlantic Ocean. A model is forced by an idealization of the annual component of the zonal wind in the Atlantic that is confined entirely to the west of 20W. Solutions are represented as expansions of baroclinic modes, and they are not dominated by a single baroclinic mode. Vertical phase propagation in the model occurs only because several modes contribute significantly. The response of a particular mode is found, not by time-stepping the equations of motion, but rather by assuming a time dependence of the form $e^{-i\sigma t}$, as in many tidal models. Open boundary conditions are specified at 10N and 10S, but the flow field is hardly affected at all by their position. Slip conditions are imposed along the coast of Africa, and this choice ensures that narrow eastern boundary currents are not significantly reduced in strength by horizontal mixing.

Because there is no forcing in the eastern ocean, the response there is entirely due to the radiation of equatorially trapped Kelvin waves generated by the wind in the western ocean. These waves superpose to form a narrow beam of energy that slopes

downward toward the east. This beam reflects from the eastern boundary as a set of Rossby beams that influence the flow field throughout the Gulf of Guinea. The most evident reflected beams are the $\ell = 1$ and $\ell = 0$ Rossby beams. The $\ell = 1$ beam is equatorially trapped, although it affects the density field most strongly somewhat off the equator. The $\ell = 0$ beam is trapped to the coast at 5N and is very similar to a beam of coastal Kelvin waves. Other Rossby beams superpose to generate coastal jets along meridional boundaries.

Some prominent features of the solution are the following. As the wind shifts from eastward to westward (so that the trades increase) there is a shift of near-surface water from the eastern to the western basin. Shortly after the wind reaches its maximum westward value, sea level reaches its lowest level throughout the eastern ocean. Sea level tilts to balance approximately the wind at the equator, and Ekman pumping deepens the pycnocline in regions of wind curl off the equator (Fig. 3). Along the 5W meridian currents are trapped to the equator and also to the coast at 5N, and they propagage upward in time. At the equator the surface flow is caused predominantly by the equatorial Kelvin beam, whereas the deeper flow is due to the $\ell = 1$ Rossby beam; at the coast the flow is caused predominantly by the $\ell = 0$ Rossby beam (Fig. 4). At 5S the coastal flow field extends much farther offshore than it does at 5N. This broadening occurs because the flow at 5S is a superposition of Rossby waves that propagate westward, rather than coastal Kelvin waves (Fig. 5). Finally, coastal currents are continuous everywhere along the coast of Africa and vertical phase propagation is evident everywhere (Fig. 6).

Many of these features compare favorably with observations. The surface dynamic height at the equator does seem to tilt to balance the wind, and large changes in dynamic height occur in regions of wind curl off the equator. Low-frequency variability in the currents and thermal structure are tightly trapped to the equator and to the coast near 5N. In addition, the upwelling signal at the coast propagates both vertically and horizontally at phase speeds consistent with those in the model. At 5S the currents and associated thermal structure extend well offshore, and there is some evidence of both offshore and poleward propagation of the annual and semi-annual components of the upwelling signal. Finally, the deep upwelling signal at Dakar is out-of-phase with the locally forced surface upwelling, and may be due to the remotely forced wave discussed in this paper.

The model is obviously too simple to be able to explain all aspects of the annual response of the tropical Atlantic Ocean. For example, strong changes in the Guinea Current from 2–4N are not present in the model, most likely due to the lack of meridional winds there. In addition, in order to find solutions as expansions of baroclinic modes it is necessary to fix ρ at the ocean surface, and so the model cannot develop any sea-surface temperature variability. Finally, the model ignores horizontal advection terms, which, at the very least, must act to modify phase information in the strong surface flows. The real usefulness of the model is that it points out in greater

detail how remote annual winds can affect the eastern ocean, both in the surface and deep ocean. The good agreement between prominent features in the model and in the observations supports the notion that remote forcing is an important cause of the annual response in the eastern Atlantic.

Acknowledgments. This research was sponsored by the National Science Foundation under grant no. OCE 79-21785 through PEQUOD, by the University of Hawaii through the Joint Institute for Marine and Atmospheric Research (JIMAR) under National Oceanic and Atmospheric Administration grant NA80RAH00002, and by the Centre National d'Exploitation des Océans (CNEXO) contract nos. 82-2651/83-2839 and by the Centre National de la Recherche Scientifique (CNRS). We are indebted to Linda T. Smith; without her programming assistance this paper would not have been possible.

APPENDIX: THE NUMERICAL SOLUTION

Most of the quantities in (9a) involve the subscript n. In the following discussion it is necessary to include additional subscripts on some of them. So for notational simplicity, the subscript n is deleted throughout this Appendix unless confusion might result from its absence.

Solutions to (9a) are evaluated on a staggered grid in the rectangular region of Figure 1 from 10S to 10N (or 20S to 20N) and from 60W to 10E. (Fields that are evaluated at land points are, of course, ignored.) The region is subdivided into an array of boxes of dimension $\Delta x = 110$ km by $\Delta y = 55$ km, so that there are $N_x = 70$ columns and $N_y = 40$ rows of boxes. Three points of the staggered grid are associated with each box: a p-point at the center of a box, a u-point at the middle of its western edge, and a v-point at the middle of its southern edge.

Second-order space differences approximate the operators ∂_x, ∂_y and ∇^2 in (9). For example, the v-equation located at point P becomes

$$\begin{aligned}(-i\sigma + A/c^2)\, v_P + \frac{1}{4}\left[f_N(u_{NE} + u_{NW}) + f_S\,(u_{SE} + u_{SW})\right] \\ + \frac{1}{2\Delta y}(p_N - p_S) - \frac{\nu_h}{\Delta x^2}(v_E - 2v_P + v_W) \\ - \frac{\nu_h}{\Delta y^2}(v_N - 2v_P + v_S) = G_P,\end{aligned} \tag{29}$$

where subscripts indicate the directions of nearest-neighbor grid points from point P (N is to the north, S is to the south, NE to the northeast, and so on). The u-equation is similar to (29) except that the Coriolis term has the form

$$-\tfrac{1}{4} f_P\,(v_{NE} + v_{NW} + v_{SE} + v_{SW}) \tag{30}$$

This formulation ensures that the set of finite difference equations conserves energy (Holland and Lin, 1975).

Boundary conditions, (13)–(15), are imposed by appropriately modifying the equations associated with grid boxes adjacent to boundaries. In the column of boxes adjacent to 60W, the u-equation becomes $u_P = 0$, and $v_W = -v_P$ in the v-equation. In the column of boxes adjacent to 10E, $u_E = 0$ in the u- and p-equations, and $v_E = v_P$ and $u_{NE} = u_{SE} = 0$ in the v-equation. These modifications insure that conditions (13) and (14a) hold at 60W and 10E, respectively. Equations adjacent to the interior boundaries of South America and Africa are modified similarly. In the row of grid boxes adjacent to 10S, the equations are replaced by $u_P = u_N$, $p_P = p_N$ and $v_P = v_{NN}$ (the subscript NN indicates the second nearest neighbor to the north). In the row of grid boxes adjacent to 10N, the u- and p-equations are replaced by $u_P = u_S$ and $p_P = p_S$, and $v_N = v_S$ in the v-equation. Note that these modifications insure that conditions (15) hold at 9.5S and 9.5N, not at 10S and 10N.

In finite-difference form, then, equations (9a) subject to boundary conditions (13)–(15) are a set of simultaneous linear equations. There are three equations in each grid box, and so the total number of equations is $a = 3N_xN_y = 8400$. The set can be summarized in the matrix form

$$AQ = B, \tag{31}$$

where A is a matrix of dimension a that consists of the coefficients of the finite difference equations, the solution Q is a column vector of the desired variables u_n, v_n and p_n at appropriate grid points, and B is a column vector of the forcing F_n and G_n at appropriate points. It is useful to order grid boxes, and also the equations associated with them, consecutively so that box 1 is in the southwest corner of the rectangular region, box N_y is in the northwest corner, box $N_y + 1$ is immediately to the east of box 1, box $2N_y$ is immediately to the east of box N, and so on. In that case, matrix A has a bandwidth of the order of $b = 3N_y = 120$, that is much smaller than a.

In many cases matrix equations like (31) can be solved approximately by iterative methods. However, Henderschott (1978) points out that, if the system of equations supports free waves, iterative methods are not likely to converge. At the annual frequency Rossby and Kelvin waves are possible in the model ocean, and they are a very important part of its response. For this reason, (31) is solved here exactly using the standard technique of Gaussian elimination by "LU decomposition" (Forsythe and Moler, 1967). Because A is sufficiently nonsingular, pivoting is not necessary. For a general matrix A, the solution of (31) on a computer using this method requires roughly a^2 words of storage and $a^3/3$ multiplications, both excessively large numbers. Fortunately, when A is properly ordered it is possible to take advantage of its bandedness, and our code for the solution of (18) requires only $2ab$ words of storage and ab^2 multiplications.

REFERENCES

Adamec, D. and J. J. O'Brien. 1978. The seasonal upwelling in the Gulf of Guinea due to remote forcing. J. Phys. Oceanogr., *8*, 1050–1060.

Anderson, D. 1979. Low latitude seasonal adjustment in the Atlantic (unpublished manuscript).

Bakun, A. 1978. Guinea current upwelling. Nature, *271*, 147–150.

Bender, C. M. and S. A. Orszag. 1978. Advanced Mathematical Methods for Scientists and Engineers, New York, McGraw Hill, 593 pp.

Berrit, G. R. 1961, 1962. Contribution à la connaissance des variations saisonnières dans le Golfe de Guinée. Observations de surface le long des lignes de navigation. Cah, COEC XIII année, 10 dec. 1961, 115–127. XIV année, 9 nov. 1962, 633–653. XIV année, 10 dec. 1962, 119–129.

Bunker, A. F. 1976. Computations of surface energy flux and annual air-sea interaction cycles in the North Atlantic Ocean. Mon. Wea. Rev., *104*, 1122–1139.

Busalacchi, A. J. and J. Picaut. 1983. Seasonal variability from a model of the tropical Atlantic. J. Phys. Oceanogr., *13*, 1564–1588.

Cane, M. A. 1979. The response of an equatorial ocean to simple wind stress patterns: II. Numerical results. J. Mar. Res., *37*, 253–299.

Cane, M. A. and D. W. Moore. 1982. A note on low-frequency equatorial basin modes. J. Phys. Oceanogr., *11*, 1578–1584.

Cane, M. A. and E. S. Sarachik. 1979. Forced baroclinic ocean motion, III. The linear equatorial basin case. J. Mar. Res., 37, 355–398.

—— 1981. The response of a linear equatorial ocean to periodic forcing. J. Mar. Res., *39*, 651–693.

Clarke, A. J. 1978. On the generation of the seasonal coastal upwelling in the Gulf of Guinea. J. Geophys. Res., *84*, 3743–3751.

Cromwell, T. 1953. Circulation in a meridional plane in the central equatorial Pacific. J. Mar. Res., *12*, 196–213.

Forsythe, G. E. and C. B. Moler. 1967. Computer Solution of Linear Algebraic Systems, New Jersey, Prentice Hall, 148 pp.

Gallardo, Y. 1981. Milieu marin et ressources halieutiques de la République Populaire du Congo. Océanographie Physique. Tr. et. doc. ORSTOM, *138*, 67–73.

Gouriou, Y. 1982. Etude des variations thermiques sur une année moyenne dans le Golfe de Guinée à 4W, entre Abidjan (5N) et 10S de 0 à 250 m. Rapport de DEA. Université de Bretagne Occidentale, sept. 1982, 43 pp.

Guillerm, J. M. 1975. Variation saisonnières des transports côtiers dans le sud-est du Golfe de Guinée. Bull. Union Océanogr. de France, *7*, 55–67.

—— 1981. Contribution à l'océanographie physique du Golfe de Guinée: hydrologie et circulation saisonnières sur une radiale au large de Pointe-Noire (Congo). Thèse d'Université, Université de Bretagne Occidentale, 203 pp.

Hastenrath, S. and P. Lamb. 1977. Climatic atlas of the tropical Atlantic and eastern Pacific Oceans, University of Wisconsin Press, 112 pp.

Hellerman, S. 1980. Charts of the variability of the wind stress over the tropical Atlantic. Deep-Sea Res., Suppl. II, *26*, 63–75.

Hendershott, M. C. 1978. Numerical models of ocean tides, *in* The Sea, *6*, Wiley Interscience, New York, 47–95.

Hickie, B. P. B. 1979. The effects of coastal geometry on equatorially trapped planetary waves. Part 1: Free oscillations in the Gulf of Guinea (unpublished manuscript).

Hisard, P. 1973. Variations saisonnières à l'équateur dans le Golfe de Guinée Cah. ORSTOM, Sér. océanogr. XI, *3*, 349–356.

Holland, W. H. and L. B. Lin. 1975. On the origin of mesoscale eddies and their contribution to

the general circulation of the ocean. I. A preliminary numerical experiment. J. Phys. Oceanogr., *5*, 642–657.

Houghton, R. W. 1983. Seasonal variations of the subsurface thermal structure in the Gulf of Guinea. J. Phys. Oceanogr., (in press).

Janke, J. 1920. Strömungen und Oberflachentemperaturen im Golfe von Guinea. Archiv der Deutschen Seewarte, *6*, 1–68.

Katz, E. J. and Collaborators. 1977. Zonal pressure gradient along the equatorial Atlantic. J. Mar. Res., *35*, 293–307.

Lemasson, L. and J. P. Rébert. 1968. Observations de courants sur le plateau continental ivoirien. Doc. Sci. Prov. CRO Abidjan, *22*, 1–6.

—— 1973a. Circulation dans la partie orientale de l'Atlantique Sud. Doc. Sc. Centre Rech. Océanogr. Abidjan, *4*, 91–124.

—— 1973b. Les courants marins dans le Golfe ivoirien. Cah. ORSTOM, Sér. Océanogr., *11*, 67–95.

—— 1973c. Circulation dans le Golfe de Guinée. Etude de la region d'origine du sous-courant ivoirien. Cah. ORSTOM, Sér. Océanogr., *11*, 303–316.

McCreary, J. P. 1980. Modelling wind-driven ocean circulation. Rep. HIG-80-3, Hawaiian Inst. of Geophys. Honolulu, HA, 96822, 64 pp.

—— 1981. A linear stratified model of the equatorial undercurrent. Phil. Trans. Roy. Soc. London, *A298*, 603–635.

——1984. Equatorial beams. J. Mar. Res., *42*, (in press).

Merle, J. 1978. Atlas hydrologique saisonnier de l'Ocean Atlantique intertropical. Travaux et documents de l'ORSTOM, *82*, 184 pp.

—— 1980a. Seasonal heat budget in the equatorial Atlantic Ocean. J. Phys. Oceanogr. *10*, 464–469.

—— 1980b. Seasonal variation of heat storage in the tropical Atlantic Ocean. Oceanol. Acta , *3*, 209–220.

Merle, J. and S. Arnault. 1983. Seasonal variability of surface dynamic topography in the tropical Atlantic Ocean. J. Mar. Res., (submitted).

Merle, J. and J. F. LeFloch. 1978. Cycle annual moyen de la température dans les couches supérieures de l'Océan Atlantique intertropical. Océan. Acta , *1*, 271–276.

Moore, D. W. 1968. Planetary-gravity waves in an equatorial ocean. Ph.D. thesis, Harvard University.

Moore, D. W., P. Hisard, J. P. McCreary, J. Merle, J. J. O'Brien, J. Picaut, J. M. Verstraete and C. Wunsch. 1978. Equatorial adjustment in the eastern Atlantic. Geophys. Res. Letters, *5*, 637–640.

Morlière, A. 1970. Les saisons marines devant Abidjan. Doc. Sc. Centre Rech. Océanogr. Abidjan, *1*, 1–15.

Morlière, A. and J. P. Rébert. 1972. Etude hydrologique du plateau continental ivoirien. Doc. Sc. Centre Rech. Océanogr. Abidjan, *3*, 1–30.

Munk, W. H. 1950. On the wind-driven ocean circulation. J. Meteor., *5*, 1–43.

O'Brien, J. J., D. Adamec and D. W. Moore. 1978. A simple model of equatorial upwelling in the Gulf of Guinea. Geophys. Res. Letters, *5*, 641–644.

Philander, S. G. H. 1977. The effects of coastal geometry on equatorial waves. J. Mar. Res., *35*, 509–523.

—— 1979. Upwelling in the Gulf of Guinea. J. Mar. Res., *37*, 23–33.

Philander, S. G. H. and R. C. Pacanowski. 1981. The oceanic response to cross–equatorial winds (with application to coastal upwelling in low latitudes). Tellus, *33*, 204–210.

Picaut, J. 1983. Propagation of the seasonal upwelling in the eastern equatorial Atlantic. J. Phys. Oceanogr., *13*, 18–37.

Picaut, J., J. Servain, Y. Gouriou, P. Lecomte, N. Mérabet, M. Séva, A. Busalacchi, J. McCreary, D. Moore and B. Burtchy. 1983. Modélisation et observations des variations thermiques basse fréquence dans l'Atlantique Tropical. CNEXO report, Université de Bretagne Occidentale, 242 pp.

Piton, B., R. Perrin and J. P. Gausi. 1977. Nouvelles considérations sur les saisons marines et la circulation superficielle dans le Golfe de Guinée. Doc ORSTOM Pointe-Noire NS, 49 pp.

Rossignol, M. 1972. Contributions à l'étude du "complexe guinéen," Doc. Sc. ORSTOM, Dakar, 143 pp.

Schopf, P. S., D. L. T. Anderson and R. Smith. 1981. Beta-dispersion of low-frequency Rossby waves. Dyn. Atmos. Oceans, *5*, 187–214.

Servain, J., J. Picaut and J. Merle. 1982. Evidence of remote forcing in the equatorial Atlantic Ocean. J Phys. Oceanogr., *12*, 457–463.

Verstraete, J. M., J. Picaut and A. Morliere. 1980. Atmospheric and tidal observations along the shelf of the Guinea Gulf. Deep-Sea Res., (GATE Supp. II), *26*, 343–356.

Voituriez, B. 1981. The equatorial upwelling in the eastern Atlantic Ocean. Report of the final meeting of SCOR WG 47, Nova Univ. Press.

Wauthy, B. 1977. Revision de la classification des eaux de surface du Golfe de Guinée. Cah. ORSTOM, Sér. Océanog., *15*, 27–99.

Received: *28 January, 1983;* revised: *10 November, 1983.*